Development and evaluation of quantitative methods of analysing single photon emission computed tomography blood flow images of the brain.

Anna Pauline Barnes, B.Sc., M.Sc.,

Department of Clinical Physics, Faculty of Medicine,

University of Glasgow.

Presented as a thesis for the degree of Ph.D.,

Department of Clinical Physics, Faculty of Medicine,

University of Glasgow, University Avenue, G12 8QQ.

May 13th 1999.

"Live as if you were to die tomorrow. Learn as if you were to live forever".

- Gandhi.

Contents

Abbreviations

(^{123}I)IBZM - iodine-123 iodobenzamide

^{123}I IMP - iodine-123 isopropyl-p-iodoamphetamine

^{123}I QNB - iodine-123 3quinuclidinyl-4-idobenzilate

^{18}F FDG - Fluorine -18 fluorodeoxyglucose.

^{57}Co - cobalt -57

^{99m}Tc ECD - technetium-99m ethyl cysteinatedimer

^{99m}Tc HMPAO - technetium-99m hexamethylpropyleneamine oxime

AC-PC - anterior commisure - posterior commisure

AnCova - Analysis of covariance

BBB - blood brain barrier

BF - blood flow

BOLD - blood oxygenation level dependent

C(^{15}O)$_2$ - radiolabelled carbon dioxide

CBF - cerebral blood flow

CBV - cerebral blood volume

CDA - change distribution analysis

CNS - central nervous system

CSF cerebral spinal fluid

CT - computed tomography

DAT - dementia of the Alzheimer's type

DFLT - dementia of the frontal lobe type

DVaT - dementia of the vascular type

EEG - electroencephalography

FHBM - functional human brain mapping

fMRI - functional magnetic resonance imaging

FWHM - full width at half maximum

gCBF - global cerebral blood flow

GLM - general linear model

$H_2{}^{15}O$ - radiolabelled water

MIPS - maximum intensity projections

MRI - magnetic resonance imaging

MTL - medial temporal lobe.

OM - orbito-meatal

PAD - possible Alzheimer's disease

PCA - principal components analysis

PET - positron emission tomography

rCBF - regional cerebral blood flow

RF - radio frequency

ROI - region of interest

SPECT - single photon emission tomography

SPM96 - statistical parametric mapping

TIA - transient ischaemic attack

VNS - vagal nerve stimulation

List of Figures

List of Tables

Acknowledgements

I have had the pleasure of working with some wonderful people during the three and half years of this project, each of whom have contributed (academically, emotionally and spititually) to this final result and I take this opportunity now to thank them all.

First of all I thank my supervisor, Prof. Dave Wyper, for having enough enthusiasm (and patience) for the both of us to get me to the end of this PhD thesis. I have learnt a lot from him not least that one can have a tremendous zest for life as well as work and I look forward to working with him for many years in the future. The same sentiments apply to Dr Jim Patterson whose sound advice and objective thoughts on this project got me through some sticky moments. Thanks also to Dr Daniela Montaldi (whose fault this all is anyway - remember our first memory activation experiment?). Daniela gave me a fascinating insight into the intracacies of the human brain but more than that she gave me her friendship which I will always treasure. I would also like to thank Dr Mike Glabus (MRC Brain metabolism unit, Edinburgh Royal Hospital, Morningside, Edinburgh) who was always on the end of an e-mail to answer some of the thorny SPM questions. Thank you to Mary-Theresa Hansen, Marlene Smeeton, Jean Winning, Marion Cresswell and Jonothan Allen who did a lot of the boring bits and made me laugh a lot.

Others in the department who deserve a thank you are Dr Donald Hadley, Dr Barrie Condon (for employing me for the last 8 mths - funded by the Robertson Trust) and Dave Brennan with whom I shared an office with the last three years and who continued to be so nice even when I was a narky so and so.

To Helen Job, thanks for all the mugs of tea and bags of chips that accompanied that shoulder to cry on. The kettles already boiling its your turn next ! Thanks to all the other trainee physicists for their encouragement and support (they have all this to look forward to).

The biggest thanks must go to my family (Polly and Paul and Charlotte) who always knew I could do it even when I thought I couldn't.

And finally to my my darling Jack, who makes my life sparkle.

Summary

Development and evaluation of quantitative methods of analysing single photon emission computed tomography blood flow images of the brain.

This thesis presents the investigations carried out on a particular method of functional human brain mapping (FHBM) analysis (SPM)[1] as to its applicability to a routine nuclear medicine neuroimaging department. Principally designed for the investigation into positron emission tomography (PET) radiolabelled water studies of normal brain function during neuroactivation experiments the technique is still relatively novel for the purposes of interpreting single photon emission computed tomography (SPECT) images of brain function.

This thesis investigates whether the functional brain mapping technique (SPM) can be extended to embrace the widely available imaging technique of SPECT and to determine whether this combination can contribute to routine diagnosis of abnormalities in brain function and to research investgiations involving functional neuroactivation.

Validation of the image standardisation facility of SPM96 applied to oblique or incomplete image data sets.

The image standardisation component of SPM96 was validated by subjecting it to a series of challenge conditions created from simulated data. The challenge conditions were chosen to reflect those that occur in clinical scans, for example, extreme misalignments to a standard reference orientation resulting in axial truncation of the image volume. The results of the software performance under these challenges showed that the image standardisation component of this software had particular problems correcting for large (15^{o}) rotations in the sagittal and coronal planes coupled with severe axial truncation. Modifications to the image

[1]Statistical Parametric Mapping, Prof K.J. Friston. Wellcome department of Cognitive Neurology, Institute of Neurology, London, U.K.

standardisation procedure were made based on these results. This involved the inclusion of a rigid body registration step prior to image standardisation and the editing of spurious voxel values, created by erroneous interpolation of edge information after re-orientation. The extra image registration step required the creation of an ideal CBF SPECT scan (whole brain coverage and orientation to a standard reference space) to which all the scans containing the challenge conditions were registered. Having established a set of working criteria for use with routine ^{99m}Tc-HMPAO SPECT scans, SPM96 was then applied to images of individual patients presenting with symptoms of dementia. The aims were:- a) To determine whether SPM maps could be produced which were consistent with the original scans. b) To ascertain whether they could assist in the reading of scans by reducing inter-rater variability.

Investigation of SPM96 as an aid to the differential diagnosis of dementia using ^{99m}Tc HMPAO SPECT images of rCBF.

To investigate the usefulness of SPM96 analysis as an aid to the visual reporting of CBF SPECT scans it was used to assist in the differential diagnosis of dementia. Usefulness was assessed by comparing inter observer reliability for diagnosis of dementia based on information from the CBF scans alone compared to diagnosis based on the scans plus information from the SPM analysis. The hypothesis was that inter observer reliability would be improved with the addition of an objective measure of CBF pattern provided by SPM96 analysis. The results obtained from this investigation failed to show any benefit to using the additional data provided by SPM96 analysis, however, it may play a role in monitoring progression of disease or the therapeutic effects of treatment.

Modification of ^{99m}Tc HMPAO SPECT acquisition protocol for SPM type analysis of neuroactivation studies: Image quality versus statistical power

To investigate the possibility of using a similar approach to PET i.e. increase the number of scans per task and accept poorer individual scan quality for SPECT studies of neuroactivation different study paradigms (replication and non-replication) were constructed. The different paradigms were created by variation of the image scanning parameters a) administered radiation activity per scan (within allowable limits) b) number of scans per task and c) scan acquisition time. Simulated neuroactivation experiments were created by the addition of pseudo activations to the images acquired under the different scanning parameters. Duplicate copies of real scans were made for the purposes of this study, in order to have a data set (activated and non-activated) that did not include noise due to natural variability of CBF or anatomy between subjects. This imposed condition of no anatomical variation makes the distinction between the paradigms clearer by removing noise due to inter and intra-subject variability without introducing bias in favour of any particular paradigm. The statistical benefits of a replication paradigms versus a non-replication paradigm were established by analysing the data sets with the SPM96 analysis. The simulation was able to show that when an SPM investigation is used for data analysis, study replication is more important than the individual image quality typically available from a high performance SPECT system.

Applications of the optimised SPECT acquisition parameters to neuroactivation studies.

To confirm the hypothesis that the addition of two further scans, allowing for each condition to be replicated (i.e. ABAB), would greatly increase confidence in the results and their interpretation, the 4 scan paradigm was used to investigate the stimulation of the vagus nerve for the treatment of epilepsy. A four scan design is also advantageous to SPECT studies of neuroactivation. The application of two additional scans, could greatly enhance the power of investigation of neuroactivation studies involving groups of normal healthy subjects, by the addition of one, or perhaps two, additional cognitive conditions (i.e., ABAC or ABCD respectively). This would enable more subtle differences in cognitive processing to be

investigated. To confirm that the addition of a further task can contribute to the teasing out of cognitive processes used in memory, a SPECT neuroactivation experiment was designed with the 4 scan paradigm to investigate the role of the medial temporal lobe in the processing of familiar and novel material.

In conclusion the first part of this investigation established that a voxel-wise analysis does not provide any benefit as an aid to differential diagnosis by visual reporting of CBF SPECT scans. However, it may provide a possible means for objectively monitoring progression of disease or treatment. The second part of this investigation was able to demonstrate that SPM can be used with SPECT to investigate functional activation studies which have, up to now, been considered to be limited to the domain of PET and fMRI. This opens up this type of study to a wider research community and establishes a role for SPECT in neuroactivation studies for experiments or subjects unsuited to the PET or fMRI environment.

Just as importantly these investigations indicate that this type of statistical mapping is applicable to the lower resolution data provided by SPECT and could therefore be applied to images of neuroreceptor function, for which radioligands are increasingly becoming available, and which can only be obtained with emission tomography.

Preface and Declaration.

This thesis comprises of my own original work carried out during the period of October 1995 and October 1998 and has not been presented previously as a thesis in any form.

The thesis presents the investigations carried out on the applicability of a particular method of functional human brain mapping (FHBM) analysis (Statistical Parametric Mapping (SPM96) - K.J Friston, Wellcome Department of Cognitive Neurology, University College London, UK) in a routine nuclear medicine neuroimaging department. The results are presented from investigations into two broadly defined areas

- The performance of the SPM method when used with non-optimal CBF SPECT images and its use as an aid in the visual reporting of these scans for the differential diagnosis of dementia.
- The optimisation of the cerebral blood flow (CBF) SPECT imaging protocol for neuroactivation experiments and its application to two different experiments.

Chapter 1 reviews the literature in the field of human brain mapping (FHBM). The first section outlines the development of functional human brain mapping in both normal and abnormal subjects and includes a short description of normal human brain function with regard to autoregulation of blood flow and its coupling with cognitive function. The second section provides a more detailed explanation of the various components of a typical FHBM analysis including image registration, image standardisation methods and statistical analysis. The advantages and disadvantages of the components are also described in order to appreciate fully the context in which the subsequent investigations were done.

Chapter 2 lists the various steps involved in using SPECT with SPM and describes the image acquisition and processing of images used in the experiments. Chapters 3 - 6 describe four different experiments linked by the overall theme of validating and optimising the methods used when analysing SPECT CBF images with SPM.

Chapter 3 outlines the methods used to create the challenge conditions devised to validate the image registration software. The results of these validations are presented and discussed in terms of providing the best methods of image standardisation for non-optimal image data sets.

Chapter 4 uses the optimal image standardisation method determined in chapter 3 to investigate the application of a SPM analysis to images of individual patients presenting with symptoms of dementia. The results are presented and the routine use of SPM in a nuclear

medicine department is discussed. The visual reporting of CBF SPECT scans was carried out by Prof. D. J. Wyper and Dr J Patterson.

Chapter 5 outlines the methods and challenge conditions used to modify the acquisition protocol of CBF SPECT images for analysis by SPM methods, in particular whether SPECT studies of neuroactivation might benefit from a similar approach used in PET, i.e. increase the number of scans per task and accept poorer individual scan quality. The results are presented and discussed in terms of their suitability for use in neuroactivation studies using SPECT.

Chapter 6 uses the optimal study design determined in chapter 5 to investigate vagal nerve stimulation as a treatment for epilepsy. Patients were recruited for this study by Dr R Duncan.

Chapter 7 uses the same design to study the role of the medial temporal lobes in novelty detection by contrasting it with their role in the encoding and/or consolidation into long-term memory of associative information. Dr D. M. Montaldi recruited the volunteers and designed the neuropsychological experiments used in this study.

Chapter 8 outlines the conclusions drawn from each of these experiments and their application to the future use of SPECT in functional human brain mapping.

CHAPTER 1

Development and evaluation of quantitative methods of analysing single photon emission computed tomography blood flow images of the brain.

This chapter outlines the development of functional human brain mapping in both patients and normal subjects and includes a short description of normal human brain function with regard to autoregulation of blood flow and its coupling with cognitive function. This is followed by a more detailed explanation of the various components of a typical functional human brain mapping analysis including image registration, image standardisation methods and statistical analysis. The advantages and disadvantages of each of the components are also described in order to appreciate fully the context in which the subsequent investigations were undertaken.

1990-1999; The decade of the brain.
Presidential proclamation 1990 (1)

1.1 Introduction

The function of the human brain can now be mapped in vivo by carefully manipulating cognitive processes while the subject is being scanned, a process referred to as neuroactivation experimentation. The dramatic images produced by the new functional human brain mapping methods of analysis might give us the impression that we are

'seeing the brain thinking' but the subtleties involved in the fractionation of cognitive processes using sophisticated experimental designs are not straightforward and the understanding of the underlying neuropsychology must not be underestimated. Likewise the fact that sophisticated statistical analysis can now be performed at the touch of a button must not stop the user having a fundamental grasp of those statistical theories on which the analysis is based. The rapid advance in technology may now have outpaced the understanding of many clinical scientists traditionally involved in functional human brain mapping principally through the investigation of lesions studies.

Inspired by these sentiments this thesis presents investigations carried out on a particular method of functional human brain mapping (FHBM) analysis (Statistical Parameteric Mapping (SPM) - Prof. K. J. Friston, Wellcome Department of Cognitive Neurology, Institute of Neurology, London, UK) with particular emphasis on its applicability to the work of a routine nuclear medicine neuroimaging department. Principally designed for the analysis of positron emission tomography (PET) radiolabelled water studies of normal brain function during neuroactivation experiments the technique is still relatively novel for the purposes of interpreting single photon emission computed tomography (SPECT) images of brain function. This thesis evaluates and develops the use of SPM for use with CBF SPECT images of cerebral blood flow and focuses on two aspects. The first part of this thesis investigates whether or not the use of a voxelwise image analysis method like SPM can improve the visual reporting of SPECT scans, by providing objective data on deviations from a normal reference database. The second part of the thesis investigates the statistical analysis component of the SPM method when using cerebral blood flow (CBF) SPECT imaging for neuroactivation experiments, to determine whether brain state replication is more important than the individual image quality typically available from a high performance SPECT system.

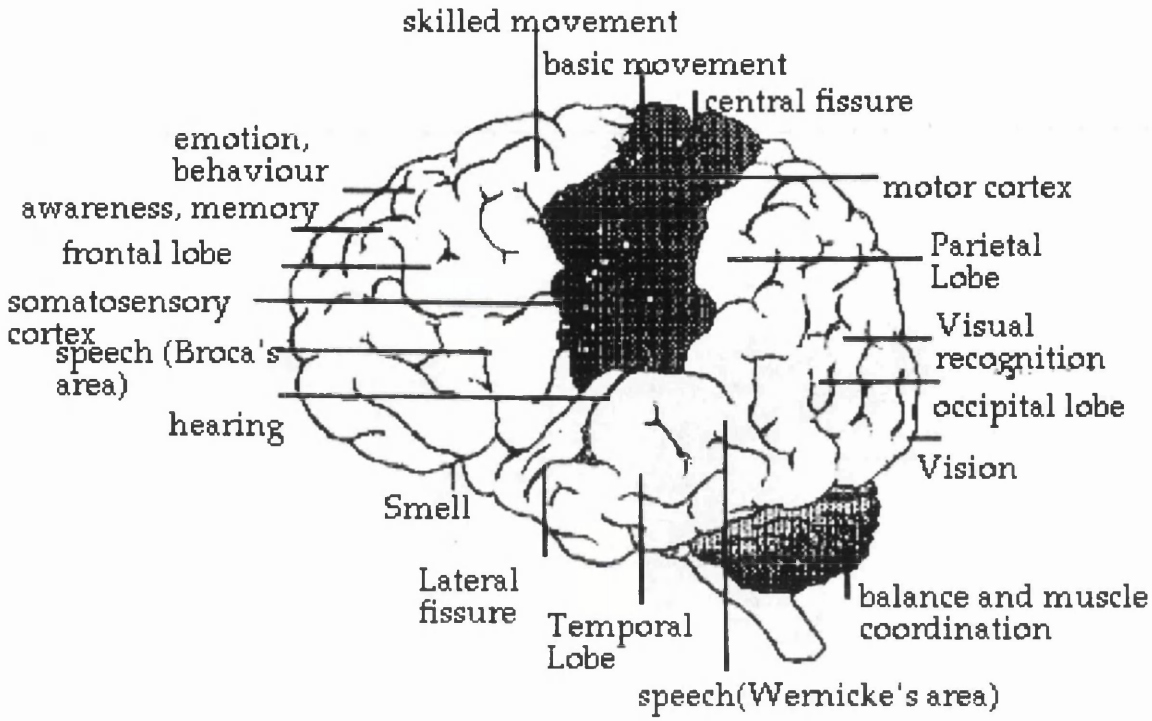

Figure 1.1 Schematic diagram of the functional anatomy of the human brain as derived from lesion studies and electrical stimulation of the cortex.

1.2 Functional Human Brain Mapping

The cutting edge of functional human brain mapping is now remote from interventional medicine but this was not always so. The original 'hands on' in vivo neuroactivation studies performed by neurologists such as Foerster in the 1920's and then Penfield and colleagues in the '30's were very much at the 'cutting edge'. Regarding each operation as an opportunity to conduct physiological experiments on the exposed cortex of conscious patients, they stimulated areas of the brain and recorded the resulting effects in elaborate detail. Penfield's results of electrical stimulation of the cortex are recorded in his book 'The cerebral cortex of man' (2) which still governs our general views of human brain functional anatomy (fig. 1.1).

Even earlier the methods of clinicopathological correlation were used as a method of functional mapping, where signs and symptoms were associated with damage or disease

located in a specific region of the brain. The names Broca's and Wernicke's areas are still with us today and refer to areas in the brain associated with damage in patients who suffered from particular language problems investigated by Paul Broca and Carl Wernicke in the nineteenth century. The study of clinicopathological correlation continued throughout the latter part of the nineteenth century and most of the twentieth century with interested clinicians recording the specific behaviour of patients afflicted with particular damage until such time as the patient's brain could be investigated pathologically. Even the invasive methods of twentieth century surgeons couldn't provide a complete picture of functional anatomy as stimulations of the exposed cortex still only provide surface topography: the surface of the cortex being the only part of the brain accessible to the scalpel or electrode.

1.3 Neuroanatomy and physiology

Neuroanatomists define the human brain in teRMS of grey matter and white matter, a distinction clearly discernible in the structural images provided by magnetic resonance scanners (fig. 1.2). The grey matter makes up the cortical layers. The white matter refers to the white nerve fibres connecting the two hemispheres together, passing sensory signals throughout the cortex.

Grey matter is one of the most metabolically active tissues in the body using almost exclusively oxygen and glucose for its function and consequently needing a continuous and plentiful supply of blood. A delicate balance of oxygen and glucose concentration is required for efficient functioning of the brain and this is entirely dependent on the body's ability to regulate the blood supply, a process referred to as autoregulation. During autoregulation the cerebral blood volume (CBV) can increase (by vessel dilation) to retain a constant rate in cerebral blood flow (CBF). Once maximum vessel dilation is reached and total blood volume can no longer increase CBF will fall. Normal mean CBF is kept constant by this autoregulation at a level of about 50-60 ml/min/100g of brain tissue. The normal flow in grey matter is slightly higher than that of the mean, at 65-85 ml/min/100g

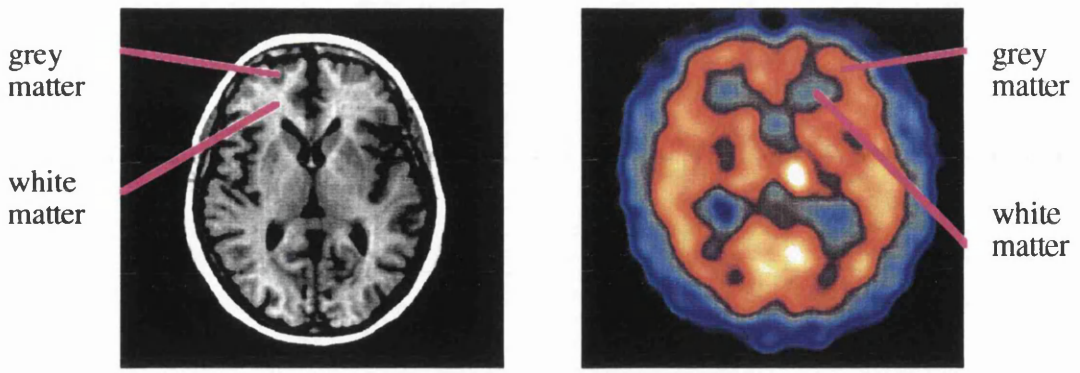

Figure 1.2. Axial images showing transverse slices through the basal ganglia. The regions of white and grey matter are clearly discernible in the T1 MR image (from a Seimens, Magnetom 1.5T scanner). The SPECT ^{99m}Tc HMPAO rCBF image (from a Strichman Medical Equipment SME810 scanner) shows how the differences in metabolic activity of in the two different brain tissues are reflected by their blood flow.

and is lower in white matter, at 27-33 ml/min/100g. Normal mean perfusion is possible down to 20 ml/min/100g CBF since the brain can compensate with a corresponding increase in oxygen extraction. Autoregulation begins to fail below this at approximately 15 ml/min/100g, causing ischaemia (restriction of blood to the tissue) which if prolonged will cause irreversible damage. The disruption of autoregulation through external injury or disease has a profound effect on the function of brain tissue. Uncontrolled increases in glucose levels after head injury or decreases in blood flow from stenosis of the blood vessels occurring in cerebral vascular disease will cause irreparable damage and eventually death of the surrounding tissue.

The level of CBF and CBV is clearly related to oxygen extraction rate and consequently the function of the brain. More than 100 years ago scientists were able to establish that the level of neuronal activity dictated the level of local blood supply in the brain. Later, when the imaging of cerebral metabolic parameters was possible using emission tomography techniques scientists were able to establish that increased blood flow was required for the increase in glucose consumption by the neuronally active areas (3,4). Interestingly they also found that the corresponding increase in oxygen consumption was slightly smaller than the rise in blood flow (5). As a result of this mismatch between demand and supply the blood leaving the activated cortical region is more oxygenated

than normal, a fact that gave rise to the now rapidly expanding field of functional magnetic resonance imaging (fMRI).

The study of CBF, therefore should enable us to investigate brain function in both the normal and diseased state. One method of doing this is to radiolabel molecules that can cross the fully functioning blood brain barrier (BBB) and so distribute according to blood flow in the brain tissue. The emission from these distributed radiolabelled molecules can then be picked up by an external detector. The first in vivo images of CBF using emission computed tomography imaging were provided by detecting the radioactive emissions from inhalation of radiolabelled $(^{15}C)O_2$ (6), and intravenous injection of $H_2(^{15}O)$ (7,8) using positron emission tomography (PET). With the development of the ubiquitous technetium-99m (^{99m}Tc) radiochemistry, single photon emission tomography (SPECT), a much more widely available technique, could be used to image CBF (9-11). Technetium-99m hexamethylpropyleneamine oxime (^{99m}Tc HMPAO) is now a well established radiopharmaceutical in nuclear medicine departments for studying CBF in various clinical conditions. This radiopharmaceutical has been shown to distribute in the brain as a function of regional CBF (rCBF) although the final distribution seems to underestimate CBF in regions of high flow (9-11). ^{99m}Tc HMPAO is administered intravenously and reaches the brain after a few seconds, 5%-6% of the total dose is extracted on its first pass through the brain where it becomes trapped in brain tissue due to a change in the lipophilicity of the molecule. This whole process takes 40-60 seconds allowing some of the tracer to diffuse back across the BBB in the first 2-3 mins after intraveneous injection (10). After this, the level of ^{99m}Tc HMPAO activity remains approximately constant over the next 8hrs (10) so that it is possible to image, much later, the actual pattern of blood flow occurring in the brain at the time of the injection. The time delay between injection and scanning is limited only by the decay time of the nuclide ($T_{1/2}$ = 6hrs).

SPECT functional brain imaging using ^{99m}Tc HMPAO is a powerful clinical tool. Several clinical applications are now well documented (12). The study of CBF using

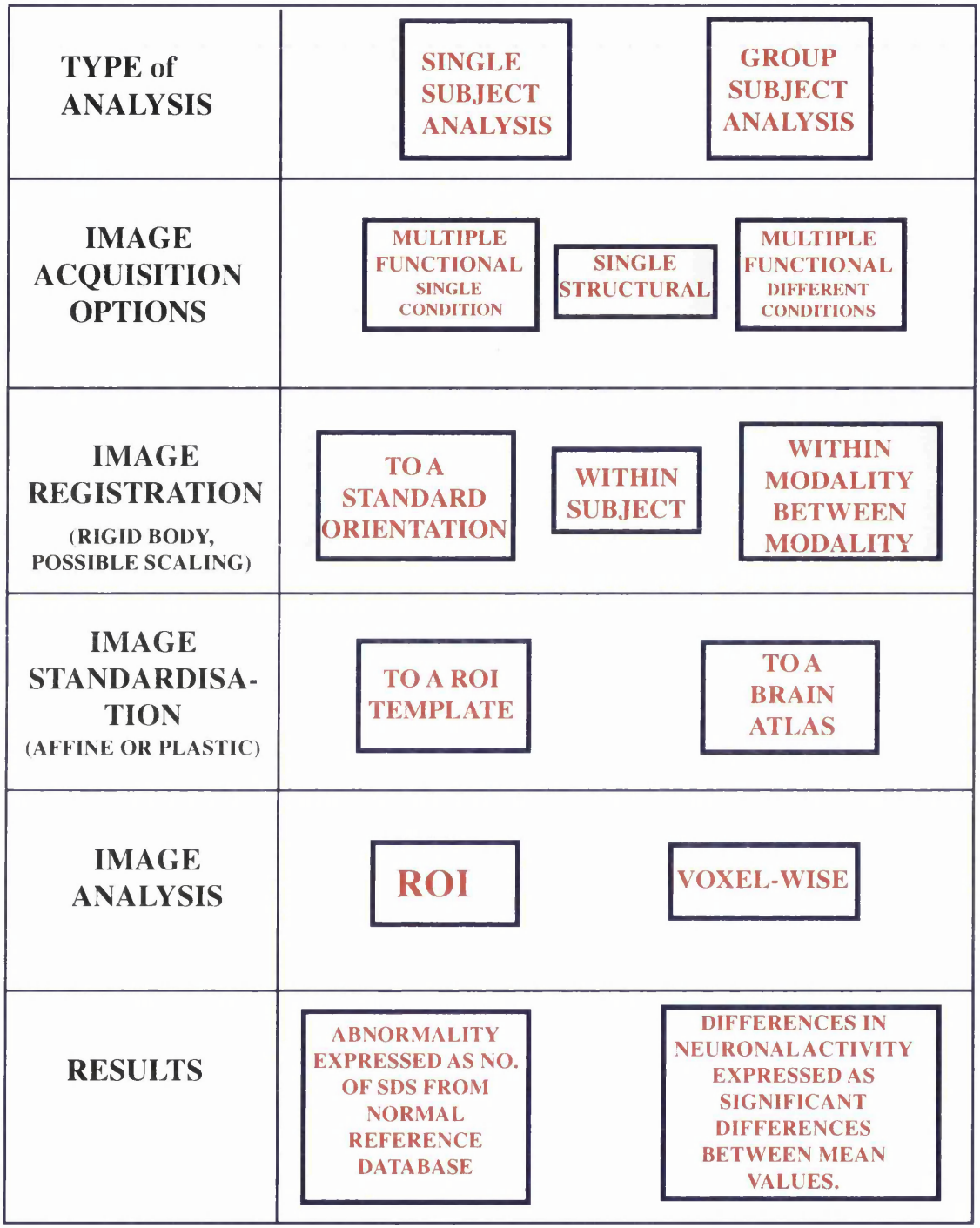

Figure 1.3. A schematic diagram of the steps taken in a functional human brain mapping analysis of an individual subject (left side of diagram) and a group of subjects (right side of diagram).
ROI - region of interest, SD - standard deviation

^{99m}Tc HMPAO has shown to be relevant to the clinical investigation of dementia, epilepsy, stroke and more recently the investigation of cognitive processing in both normal and abnormal brains (13-15), referred to as functional human brain mapping (FHBM).

1.4 Functional Human Brain Mapping Tools.

A functional human brain mapping investigation consists of:

- scanning to acquire images,
- image re-alignment to ensure common orientation,
- a method of anatomical standardisation for between subject analysis,
- statistical analysis, using either regions of interest or voxel-wise measurements.

The next section describes each of these components (see figure 1.3) to appreciate fully the context in which the subsequent investigations in chapters 3-6 were undertaken.

1.5 Imaging modalities

Advances in neuroimaging technology have meant that high resolution (temporal and spatial) functional and structural imaging are now routinely available. Magnetic resonance imaging (MRI), x-ray computed tomography (CT) and single photon emission computed tomography (SPECT) are now fundamental to the hospital departments of radiology and nuclear medicine. Positron emission tomography (PET) although usually in residence at centres of excellence (due to high capital and running costs) is nevertheless also used for clinical investigation.

X-ray CT is used for structural imaging and is made possible due to the differences in linear attenuation of x-rays by different types of body tissue and is excellent for imaging bone defects (see fig 1.4). However, contrast agents are needed to image blood flow and this method provides almost no contrast between white and grey matter in the brain.

	X-RAY CT	MRI	PET	SPECT	BOLD fMRI
	structure	structure	function	function	function
CBF	with contrast agent	with contrast agent	with $(^{15}C)O_2$ and $H_2(^{15}O)$	with ^{99m}Tc HMPAO	special pulse sequence
NEURO-RECEPTORS	NO	NO	YES (various imaging agents)	YES (various imaging agents)	NO
COST	LOW	MODERATE	HIGH	MODERATE	HIGH
AVAILABILITY	widespread	widespread	limited	widespread	limited
SPATIAL RESOLUTION	<1mm	< 1mm	2~3mm (very best) 4-6mm (typically)	~ 6mm (very best) 8-9mm (typically)	< 1mm
TEMPORAL RESOLUTION	N/A	N/A	$H2^{15}O$ 1-2 minutes $^{18}FFDG$ 20mins	^{99m}Tc HMPAO 45 secs.	seconds
NO. OF STUDIES PER SUBJECT	N/A	N/A	12 (max)	4 (max)	unlimited
INTERSTUDY INTERVAL	N/A	N/A	minutes	hours (splitdose) days	seconds
INTRUSIVENESS OF STUDY ENVIRONMENT	N/A	N/A	MODERATE experiments must be performed inside the scanner	LOW experiments can be performed anywhere	HIGH high magnetic field levels, high noise levels during scanning

Table 1.1 Comparative advantages and disadvantages of x-ray CT, MRI, PET, SPECT and fMRI for scanning of the human brain.

CT - computed tomography, MRI - magnetic resonance imaging, PET - positron emission tomography, SPECT - single photon emission computed tomography, BOLD -blood oxygenation level dependent, fMRI - functional magnetic resonance imaging, CBF - cerebral blood flow, HMPAO - hexamethyl-propylene-amine-oxime.

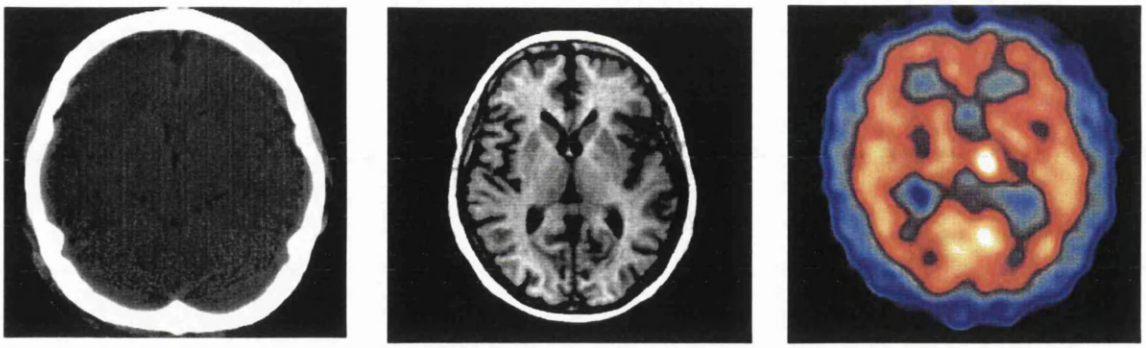

Figure 1.4 Three different kinds of imaging modality of an axial slice taken through the basal ganglia; x-ray computed tomography (CT), magnetic resonance imaging (MRI-T1) and emission tomography (SPECT).

Conversely MRI (also used for structural imaging) provides very good contrast between white and grey matter but poor information on bony structures of the skull (fig 1.4). MRI, is able to distinguish between different tissue types by manipulating radiofrequency pulses to excite hydrogen nuclei within the body. This is done by detecting the differences in the resulting radiofrequency emissions due to the different tissue environments from the de-exciting nuclei. Functional imaging techniques PET and SPECT are based on the ability to detect gamma rays emitted from the human body after the introduction of trace radioactive substances or radiopharmaceuticals. By careful design of the radiopharmaceutical a range of physiological parameters in the body can be measured. In particular cerebral function can be assessed by measuring blood flow (fig. 1.4) and volume, oxygen extraction, glucose transport and metabolism, and neurotransmitter function. For example, radiopharmaceuticals such as ^{99m}Tc HMPAO and ^{99m}Tc ECD with SPECT are used to image CBF; and (^{123}I)IBZM is used with SPECT, to investigate dopamine receptor function. ^{18}F FDG is used with PET to look at glucose consumption, and $H_2{}^{15}O$ and $C(^{15}O)_2$ to investigate CBF. More recently MRI has been able to provide functional information using a scanning sequence referred to as blood oxygenation level dependent (BOLD) contrast (5). This MRI technique can be used to detect an increase in oxygen levels of blood leaving a region associated with increased neuronal activity in the brain. The small changes in the external magnetic field produced by the difference in the magnetic properties of oxyheamoglobin and de-

oxyheamoglobin can be detected when using the appropriate RF pulse manipulations. The advantage of this type of functional imaging over emission tomography techniques is that it involves no ionising radiation. However, the high magnetic fields used do pose a problem when imaging subjects with metal implants and the loud noise during acquisition makes mapping of any auditory stimulation difficult. Although a certain degree of spatial information is provided by an emission tomography functional image the anatomical detail is not apparent and the anatomical location in fMRI is only referenced to its structural MRI acquisition provided there is no movement by the subject between the two. As a consequence a method of linking structural information from either MR or CT to the functional information obtained from either SPECT, PET or fMR images is crucial.

1.6 Image Registration

Diagnostic imaging often involves combining structural images with sequential functional images (fig. 1.5) to monitor the progress and treatment of diseases such as dementia, cerebrovascular disease and brain tumours. The wide accessibility to these techniques has also allowed neuropsychologists to use them to assess brain function in groups of normal subjects. Multiple functional (and sometimes structural) images of each subject are required during several cognitive processing tasks to provide information for the subsequent analysis. Crucial to both these types of comparison is that the scans be aligned to precisely the same orientation so that the observer is looking at exactly the same view of the brain across all scans from the subject's data set or the same view across a group of subjects. To achieve this, various methods of image co-registration have been developed which reorientate one of the scans (the sample scan) until each anatomical location corresponds exactly with the other (the reference scan). This process can be extended so that the data is also aligned along an accepted anatomical reference line (an aligned reference scan) to allow both inter and intra-modality comparisons.

Image registration is the term used to describe the method of determination of one to one mapping between co-ordinates in one (reference) image to those in another (sample)

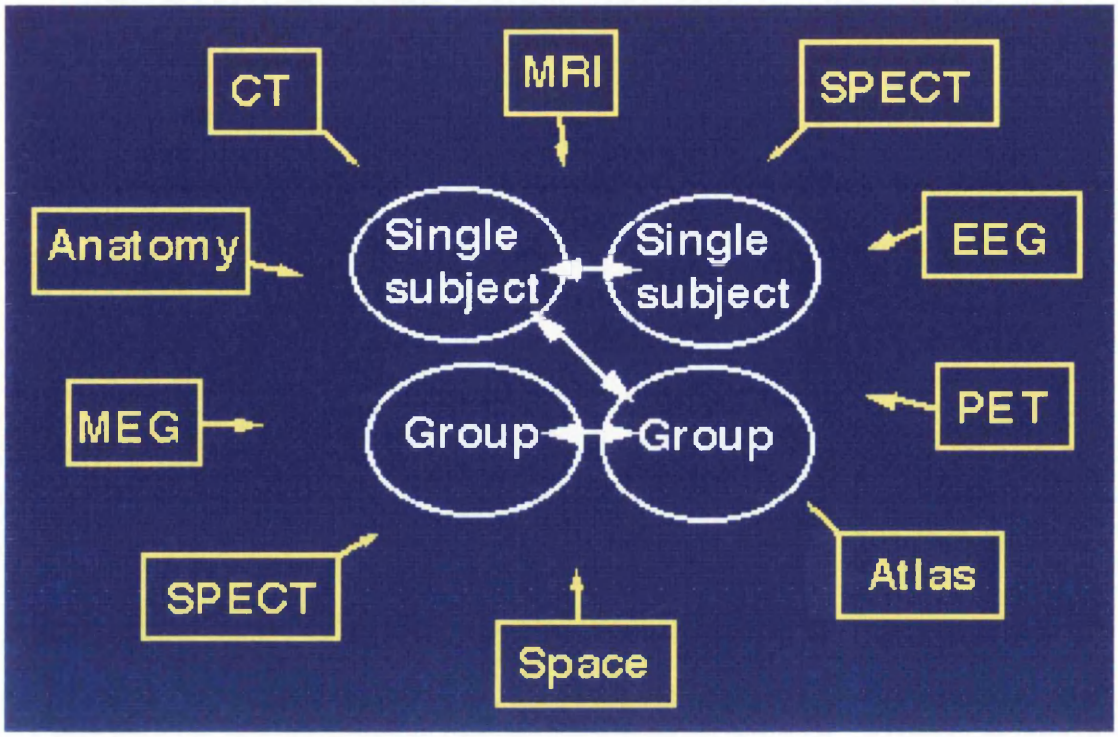

Figure1.5 Various different types of data that can be registered (yellow) for different comparisons (white).

image such that the points in each correspond to the same anatomical location. The simplest mapping or affine transformation is a rigid body transformation and can be described in matrix notation as follows:

$$\begin{pmatrix} S1 \\ S2 \\ S3 \\ 1 \end{pmatrix} = \begin{pmatrix} 1 & 0 & 0 & Xtrans \\ 0 & 1 & 0 & Ytrans \\ 0 & 0 & 1 & Ztrans \\ 0 & 0 & 0 & 1 \end{pmatrix} * \begin{pmatrix} R1 \\ R2 \\ R3 \\ 1 \end{pmatrix} \qquad S = MR \text{ (in matrix notation)}$$

A rigid body transform consists of 6 parameters, 3 rotation and 3 translation, and is used when the distance between the points within the sample image is to be preserved for example for within subject imaging. The affine transform can be extended to 9 parameters to account for scaling differences that may be needed for inter-modality registration. Further parameters (usually another 3) can be added to transform differences in overall brain shape and are the basis of image standardisation techniques.

The following sections describe the various techniques used to derive the transformation described above beginning with the rigid immobilisation techniques used by surgeons performing stereotactic surgery to the more sophisticated techniques utilising voxel similarity measures and high speed computing.

1.6.1 Image registration by immobilisation

Immobilisation methods are used to locate brain images in 3D space for the purposes of stereotactic surgery and radiotherapy. Surgeons use stereotactic frames bolted to the patient's skull, to locate lesions within and across different imaging modalities and to locate lesions within their operating space (fig. 1.6). These invasive methods are acceptable where a general anaesthesia has already been administered for the subsequent surgical procedures. For radiotherapy treatment less invasive methods of immobilisation have been developed when patient positioning must be reproducible on a daily basis over a treatment of 6 weeks. Immobilisation methods for radiotherapy are based on the fitting of individual moulds to either a patient's whole head (16) or their teeth (17,18). Published data report that reproducibility of positioning is of the order of 2mm (17-19) and sufficient for the purposes of radiotherapy beam treatment. Radiologists and surgeons commonly use different types of imaging to assist in diagnosis or in the planning of treatment. PET/SPECT imaging of a brain tumour may be required alongside the patient's MRI scan for a better representation of the extent of tumour volume or assessment of recurrence. MRI and x-ray CT images may be combined for a patient's radiotherapy planning so that better delineation of the brain lesion is obtained from the MRI while the CT image provides information essential to radiation dose volume calculations. Visualising between modalities when using immobilisation devices is easily achieved by fixing external markers to the patient's head frame/holder. The markers can then be filled with an appropriate material for visualisation between imaging modalities e.g. copper sulphate filled tubes and spheres, glass beads, vitamin E tablets,

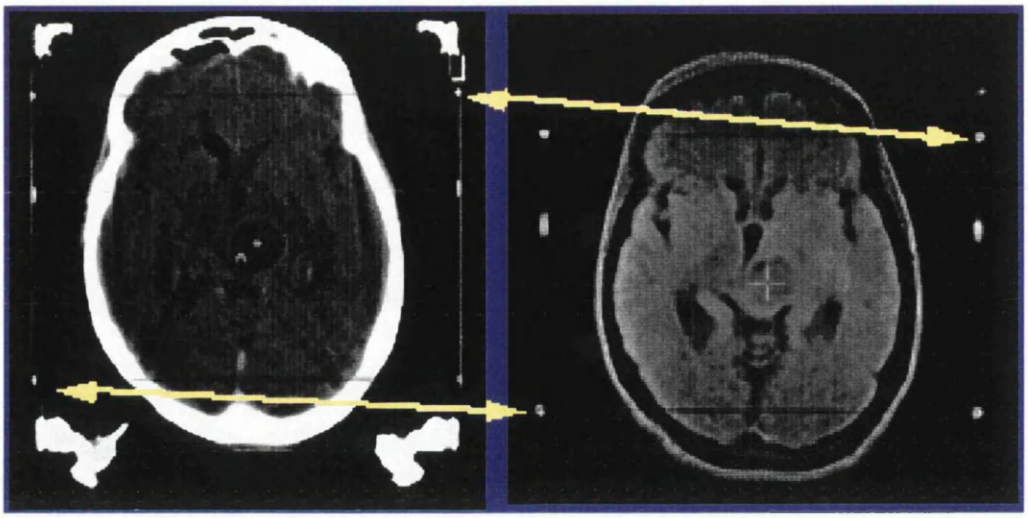

Figure 1.6 shows the use of a stereotactic frame visible in both CT (left picture) and MRI (right picture) External markers (or fiducial points) are used to register these two images of the same patient to one another.

oil filled tubes, staples, polyvinyl alcohol gel markers, spheres/discs of ^{99m}Tc and v-shaped markers of aqueous solutions of gadolinium are all suitable.

1.6.2 Image registration by external landmark matching.

Immobilisation devices are not 'patient friendly' and rigid fixation is unacceptable for the ever increasing numbers of serial diagnostic scans being carried out and for normal subjects being scanned for research studies where the position of the head in the scanner for any one scan is not crucial to the treatment/study process. Neuroimaging scientists recognised that if fiducial markers could be fitted to immobilisation frames for visualisation between imaging modalities (prospective image registration) they could also be used to achieve the registration retrospectively. Evans et al at the McConnell Brain Imaging centre in Montreal, as part of their optimisation of techniques for the functional imaging of patients (20), developed a method that involved the use of a 'soft frame' on which to mount the fiducial markers in conjunction with a rigid head mould immobiliser. Thin catheters were mounted on elastic strips which could be pulled over the head and held in place by elastic chin straps and Velcro. Other groups (21,22) used the skull as the frame and fitted fiducial markers directly to the skin in low movement places such as the

naison (connection between the nasal and frontal bones of the skull) and the preauricular points (just in front of the earholes). Registration of the images is then achieved, after acquisition, by the user locating the fiducial markers within both image volumes and a computer algorithm finding the minimum distance between these point pairs by some iterative minimisation calculation.

1.6.3 Disadvantages of image registration by external landmark matching.

Although markers have the advantage that inter-modality registration is possible as long as the marker is visible in each modality this method has a number of disadvantages. First there is the problem of movement of the markers from their position between scans which will occur whether they are attached to skin or an elastic strap. Secondly all scanning needs to take place on the same day to ensure consistency otherwise semi-permanent ink/tattoo is used to mark the position of the fiducials before they are removed, certainly with some degree of inconvenience to the subject. This movement is not insignificant. Strother et al 1994 (23) declare that in a comparison of 6 different methods including principal axes, surface contours and anatomical landmark techniques "fiducial markers that are not rigidly fixed to the skull are inaccurate compared to other techniques". Thirdly time taken to locate the markers in each image increases with number of markers required for accurate registration. Although no expertise is required the task can be lengthy and tedious. The errors associated with the location of the centre of the marker due to partial volume effects, interslice gaps in the data and point spread functions inherent in tomographic scanning can also effect the accuracy of this technique. Some groups have developed methods to combat this (21) but require elaborate construction of 3d markers. This solution brings with it its own problems. The larger the marker the more they may impinge on the data acquisition. For example oil filled beads while ideal for achieving a uniform distribution of isotope cannot be used in MRI because the chemical shift induced by the field will introduce distortion in the reconstructed image. For SPECT, ^{57}Co is the isotope of choice for markers and has an energy of

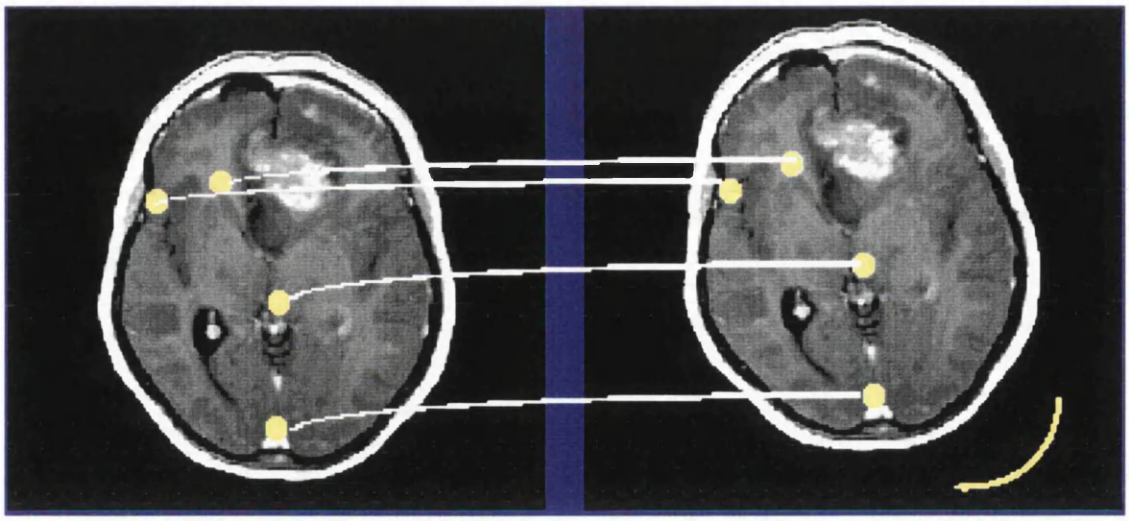

Figure 1.7 shows an example of how internal/anatomical landmarks can be used to register two serial MR images from the same patient.

120keV while ^{99m}Tc, the most commonly used SPECT isotope, has an energy of 140KeV. Dual energy acquisitions are easily obtainable but care must be taken to make the activity in the fiducials hot enough that the markers are not swamped by the scatter of ^{99m}Tc but not so hot as to cause streaking in the main body of the image.

1.6.4 Image registration by internal landmark matching

A solution to some of these problems is to use the brain structure itself. Well defined anatomical markers (fig. 1.7) inherent in the brain would avoid errors associated with skin movement, repositioning and artefact produced by the marker medium. Evans et al, who in 1991 (24) had been using the external fiducial marker technique recognised the value of the internal marker method and developed a protocol that used 10-20 anatomical landmarks (25). Identification of the landmarks took approximately 20-30 mins. per subject and included such structures as; head of caudate, thalamus, frontal, temporal, occipital poles, sylvian fissure, occipito-cerebellar junction and the superior lateral aspect of the parietal lobe. Other groups using these types of methods included Hill et al 1991 (26) to register CT and MR images as an aid to radiotherapy treatment planning, and Ge et al 1994 (27) by identifying the inter-hemispheric fissure.

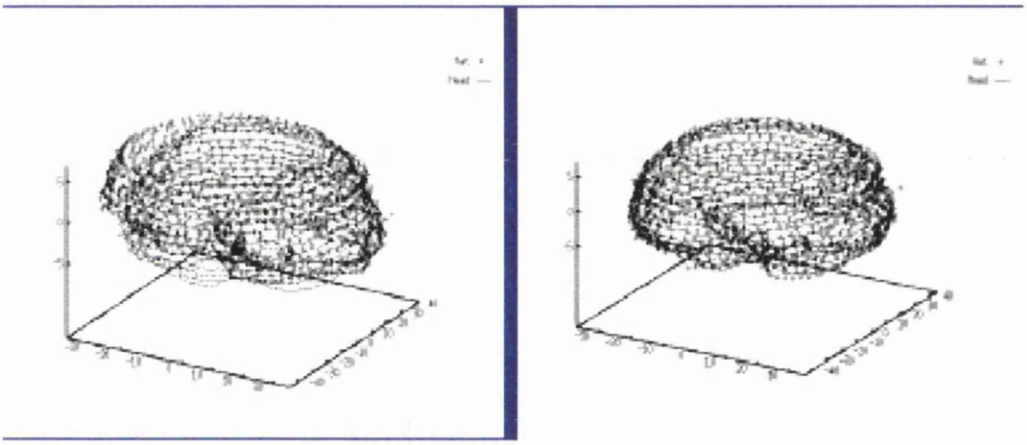

Figure 1.8 Contours used to define the surface of the brain for use in the "head and hat" method of image registration.

1.6.5 Disadvantages of image registration by internal markers

The biggest errors incurred using this type of image registration are associated with the mismatch of information between the different image types. It takes skill and time to locate enough common landmarks between an MRI and a CBF SPECT image and is therefore not entirely suited to use in a busy routine imaging department where time is a premium. Nevertheless, they are particularly good for registering images where there is not a substantial amount of overlapping information. An alternative method of registration using internal markers is to use the surface of the brain itself (28) (fig. 1.8). This surface matching technique is more commonly referred to as the "head and hat" method, where a set of points defining the surface contours of the brain in one image (the hat) is matched to another set of points defining the surface contours in another image (the head). The hat is 'put on' to the head by using the same kind of iterative minimisation algorithm that the previous marker methods use. The points to be matched are the intersections with the head surfaces of a ray drawn from a contour in the transformed hat to the centroid of the head surface contour. Surface contour methods are an improvement on point landmarking methods for inter-modality registration of whole brain images since the surface of the brain is easy to determine, independent of image type. However, they do not perform well in situations where there is not much overlapping information. For

example neither MRI or x-ray CT routinely include the whole head surface. Despite this, the technique remains popular, with some modifications such as the automatic detection of the surface contours using edge detection algorithms (29,30).

1.6.6 Image registration by voxel similarity methods.

The ultimate goal of any image registration method is that it should be objective and robust. By replacing the observer/user with a similarity measurement that can be evaluated by computer between the two images, automated methods of image registration are the ultimate in objectivity, if not robustness. Methods that allow the accuracy of a registration to be assessed by matching corresponding voxels between datasets have come to be known as voxel similarity measures. Image registration using a voxel similarity method is achieved by optimising a measure or cost function based on pairs of overlying voxels.

In 1983 Venot et al (31) used a similarity measurement based on an evaluation of a stochastic sign change function in order to centre an image with respect to some standard axes to correct for rotation in the axial plane. Mintun et al 1990 (32) subsequently exploited this method to correct for rotation in the axial and coronal plane before fitting an estimate of axes orthogonal to a line through points defined by anatomical landmarks (anterior aspect of the corpus callosum, the most anterior point of the frontal lobe and the posterior of the occipital lobe). A similar technique was developed by Junck et al 1990 (33) using an index of similarity that corresponded to maximisation of the cross correlation product between the left and right hemispheres. No attempt was made to align the images with respect to standard axes, instead the method was used to ensure the registration of serial emission tomography images of the same patient.

Over the next decade a myriad of techniques were developed which used the similarity measures of two images as a means of registration; stochastic sign change (34,35), correlation function (33), correlation coefficient (36), sum of absolute differences (37),

optical flow (38), edge detection (29) relative entropy (39), variance (40) and sum of squares (41). An excellent review comparing some of these techniques are given in the book Interactive Image-Guided Neurosurgery (42) and the Journal of Computer Assisted Tomography (1996) "Comparison and Evaluation of Retrospective Intermodality Brain Image Registration Techniques" (43).

1.6.7. Disadvantages of image registration using voxel similarity measures.

Criticisms levelled at these methods are that they are computationally expensive and cannot be employed for intermodality image registration. The former criticism is now no longer applicable with the ultra fast generation of co-processors of the order of 300MHz and the manipulation of computer algorithms to perform complex matrix operations allows registration of image pairs to be performed in a matter of minutes. The latter problem of intermodality registration has been tackled by various groups who have used pseudo emission tomography images. In this the structural images (usually MR) are transformed into emission tomography images (usually $H_2(^{15}O)$ PET) by assigning each tissue type (grey and white matter, CSF) a corresponding PET intensity value e.g. a 1:4 ratio of voxel values in white compared to grey matter, convolving the image with a Gaussian spatial smoothing filter and adding noise to produce a pseudo functional image of blood flow. This pseudo functional image can then be registered with the true functional image, the transformation parameters of which can then be applied to the true structural image to achieve registration with the true functional image. This rather ingenious way of dealing with the problem (illustrated in fig. 1.9) is now a firmly established method of inter-modality image registration (41,44) although other more direct methods are available (39). However, with this method of image registration, robustness is still a problem and deviations in normal anatomy or truncation of image volume still remain a problem for most of these techniques due to the possibility of these types of iterative algorithms getting stuck in a local minimum.

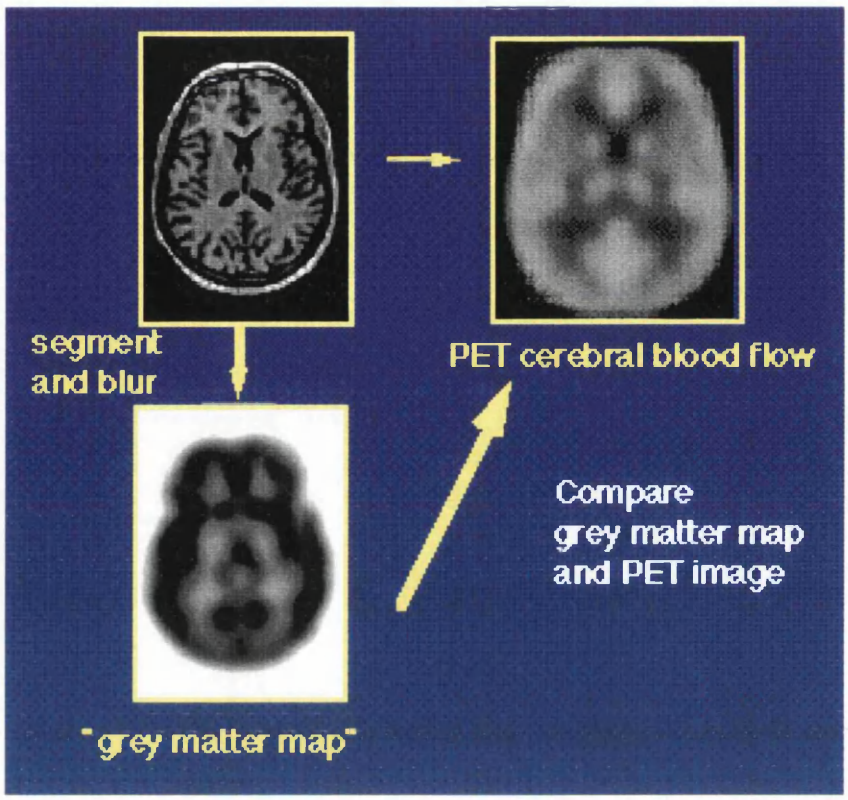

Figure 1.9 shows how inter-modality image registration by voxel similarity measures is achieved using pseudo functional images.

The goal of all these image registration techniques is to ensure that the signals measured accurately reflect the functional location in the corresponding structures. The algorithms described above account for differences in alignment of serial images of the same subject, location in reference space for inter-subject comparisons and even account for overall changes in brain size and shape. However, there still remains a significant error due to differences in individual gyral anatomy between subjects.

1.7 Image standardisation .

As the number of groups involved in neuroactivation imaging studies increased it became clear that a common reference frame with which to compare measurements between different subjects and imaging centres was needed (fig. 1.10). Fox et al 1984 (45) using

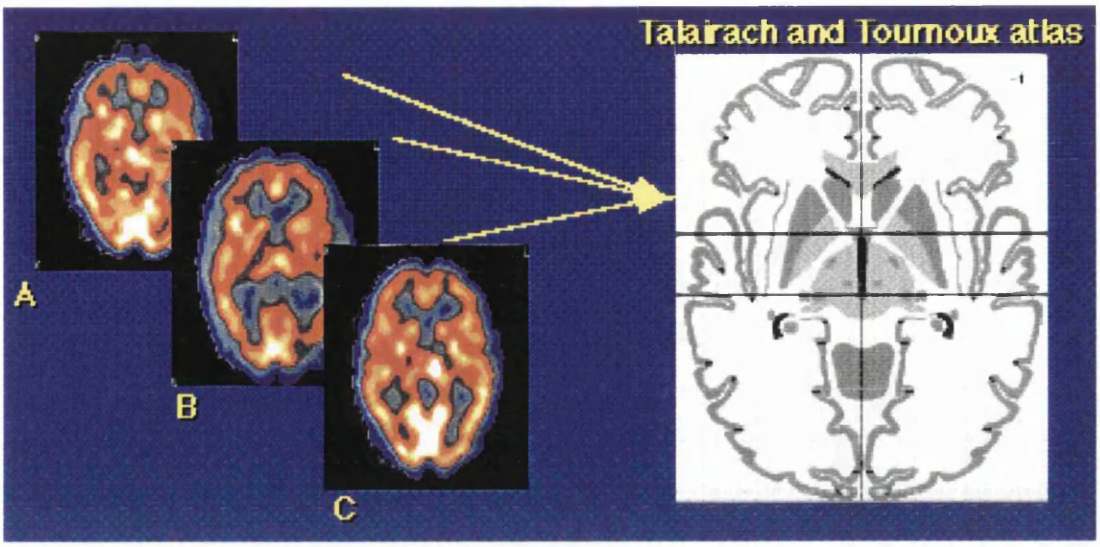

Figure1.10 Illustrates how a common reference frame can be used to compare functional scans from different subjects.

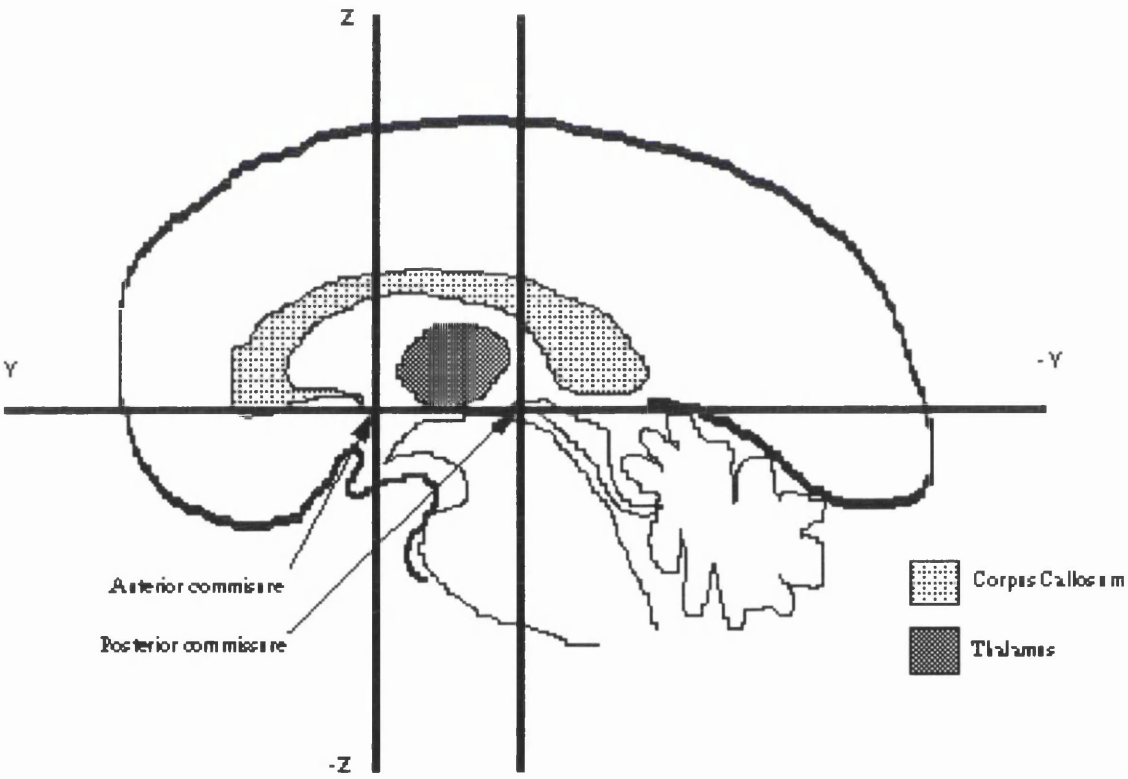

Figure 1.11 Show the position of the 'Talairach axes' through the mid sagittal plane. The positive X-axis being orthogonal to both Y and Z is orientated out of the page.

the principles of anatomical landmark image registration developed a method of locating functional images within a standard space based on the identification of the line through the anterior and posterior commissures (AC-PC line). The orthogonal co-ordinate system Fox described had been developed originally by Talairach and Tournoux in 1967 (and later published as an atlas in 1988 (46)) to be used in conjunction with an atlas of a middle aged, French woman's brain labelled with anatomical references in 4mm thick axial slices. This co-ordinate system, now commonly referred to as "Talairach space", is set up so that the Y axis runs along the AC-PC line, the Z axis at right angles to this through the mid point of the AC-PC to the vertex of the skull and the X axis orthogonal to both of these (fig. 1.11). Since the AC-PC line is very difficult to identify on functional images Fox et al 1984 (45) transformed the functional data into Talairach space by identifying points relative to the AC-PC line. A line drawn through the glabella and inion as defined from a lateral skull x-ray film was assumed to be parallel to the AC-PC line and used as a reference from which to estimate this line. Results showed that estimation of the AC-PC line using this method was robust and that the location of the estimated AC-PC line was always rostral to the true AC-PC line and roughly parallel with a mean angle 1.05^{o}, converging anteriorly. With these adjustments the estimated AC-PC line approximated the true AC-PC line well. Since Fox's method required each subject to go through an extra procedure, groups wanting to make the whole experience for normal volunteers as simple as possible developed methods that avoided the use of structural imaging altogether and were able to identify the AC-PC line directly from functional images. Friston et al 1989 (47) developed a technique that required the user to identify the ventral aspects of the anterior and posterior corpus callosum, the thalamus and the occipital pole directly from the coronal slices of a perfusion PET scan. A regression calculation was applied to these points to find the best straight line fit which was then assumed to be an approximation of the true AC-PC line. Results showed that this method agreed well with the accuracies reported by Fox et al in 1985 (45) with the estimated AC-PC line being rostral to the true AC-PC line and the mean angle of convergence being 0.13^{o}. These methods remain popular with modifications to remove user interaction and

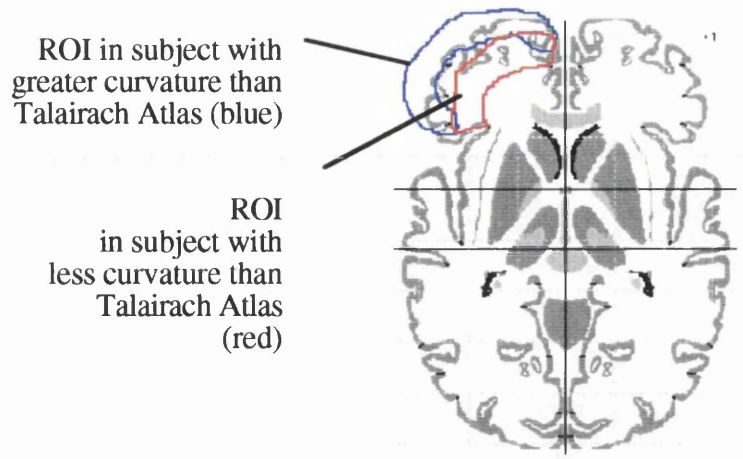

Figure 1.12 The figure above shows how a signal may be 'diluted' when averaging across different subjects due to differences in individual gyral anatomy.

extend the algorithms to take account of individual variations in brain shape and structure (35,48).

This method of standardising space became fundamental to the expanding field of in-vivo functional brain mapping. While the need to locate structure and function within a standard reference frame is necessary for individual patient assessment, and in some cases their consequent surgery, the facility to match exactly each person's individual gyral structure to that of a reference is also important when performing neuroactivation experiments across a group of subjects. The standard protocol to maximise the signal produced by neuroactivation paradigms is to pool data from multiple subjects. If it were possible that all brains could be made identical anatomically by exactly registering them with one another then the problem is solved. Unfortunately, even after accounting for differences in orientation and size there are still residual errors in individual detail anatomy which may have serious consequences for subsequent measurement techniques. For a subject with relatively less curvature (red region of interest (ROI) in fig 1.12) than the Talairach brain over the frontal lobe, the location of a cortical region as defined by the Talairach atlas may in fact lie over extracerebral structures. For an individual with greater curvature (blue ROI in fig1.12) this same Talairach region may lie over white matter. A simple solution is to smooth all the images before analysis, using a Gaussian spatial filter to reduce this effect of anatomical mismatching by smearing out structures to get more of

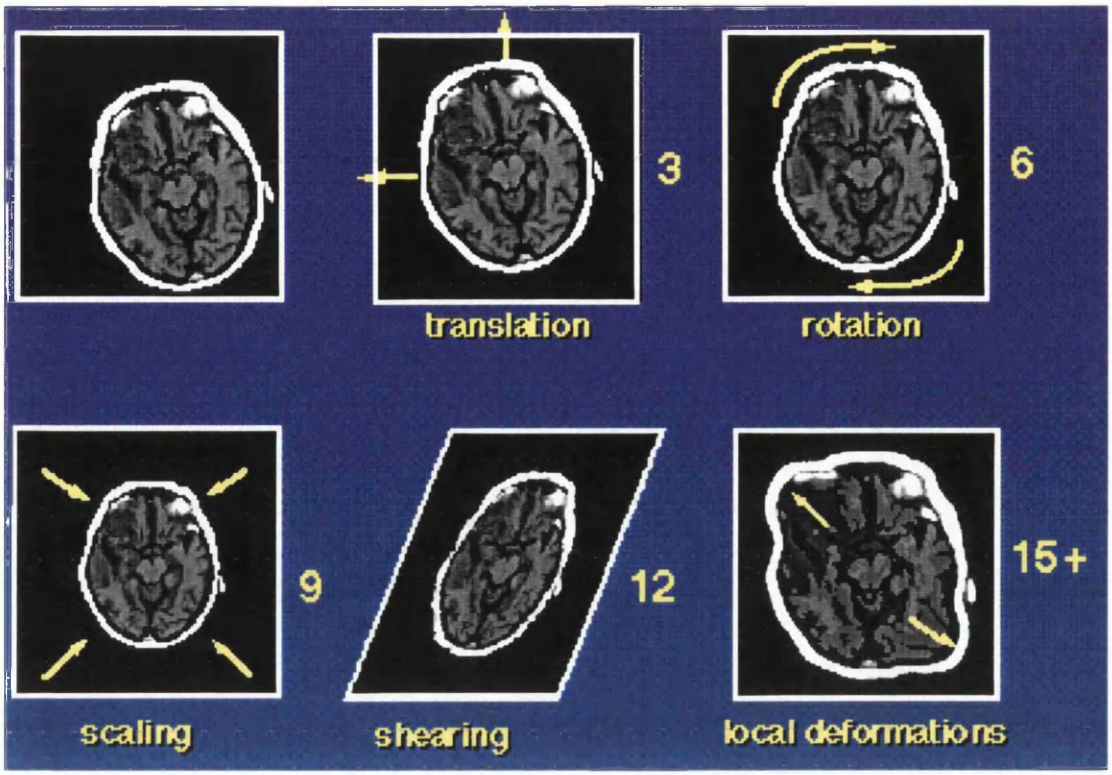

Figure 1.13 A schemtaic of the Rigid body, affine transfoRMS and plastic transformations used for image registration.

an overlap between subjects. However, this smearing also has the obvious effect of reducing the resolution of the image and diluting the amount of change in measured signal in each individual. Groups that had already extended the 6 parameter rigid body transformation to a 9 parameter affine transform to allow for scaling in the 3 axes were able to extend the transform to 12 parameters (38,49)(fig. 1.13). These 3 extra parameters accounted for differences in overall brain shape by introducing shearing transformations to the registration method which reduces the problem described above, removes the need for such heavy smoothing but leaves the problem of individual gyral anatomy, a significant problem when unsmoothed PET images regularly achieve resolutions of the order of 6mm.

Matching of images at this level can be achieved using nonlinear or "plastic" transformations (bottom row fig. 1.13). These transformations can be carried out by matching structures recognisable in both the atlas/template and individual brain image

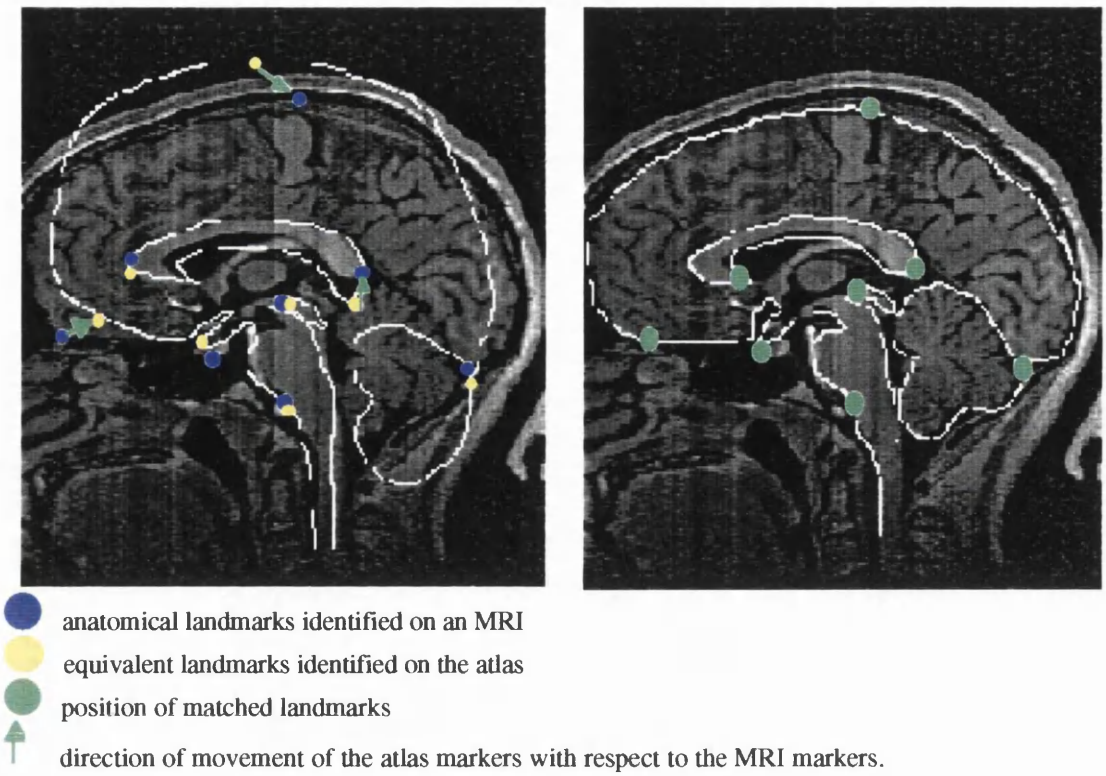

Figure1.14 shows how a standard brain template outline can be deformed to fit an individual subject's MR scan. Slices taken through the midline sagittal plane of a T1 MRI.

such as points or edges representing anatomical structure (50-52) (fig.1.14). A standard schematic anatomical ROI template derived from the Talairach atlas or a cryosectioned post mortem brain (see fig 1.14) can be altered to fit the subject's own anatomical structure. A computer algorithm records the changes made in the template and applies them to the subjects images so that they now look like the standard template. Alternatively, automatic techniques based on pixel intensity distribution (48,53) can be used to match a subject's images to a standard image template. A standard image is obtained by averaging brain images closely representing Talairach space (see fig 1.15). A standard distribution of voxel intensity is derived from the standard image, which can then be used to map the distribution of voxel intensities from an individual subject's image.

Original standardisation techniques relied on the information provided from a single subject's anatomy (46,52,54). However, more recent methods have attempted to define

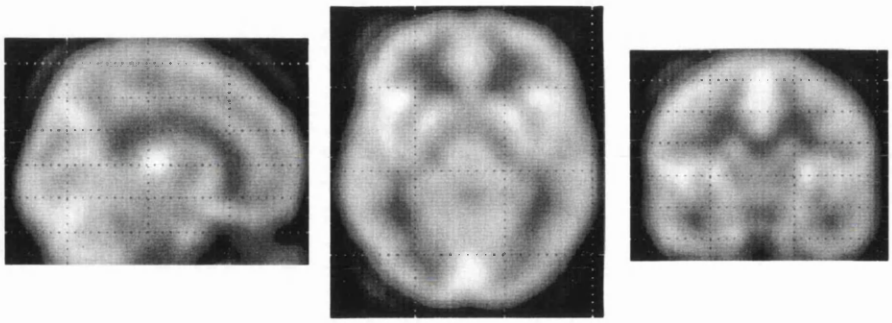

Figure 1.15 shows 3D sections through the sagittal, axial and coronal planes respectively of the PET CBF template used by SPM96.

the standard template in teRMS of an average of the general population. The PET template used by Friston and colleagues to spatially normalise all emission tomography is an average of 6 PET $H_2(^{15}O)$ images obtained routinely that best represented Talairach space on visual inspection (fig. 1.15). Evans and colleagues (25) expanded their single MRI template from a single individual to include 50 high resolution MRI 3D brain images on which a team of experts defined various gyral and sub-cortical structures. This template can be accessed via the internet where a database of both Talairach labels and statistical probability maps of normal anatomical structure can be found (http://ric.uthscsa.edu/projects/talairachdaemon.html) (fig. 1.16). The anatomy as defined by the statistical probability maps is based on regions defined by the 50% likelihood of finding a particular anatomical boundary within the population of 50 normal MR images of the brain.

1.8 Image analysis

The end point of this image standardisation is to assess the content of the images, either qualitatively or quantitatively. The rest of this section describes two different methods of obtaining quanititative data from functional images of the brain; region of interest measurements and voxel-wise statistical analysis.

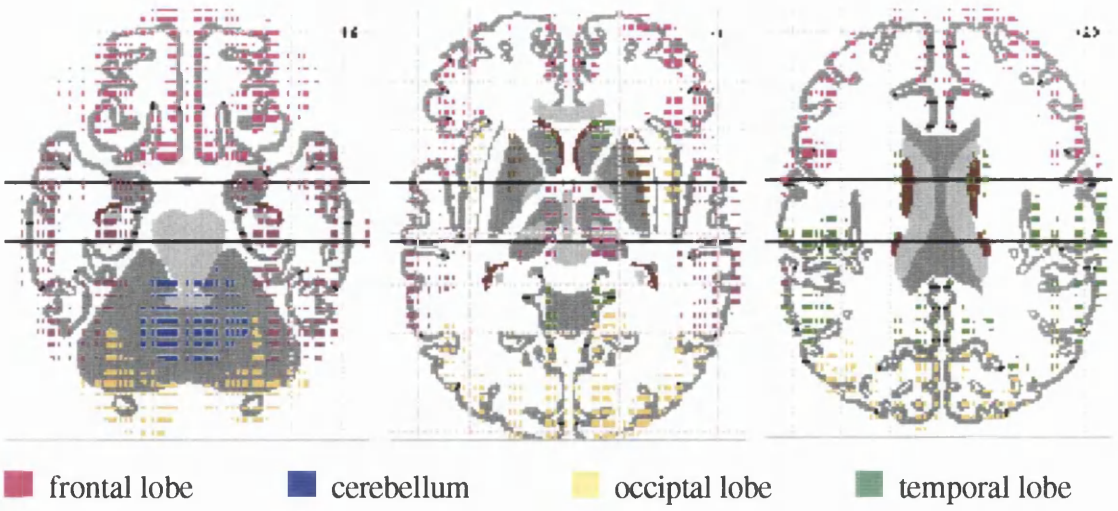

Figure 1.16 shows axial slices (ac-pc -16mm, ac-pc +1mm and ac-pc +20mm) from the Talairach Daemon (http://ric.uthscsa.edu/projects/talairachdaemon.html). The atlas is colour coded according to the statistical probability maps based on regions defined by the 50% likelihood of finding a particular anatomical boundary within the population of 50 normal MR images of the brain.

1.8.1 Image analysis by region of interest methods.

In clinical practice, emission tomography scans are valuable tools where qualitative features of an image provide diagnostic and prognostic guidance, but problems arise when quantitative data is needed. The immense number of individual picture elements (pixels) in each scan means that extensive computation is inevitable and the localisation of the quantitative measures in teRMS of their anatomical location assumes expertise in neuroanatomy. Conventional methods of analysing brain PET and SPECT images involve the placement of a number of regions of interest (ROI) on the image and measurement of the mean counts within those regions. Global differences in the overall number of counts due to differences in administered dose, uptake fraction in the brain as well as physiological changes in the subject (mood changes, physical activity) are accounted for either by dividing each ROI value by the average global value or by a suitable reference region such as a whole slice ROI value or the cerebellum ROI value. Regions of interest drawn either directly on to the emission tomography scan or with reference to the same individual's anatomical scan provide both data reduction and a means of establishing an anatomical reference (fig. 1.17).

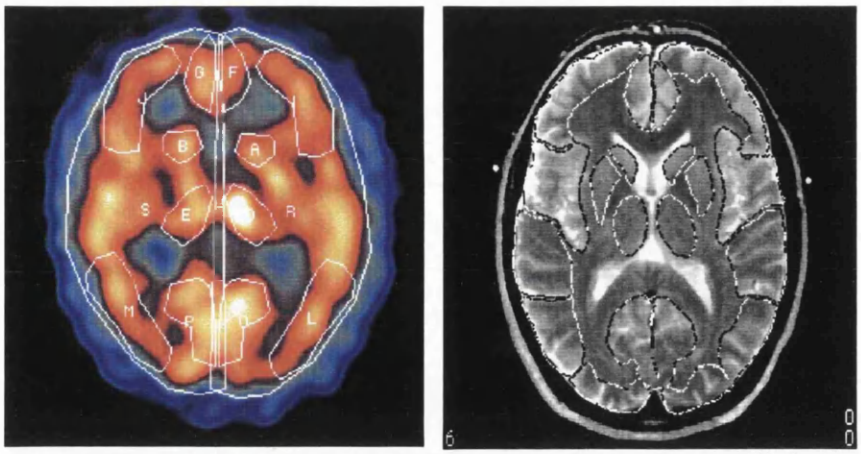

Figure 1.17. a) ROIs drawn directly on to a SPECT image of blood flow and b) the regions drawn on an MRI before superimposing on to the same individual's functional image.

1.8.2 Disadvantages of image analysis by region of interest methods.

The reduction of data by collapsing a group of contiguous pixel values into a single mean value although useful as a data reduction step runs the risk of losing potentially valuable information. Large ROIs may lump functionally distinct areas together and so 'hide' changes or abnormalities affecting only part of the ROI or if a significant change is detected the ROI may cross functional boundaries hiding the true location of the change. The anatomical localisation aspects of ROI methods also have certain drawbacks. The placing of an ROI is entirely dependent on the investigator's ability to identify brain structures and a degree of expertise in human neuroanatomy is needed for this. The size and shape of the region is also important since the more closely the dimensions of a region conform to the area of change the greater the measured magnitude of change will be so a small ROI will detect a regional difference with greater sensitivity than a large ROI. Small ROIs, however, have greater chance of missing the area of change altogether if the placement accuracy is wrong by even a small amount. Similarly an ROI that confoRMS precisely to the shape of the structure will detect a change with greater sensitivity than a geometrically regular shape, but accuracy of positioning is paramount to this sensitivity.

In an attempt to combat the limitations of traditional ROI methods of analysis, various groups began to develop computer based algorithms designed to make the process more objective and less time consuming. Junck et al 1988 (33) used an automated routine to draw ROIs directly onto the functional image to remove observer bias in the placement of ROIs. Following image registration the cortex of the brain was defined by the automatic delineation of the outer rim by thresholding of the voxels at 30% of the global mean and a concentric ring 1.5cm inwards. Cortical regions were then defined by 8 regions per hemisphere approximately $4cm^2$ with the cerebellum defined manually. Although observer bias is removed using this method there remains the problem of these regions 'lumping' together functionally distinct regions or crossing functional boundaries. Other methods removed observer bias and to some extent removed the problem of 'lumping' functionally distinct regions together by using ROI templates defined by a standard template of brain structure (20,52,55) that could be warped to fit each individual's scan. Evans et al 1988 (20) used a high resolution MRI from a single subject and later (25) an average of approximately 50 individual MR scans to define a template with 56 different ROIs. Seitz et al 1990 (56), Toga et al 1994 (52) and Bohm et al 1989 (55) all used an individual cryosectioned human brain at 4 slices per 1mm to define their ROI template of over 250 separate ROIs. High speed computers allowed the lookup tables storing the ROIs to be easily usable if not completely objective. The template can be scaled and translated to fit the individual's anatomy using powerful graphical tools that, although automated require a certain degree of user input. Each ROI can be re-drawn, if needed, to fit more closely the subjects anatomy before it is superimposed on to the functional image. The functional value for each ROI is calculated as the area weighted average which can then be grouped into larger anatomical areas if needed. Further volumetric data can be obtained by summing these areas over a number of slices from the image. Although these methods of using predefined ROI templates do not need the abilities of an expert anatomist, Collins et al (25) noted that misplaced ROIs (due to mis-registration) could lead to a reduction of 50% in measured signal. The ultimate solution to problems of observer bias and the anatomical versus functional structure definitions is the

development of voxel based statistical analyses, where the regions are effectively reduced to single voxels.

1.8.3 Image analysis by voxel-wise methods.

The methods described above stemmed from the need to find quick, reliable and objective methods of handling the vast amount of functional data acquired from patient scans. But in another branch of assessing human brain function, scientists were looking to find ways of measuring the changes in the brain produced not by disease or drugs but by thought. In this area there is no preconceived notion of structure. The original electrical external stimulation experiments in the early 20th century had been able to map the cortex associated with the senses. Indeed the initial "activation" experiments performed on normal humans in the early 80's using straight forward paired functional image subtraction and ROIs easily detected the robust regional changes that occur in the primary sensory and motor cortex due to some external stimulation (32,57). However, the more subtle activations of human functions such as memory or learning were proving to be less easily detectable using these methods and required a different "top-down " approach - a method that did not depend on anatomically defined ROIs. Instead neuroscientists exploited the field of parametric statistics in attempts to maximise the potential information contained in the tens of thousands of pixels within each scan (57-61).

The small changes in regional cerebral blood flow that must be produced by neuronal activity within the brain when performing higher cognitive processing were proving elusive and so groups looked towards the traditional methods of functional brain mapping for a way to enhance these small changes against the background of noise. Electrically evoked potential studies had long been using methods of signal averaging over time as a way of finding the tiny electrical signals produced by the brain in response to a particular stimulus. Fox et al 1988 (57) used the same principle to average a detected signal over space. By averaging the measured signal across multiple images of the same brain state, random background noise will cancel out while consistent focal responses will sum and

therefore increase the signal to noise ratio. Fox's method reported these regions of local minima or maxima as spherical ROIs of fixed size placed at the centre of mass of the regional change and its location in three dimensional space. The signal was then discriminated from noise using omnibus testing by the gamma-2 statistic. Significance on a local level was further determined by performing a t-test on voxels in those regions that survived the omnibus testing. The advantage of this approach was that by identifying only the location and magnitude of change without attributing shape or extent, this technique ensured no signal loss implicit in the use of preselected ROIs. Fox's method of locating significant blood flow change in space is referred to as change distribution analysis (CDA). Other similar voxel-wise analyses developed subsequently (58,59,61,62), owe much to the form that Fox's change distribution analysis takes, their final form being dependent on the methods of voxel intensity normalisation, modelling variance, testing for local significance and experimental design (group comparisons or individual subject assessment).

- Voxel-wise analysis of individual patient data.

This type of analysis involves the comparison of the patient scan with a normal or disease reference data set. These voxel comparisons can be expressed as Z-scores (the number of unit standard deviations from the reference mean) (63), (64) or in terms of a principal components analysis (PCA) (65), (66) where the distribution pattern of voxel intensity in the patient scan is compared with the known distribution pattern of voxel intensity in the reference scans. Significance is assigned to how well the two patterns match. These methods rely on one measure (scan) per subject per brain state and use a proportional scaling method to account for global voxel intensity differences.

- Voxel-wise analysis of different groups.

This type of analysis involves the comparison of groups of scans by testing for the differences in the means of the two data sets taking in to account the variance in the data. The variance is modelled either at a local level for each voxel included in the analysis

(59,67) or at a global level using an average variance for all voxels included in the analysis (61).

1.8.4 Limitations of image analysis by voxel-wise statistical methods.

The disadvantages of using voxel-wise methods for the analysis of functional brain images is that they are very sensitive to any pre-processing of the images and underlying statistical assumptions made about this data.

Pre-processing of the images includes image registration/standardisation, spatial smoothing and removal of global voxel intensity differences. Errors in standardisation of the images are assumed random across a group of subjects and are likely to manifest themselves as false negative results (type II errors) in the statistical analysis, a problem not confined to voxel-wise analysis (see the ROI definition displayed in fig 1.12 frontal lobe curvature). Spatial smoothing is performed prior to analysis to improve the signal to noise ratio, with filter sizes ranging from 10mm FWHM - 20mm FWHM for emission tomography images. The amount of smoothing affects the estimate of variance used for any subsequent statistical analysis; too much smoothing resulting in type II errors and too little smoothing results in type I errors (false positive results). Differences in global intensity voxel values must be accounted for (global intensity normalisation) if the local changes in voxel values are to be measured. Global differences can be removed either by scaling all the images in the data set to some reference voxel value (much like the method used in conventional ROI methods) or by including the global differences in the statistical analysis itself by modelling it as a confounding covariate in an analysis of covariance (AnCova) method. Traditionally scaling has always been the method of global intensity normalisation but for normal subjects where the average global voxel value is not going to differ much between subjects it is thought that the AnCova model is more appropriate, avoiding the occurrence of type II errors.

Statistical assumptions made about the data include the use of parametric analysis methods that assume that the population distribution from which the sample is drawn is known. This assumption is the basis on which the rest of the analysis rests. The variance in the images that remains after the pre-processing steps is calculated either at each voxel (59) or an average variance is calculated for all the voxels included in the analysis (61) before being used in the statistical test at each voxel. A smoothing estimator is then used to calculate the variance (61). This estimation of variance will have a profound effect on the subsequent test statistic used. Finally there are differences in the interpretation of the significant results obtained from an omnibus testing of the data. Significance of regions of change in the presence of multiple statistical tests can be based either on the number of voxels (extent) (68) reaching significance after omnibus testing or on the value of these voxels (height) (59), bearing in mind the non-independent nature of the smoothed voxels included in the analysis. The most recent developments in voxel-wise statistical analysis include tests for significance based on both extent and height of voxels (69,70).

A considerable amount of investigations have been published using these voxel-wise statistical methods. Initial reports confirmed the results of brain lesion studies and some PET investigations have been cross-replicated but with the number of investigations increasing there appear to be more and more discrepancies. Despite the scope for differences in the statistical methods described above it would seem that these discrepancies may be more to do with the differences in acquisition parameters and paradigm design than with the validity of the voxel based analyses themselves (58). This method of image analysis was developed for PET and later extended to fMRI investigations of neuroactivation where the ability to perform multiple image replications of brain states lends high statistical significance to their results. More recently, however, investigations are being performed with fewer numbers of subjects and limited numbers of replications per brain task. In particular SPECT studies of neuroactivation, where there are difficulties in performing replications of tasks due to the nature of the

radiopharmaceutical used with this technique, are vulnerable to false negative errors due to the consequently limited degrees of freedom.

1.9 *Plan of investigations and aims.*

The future of functional brain mapping must include the development of a standardised system that includes all of the elements described in this chapter; anatomical location in 3 dimensional space, the applicability of this method across subjects and imaging modalities and the careful design of statistical analysis methods used to isolate regions of the brain responsible for particular cognitive processes. But "the exchange of information, the credibility of results and the power of these techniques will in part be determined by our ability to find standardised, reproducible and accurate methods of analysing data from these sources", cautions Mazziotta in an extract from his editorial in a 1984 edition of the Journal of Cerebral Blood Flow and Metabolism (71). This thesis describes the investigations used to establish - from existing methods - a standardised, reproducible and accurate method of analysing data from ^{99m}Tc HMPAO SPECT images of cerebral blood flow.

Chapter 1 outlined the development of functional human brain mapping in both normal and abnormal subjects and included a short description of normal human brain function with regard to autoregulation of blood flow and its coupling with cognitive function. This was followed by a more detailed explanation of the various components of a typical FHBM analysis including image registration, image standardisation methods and statistical analysis. The advantages and disadvantages of the components were also described in order to appreciate fully the context in which the subsequent investigations were done. Chapter 2 lists the various steps involved in performing a FHBM analysis with SPECT and describes the image acquisition and processing of images used in the experiments. Chapters 3 - 7 describe five different experiments linked by the overall theme of validating and optimising the methods used when analysing SPECT CBF with SPM. Chapter 3 outlines the methods used to create the challenge conditions devised to validate the image standardisation facility. The results of these validations are presented

and discussed in teRMS of providing the best methods of image standardisation for non-optimal image data sets. Chapter 4 uses the optimal image standardisation method determined in chapter 3 to investigate the application of a SPM analysis to images of individual patients presenting with symptoms of dementia. The object was not to use the method to automate the diagnostic interpretation of images but to determine whether it could provide an objective measurement of abnormality which might assist in the expert reading of scans. The results are presented and the routine use of SPM in a nuclear medicine department is discussed. Chapter 5 outlines the methods and challenge conditions used to modify the acquisition protocol of ^{99m}Tc HMPAO SPECT images for analysis by SPM methods, in particular whether SPECT studies of neuroactivation might benefit from a similar approach used in PET, i.e. increase the number of scans per task and accept poorer individual scan quality. The results are presented and discussed in teRMS of their suitability for use in neuroactivation studies using SPECT. Chapter 6 uses the optimal study design determined in chapter 5 to investigate vagal nerve stimulation as a treatment for intractable epilepsy. Chapter 7 uses the same design to study the role of the medial temporal lobes in novelty detection by contrasting it with their role in the encoding and/or consolidation into long-term memory of associative information. The results for each of these neuroactivation studies are discussed in teRMS of their contribution to the knowledge of human brain function. Finally chapter 8 outlines the conclusions drawn from each of these experiments and their application to the future use of SPECT in functional human brain mapping.

CHAPTER 2

Image acquisition and image analysis tools.

This chapter describes the various steps involved in using SPECT with the functional human brain mapping software (SPM) including image acquisition, image registration, image standardisation, image reslicing, smoothing, global normalisation, statistical analysis and statistical inference common to all the subsequent investigations (Chapters 3-7).

2.1 Image acquisition

All images were acquired using the SME 810 Novo (Strichman Medical Equipment) dedicated SPECT section scanner which consists of an annular array of 12 detectors with an 8 inch diameter field of view. There is no rotation of detectors. Each has a point focused 800 hole collimator, and performs 3D rectilinear translations orthogonal to its axial direction. Each detector of an opposing pair is responsible for scanning the half volume nearest to it and produces an image of the radioactive distribution that is in the field of focus, which will also contain additional blurring from regions above and below the focal plane. An iterative procedure is then used to back project the data and restore the activity lost to attenuation. First the head boundary is determined by fitting an ellipse to each slice in the image such that the concentration of the activity is zero outside the ellipse and non-zero inside. Then, assuming that the attenuation coefficient is homogeneous along the absorption length as the photon travels through the brain tissue, skull and scalp

Figure 2.1 Schematic arrangement of the detectors and the rectilinear motion during scanning of the SME810 brain SPECT gamma camera.

and using a 'Chang like' attenuation correction (72) an attenuation map is constructed. This map is constructed for each of the 12 detectors and specifies, for every point in the field of view, the probability that a photon emerging from that point will reach the detector. The map can be applied iteratively (minimum of 1 iteration and a maximum of 3 iterations) to the raw data to obtain an estimate of the radio-tracer distribution in the head.

The scans were acquired using either 500MBq ^{99m}Tc HMPAO described as 1 unit dose, slice thickness is 12mm, scanning time is 120secs per slice (1 unit time), and slice spacing 6mm (6mm = 1unit separation) or 250MBq ^{99m}Tc HMPAO (1/2 unit dose), slice thickness is 12mm, scanning time is 240secs per slice (2 unit time), and slice spacing 8mm. These acquisition parameters provide an in-plane resolution of 8mm and longitudinal resolution of between 10mm and 12mm. For a full description of this scanner and the reconstruction algorithm the reader is referred to the paper "New multi-dimensional reconstructions for the 12-detector, scanned focal point, single-photon tomograph." by Stoddart and Stoddart 1992, Physics in Medicine and Biology (36). Optimum scan orientation is approximately parallel to the orbito-meatal (OM) line and head movement during the scanning procedure is minimized by subject co-operation and assisted by placing foam supports either side of the subject's head which are held in place by Velcro. ^{99m}Tc HMPAO is injected intravenously while the patients are supine on the

scanning couch under standard resting conditions of eyes closed and minimum auditory stimulus, unless the subject is taking part in an activation task in which case they will be injected as the experimental protocol requires. Image acquisition begins approximately 15mins after injection with a total acquisition time 30-60 mins. depending on the slice thickness acquisition parameter and the size of the patient's head. After reconstruction all scans are converted to ANALYZE™ [1] compatible format using customised MATLAB[2] scripts (courtesy of MG[3]) and transferred to a SUN ULTRAsparc[4] workstation for further process/analysis.

2.2 Image analysis - Statistical Parametric Mapping.

There are several voxel-wise analysis techniques available either commercially or as freeware (SPM96, MEDx3.0, IDL, AFNI, Hermes)[5]. The analysis used for the investigations presented here was Statistical Parametric Mapping (SPM95/96). Statistical Parametric Mapping (SPM) was originally developed by Karl J Friston and colleagues at the MRC Cyclotron Unit, Hammersmith hospital, London, UK. The latest versions, SPM95 and SPM96, were developed at the Wellcome department of Cognitive Neurology, under the direction of Professor Friston. The software is freely available from the web site (http://www.fil.ion.bpmf.ac.uk/spm) and is written both in MATLAB code to run on a UNIX platform and C programming language to run on a Windows95 platform. Online technical support is provided by the group via a mailbase service for all users (http://www.mailbase.ac.uk/lists/spm).

SPM is software used for the intersubject averaging of functional brain images and their statistical analysis (73). It consists of 3 main modules:

---

[1]Mayo Medical Ventures, USA (http://www.mayo.edu/bir/analyze/ANALYZE_main.html
[2]The Mathworks Co, UK (http://www.camcontrol.co.uk)
[3]MG-Dr Mike Glabus, neurophysicist, MRC Brain Metabolism Unit, University of Edinburgh, Edinburgh, UK.
[4]SUN Microsystems, London, UK (http://www.sun.co.uk)
[5] SPM96 Statistical Parametric Mapping, Wellcome Department of Cognitive Neurology, Inst. of Neurology, London, UK (http://www.fil.ion.bpmf.ac.uk/spm)
MEDx3.0 - Sensor Systems Inc., USA (http://www.sensor.com)
IDL - Research Systems Inc., UK (http://www.rsinc.com)
AFNI - Robert Cox, Biophysics Research Inst., Medical College of Wisconsin, USA (http://varda.biophysics.mcw.edu/~cox/index.html)
Hermes - Nuclear Diagnostics Ltd., Kent, UK.

- module one image registration,
- module two image standardisation (spatial normalisation) and
- module three statistical analysis.

SPM uses an automatic and general multidimensional non-linear spatial transformation technique to standardise brains from different subjects (49). There are two components to this transformation; one is spatial and the other involves the intensity values of the voxels within an image. The assumption on which this model is based is that the differences between the subject's brain (object image) and the standard brain (target image) are slowly varying with position in the images. Any physiological/functional differences that we are trying to measure manifest themselves as differences in voxel intensity values between the two images which are considered to be rapidly changing and can be regarded as residual error (48). The statistical analyses used by SPM are based on the general linear model (GLM) (59). In its simplest form it can be described as testing for the null hypothesis that two mean images are the same using a paired t-test at every single voxel in the mean images. The statistical parametric maps that are produced from this type of analysis represent the significance changes in rCBF not absolute or relative percentage changes in rCBF. The statistical methods used in this module are parametric in nature since it is assumed that the underlying probability distribution of the data is known.

2.2.1 MODULE ONE:- Image Registration.

Image registration by voxel similarity methods

Spatial transformations for intra-modality, intra-subject registration:-

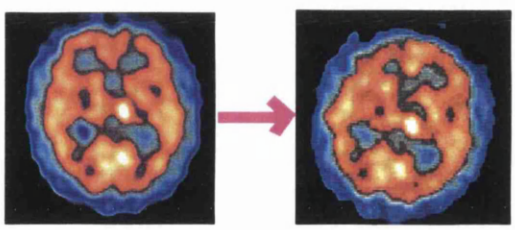

The spatial transformation used to map the object image on to the target image is an affine transform which in its simplest form has 6 rigid body parameters describing translation and rotation in space. In order to map one image on to another using a transformation the

parameters must first be calculated. SPM uses a directed iterative least squares calculation to do this. The algorithm used (49) is based on a Gauss - Newton optimisation using a first order approximation of a Taylor expansion. Since using only the first order approximation of a Taylor expansion means that the solution may become trapped in a local minimum, the developers of SPM suggest that the starting estimates of the transformation parameters are not too far from the solution. This means that the object image must already be fairly close to the same orientation as the target image. In addition to these close starting parameters the initial iterative steps are performed with smoothed images which also reduce the likelihood of the solution becoming trapped in a local minimum. Once the registration is close to optimum the calculation can then be continued with the unsmoothed images.

Spatial transformations for inter-modality, intra-subject registration:-

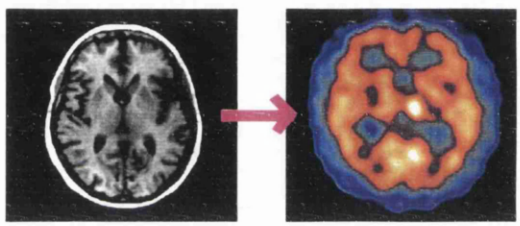

To achieve registration between two different imaging modalities SPM changes the structural image into a pseudo functional image before using a nine parameter transform (6 rigid body and 3 scaling) to register this with the true functional image (41). That is the structural images (usually MR) are transformed into pseudo emission tomography images (usually of blood flow) by assigning each tissue type (grey and white matter, CSF) a corresponding PET intensity value e.g. 1:4 white:grey matter, convolving the image with a Gaussian spatial smoothing filter and adding noise. This pseudo functional image can then be registered with the true functional image, the transformation parameters of which can then be applied to the true structural image to achieve registration with the true functional image.

2.2.2 *MODULE TWO. Image standardisation.*

Image standardisation using a voxel similarity method.

Intensity transformations for intra-modality and inter-subject registration:-

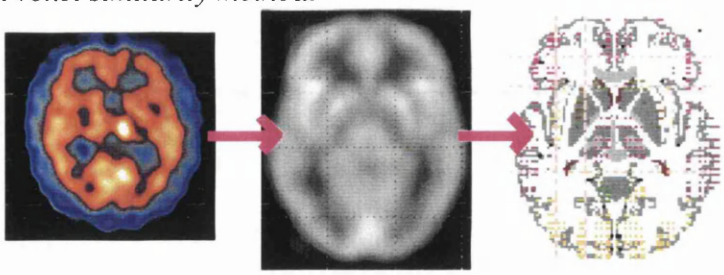

This component uses a 12 parameter transform (6 rigid body, 3 scaling and 3 shearing) and an optional non-iterative non-linear resampling of image data to remove non-linear differences in brain shape to match to a standard template. Before this can proceed brain template must be defined using one of 4 different options a) template defined by an average of 305 MR T1 images b) template defined by the SPM95 template derived from a single subject PET scan c) template defined by the SPM96 template of an average of 6 PET scans d) template defined by the user [6]. Option a) is preferred since the final statistical parametric maps of brain activation can be referred to the on-line probabilistic anatomical maps defined by the Talairach deamon also defined by a subset of 305 MR T1 images (http://ric.uthscsa.edu/projects/talairachdaemon.html)

Once the images have been transformed into perfect anatomical register using the 12 parameter transform to account for overall differences in brain size and shape the user can specify a further optional non-linear spatial transformation that adjusts the object image to fit the cortical gyral anatomy of the target image more closely (49). The algorithm can be described more simply in terms of reducing it to a function which is based on the integral of all pixel values in the template image divided by the integral of all the pixel values in the object image and an error term which is then convolved with the original pixel values in the object image and a Gaussian spatial filter to reduce the errors in the transformation due to rCBF differences. A graphical example of this is given in figure 2.2.

---

[6] References to these options can be found in the SPM documentation at web site http://www.fil.ion.bpmf.ac.uk/spm/dox.html

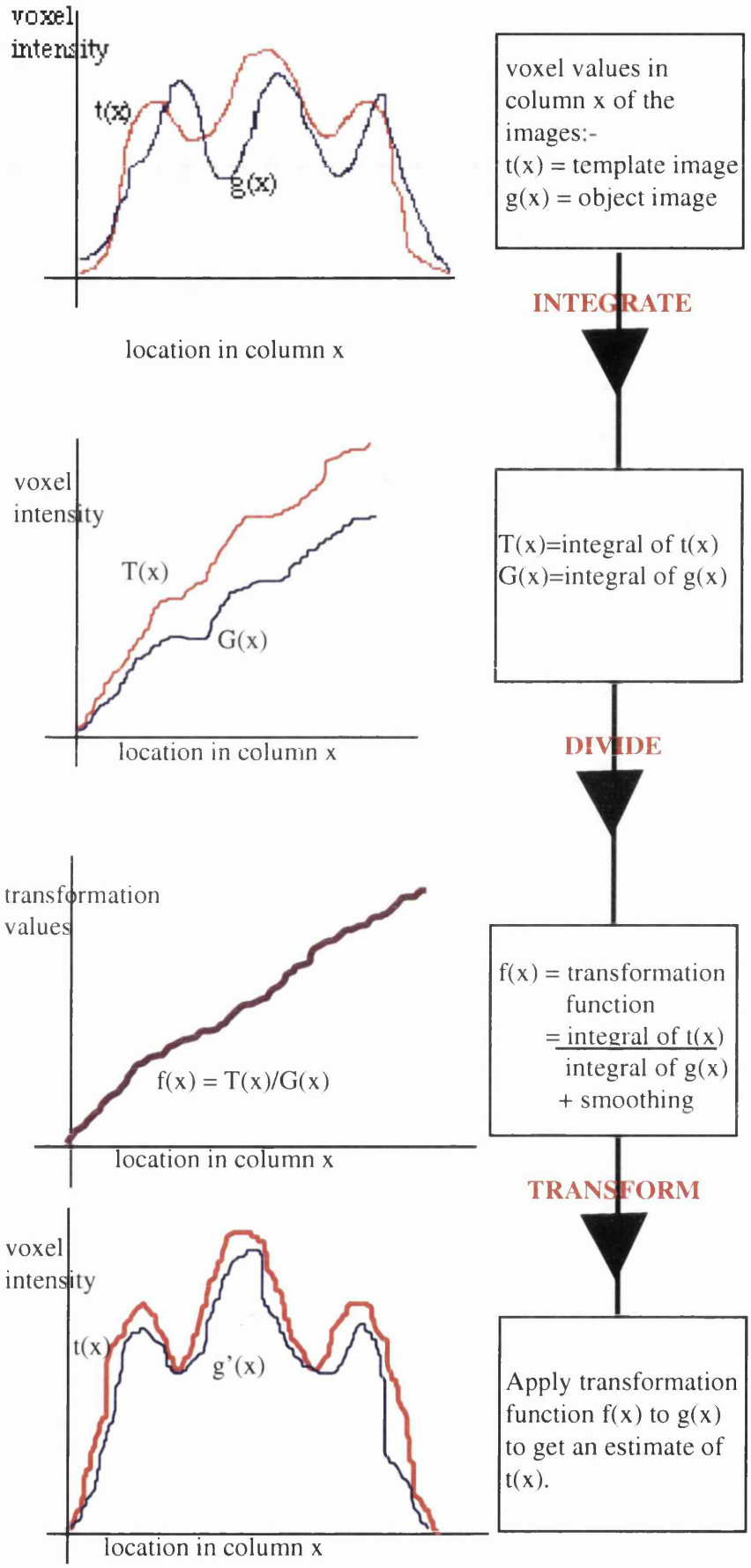

Figure 2.2 shows graphically how the computer algorithm matches the sample image to the template image by reducing each image to the integral of the voxel values (voxel intensity) in each column x (pixel x location) before applying the intensity transformation.

SPM95 implemented this transformation by calculating the sum over all the rows, transforming the image and then summing over all the columns and then transforming the image again. This made the assumption that the transformation was commutative i.e. rows then columns is the same as columns then rows.

SPM96 extended this model to include 3 dimensions avoiding the error introduced by assuming the commutative nature of the method (49). This intensity transformation has been described by the developers of SPM as being better suited to adjusting cortical anatomical differences rather than sub-cortical differences (48). As a consequence only the 12 parameter linear transformation is used for image standardisation of ^{99m}Tc HMPAO SPECT images of CBF used in chapters 3-6.

Intensity transformations for inter-modality and inter-subject registration:-

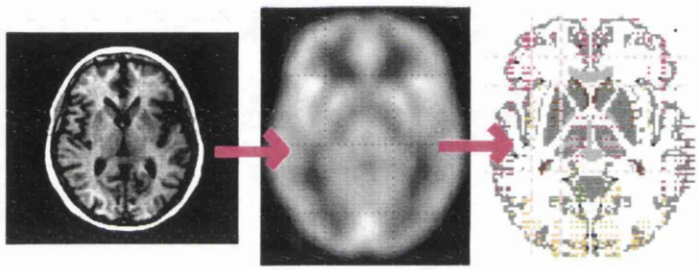

There are two ways of applying the method described above to standardise structural with functional images a) standardise the high resolution structural image to the MR template provided with SPM and then use the same transformation on the corresponding previously registered functional image or b) standardise the functional image to the PET template provided with SPM and then use the same transformation on the corresponding previously registered structural MR image.

Since the object MR image must have contrast/acquisition parameters (of which there are a huge number of permutations) very close to that of the template or the standardisation algorithm will fail, option b) is preferred

Reslice parameters:- Once image registration and image standardisation has been completed the registered object images have to be resliced. There are 3 options for the interpolation method a) nearest neighbour b) bilinear c) sinc interpolation. Option b) is

preferred for ^{99m}Tc HMPAO SPECT rCBF images based on empirical evidence (see appendix A) and advice from the SPM developers (personal communication from John Ashburner 26/01/98)[7].

2.2.3 MODULE THREE. Statistical Analysis.

Image analysis by voxel-wise methods.

The statistical analyses used by SPM are based on the general linear model (GLM) (59), in which a variation in the signal that is being measured can be expressed in teRMS of a linear combination of explanatory variables and an error term: i.e.

$$Y = XB + e \qquad (1)$$

where Y = the response variable (the signal we are trying to measure) X = the explanatory variable (cognitive task) B = unknown parameter and e = an error term (that includes stochastic noise from the scanner, and biological noise from the subjects, and is modelled as a normal distribution).

This means that if the GLM holds true for the data then both data sets will have the same distribution and therefore a simple t-test can be used to test for the null hypothesis that two mean images are the same using a paired t-test at every single voxel in the mean images.

Smoothing:- Before statistical analysis is carried out the images must be spatially smoothed using a Gaussian spatial filter so that a) the data conform more closely to a Gaussian field model which is used to make statistical inferences about the SPM(t) maps produced b) the noise is reduced in the scan by smearing out the signals at higher spatial frequencies usually attributable to noise and c) it removes very small differences in the functional anatomy between subjects (59).

---

[7]SPM-mailbase letter dated Jan/98 at http://www.mailbase.ac.uk/lists/spm/1998-01/0078.html

There is no 'best' smoothing filter, only general guidelines that for the data to be compatible with the Gaussian field theory, the full width at half maximum (FWHM) of the smoothing filter must be at least twice the voxel size of the original image in all directions (61). It should also match the expected extent of the signal (which of course is unknown) produced by the change in rCBF. A spatial filter with a small FWHM (i.e. less than the extrinsic resolution of the system filter) will preserve amplitude [u] of activation but leave some stochastic noise from the scanner and radioactive decay processes which will adversely affect the overall signal [c], whereas a larger filter (i.e. greater than the extrinsic resolution) will increase the extent, (number of significant voxels) [k] of an activation region but may introduce noise from other structures again reducing the overall signal [c]. It follows that there must be an optimum filter size for the data sets available where u, k and c are at a maximum or in teRMS of the reporting of SPM(t) maps p_u, p_k and p_c are at their most significant where p is the significance of the signal changes in the data.

Review of the literature reveals a range of Gaussian spatial filters used, presumably dependent on the machine and/or back-projection method used (which will also include a certain degree of spatial filtering). However, it was not possible to simply transfer this information supplied by PET or conventional SPECT users of SPM to our data since the detector arrangement and performance characteristics of the SME 810 dedicated brain SPECT scanner differs from conventional gamma cameras. It was necessary, therefore, to decide empirically which filter gave the optimum results for our data sets (see appendix A). The optimum filter size determined by our measurements for a unit dose (500MBq) of ^{99m}Tc HMPAO is 10mm FWHM and for a half unit dose (250MBq) of ^{99m}Tc HMPAO is 12 mm FWHM.

SPM Experimental Design:- The experimental design is a crucial component in applying SPM and there are a number of design options to chose from. The three different designs used in this thesis are:

- multi-subject; different conditions, (equivalent to a blocked analysis of variance)
- multi-subject; replication of conditions (equivalent to a blocked analysis of variance with replications)
- compare groups; one scan per subject. (equivalent to an analysis of covariance or unpaired t-test)

Contrasts:- Contrasts are used to describe the changes that the experiment is searching for and consist of matrices containing a series of 1's, -1's and 0's (73). For example, once the scans have been selected in order of subject and then condition, a multi-subject; different conditions experiment of the form A B C D denoting four different cognitive tasks would be constructed in the following way to look at a simple subtraction paradigm.

contrasts

Tasks
A B C D

$$\begin{pmatrix} 1 & -1 & 0 & 0 \\ -1 & 1 & 0 & 0 \\ 0 & 0 & 1 & -1 \\ 0 & 0 & -1 & 1 \end{pmatrix}$$

A-B
B-A
C-D
D-C

All scans of subjects performing task A compared to all scans of subjects performing task B etc ..

These contrasts could be extended further to look at the difference in the differences (an interaction). For example

contrasts

Tasks
A B C D

$$\begin{pmatrix} 1 & -1 & -1 & 1 \\ -1 & 1 & 1 & -1 \end{pmatrix}$$

(A-B) - (C-D)
(B-A) - (D-C)

Using this simple notation the comparison of conditions can be constructed in such a way as to be more than just a cognitive subtraction (74) (see CH7).

Global Intensity Normalisation:- Before the difference in means can be calculated some adjustment for differences in global blood flow between scans of the same subject and scans of different subjects must be made. These global differences can be attributed to differences in administered dose and uptake fraction in the brain as well as physiological changes in the subject (mood changes, physical activity). All of these changes will interfere with the actual rCBF change that is being measured.

Global CBF (gCBF) is measured as the mean value over all intracerebral voxels, where the intracerebral voxels are calculated as being the voxels with a value above 80% of the global mean of all voxels in the scan. The statistics are then performed on the voxels that survive an 80% threshold of the mean gCBF value (grey matter threshold). This means in effect that the volume of the brain analysed will be equivalent to that of the smallest volume in any individual brain scan included in the analysis. There are two different ways that SPM can remove differences in gCBF a) Proportional Scaling and b) Analysis of Covariance (AnCova) (59). Proportional scaling removes differences in gCBF by scaling all voxels within a scan to the mean gCBF of each scan and assumes the change in rCBF will be dependent on the gCBF. AnCova removes differences in gCBF by modelling the mean gCBF for each scan as a confounding covariate and so removes most of the error variance due to gCBF leaving only the variance due to the differences in rCBF induced by the activation task being investigated. This assumes that the measured change in rCBF is an additive effect, the size of which is independent of the gCBF, as opposed to proportional scaling which assumes the change will be dependent on the gCBF.

For the purposes of normalising ^{99m}Tc HMPAO SPECT images option a) is preferred. The developers of SPM recommend that for qualitative measures of rCBF (such as ^{99m}Tc HMPAO scans) where the differences in global counts between subjects can be quite large, the proportional scaling method is used in preference to AnCova (personal communication from Dr Andrew Holmes 02/02/98)[8].

[8] SPM-mailbase letter dated feb/98 at http://www.mailbase.ac.uk/lists/spm/1998-02/0001.html

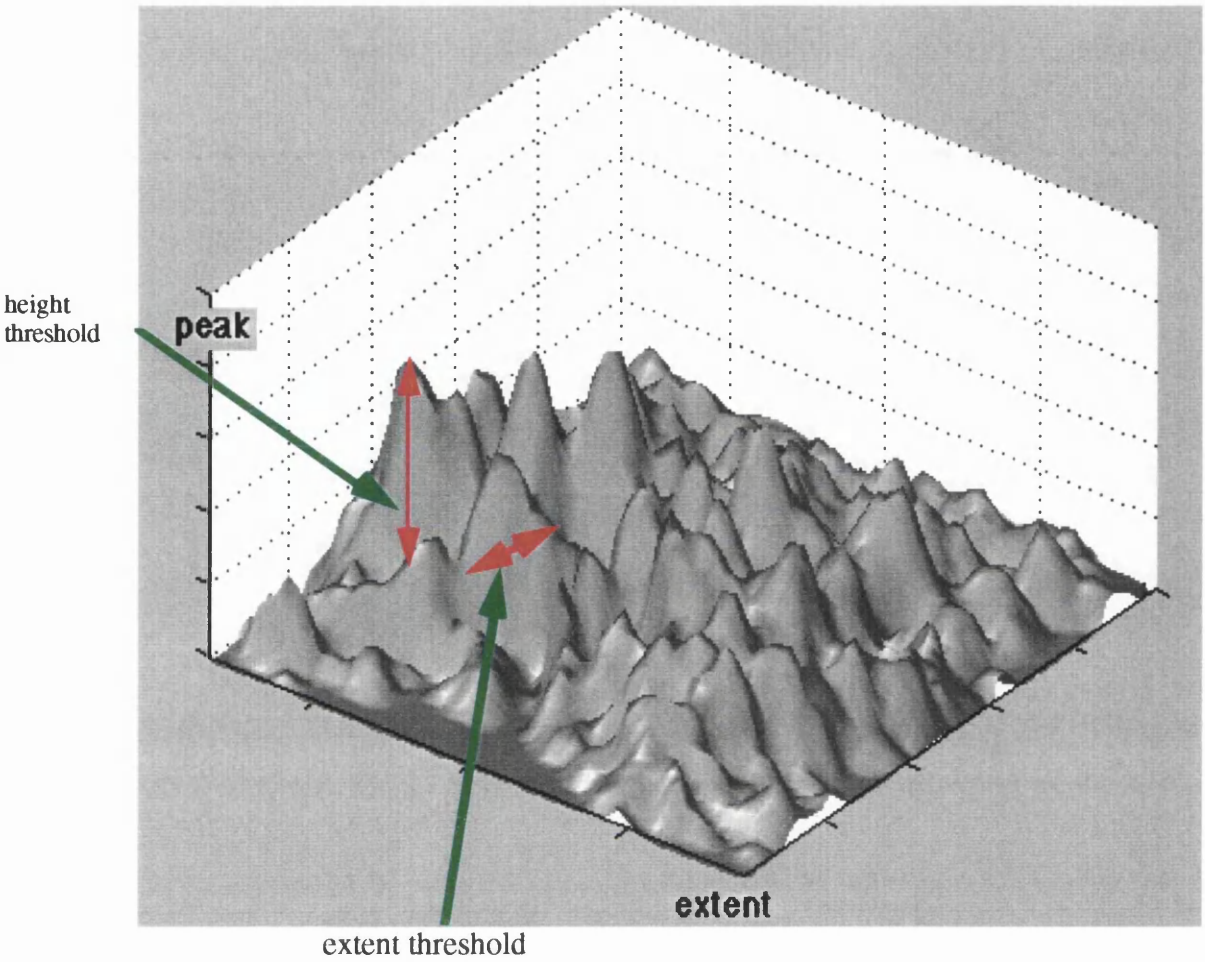

Figure 2.3 shows a 3d representation of a slice through an SPM (t) to demonstrate the difference between significance in activation height and activation extent.

Presentation of Results

After smoothing and global intensity normalisation a t-test is performed on every intracerebral voxel to produce a statistical map SPM(t) which represents change significance. Having computed a t value for each voxel in the data set (SPM(t)) constructed using the appropriate experimental design and contrast, the values are transformed to the unit Gaussian distribution and expressed as Z-scores (unit standard deviations from a mean of zero). These 'maps' are then displayed as maximum intensity projections (MIPS) in 3 planes; axial, sagittal and coronal (see fig 2.4). The data can also be rendered on to cortical surfaces or MRI sectional planes. To display the SPM(t) MIPS a significance threshold must be selected. All voxels surviving the threshold will be displayed.

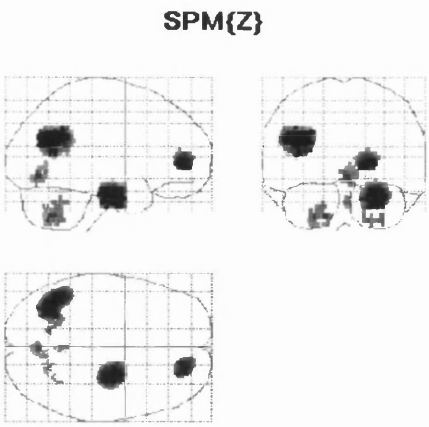

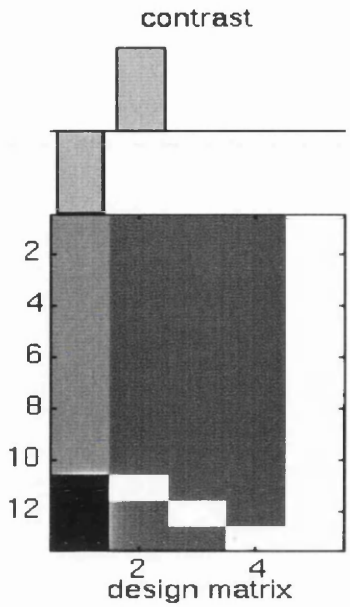

P values & statistics ../abarnes

set-level {c}	cluster-level {k,Z}	voxel-level {Z}	uncorrected k&Z	x,y,z {mm}
1.000 (1)	**0.000 (795, 8.45)**	**0.000 (8.45)**	**0.000 0.000**	**-36 -62 28**
	0.000 (555, 8.36)	**0.000 (8.36)**	**0.000 0.000**	**26 -16 -24**
	0.000 (212, 8.04)	**0.000 (8.04)**	**0.000 0.000**	**18 50 4**
		0.000 (6.74)	0.000 0.000	26 52 4

Height threshold {u}=3.09, p=0.001
Extent threshold {k}=3.258e-01 voxels, p=0.5
Expected voxels per cluster, E{n}=0.8
Expected number of clusters E{m}=81.2

Volume {S}=121942 voxels
Degrees of freedom = 9
Smoothness FWHM {mm}=3.9 3.9 7.4
{voxels} = 2.0 2.0 1.9

Figure 2.4 shows the SPM (t) table printed after a typical SPM96 analysis of 3 individual sample scans contrasted with a reference group. See text for details.

Height and extent threshold:- The Z-score map that is produced can be considered significant on two levels a) height of change significance of rCBF and b) extent of the number of voxels with significant change of rCBF (59) (see figure 2.3 for graphical representation of peak significance and extent significance).

Corrected significance (multiple statistical tests):- When performing multiple statistical tests a correction must be made for the number of tests being performed. Usually this takes the form of a Bonferroni correction i.e. the level of significance divided by the

number of independent statistical tests performed. In its simplest form this would mean that for a voxel-wise analysis the significance level would have to be divided by the total number of voxels in the data set, typically tens of thousands and would wipe out any statistically reliable activation signals. However, intrinsic resolution of the scans and the spatial smoothing filter which is applied to the data prior to analysis means that the voxels are not independent of one another. Instead an estimate of smoothness is used so that an equivalent number of tests can be calculated and an alternative "Bonferroni type" correction for multiple testing is made (59).

Corrected significance based on height and extent:- A further calculation is made that combines the significance of the extent of the activation with its height corrected for multiple comparisons; so that a change in the voxel height (representing ΔrCBF) although small (<2%) may still be considered a significant region of change if it occurs over a significant number of voxels (69).

Statistical Inference:- If one is considering a hypothesis driven experiment where the cognitive tasks have been manipulated in such a way that a particular brain region is expected to show significant change then the significance threshold can be set at $p<0.01$ (uncorrected height threshold) and $p=1.00$ (uncorrected extent threshold). If the experiment is more exploratory then the thresholds can be set at $p<0.001$ (uncorrected height threshold) and $p<0.1$ (corrected height threshold) or $p<0.05$ (corrected extent threshold).

Figure 2.4 shows the MIPS viewed on 3 orthogonal sections of a 'glass brain'. To the right of this is the contrast representation, in this case (-1 1 0 0), and the design matrix used commonly by statisticians when performing an AnCova. Below this is the list of data defining the location and Z-scores for the most significant voxels surviving a predetermined significance threshold. Reading the columns from right to left; column 1 gives the x, y, z co-ordinates of the most significant voxel in Talairach space, column 2 lists both the uncorrected significance of the height and the extent of the change in voxel

value (or ΔrCBF), column 3 lists both the Z-score and the corrected (for multiple tests) significance of the height of the change in voxel value, column 5 lists the Z-score, the number of voxels and the corrected significance (multiple tests and extent), column 6 lists the significance of the number of clusters of continuously significant voxels detected.

For a more in depth review of all of these steps the reader is referred to http://www.fil.ion.bpmf.ac.uk/spm.

CHAPTER 3

Validation of the image standardisation facility of SPM96 applied to oblique or incomplete image data sets.

This chapter describes the methods used to validate the image standardisation facility of SPM96 by performing a series of challenge conditions analogous to those present in routine clinical data. Section 3.1 describes the problems inherent in validating *between subject* and *between modality* image registration in the situation in which there is no one-to-one correspondence. Section 3.2 lists the steps taken to create the simulated "non-optimal" data sets, i.e. the challenge conditions. Section 3.3 describes the assessment of errors and lists the results for the overall performance of the image standardisation facility. Section 3.4 discusses these results in teRMS of finding the optimal method of image standardisation for clinical ^{99m}Tc HMPAO SPECT cerebral blood flow images.

3.1 Introduction.

Despite fixed protocols for positioning patients within the field of view of a SPECT camera for some seriously ill patients correct positioning is almost impossible. The developers of SPM recommend that differences in orientation between scans or with respect to a template be no more than a few degrees because of the possibility of the result getting stuck in a local minimum. In some seriously ill or elderly patients, positioning within the field of view is difficult, and images may have as much as

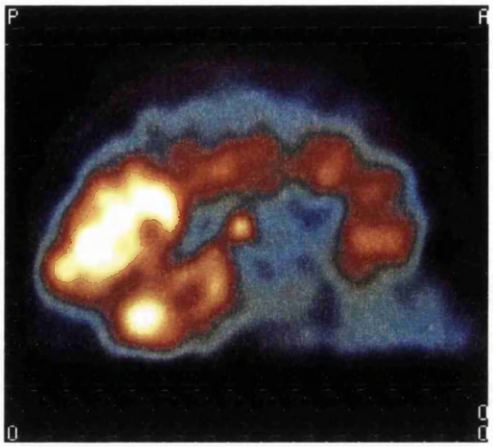

Figure 3.1a shows a section through the mid sagittal of ^{99m}Tc HMPAO scan that has a good field of view covering the whole head.

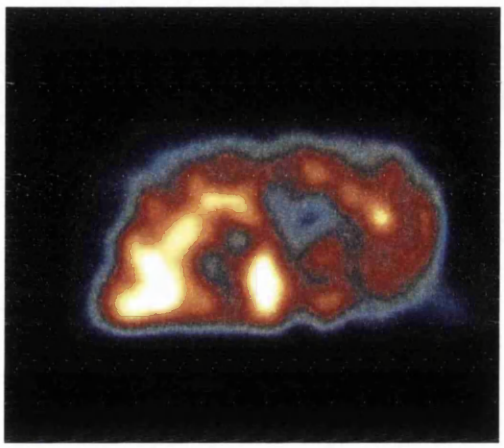

Figure 3.1b shows what happens when the patient's head is tilted backwards in the sagittal plane (usually caused by the difficulty many older patients have in lying on the poorly designed scanning couches when they have a marked curvature of the spine) which results in only the top half of the cerebrum being in the field of view.

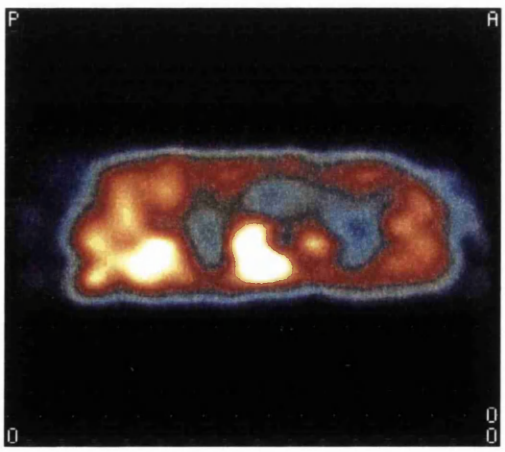

Figure 3.1c shows what happens when there are problems positioning a seriously ill patient and that patient finds it difficult to lie in the scanner for any length of time. Both the cerebellum and the superior axial slices are missing from the field of view.

Figure 3.1 shows how positioning of the patient within the confinces of the scanner can effect the field of view and hence the volume of brain contained within the images. Figure 3.1 a typical image from the SME810 scanner with good coverage of the whole brain. Figure 3.1b shows what can happen if there are problems positioning the patient. Figure 3.1c shows what might happen if that patient also finds it difficult to lie in the scanner for any length of time.

a 20° pitch misalignment from one another or from a standard reference position and 5°-10° roll and/or yaw. For a section scanner this results in a loss of data from either the top or bottom regions of the brain image data set (axial truncation) and only a small area of overlapping data between two images to be registered (be they repeat SPECT/PET scans or an ideal template) may be available, as illustrated in figure 3.1. Even for conventional rotating gamma cameras positioning of the camera head so that the shoulders of the patient are avoided can also result in a loss of information from the lower parts of the field of view (the cerebellum). In addition routine MR and CT acquisitions quite often do not include the top of the head.

Although whole brain coverage is not essential for the clinical reporting of scans, the performance of automated image registration software can be hampered by axial truncation. No specific problems have been reported by the developers of SPM96 but other developers of image registration software (39) suggest that partial data sets may pose a problem for automated registration and the experience of this department suggests that in severely compromised data sets there may be a particular problem with alignment in the sagittal or coronal planes.

3.1.1 Validation of accuracy and precision of image registration and standardisation methods.

A comprehensive study by Strother et al 1994 (23) comparing the merits of 'correlation of similarity' with other methods of image registration found that overall the former method was more accurate. Not surprisingly the smallest errors were incurred for intra-modality matching, particularly for MR to MR images of the brain. Landmark matching (both internal and external) fared particularly badly for inter-modality matching due to the difficulties in locating the same points between structural and functional images as well as problems locating the centre of a marker in the lower resolution functional images.

The surface contour method performed only marginally worse for inter-modality compared with intra-modality matching (2mm for MRI/PET compared to 1mm for

MRI/MRI) but was not as good as the correlation of similarity method (1mm for MRI/PET compared to 0.25mm for MRI/MRI).

The above study assessed these techniques by their positional accuracy with reference to some standard position rather than by the resultant error in computing the significance of change or abnormality. Is a 1^{o} error about the x axis better or worse than a 1mm translation along the y axis ? To answer this question it is more appropriate to investigate directly the effect of positional errors on the parameters used in this study i.e. the resulting change in the number of counts in each ROI (40) or the effect on a typical Z-score value in a voxel-wise analysis. However, the validation of image registration accuracy is not straightforward. As Pelizzari et al 1994 (75) states, "the measurement accuracy of co-registration methods on real human studies is inherently difficult". Even for intra-subject, within modality co-registration there can be no one-to-one correspondence between the data sets due to the natural variability in cerebral blood flow and stochastic noise generated by the radioactive decay processes and the detector instrumentation. For inter subject co-registration the individual variations in anatomy, despite attempts at standardization, will add to the overall mis-registration. In short there is no absolute 'gold standard' against which image registration algorithms can be tested. It is better then to consider precision (or relative accuracy) rather than absolute accuracy, when considering image co-registration, as any transformation will have residual errors. The best that can be achieved is to compare the final co-registration result achieved with a full data set with that obtained during any of the situations where only a compromised or restricted data set is available. The key to the use of this method of validation is that the full data set becomes the 'gold standard' to which the sample (challenge condition) data sets may be compared. To measure the precision in an automated co-registration algorithm a single data set (sample scan) is manipulated prior to co-registration to provide a series of challenge conditions.

3.2 *Methods*

To create the challenge conditions for testing the image standardisation component of the software the following method was used:-

- Create a reference dataset
- Create the challenge conditions
- Determine the optimum image standardisation method

3.2.1 Creating a reference data set

The method used to create the reference data set is fully illustrated in figure 3.2. Because there is no known result to these challenge conditions the deviations from a known constant condition were used to measure the relative accuracy of the image standardisation facility. First a reference database of scans was created to provide the reference data set against which each of the challenge conditions could be compared. Ten scan pairs were selected from a previous study where each subject had been scanned twice . The scans in each of these pairs were co-registered with one another and an average image was created from each pair. Each of these 10 average scans were then co-registered to the image in the group that was most closely aligned with the ac-pc line orientation. These 10 re-aligned scans were then denoted as the reference group. To create the sample image, the reference group was then averaged into one single scan. The challenge conditions were then superimposed on to the sample image. Although the premise in this investigation was to monitor the effect of each challenge condition against a known reference, the use of an averaged scan as a sample image rather than a single image from an individual removed any possibility of a systematic result occurring as a consequence of that one individual's anatomy.

3.2.2 Creating the challenge conditions

In order to follow the effects of the challenge conditions on the statistical output known changes in rCBF had to be created in the sample scan.

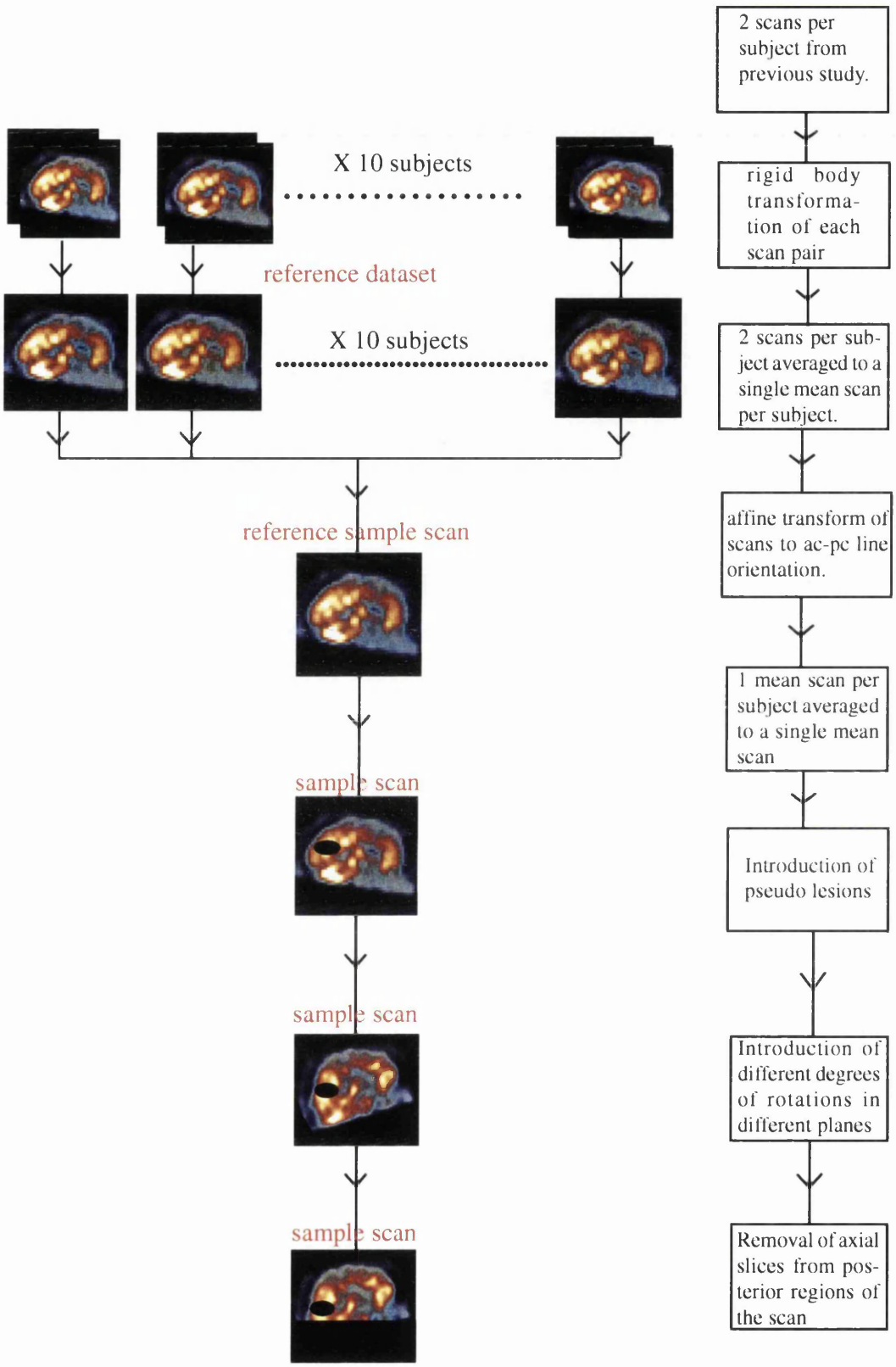

Figure 3.2. A schematic flow diagram showing the steps involved in producing the simulated data for validating the image standardisation facility in SPM96.

The pseudo differences between the scans were achieved by using a customised graphics package[9], to place a region of 'abnormality' in the sample scan. The image data was manipulated in ANALYZE™ format as single images representing axial slices through the brain. A region was drawn in the left and right parietal lobes on three axial slices through the parietal cortex. The mean value of each of these slices was calculated and 30% of the slice mean was added to each pixel in the designated region in each slice. The slice mean was calculated as the number of counts in those pixels with a non-zero value in that slice divided by the area (mm^2) within the threshold boundary.

Rotations in the sagittal, coronal and axial planes of varying degrees were introduced using the display facility in SPM96.

Axial truncation was achieved using a customised graphics program (mri3d)[10] by removing slices from the inferior parts of the sample image after introduction of a rotation.

DIRECTION OF ROTATION	DEGREE OF ROTATION	AXIAL TRUNCATION
sagittal	0^0	0slices
coronal	6^0	3slices (18 mm)
axial	9^0	5slices (30mm)
	12^0	
	15^0	

Table 3.1 gives a summary of all the challenge conditions. Each challenge condition was created from different permutations of these parameters e.g. direction of rotation: sagittal, degree of rotation: 15^0, axial truncation: 3slices (18mm).

3.2.3 Determining the optimum image standardisation method:

Three different methods were examined and are illustrated in figure 3.3.

[9]xpaint is a Xwindows, UNIX application available with Solaris 2.7.
[10]customised image display software runs on a UNIX platform, courtesy of Martin Connell, Department of Clinical Neuroscience, University of Edinburgh, Western General Hospital, Edinburgh, UK.

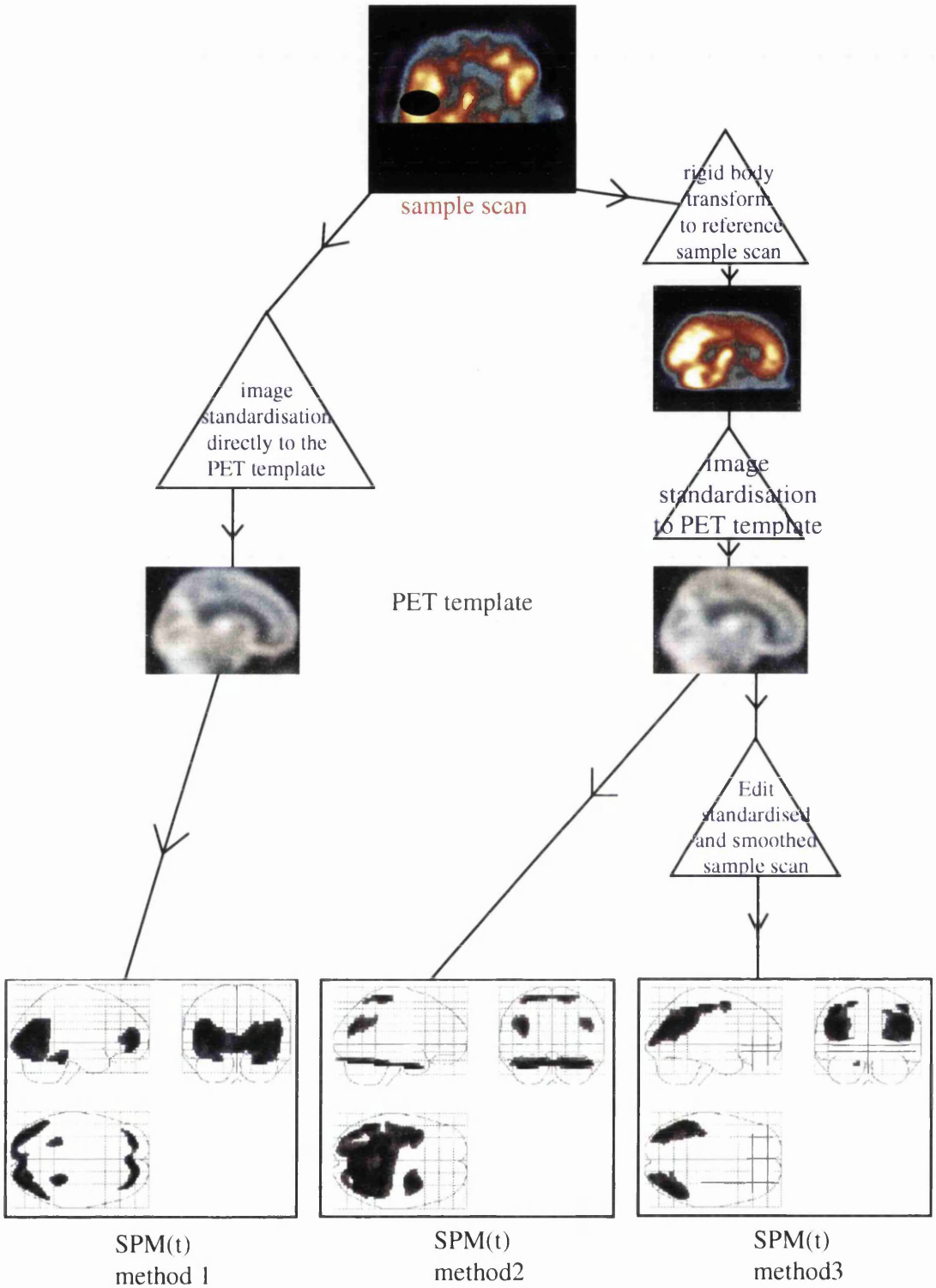

Figure 3.3 A schematic flow diagram showing the 3 different methods used to achieve image standardisation under a series of different challenge conditions.

The **first method** involved image standardisation of each of the challenge condition sample images by direct matching to the standard PET template supplied with SPM96, linear spatial standardisation function.

The **second method** used a rigid body registration step prior to standardisation. Each challenge condition sample image was co-registered to the reference image (the sample image no rotation, no truncation) using a 6 parameter rigid body transform before it was matched to the PET template.

The **third method** includes editing of the final standardised sample image after co-registration, standardisation and smoothing to remove spurious data contained in the smoothed edges.

3.3.1 Reporting image standardisation results:

The results from each of the challenge conditions were analysed using the "compare groups: 1 scan per subject" option where group 1 was the 10 average scans in the reference data set and group 2 was a single challenge condition sample scan. Global blood flow normalisation was achieved using the proportional scaling option and SPM(t) maps were generated using the default thresholding of $P_u<0.001$, and $P_k<0.5$ (uncorrected). Results were calculated in teRMS of the average in absolute change in Z score and root mean squared error in location (defined by Talairach co-ordinates) of the most significant voxel within the two pseudo lesions with respect to that reported in the reference scan. Aggregate errors particular to the method of image standardisation used or the challenge condition being corrected were used to provide an overall view of the performance of the image standardisation facility.

3.3 Results

Figure 3.4 shows the reference results to which all other subsequent results were compared. Figures 3.5 - 3.7 show the results of the 3 different methods of image

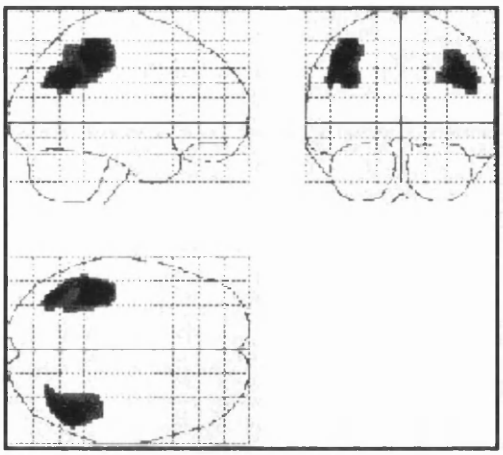

Figure 3.4. **Reference result**

SPM (t) map of the results of standardising the reference image to which all other subsequent sample scans were compared.

$Z_L = 4.84$ $(x\ y\ z)_L = -40\ -40\ 52$

$Z_R = 4.25$ $(x\ y\ z)_R = 48\ -56\ 36$

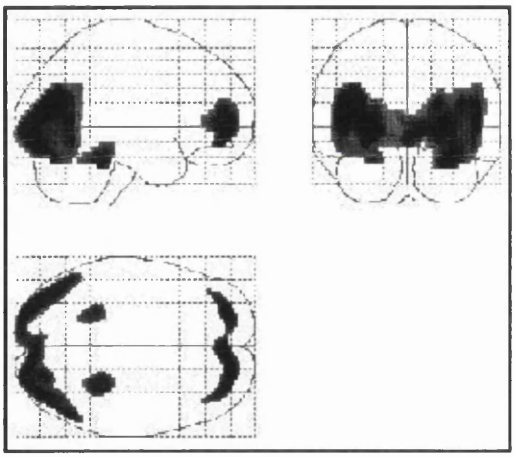

Figure 3.5. **Method1**:- spatial normalisation to PET template directly.

SPM (t) map of the results of method1 image standardisation on the significance and location of the pseudo lesions.

$|\Delta Z| = 0.59$ RMS(x y z) = 53 mm

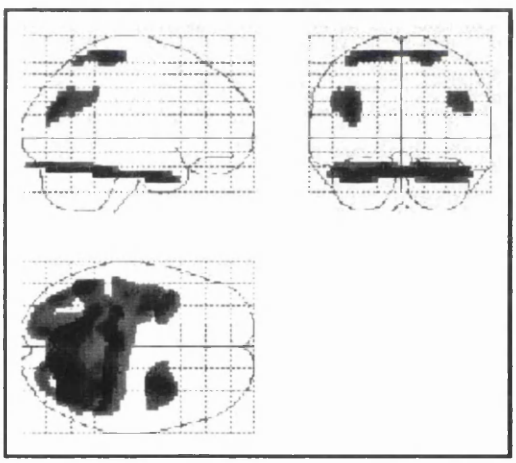

Figure 3.6. **Method2**:- co-registration to reference sample image prior to spatial normalisation.

SPM(t) map of the results of method2 image standardisation on the significance and location of the pseudo lesions.

$|\Delta Z| = 0.82$ RMS(x y z) = 9.8 mm

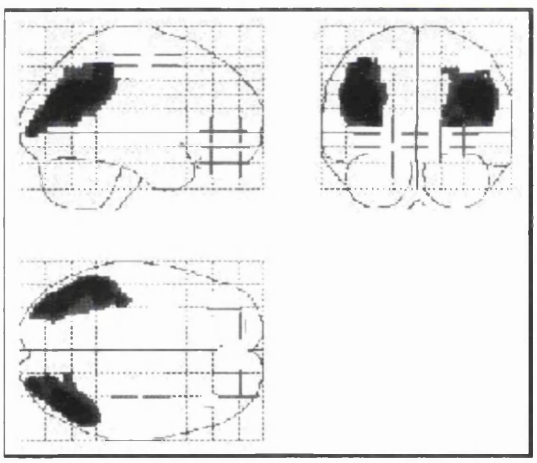

Figure 3.7. **Method3**:- editing of smoothed edges after standardisation but prior to statistical analysis.

SPM(t) map of the results of method3 image standardisation on the significance and location of the pseudo lesions.

$|\Delta Z| = 0.12$ RMS(x y z) = 5.7 mm

standardisation on the challenge condition; direction of rotation: sagittal, degree of rotation: 15°, axial truncation: 5 slices (30mm).

The results from the first method (figure 3.5) show that the image standardisation procedure has failed to correct for the rotation in the sagittal plane made evident by the fact that the pseudo lesions originally located bi-laterally in the parietal lobes are now located in the occipital lobe and the appearance of a further significant lesion in the anterior frontal lobes bi-laterally. The size of both the average absolute difference in Z-score (0.59) and the RMS error in location (53mm) recorded in this example would undoubtedly give erroneous information if the same situation had arisen in a clinical scan. The results from the second method (figure 3.6) show that the rotation in the sagittal plane has been corrected. This is clear from the large reduction in the RMS error in location (9.8mm). However, another problem becomes apparent in this case. The large areas of significance produced at the top and bottom of the SPM map are a result of the statistical calculation detecting voxel values at the edge of the resliced sample scan volume as unexplained variance. The consequence of this is that the significances of the voxel values in the pseudo lesion are reduced (causing a larger difference in absolute in Z-score than in method 1) with respect to the reference group as a direct affect of the increased overall variance of the resliced sample scan. Finally the results of using method 3 on this example are shown in figure 3.7. The voxel values produced by the interpolation of edge information after reslicing of the sample image are removed by manually editing these parts of the scan. This allows the pseudo lesion voxel values to be identified at a higher significance level, differing from the original z-score value by just 0.12 but doesn't entirely remove the RMS error in location (5.7mm). The residual differences in both Z score and RMS could be a result of the interpolation of the voxel values within the lesion itself after reslicing and therefore some caution must be observed when interpreting SPM maps produced from clinical scans if acquired under the same situations of extreme rotation and axial truncation.

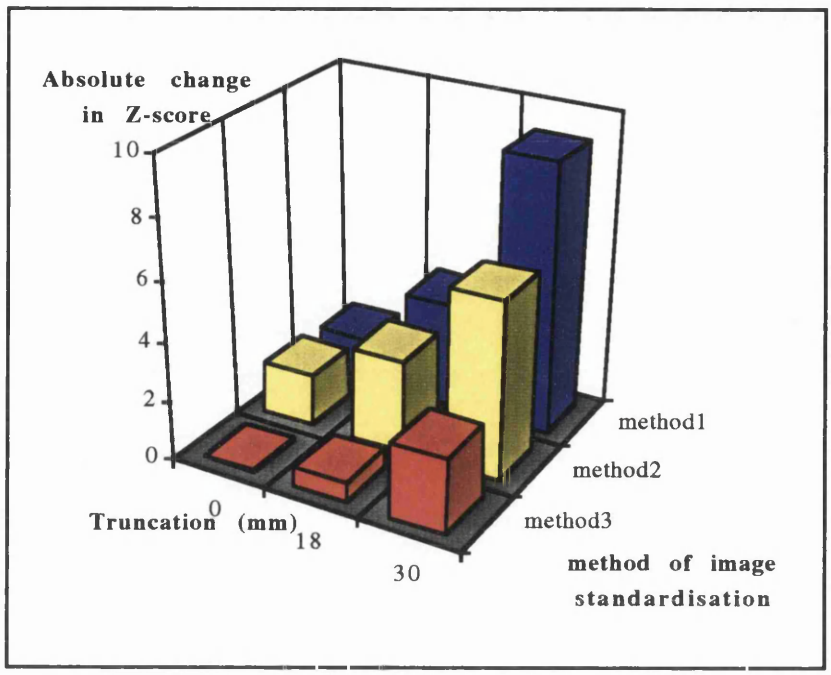

Figure 3.8 a. shows the total sum of errors in $|\Delta Z|$ the most significant voxel with respect to the reference sample image determined by the method of image standardisation used. The largest errors are associated with the largest volume of image removed (5 slices @ 6mm thick) regardless of the image standardisation method used. To minimise this effect method3 should be used for image standardisation.

Method1:- spatial normalisation to PET template directly.
Method2:- rigid body transform to reference sample image prior to spatial normalisation.
Method3:- editing of smoothed edges after standardisation but prior to statistical analysis.

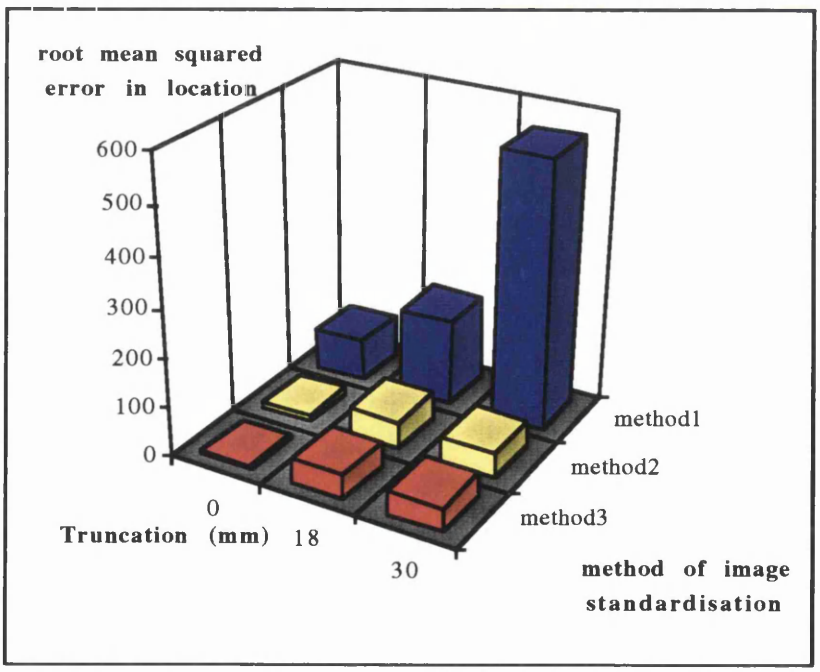

Figure 3.8 b. shows the total sum of RMS errors in location of the most significant voxel with respect to the reference sample image determined by the method of image standardisation used. The largest errors are associated with the largest volume of image removed (5 slices @ 6mm thick) regardless of the image standardisation method used. To minimise this effect method3 should be used for image standardisation.

Method1:- spatial normalisation to PET template directly.
Method2:- co-registration to reference sample image prior to spatial normalisation.
Method3:- editing of smoothed edges after standardisation but prior to statistical analysis.

Although the results illustrated in figures 3.5-3.7 are from one of the most extreme challenge conditions and consequently show the largest errors, this pattern of being able to reduce the error in Z score and location by applying method 3 is consistent for all challenge conditions. To gain an overall view of this result all the measurements of average absolute differences in Z score were summed over all directions of rotation for each axial truncation depending on the method of image standardisation used. For example the $|\Delta Z|$ for all the rotations sagittal, coronal and axial at 15^{o}, 12^{o}, 9^{o}, 6^{o}, 0^{o} for the axial truncation of 30mm were summed together (e.g. 0.69+0.74+0.79+0.82+0.09+0.11+0.82+0+0.49+0.48+0.48+0.48 = 5.99) then the same for the axial truncation of 18mm and finally for 0mm. These aggregate results are shown in figure 3.8 and provide a performance measure of each of the image standardisation methods under investigation regardless of the direction or size of rotation but affected by the amount of axial truncation present in the sample image. Both figures 3.8a and 3.8b show that all methods are poor when performed on severely truncated data. Method 3 produces the most improvement in terms of Z-score difference but methods 2 and 3 work equally well with regard to improvement in RMS error in location.

A further overall view of the results of this investigation in to the image standardisation facility are shown in figure 3.9 and illustrate the type of situations (challenge conditions) that will produce the biggest errors regardless of the method of image standardisation used. This investigation shows that because there still remains a residual error in location even after using image standardisation method 3, any SPM analysis of images that contain a restricted amount of data because of large rotations in the sagittal or coronal planes (axial truncation = 30mm and sagittal rotation 15^{o} i.e. no cerebellum) must be interpreted with caution. A complete listing of results for each of the challenge conditions are included in appendixB.

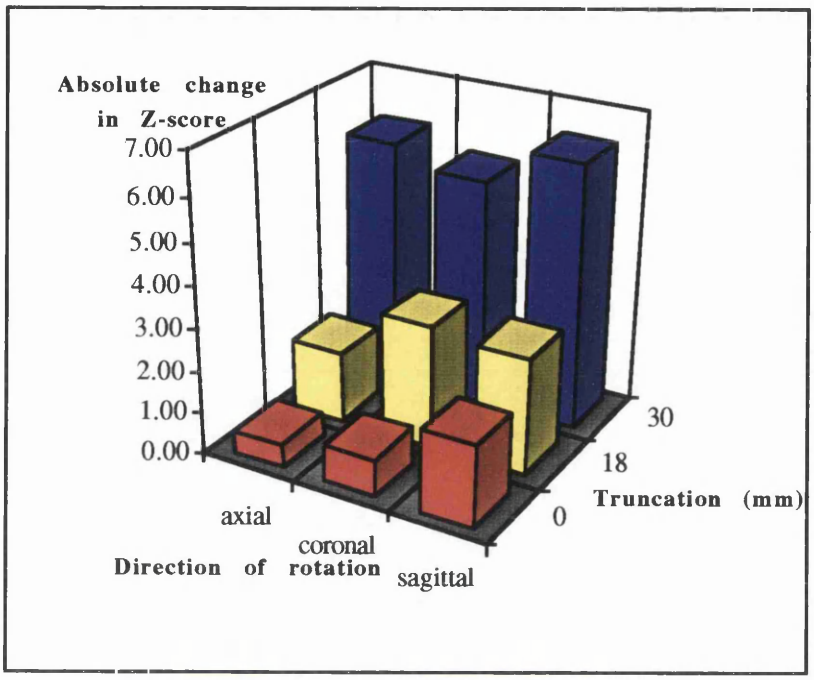

Figure 3.9 a. shows the total sum of errors in $|\Delta Z|$ of the most significant voxel with respect to the reference sample image determined by the challenge condition. The largest errors are associated with the largest volume of image removed (5 slices @ 6mm thick) in conjunction with a rotation in the sagittal plane.

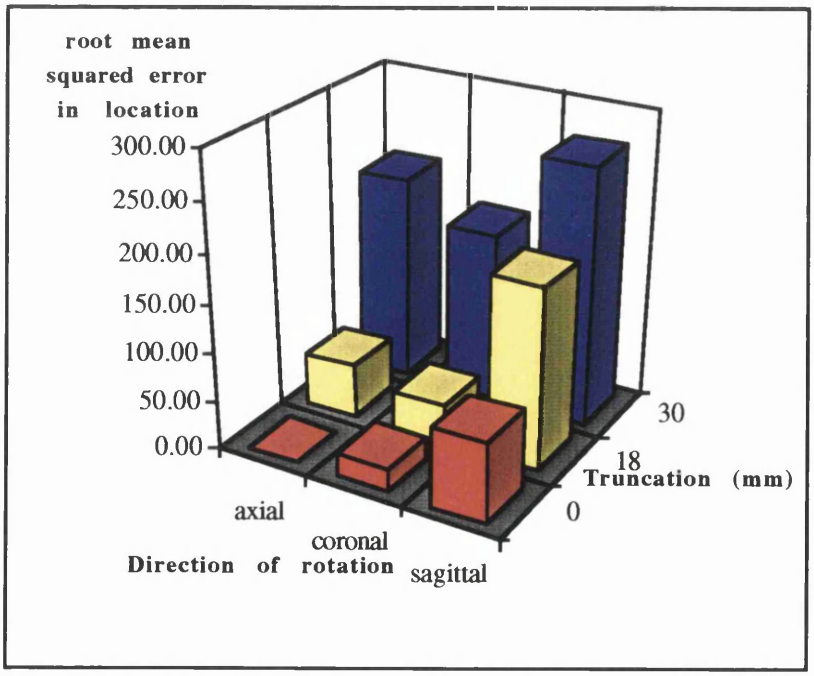

Figure 3.9 b. shows the total sum of RMS errors in location of the most significant voxel with respect to the reference sample image determined by the challenge condition. The largest errors are associated with the largest volume of image removed (5 slices @ 6mm thick) in conjunction with a rotation in the sagittal plane.

The results of the investigation in to the spatial normalisation facility of the SPM software demonstrated that relying on the spatial normalisation facility (method 1) alone was unreliable in situations where starting parameters were far from ideal (axial truncation = 30mm and sagittal rotation 15^{o} i.e. no cerebellum). Results were improved by performing a rigid body co-registration of the sample images to an average ^{99m}Tc HMPAO SPECT reference image prior to spatial normalisation (method 2). A further reduction in errors could be made if the smoothed edges (containing spurious voxel values) were removed after spatial normalisation but prior to statistical analysis (method 3).

3.4 Discussion

This study investigated three different methods of image standardisation for use with non-optimal image data sets. The chronology of the methods were such that the second method was developed as a solution to the problems incurred using the first method (the SPM96 image standardisation facility) and the third method was developed as a solution to the problems encountered using the second method. They have been presented together for clarity.

The method of validation described requires that a full data set becomes the 'gold standard' to which the sample (challenge condition) data sets may be compared. To measure the precision in an automated co-registration algorithm a single data set (sample scan) was manipulated prior to co-registration to provide a series of challenge conditions. These challenge conditions were chosen to reflect those present in routinely acquired clinical data (large rotations from a standard reference position resulting in axial truncation of the image volume). This method is similar to that employed by Minoshima et al 1991 (35). A series of simulated PET images were used to apply a number of challenge conditions, involving both rotations and translations, to a sample image before employing a correlation of similarities method (stochastic sign change evaluation) to register this sample image to the original reference image. Results show that the precision accuracy for this method gave a mean rotational error of 0.03^{o} and a translation error of 0.5 pixels.

In anticipation of using this method to register images of abnormal brains they also simulated various lesions (typical of the clinical groups they would be investigating) within the sample image before applying additional rotation and translation. The consequential mis-registration errors tended to increase with larger lesion volumes, with the largest error (>1.0^{o}) due to rotation in the coronal plane and a single lesion volume of 32% of the total brain volume. Minoshima et al concluded from this that their method of image registration would still perform well in the presence of large lesion deficits typical of an abnormal brain. Similarly, Studholme et al 1997 (39) tested the precision of their image registration by correlation of similarities method (maximum entropy) by re-registering clinical images to themselves after the introduction of random rotations and translations. An additional challenge of axial truncation of these images was introduced to model the problem that section scanners have when trying to obtain images of the whole brain. They found the test registrations carried out using their technique failed when used on these truncated image volumes. Friston et al 1991 (48) used a similar concept of precision accuracy to validate their method of image standardisation by measuring the precision with which stereotactic anatomical locations could be defined within and between subjects registered to a standard template. They were able to show that the residual error after both within subject and between subject matching was reduced after a plastic transformation was performed, concluding that better image standardisation was achieved by the use of a plastic image transformation. Assumptions needed for Friston's method to work are that the functional residual differences, (e.g. the differences in rCBF that are actually being measured) are small. This is because the premise on which the final image registration result is based is that the observed distribution of voxel intensities within the sample image will correspond to that of the reference image/template. If this is not the case then differences in rCBF due to lesion deficits, for example, may result in the plastic transformation trying to compensate by shifting voxel values to fill the gap. This condition has not been explicitly modelled by Friston et al in their validation of automated image standardisation.

In the present study the image standardisation facility of SPM96 performed adequately in the most extreme conditions as long as appropriate modifications to the process were made. The maximum errors or changes in Z-score and location were induced by severe truncation of volume coupled with rotations in the sagittal plane and the coronal plane corrected by spatial normalisation to the PET template alone. For example, for a particular challenge of 30mm axial truncation + 15^{o} axial rotation the maximum error in absolute Z-score in the pseudo primary lesion was $|\Delta Z|=0.89$ and therefore likely to affect the acceptance of this region as significant at the default threshold levels of $P_u<0.001$ and $P_k<0.5$. This errors was reduced to $|\Delta Z|=0.48$ by initially co-registering the sample scan with the reference scan prior to spatial normalisation. Although method 2 coped well with large rotations the statistical analysis proved a little more sensitive. As a result of the initial extreme orientations and missing data new edges appeared in the interpolated and resliced data. The new edges become a problem when each image is smoothed prior to analysis, 'smearing' the edges and creating spurious voxel values. Despite the thresholding of voxels and the masking of images to ensure matching volumes across comparisons in the statistical analysis, some of this smeared edge information is included in the analysis and inherently includes lower values in these voxels than in the reference group. The inclusion of these lower value voxels alters the overall global mean value so that the previously significant change in voxels within the lesion is no longer significant. Instead it is these 'edge' voxels that are mapped as significant swamping the true lesion significance in the main body of the scan. This problem has recently been reported by others in the SPM user community (personal communication from B Swartz, 02/04/98)[11] and the next version of SPM (SPM99) will prevent the inclusion of these smeared edges in the analysis[12]. By preventing voxels with zero intensity being included when the image is being convolved with a spatial smoothing kernel the creation of false information will not occur. In the meantime, however, the only way around this problem is to intervene manually and edit the smeared edges from each slice in each individual scan (see figure 3.10). These new edited scans can now be run through the same statistical

[11]SPM help line letter dated - http://www.mailbase.ac.uk/lists/spm/1998-04/0014.html
[12]SPM technical notes http://www.fil.bpmf.ion.ac.uk/spm/spm99.html

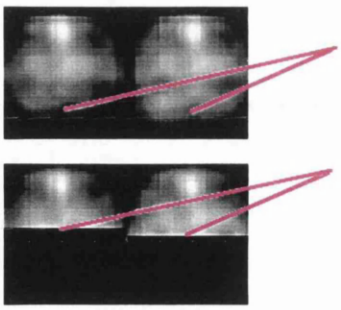

Figure 3.10 Shows how the scans were edited to remove the smoothed edges containing spurious voxel values from a standardised and smoothed sample scan.

analysis as before, this time without the interference of false information. Further correction can be made (reducing the error from $|\Delta Z|=0.48$ to $|\Delta Z|=0.09$) by removing the smeared edges from the co-registered and spatially normalised sample scan. Time taken to perform method 3 takes approximately 15 minutes per sample scan.

The biggest changes in location of the voxel with maximum Z-score were of the order of 55mm and may present a more serious limitation in the location of the primary lesion with respect to known anatomical structure. (e.g. a move of 55 mm could place the lesion in the occipital cortex instead of the parietal cortex - see fig 3.4 and 3.5) but by following the co-registration and editing procedure the RMS error was reduced from 55mm to 9mm and in most cases to zero. If there is potential for error (e.g. when analysing images that are non-optimal) the facilities provided by SPM96 allow the user to "click" around the significant region. Rather than rely solely on the location of maximum Z-score voxel, one can use the whole structure of the significant region to determine in which anatomical structure most of the contiguous voxels lie. Of course this is subjective and may diminish the overall automation of the process unless one recognises that the match between Talairach and Tournoux atlas and the template used for spatial normalisation is at best a good estimate (personal communication from Karl Friston 23/06/98)[13]. In recognition of the problem of defining a standardised anatomical map Collins et al 1994 (25) set up their

[13]SPM help line letter dated - http://www.mailbase.ac.uk/lists/spm/1998-06/0076

own standard map based on the co-ordinate convention used by Talairach and Tournoux 1988 (46) but with additional information provided by the collection of anatomical data delineated by experienced neuro-anatomists from over 50 normal high resolution 3D MRI scans. The new atlas is expressed in terms of probability maps and the borders of anatomically distinct areas delineated at the 50% probability mark. The reported errors in Z score that these results predict for certain starting conditions become less significant when one views them in the context of the data provided by Collins and colleagues.

3.5 Conclusion

This investigation showed that when data from a severely restricted (non-optimal) image volume of CBF ^{99m}Tc HMPAO are to be analysed using SPM96 the image standardisation procedure must be modified to include:-

- a rigid body co-registration between the non-optimal data set and an ideal reference optimal data set of the same imaging modality and acquistion parameters.
- manual editing of the voxel values created by the interpolation of edge information (this should be after image standardisation and smoothing prior to statistical analysis).

CHAPTER 4

Investigation of SPM96 as an aid to the differential diagnosis of dementia using ^{99m}Tc HMPAO SPECT images of rCBF.

This chapter describes the application of SPM96 analysis to clinical image data using the optimal method of image standardisation determined in chapter 3. Section 4.1 describes the difficulties in making a differential diagnosis of dementia both clinically and with imaging and the benefit that an objective method might make. Section 4.2 describes the methods and materials used to establish any benefits of using SPM96 on clinical images of cerebral blood flow. Section 4.4 discusses the role that SPM96 may have in the routine reporting of diagnostic images of cerebral blood flow.

4.1 Introduction

In most hospitals the reporting of images is done by an experienced consultant in nuclear medicine and neuroradiology (sometimes with the participation of an experienced imaging physicist). This is generally sufficient to arrive at the desired interpretation of the image being reported. In the specific case of the interpretation of ^{99m}Tc HMPAO CBF scans it is not difficult to spot the perfusion deficit produced by, for example, a massive cerebral infarct, or the typical CBF pattern of a patient in the later stages of dementia of the Alzheimer's type (DAT). Even the more subtle differences between an ictal and inter-ictal scan of an epilepsy sufferer can, with experience, be reliably detected visually.

However, there are some cases where this is not always so and interpretation of the scan is more difficult. For example patients in the earlier stages of DAT might exhibit the classical pattern of reduced perfusion bilaterally in posterior temporal and parietal cortex. Those patients in later stages of the disease might also have superimposed vascular abnormalities that would result in a less obvious match to the typical DAT CBF SPECT pattern. Would an objective and consistent method of image analysis be of value in interpreting these scans ? This investigation focused on whether the application of a voxel-wise image analysis technique (SPM96) could impact on the reading of scans. To do this SPM96 was used to aid in the differential diagnosis of dementia from SPECT images of CBF. A measure of inter observer agreement was used as an indicator of the software's usefulness, where an improved level of agreement would be interpreted as a positive finding (less equivocal diagnoses) and a lowered level of agreement a negative finding.

The measurement of regional cerebral blood flow (rCBF) using SPECT has been shown to contribute to the differential diagnosis of dementia due to the different perfusion patterns detected in the classical foRMS of each condition (76-83) and it has been proved useful for the differential diagnosis of dementia. SPECT images of probable Alzheimer's disease (PAD) as defined by DSM IV R criteria (84) show regional deficits in the parieto-temporal cortex (sometimes asymmetrical) (42,63,85), those of dementia of the frontal lobe type (DFLT) show characteristic reductions in the anterior regions of the cortex including anterior aspects of the temporal lobe (86) while multi-focal lesions throughout the cortex indicate the presence of dementia of the vascular type (DVaT) (63,87). Using these characteristic SPECT rCBF patterns new automated techniques for analysing cerebral blood flow scans are being developed with the goal of obtaining an objective and accurate method of analysis to enhance the diagnostic performance of this procedure.

A number of automated methods have been reported in the literature (42,63,79,85,87-91), with some spectacular results (sensitivity and specificity in some studies of 85-95%) but most have relied on testing their methods using patients fulfilling strict clinical criteria

and in whom diagnositic probability was already high. Those studies less restrictive with their patient groupings have found more mediocre sensitivity and specificity of a diagnosis based purely on neuroimaging information (sensitivity and specificity of 43-60% and 60-75% respectively (92-94)). However, these less successful methods although correct in their patient selection used conventional ROI methods of reporting and did not take full advantage of the extensive and sophisticated image analysis packages currently available free from the internet or commercially (SPM96, MEDx3.0, Hermes) for this kind of study.

Very few of the studies listed above had post mortem confirmation of dementia type (with the exception of Bonte et al 1997 (90) and Jobst et al 1995 (85)) preferring instead to use the diagnosis given clinically at a follow up investigation of between 10 months and a few years after initial presentation of symptoms. The present study also lacks post mortem confirmation, however, it differs fundamentally from the other studies mentioned. Rather than using the new voxel-wise image analysis to improve correct diagnosis of dementia the method is being investigated for its potential as an aid to improve the consistency of visual interpretation of CBF scans between observers i.e. it assessed the *confidence* rather than the *correctness* of classifying scans.

Having established a set of working criteria for use with routine ^{99m}Tc-HMPAO SPECT scans, SPM96 was then applied to images of individual patients presenting with symptoms of dementia. The aims were:-

- To determine whether SPM maps could be produced which were consistent with the original scans.
- To ascertain whether they could assist in the reading of scans by reducing inter-rater variability.

4.2 Methods

4.2.1 Recruitment of Subjects.

Patients:- 39 patients who had been referred to the Institute of Neurological Sciences by "Old Age Psychiatrists" or Neurologists during the period April 1994 to December 1996 whose differential diagnosis included dementia, were recruited retrospectively for the purposes of this study. Ethics permission for the study was given by the Southern General Hospital-NHS Trust ethics committee. Scans of patients were included regardless of the results of initial investigation and therefore this unselected group was typical of those seen routinely in the department for diagnostic assessment of dementia. Initial examination included neuropsychological evaluation, neurological examination and ^{99m}Tc - HMPAO SPECT scan.

Controls:- In order to perform a voxel-wise statistical analysis on each patient a database of 32 (number of patients recommended for a reference data base - personal communication from Karl Friston, 02/12/97)[14] ^{99m}Tc HMPAO SPECT scans was constructed from archived scans of patients referred to the department for investigation between March 1993 and March 1998 whose SPECT scans were subsequently reported as normal and who had had no further history of neurological investgation. To account for systematic differences in rCBF due to age, of approximately 100 scans reviewed only scans of the 32 controls over the age of 45 were included. (age range 46-68). Other criteria for inclusion concerned the quality of the archived scans; images had to include the whole brain (from below the cerebellum to the top of the head) and low extra-cerebral uptake. To confirm no missed abnormalities in these scans we used a jackknife analysis (63) of testing each scan against the rest of the normal group using SPM96. First, normal reference data were calculated from 31 subjects excluding one subject. SPM(t) maps of the excluded subject were then calculated in comparison to the normal reference data created from the rest of the normal controls. This procedure was repeated 32 times to generate individual SPM(t) maps for each normal control.

---

[14]SPM help-line http://www.mailbase.ac.uk/lists/spm/1997-12/0009.html

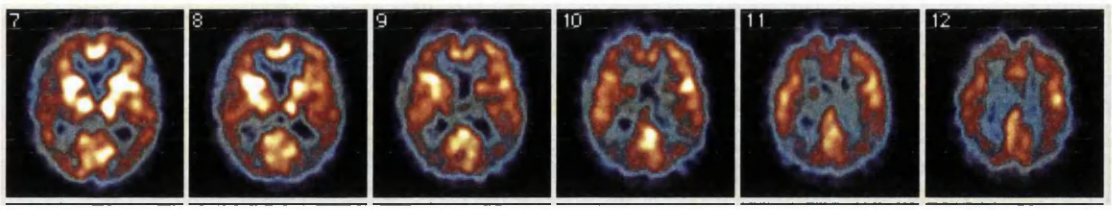

Dementia of the Alzheimer's Type (DAT) -
PL,pTL,(bilateral, occasionally unilateral) FL involved in advanced disease,

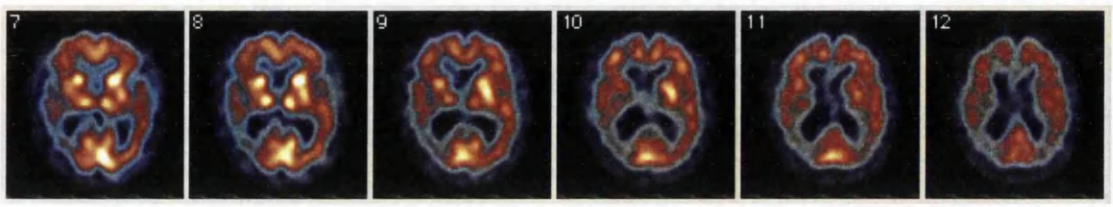

Dementia of the Alzheimer's Type (DAT) - asymmetrical defects

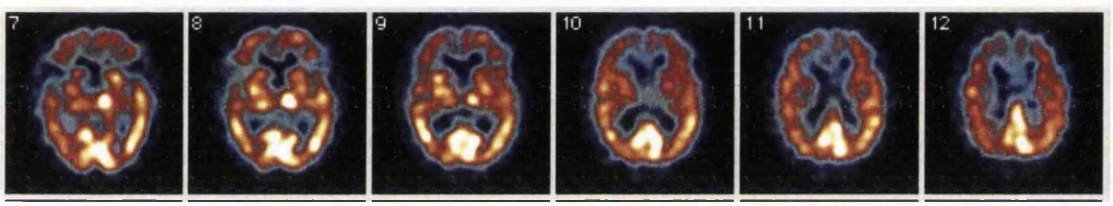

Dementia of the Frontal Lobe Type (DFLT) - Med, Lat iFL (bilateral, obvious atrophy) aTL (bilateral)

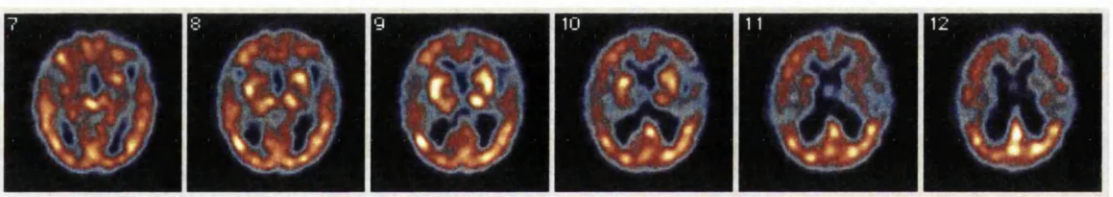

Dementia of the Vascular Type (DVaT) - Multiple small cortical perfusion defects, Clear MCA territory (usually the insula), Classic watershed region infarction.

iPL - Inferior parietal Lobe, pTL - posterior temporal lobe, iFL - inferior frontal lobe, aTL - anterior temporal lobe, Med - medial, Lat - lateral, MCA - middle cerebral artery, CBF - cerebral blood flow, SF - sylvian fissure.

Figure 4.1 shows axial slices of different ^{99m}Tc HMPAO scans of CBF to illustrate the guidelines used for the categorisation of dementia in terms of CBF pattern.

4.2.2 Data Analysis

Visual reporting:- Qualitative reporting was done using Strichman Medical Equipment display software, provided with the scanner, run on an Apple Macintosh computer, system 7.5 or less. Each scan was reconstructed and displayed on a colour monitor in axial slices at a thickness of 6mm. The SME software allows 3D manipulation of the data sets providing a manual adjustment facility, to allow axial slices to be resliced parallel to the plane through the anterior and posterior commisure for assessment. The colour scale used for display purposes is an 8bit scale with white representing maximum activity and blue/black representing minimum. During reporting the colour level was interactively manipulated by the observer. Following this review probabilities were assigned to each of the following diagnostic categories: dementia of the Alzheimer's type (DAT), dementia of the frontal lobe type (DFLT), dementia of the vascular type (DVaT), some other dementia e.g. Korsakoff's (other), normal (normal). The reading of the scans was assisted by comparison with an "ideal" ^{99m}Tc HMPAO SPECT scan and followed specific guidelines as described by Holman et al 1992 (77) and Talbot et al 1997 (78). (These guidelines are given in Figure 4.1. along with corresponding CBF SPECT data). The "ideal" scan (figure 4.2.) was constructed from 10 scans in the control database, spatially normalised to the PET template and then averaged to produce a mean normal scan. Images were interpreted by two independent observers, experienced in the interpretation of cerebral perfusion images of patients with dementia and normal control subjects, using the procedure described above and knowledgeable of the criteria for abnormality but without prior knowledge of the clinical data. The location and severity of the perfusion defects were noted and a percentage likelihood of final diagnosis as interpreted from the rCBF data was reported.

Image processing of individual SPECT data:- Image registration and smoothing was performed on each patient's scan. Any non-optimum starting estimates (see chapter 3) had to undergo a certain amount of image processing before statistical analysis could be performed. As defined by the results from the previous chapter (Chapter 3 -*Validation of the image standardisation facility of SPM96*), this involved a rigid body co-registration of

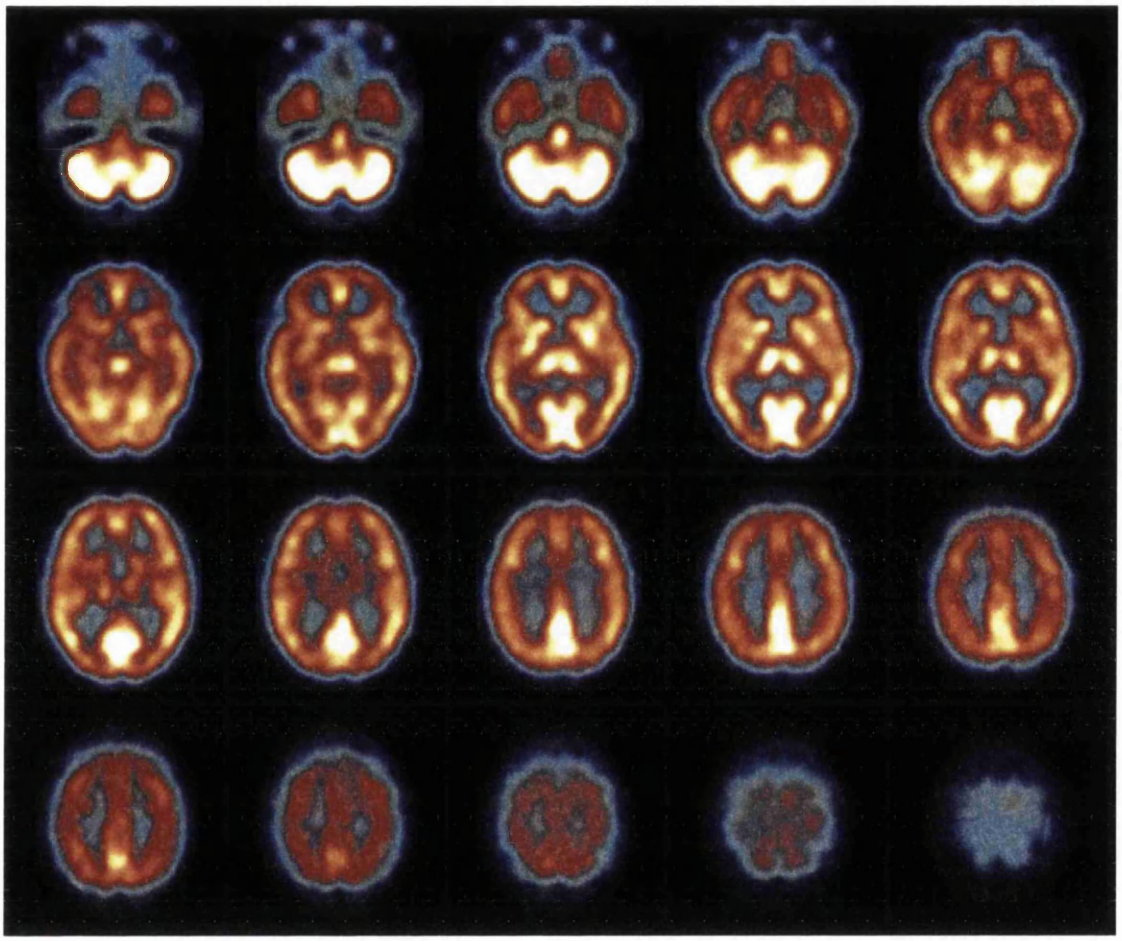

Figure 4.2. Average normal SPECT scan used for visual reporting, constructed from 10 scans in the control database, spatially normalised to the PET template and then averaged to produce a mean normal scan..

each of the non-optimal images to an "ideal" SPECT scan, prior to image standardisation. The co-registered and standardised images were then exported to a customised graphics package (mri3d) after smoothing so that partial axial slices could be edited to delete the spurious voxel information produced by smoothing of edges.

Voxel-wise statistical analysis:- Once the images had been edited the statistical option "compare groups, 1 scan per subject" available with the SPM96 statistics module was used to compare each individual patient data to a reference data base. These SPM(t) results were then used by the two observers in conjunction with the original scans to give a revised diagnostic estimate. To quantify the agreement between the 2 observers, a Kappa (K) statistic was calculated (95).

4.3 Results.

The results of the percentage differential diagnosis from each of the observers for the 39 patients are listed in appendix C. Some of these cases are described. Both the original CBF scan and the corresponding SPM(t) map are included to demonstrate how typical CBF patterns for the five dementia categories are represented in significance space (SPM(t)).

CASE 1

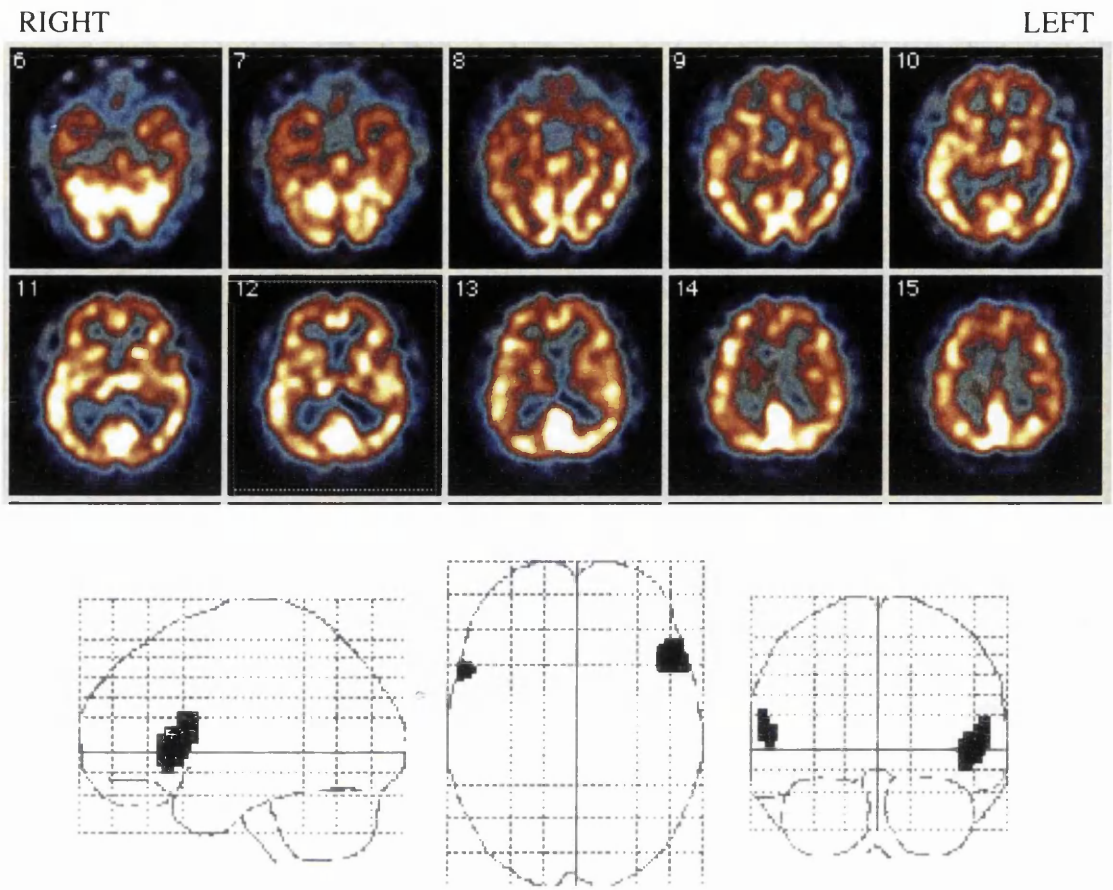

Figure 4.3 shows 10 axial slices from above and below the ac-pc line of a ^{99m}Tc-HMPAO scan acquired from a patient whose clinical differential diagnosis included dementia. Below this is the glass brain display of the results (SPM(t)) calculated by the SPM96 analysis option "compare groups; 1 scan per subject". The results are thresholded at Pu<0.001 and Pk<0.5 (uncorrected).

The case shown in figure 4.3 was originally reported by observer 1 (20% DVaT + 80% normal) and observer 2 (100% normal) based on the CBF SPECT scan information alone. This diagnosis remained unchanged with evidence from SPM(t) for observer 1 but changed for observer 2 (10% DVaT + 90% normal).

The small areas of reduced perfusion in the cortex located by the SPM(t) map are in the area of the insula in both hemispheres. This area is often implicated in cases of cerebral vascular disease which is why observer 1 and 2 reported the possible presence of DVaT from evidence provided by the SPM(t).

CASE 2

RIGHT LEFT

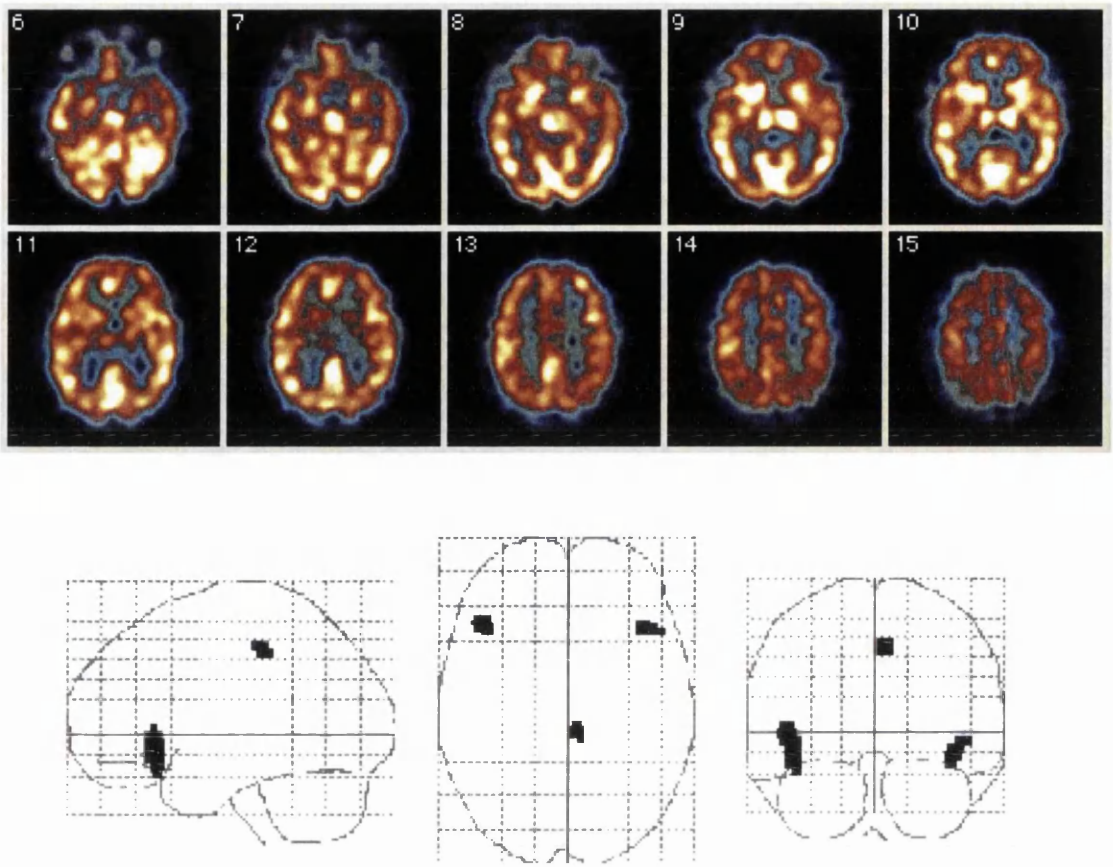

Figure 4.4 shows 10 axial slices from above and below the ac-pc line of a ^{99m}Tc-HMPAO scan acquired from a patient whose clinical differential diagnosis included dementia. Below this is the glass brain display of the results (SPM(t)) calculated by the SPM96 analysis option "compare groups; 1 scan per subject". The results are thresholded at Pu<0.001 and Pk<0.5 (uncorrected).

The case shown in figure 4.4 was originally reported by observer 1 (100% normal) and observer 2 (100% normal) based on the CBF SPECT scan information alone. This diagnosis remained unchanged with evidence from SPM(t) for observer 1 but changed for observer 2 (10% DVaT + 90% normal).

The small areas of reduced perfusion in the cortex located by the SPM(t) map are in the area of the insula in both hemispheres. Again this prompted observer 2 to report the possible presence of DVaT from evidence provided by the SPM(t).

CASE 3

RIGHT LEFT

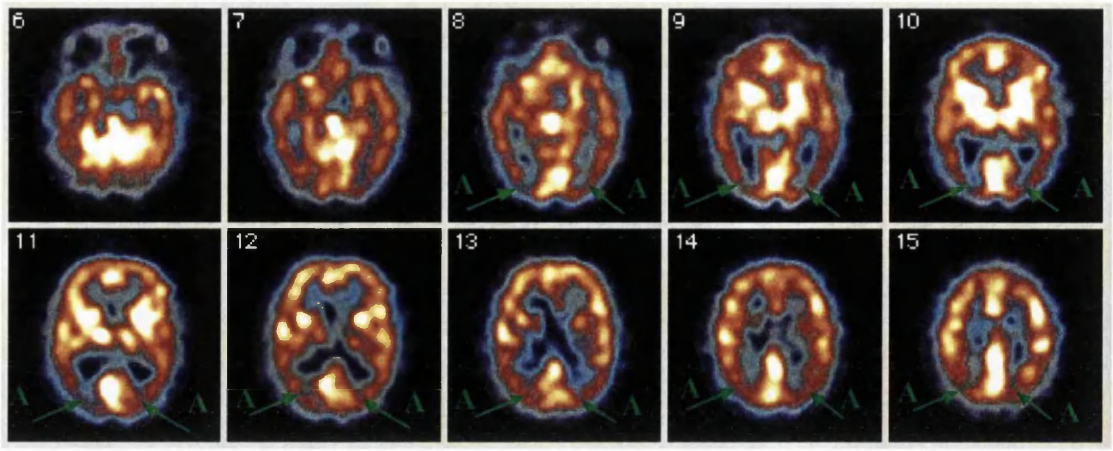

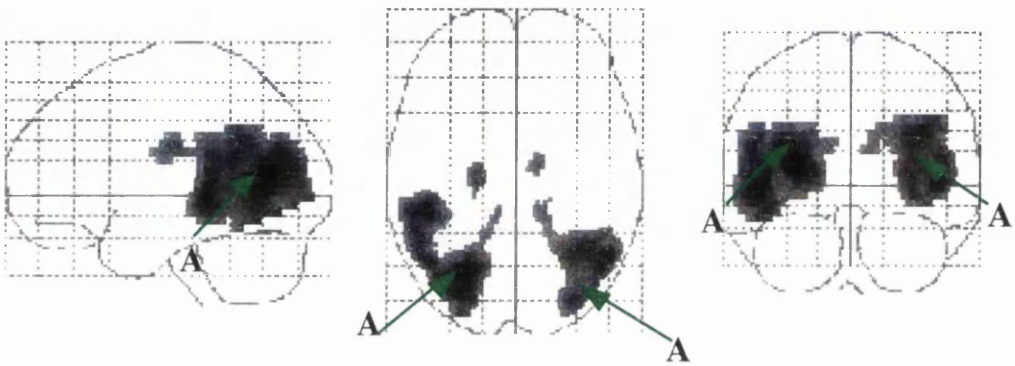

Figure 4.5 shows 10 axial slices from above and below the ac-pc line of a ^{99m}Tc-HMPAO scan acquired from a patient whose clinical differential diagnosis included dementia. Below this is the glass brain display of the results (SPM(t)) calculated by the SPM96 analysis option "compare groups; 1 scan per subject". The results are thresholded at Pu<0.001 and Pk<0.5 (uncorrected).

The case shown in figure 4.5 was originally reported as DAT by observer 1 (100%) and observer 2 (100% DAT) based on the CBF SPECT scan information alone. This diagno sis was confirmed with evidence from SPM(t) with observer 1 (100% DAT) and observer 2 (100% DAT).

Areas of reduced perfusion in the cortex evident in the CBF SPECT scan that match up with areas located by the SPM(t) map are labelled with green arrows (A). These areas are the parietal lobes (A) with the right hemisphere being slightly worse than the left and are consistent with areas associated with DAT reported by other imaging studies.

CASE 4

RIGHT **LEFT**

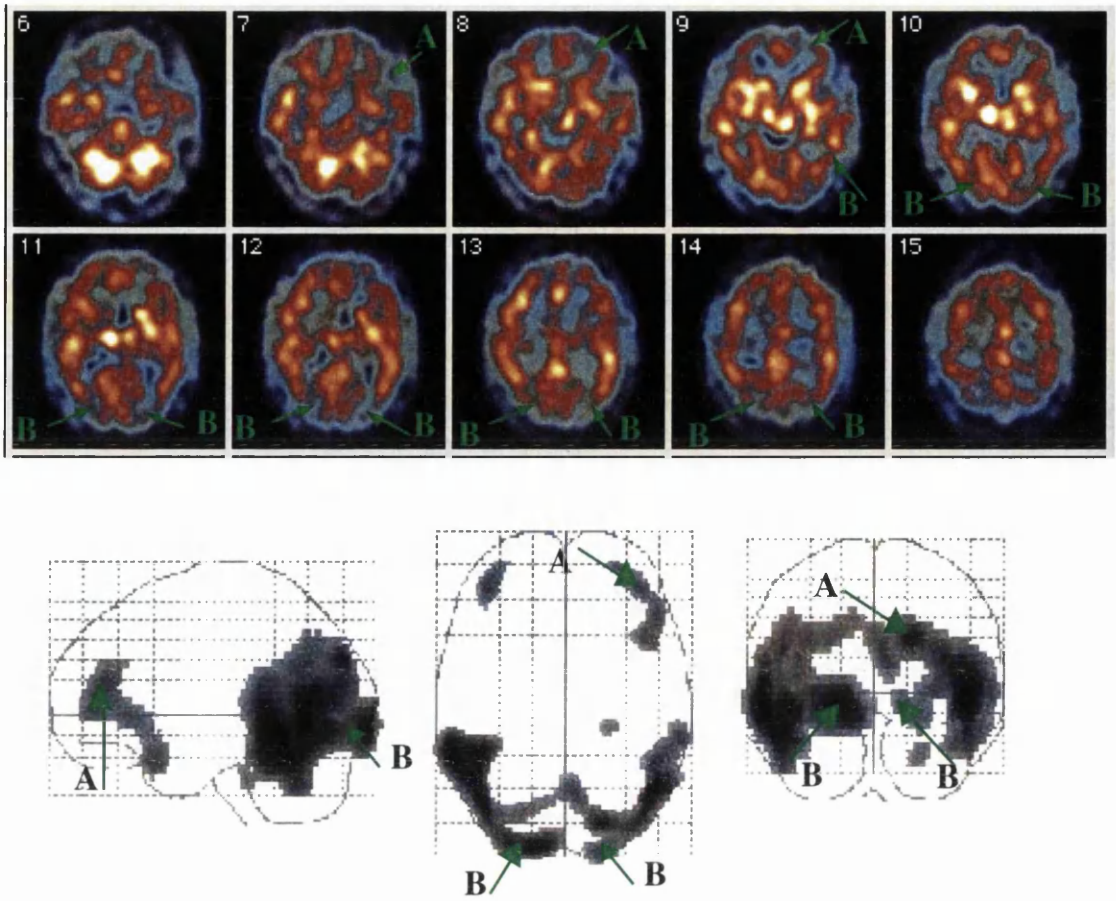

Figure 4.6 shows 10 axial slices from above and below the ac-pc line of a ^{99m}Tc-HMPAO scan acquired from a patient whose clinical differential diagnosis included dementia. Below this is the glass brain display of the results (SPM(t)) calculated by the SPM96 analysis option "compare groups; 1 scan per subject". The results are thresholded at Pu<0.001 and Pk<0.5 (uncorrected).

The case shown in figure 4.6 was originally reported by observer 1 (30% DAT + 10% DFLT + 30% DVaT + 30% other) and observer 2 (40% DAT + 20% DFLT + 20% DVaT + 20% other) based on the CBF SPECT scan information alone. This diagnosis was later changed, with evidence from SPM(t), to 90% DAT + 10% DVaT by both observers.

Areas of reduced perfusion in the cortex evident in the CBF SPECT scan that match up with areas located by the SPM(t) map are labelled with green arrows (A,B). These areas are the frontal lobe(A) and bilateral parietal lobes (B) and are consistent with areas associated with DAT reported by other imaging studies. Reduced perfusion in the frontal lobes has been reported in later stages of the disease.

CASE 5

RIGHT LEFT

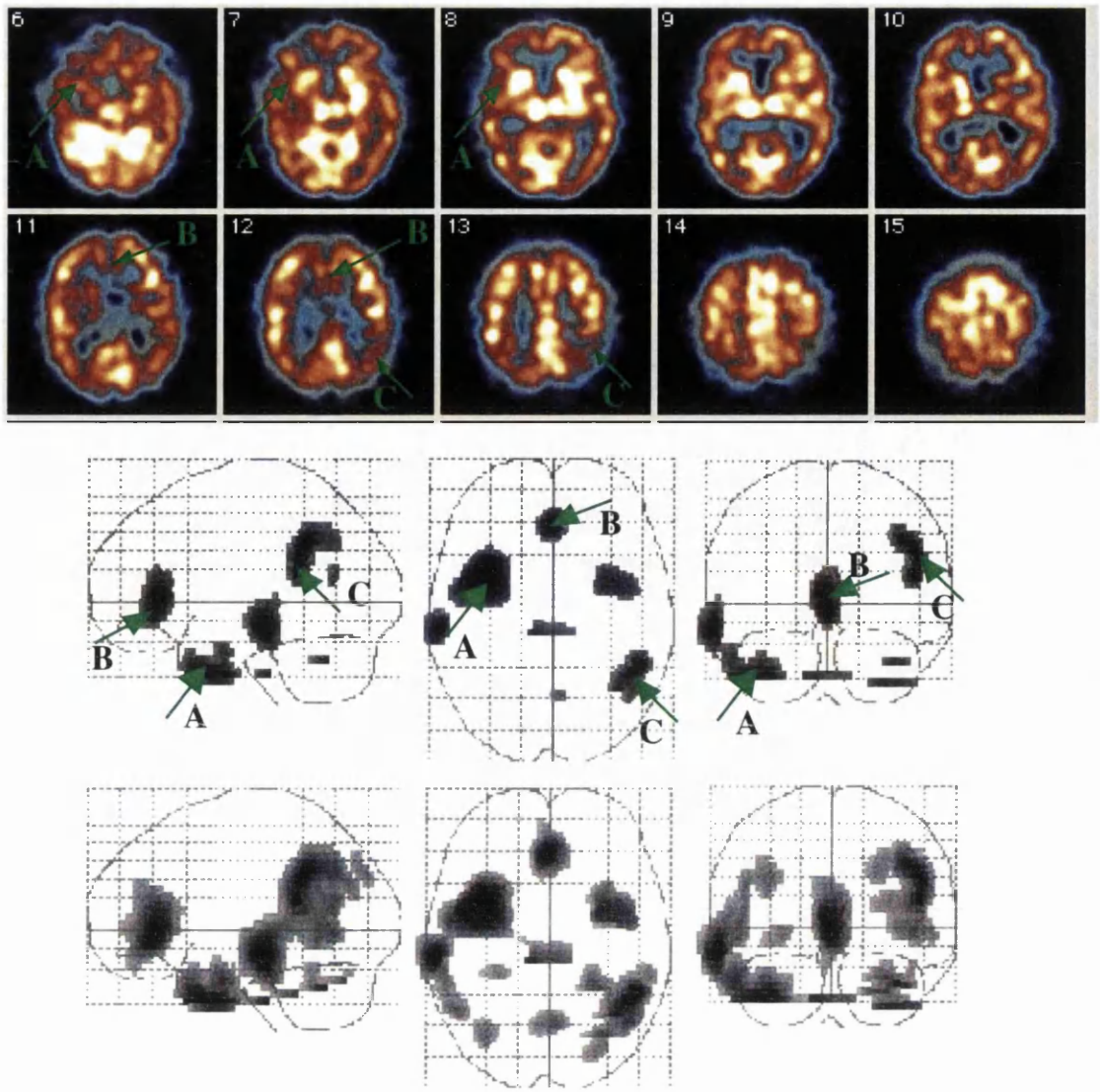

Figure 4.7 shows 10 axial slices from above and below the ac-pc line of a ^{99m}Tc-HMPAO scan acquired from a patient whose clinical differential diagnosis included dementia. Below this is the glass brain display of the results (SPM(t)) calculated by the SPM96 analysis option "compare groups; 1 scan per subject". The results are thresholded at Pu<0.001 and Pk<0.5 (uncorrected) in the first row and then Pu<0.01 and Pk<0.5 (uncorrected) in the second row..

The case shown in figure 4.7 was originally reported as DAT by observer 1 (100%) and observer 2 (90% DAT + 10% DVaT) based on the CBF SPECT scan information alone. This diagnosis was confirmed with evidence from SPM(t) with observer 1 (90% DAT + 10% DVaT) and observer 2 (95% DAT + 5% Normal).

Areas of reduced perfusion in the cortex evident in the CBF SPECT scan that match up with areas located by the SPM(t) map are labelled with green arrows (A,B,C). These areas are the medial temporal lobe(A), anterior cingulate (B) and parietal lobe (C) and are consistent with areas associated with DAT reported by other imaging studies.

CASE 6

RIGHT LEFT

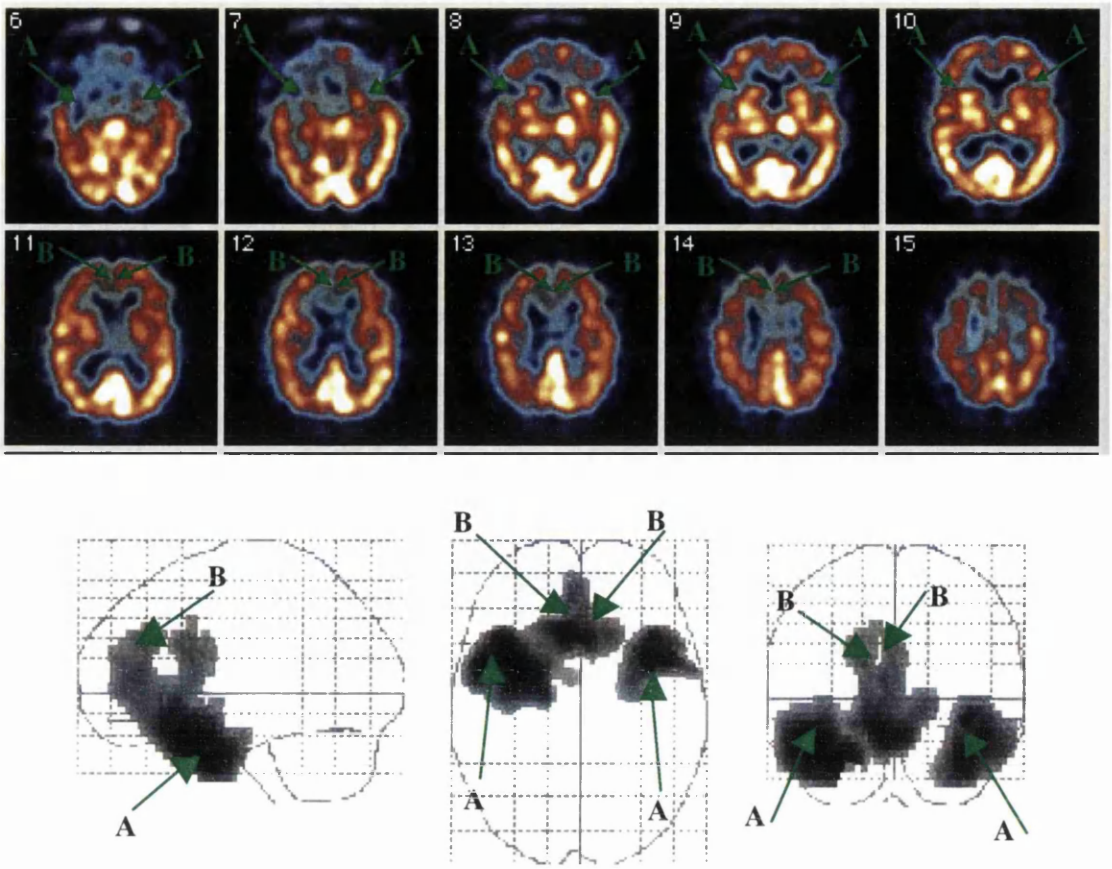

Figure 4.8 shows 10 axial slices from above and below the ac-pc line of a ^{99m}Tc-HMPAO scan acquired from a patient whose clinical differential diagnosis included dementia. Below this is the glass brain display of the results (SPM(t)) calculated by the SPM96 analysis option "compare groups; 1 scan per subject". The results are thresholded at Pu<0.001 and Pk<0.5 (uncorrected).

The case shown in figure 4.8 was originally reported by observer 1 as 90% DFLT + 10% DAT and observer 2 as 100% DFLT based on the CBF SPECT scan information alone. This diagnosis was later changed with evidence from SPM(t) with observer 1 (90% DFLT + 10% DAT) and observer 2 (30% DFLT + 70% DVaT).

Areas of reduced perfusion in the cortex evident in the CBF SPECT scan that match up with areas located by the SPM(t) map are labelled with green arrows (A, B). These areas are the anterior temporal lobes (A) - the right is worse than the left - and the anterior cingulate(B) and are consistent with areas associated with DFLT reported by other imaging studies.

CASE 7

RIGHT LEFT

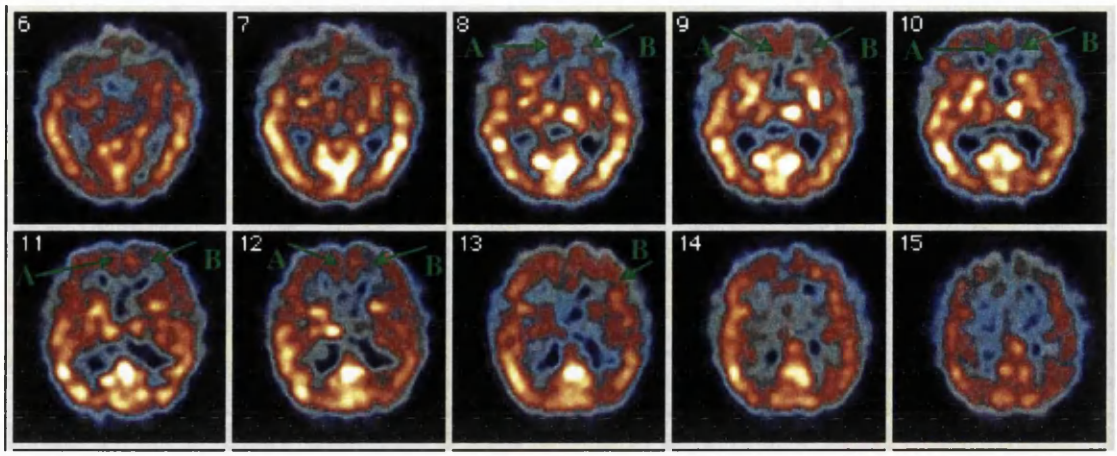

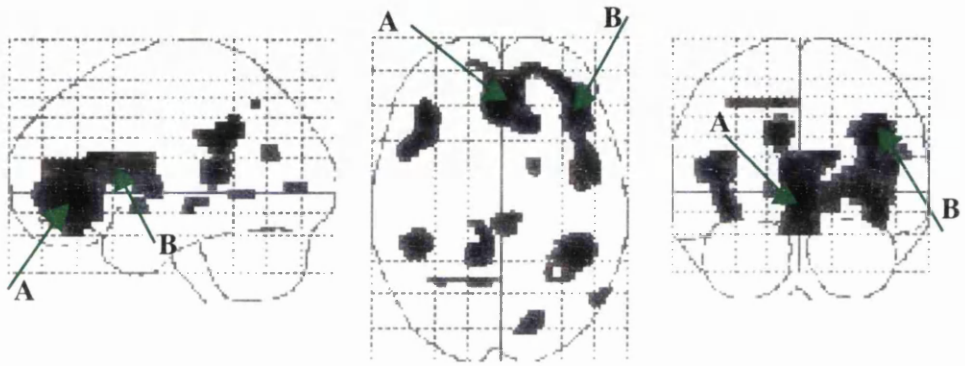

Figure 4.9 shows 10 axial slices from above and below the ac-pc line of a ^{99m}Tc-HMPAO scan acquired from a patient whose clinical differential diagnosis included dementia. Below this is the glass brain display of the results (SPM(t)) calculated by the SPM96 analysis option "compare groups; 1 scan per subject". The results are thresholded at Pu<0.001 and Pk<0.5 (uncorrected).

The case shown in figure 4.9 was originally reported as DFLT by observer 1 (100%) and observer 2 (60% DFLT + 20% DVaT + 20% other) based on the CBF SPECT scan information alone. This diagnosis remained unchanged with evidence from SPM(t).

Areas of reduced perfusion in the cortex evident in the CBF SPECT scan that match up with areas located by the SPM(t) map are labelled with green arrows (A,B). These areas are the anterior cingulate (A), and left frontal lobe (B) and are consistent with areas associated with DFLT reported by other imaging studies.

CASE 8

RIGHT LEFT

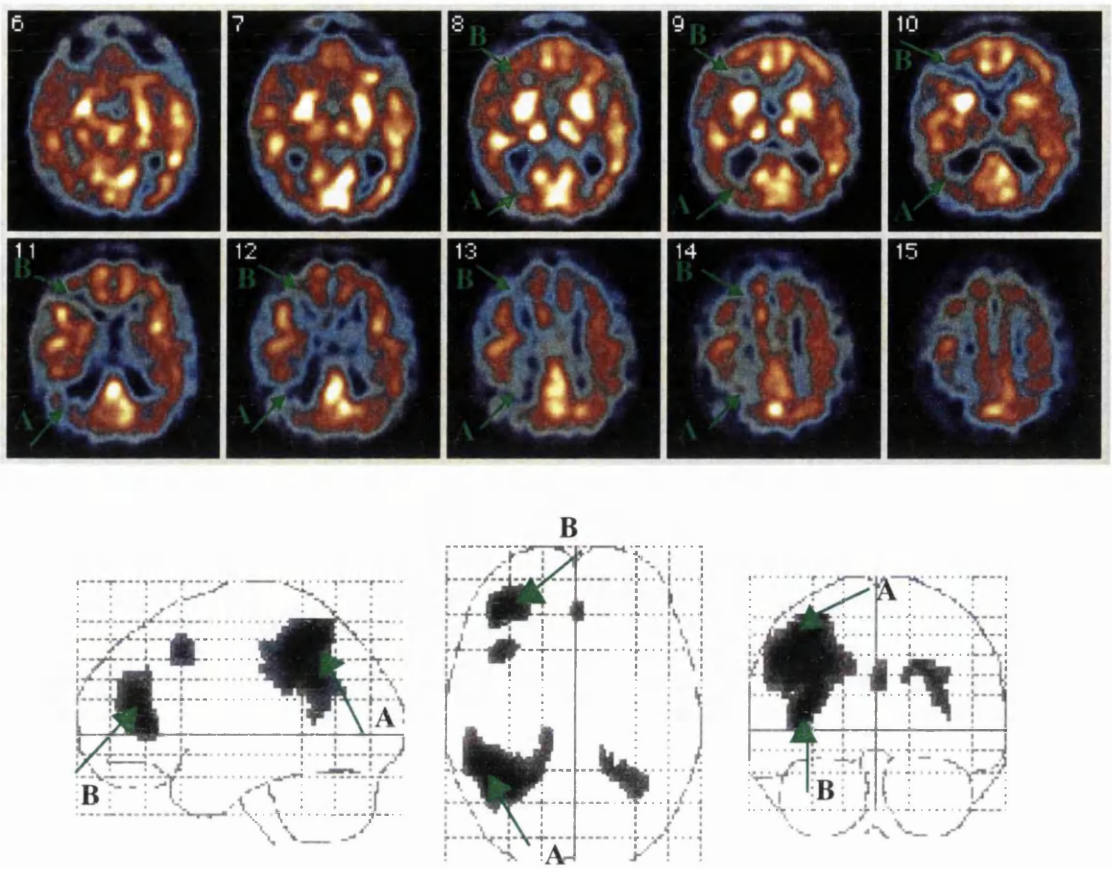

Figure 4.10 shows 10 axial slices from above and below the ac-pc line of a ^{99m}Tc-HMPAO scan acquired from a patient whose clinical differential diagnosis included dementia. Below this is the glass brain display of the results (SPM(t)) calculated by the SPM96 analysis option "compare groups; 1 scan per subject". The results are thresholded at Pu<0.001 and Pk<0.5 (uncorrected).

The case shown in figure 4.10 was originally reported as DVaT by observer 1 (100%) and observer 2 (100% DVaT) based on the CBF SPECT scan information alone. This diagnosis remained unchanged with evidence from SPM(t).

Areas of reduced perfusion in the cortex evident in the CBF SPECT scan that match up with areas located by the SPM(t) map are labelled with green arrows (A, B). These areas are the right parietal lobe (A), and right anterior frontal lobe (B). Their appearrance is consistent with that associated with DVaT reported by other imaging studies.

CASE 9

RIGHT LEFT

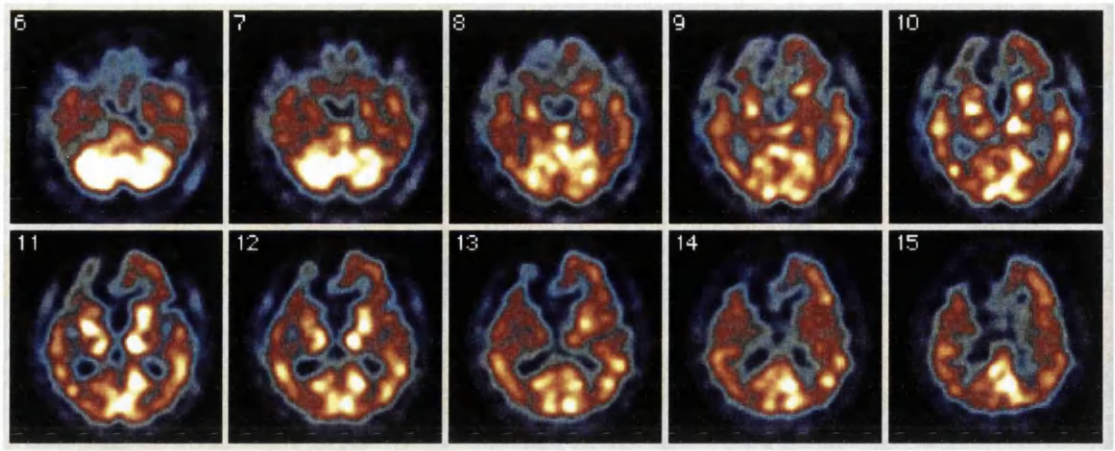

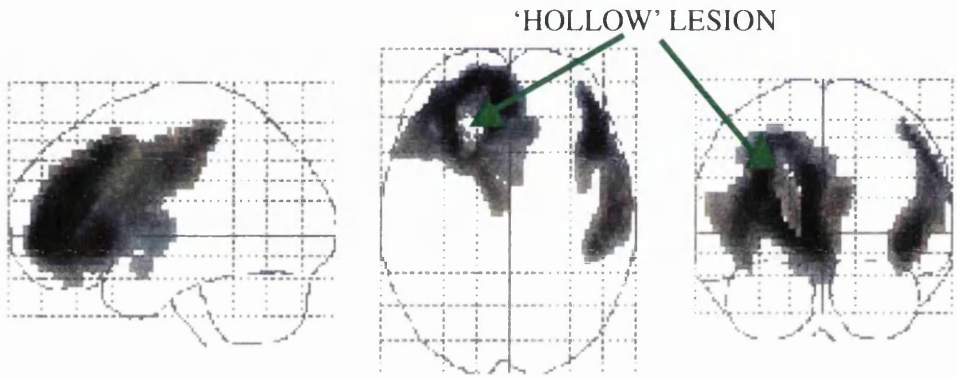

Figure 4.11 shows 10 axial slices from above and below the ac-pc line of a ^{99m}Tc-HMPAO scan acquired from a patient whose clinical differential diagnosis included dementia. Below this is the glass brain display of the results (SPM(t)) calculated by the SPM96 analysis option "compare groups; 1 scan per subject". The results are thresholded at Pu<0.001 and Pk<0.5 (uncorrected).

The case shown in figure 4.11 was originally reported by observer 1 and observer 2 (100% DVaT) based on the CBF SPECT scan information alone. This diagnosis remained unchanged with evidence from SPM(t).

The area of reduced perfusion in the cortex is the site of the main cerebral infarction in the right frontal lobeand is clearly visible in the SPM(t) map. This case is a good example of how the thresholding facility that SPM96 uses to include only intra-cerebral voxel values can fail. In this case the values of the voxels representing the infarct have such a low value they are not included in the statistical analysis and this results in the lesion looking 'hollow' on the SPM(t) map (green arrow).

CASE 10

RIGHT LEFT

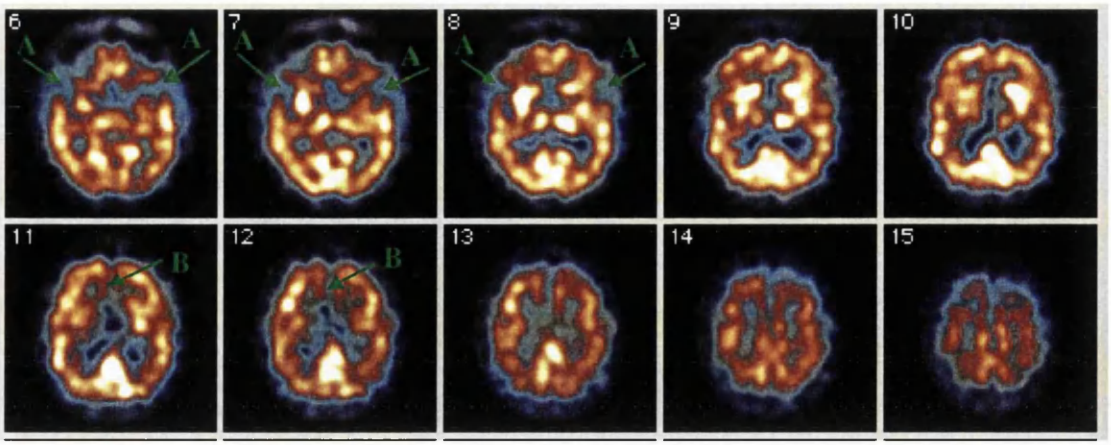

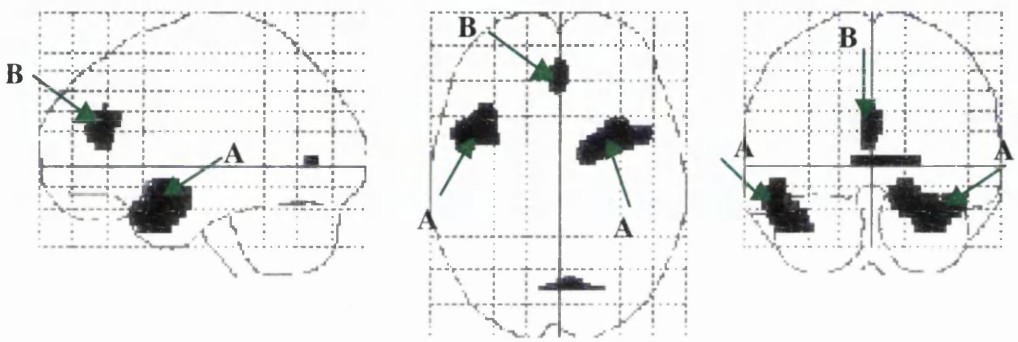

Figure 4.12 shows 10 axial slices from above and below the ac-pc line of a ^{99m}Tc-HMPAO scan acquired from a patient whose clinical differential diagnosis included dementia. Below this is the glass brain display of the results (SPM(t)) calculated by the SPM96 analysis option "compare groups; 1 scan per subject". The results are thresholded at Pu<0.001 and Pk<0.5 (uncorrected).

The case shown in figure 4.12 was originally reported by observer 1 (60% DVaT + 20% other + 20% normal) and observer 2 (20% DVaT + 80% normal) based on the CBF SPECT scan information alone. This diagnosis later changed with evidence from SPM(t) to observer 1 (20% DFLT + 60% DVaT + 20% other) and observer 2 (40% DVaT + 60% normal).

Areas of reduced perfusion in the cortex evident in the CBF SPECT scan that match up with areas located by the SPM(t) map are labelled with green arrows (A, B). These areas are the anterior parts of the temporal lobe bilaterally (A), and the inter-hemispheric fissure (B).

To quantify the agreement between the 2 observers for the two different reporting methods (visual and visual+SPM96), a Kappa (K) statistic was calculated and is defined as :

$$K = (Po - Pe)/(1 - Pe) \quad (2)$$

where Po = observed proportional agreement, Pe = chance proportional agreement which includes a correction for the fraction of agreements expected by chance. K=1 only when complete agreement is observed. Interpretation of the level of agreement is as follows; 0.0 - 0.2, slight; 0.2 - 0.4, fair; 0.4 - 0.6, moderate; 0.6 - 0.8, substantial, and 0.8-1.0, almost perfect. Values below zero represent less agreement than expected by chance. The K statistic was computed for between observers agreement of visual reporting of ^{99m}Tc HMPAO SPECT scans before and after SPM96 revised reporting. The K statistic was calculated by categorising the diagnosis with the highest score (and reassigned a value of one) to be taken as the actual diagnosis for each patient (see appendix C). The K statistic for this overall assessment is listed in the first row of Table 4.1.

Disease	observer1 /observer 2	observer1* /observer2*
+overall	0.584	0.507
DAT	0.593	0.543
DFLT	0.682	0.4
VD	0.591	0.498
normal	0.54	0.53

Table 4.1 . Lists the measured agreement between observers.
+ overall kappa statistics where the highest score in a diagnostic category was assumed to be the actual diagnosis and given a value of one.
* using SPM96 results.

K = Kappa 0-0.2 poor, 0.2-0.4 fair, 0.4-0.6 moderate, 0.6-0.8 Good, 0.8-1.00 very good.

The weakness of this calculation is that it takes no account of the degree of disagreement since all disagreements are treated equally. Instead a weighted Kappa statistic can be calculated where observations near to the diagonal, representing a difference of only one category, are considered less serious than those where a discrepancy is two or more

categories. A weighted K statistic was calculated for the agreement between observers for each disease category and are listed in full in appendix C. Results for this test are shown in table 4.1 rows 2-4 and give similar values to that obtained from the overall measure. In all categories the level of agreement is lowered when using additional information from the SPM96 analysis.

The likelihood of diagnosis for each subject given by observer 1 and observer 2 for both methods of reporting are listed in appendix C along with the kappa tables and calculations used to calculate the levels of agreement between the observers.

4.4 Discussion

Before SPM(t) maps could be calculated for each individual patient a normal database had to be constructed. Official bodies responsible for monitoring the administration of radioactive substances are understandably keen to keep unnecessary exposure of the general population to a minimum. It was therefore not possible to build "from scratch" a new database of ^{99m}Tc HMPAO scans of the normal general population. Instead the database was constructed from archived scans of patients referred to the department from neurologists and psychiatrists for the investigation of suspected transient ischaemic attacks (TIA) and mild memory problems, between March 1995-March 1998 but whose SPECT scans were subsequently reported as normal. Justification of this method is needed. Apart from ensuring that the scans included in the database were from individuals who were not subsequently found to have any abnormality a jackknife type method (63) of testing each scan against the rest of the normal group using SPM96 was used to check for rCBF abnormalities that may have been missed by visual reporting (there were none). Other criteria for a scan's inclusion in the database included low extra cerebral uptake and good coverage of brain including cerebellum.

Further justification for this method of constructing a normal database is obtained by reference to the more usual approach of advertising (both internally and externally) for volunteers. In this situation we were able to examine retrospectively each scan initially

reported as normal. There was no bias from the subjects themselves for their reason to be included in the study. One has to question the reasons why an individual would volunteer themselves as subjects. Family members of patients who wish to contribute whatever they can to help their suffering relative are few and far between. It is more likely that those presenting themselves as subjects are concerned about their own physical and mental health. Only after a lengthy battery of tests, which all subjects recruited for a study must undergo, can those subjects who are genuinely worried and may turn out to be "not normal" be weeded out. Using this method of retrospective selection we were better able to establish a representative database of normal CBF scans from our own archives without incurring the difficulties involved in subject recruitment.

To account for the global differences in cerebral perfusion across subjects it is necessary to globally normalise the voxel intensities within an image. There are two options for doing this in SPM96; AnCova and proportional scaling (see CH2 pg47). For the purposes of this study the proportional scaling method was used in preference to AnCova since use of the latter method with data where similar global uptake of the radiopharmaceutical cannot be guaranteed is not recommended. In our control group the mean global counts ranged from 61.2 to 123.3 and in the patients 33.8 to 128.5. The proportional scaling method of accounting for global CBF differences uses whole brain as the reference region to which to normalise. Other reference regions commonly used include, calcarine cortex, cerebellum, thalamus and basal ganglia (42,63,88,96). Although the SPM96 proportional scaling normalisation facility does not allow other reference regions to be defined it is possible (using MATLAB scripts, courtesy of MG)[15] to pre-normalise the data prior to SPM analysis and then switch off the normalisation facility within SPM96. It was decided however, that this would not be appropriate and that global mean value would be used as the normalisation factor for two reasons. Firstly, the cerebellum could be rejected as suitable reference regions quite simply because in some of the images all or part of this information was missing and in one

[15] Dr Mike Glabus Neurophysicist, MRC Brain Metabolism Unit, Royal Edinburgh Hospital, Edinburgh, EH10 5HF, UK.

image the lower part of the calcarine cortex was missing. Secondly, normalising to the thalamus and basal ganglia while adequate for assessment of DAT, since these areas are relatively spared in the progression of the disease, would not always be appropriate in the case of DVaT. For example, small infarcts in the perforators branching from the middle cerebral artery will almost certainly result in lowered perfusion in the thalamus. Minoshima et al 1995 (63), Bartenstein et al 1997 (42) make allowances for this by only using the higher value thalamic activity from either hemisphere. However, this would need apriori knowledge of the disease state which would have been unacceptable for the purposes of this study.

The results from this study failed to show that SPM could improve/enhance the interpretation of CBF scans as an aid in the differential diagnosis of dementia. The study results of the inter observer reliability (overall agreement measured K= 0.584 and K_{spm}=0.504) in fact show a slight decrease in overall agreement between the observers. This was also reflected in the measurements made using the weighted kappa statistic for each disease category. Although SPM aided reporting seemed to increase the amount of disagreement between observers overall, anecdotal evidence from both the observers suggested that the SPM(t) maps strengthened the confidence of the initial percentage probability diagnosis based on evidence from the scan alone and therefore speeded up the process of visually reporting the scans. In addition further inspection of the results of CBF SPECT scans and their associated SPM(t) maps from 10 cases out of the original 39 shows that the SPM analysis was robust in detecting blood flow abnormalities in the cerebral cortex but that the interpretation of these maps by the two observers could be different. It is useful to study these cases in more detail.

Case 1 and 2 are good examples of the CBF SPECT scans that were reported normal on visual inspection alone. The SPM(t) map detects areas of reduced perfusion (with respect to the reference group) in the insula for both scans, an area often implicated in cases of cerebral vascular disease. Looking at the scans again it is clear that there is a widening of the left sylvian fissure for case 1 and bilaterally in case 2. This may have been initially

dismissed as localised atrophy in this area consistent with the patients' age but other studies using SPM have confirmed that relative blood flow deficits detected in this way cannot be attributed solely to the effects of atrophy (97). The SPM results confirmed observer 1's suggestion that DVaT may be present in case1 and introduced the possibility of DVaT in case 2. Observer 2 had originally reported both scans as 100% normal but introduced the possibility of DVaT on evidence from the SPM(t) for both case 1 and 2.

Case 3 was originally reported as 100% DAT by both observers and remained unchanged with the evidence from the SPM(t). This result is interesting because neither the CBF SPECT scan or the SPM(t) show any evidence of reduced blood flow in the area of the medial temporal lobe an area associated with structural abnormalities detected in CT and MRI as decreases in the thickness of the cortex (85). This absence of medial temporal lobe reduced perfusion has also been recently reported by a study using PET with 2(^{18}F)FDG to examine the differences between normal controls and patients with probable mild DAT (98,99).

Case 4 is a good example of how an SPM analysis can help in some particular cases where the diagnosis based on the CBF SPECT scan remains equivocal. Initially this scan was reported by both observers of having an almost equal likelihood of any of the dementias [obs1 - (30% DAT, 10% DFLT, 30% DVaT, 30% other) obs 2 - (40% DAT, 10% DFLT, 20% DVaT and 30% other)]. The evidence from the SPM(t) map for this case shows significant reductions in the parieto-temporal regions and a slight reduction in the medial temporal area, all implicated in DAT and making the likelihood of DAT much more probable (90%). The patchy appearance of the rest of the cortex, however, also suggests the presence of DVaT superimposed on the classic DAT pattern reflected by both observer 1 and observer 2 including it as a possible diagnosis (10%).

Case 5 was originally reported as a definite case of DAT with the suggestion of the presence of DVaT by observer 2. The SPM(t) map, however, shows much smaller numbers of voxels with significant reduction in the parieto-temporal regions evident in the

previous two cases, although the abnormalities in the SPECT scan are quite clearly located in the map. This SPM(t) map was re-thresholded at a lower significance of $P_u<0.01$ ($P_k<0.5$) and the classic DAT pattern in CBF became more apparent. This case highlights the problems that may occur should an SPM(t) map be used without the original evidence from the CBF scan and without the appreciation of the various parameters that can be adjusted within SPM96. If an SPM analysis is to be used to assess the CBF pattern in an individual patient, as confirmation of an already suspected diagnosis, a choice should be made as to what significance threshold should be used. The developers of SPM provide the guidelines that, the results of an apriori hypothesis can be thresholded at $P_u<0.01$ and $P_k=1.00$ but that an exploratory investigation must always be displayed at a higher threshold of $P_u<0.001$ and $P_k<0.5$. Interpreting these guidelines for the SPM analysis of an individual patient's scan, rather than for studies of neuroactivation, where groups of scans are analysed together and the changes in blood flow being measured are only a few percent, choosing a less strict threshold would seem valid. In some cases however, if the blood flow deficit is very widespread an SPM(t) map at this level would show almost all the voxels analysed as being significant and therefore, hide any predominant pattern. It is more appropriate in this case to use a higher significance level. This might give the impression that the choice is arbitrary but the guideline should be:-

- if the possibility of false negatives is to be minimised then a lower threshold should be used,
- if this results in too many voxels being significant and so obscuring localised information within the SPM(t) map then a more stringent threshold should be applied.

Cases 6 and 7 were both initially reported as DFLT based on the CBF SPECT scan information alone. For case 6 the SPM(t) map quite clearly shows the perfusion deficits in the anterior cingulate and anterior parts of the temporal lobe both areas are consistent with that reported in the literature (100). This result confirmed the diagnosis for observer 1 but caused observer 2 to change the definite DFLT diagnosis to possible DVaT (70%),

highlighting that the lack of agreement between the two observers is not that the abnormalities are not being detected by them and the SPM analysis but rather it is dependent on the interpretation of this information. In the SPM(t) map of Case 7 again there is a good correspondence between the abnormalities seen in the cortex and those detected by SPM, confirming the original diagnosis for both observers.

Case 8 and 9 are both examples of a definite diagnosis of DVaT quite clearly evident in the CBF SPECT scan of both patients and confirmed with evidence in the SPM(t) maps. Case 9 shows a good example of a particular problem inherent in SPM when measuring gross deficits in blood flow. As described in Chapter 2 pg47 a SPM analysis only includes what is considered to be intra-cerebral voxels. The voxel values within this lesion fall well below this threshold and are therefore not included in the analysis and as a result the lesion displayed looks hollow on the SPM(t) map. The way round this problem is to reset the threshold for intra-cerebral voxels using a facility in the SPM software. However, for the purposes of this study where the location of the lesion was more important than the size this step was not necessary. If, however, the SPM(t) map was to be used as a means of measuring the size of the lesion volume then the intra-cerebral voxel level would have to be reset and a sensible level would have to be determined.

Case 10 is a good example of where the diagnosis remained equivocal even after the information from the SPM(t) was made available. In the first instance both observers included the possibility of the presence of DVaT (60% and 20% respectively) based on the appearance of the insula regions in the SPECT scan which are often involved when infarcts occur in the middle cerebral artery. However, the blood flow deficits detected by the SPM analysis appears to put these areas more firmly in the anterior parts of the temporal lobe. The SPM(t) map also shows a deficit in the area of the anterior cingulate possibly reflecting the widening of the inter-hemispheric fissure clearly evident in the CBF SPECT scan. Perfusion deficits in both these areas have been described as typical of the CBF patterns seen in patients suffering from DFLT. While observer 1 still gave the most likely cause for this CBF pattern to be DVaT the possibility of DFLT (20%) was

also included based on the SPM(t) result. Observer 2 on the other hand, whose original diagnosis had been normal (80%) with the possible presence of DVaT (20%), increased the likelihood of vascular dementia as a diagnosis on the evidence from SPM(t) DVaT (40%) with normal (60%) remaining as the most likely diagnosis. As with case 6 the problem here is not whether this method of using SPM96 is capable of detecting blood flow deficits in the cortex of individual CBF SPECT scans but rather the observer's ability to use this information to make a diagnosis.

An SPM type analysis of individual patients clearly does not remove the observer variability in interpretation. These results may be interpreted therefore, not as the inability of the SPM method to find significantly abnormal regions of CBF - indeed the SPM(t) maps presented in the results section certainly confirm the validity of the SPM technique in detecting areas of abnormal cortical perfusion in individual patients - but rather in teRMS of the observers uncertainty in interpreting these patterns with respect to dementia type. It might be that in future each observer may have to ascend a learning curve with regard to the incorporation of information from a SPM(t) map to the routine visual reporting procedure. The "ideal" ^{99m}Tc HMPAO scan created for this study is now being routinely used to train junior radiologists and physicists in the visual reporting of CBF SPECT scans.

Finally it may be that an objective image analysis software of this kind could prove valuable as a way of monitoring the progress of a disease like dementia. Often it is difficult to visually interpret the amount of change that has taken place when comparing serial diagnostic scans of the same patient. The example in figure 4.13 shows the case of a patient whose consultant psycho-geriatrician requested a ^{99m}Tc HMPAO CBF SPECT scan for confirmation of DAT. The initial scan, without additional information from an SPM(t) map, was reported as normal taking into consideration the patient's age.

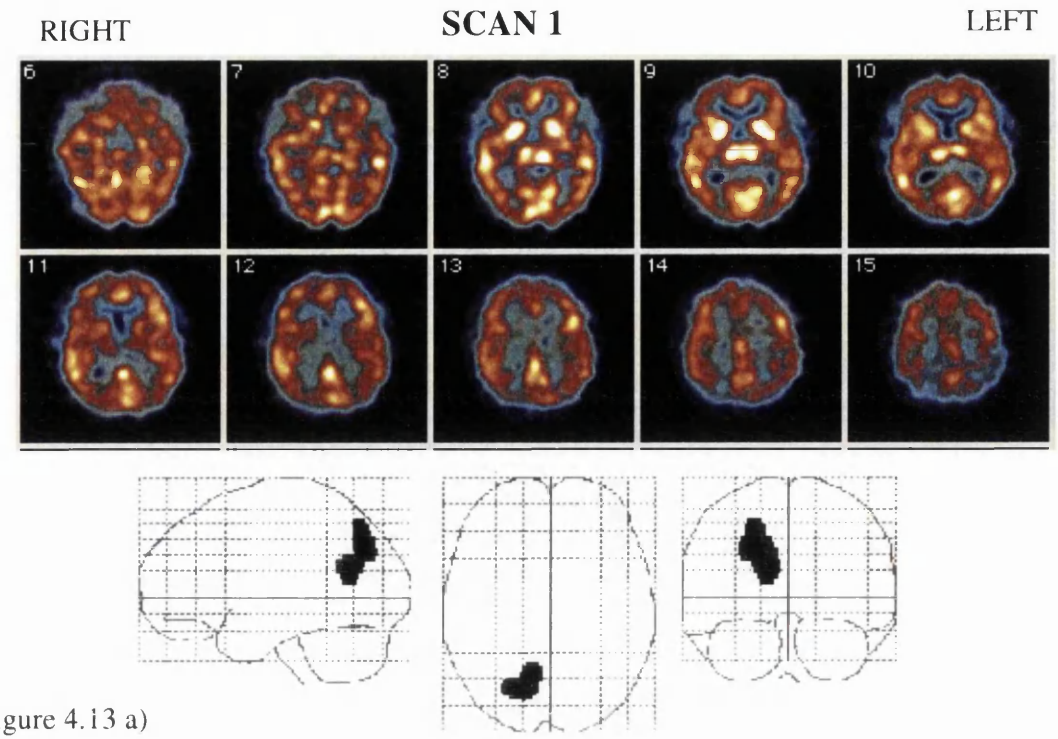

Figure 4.13 a)

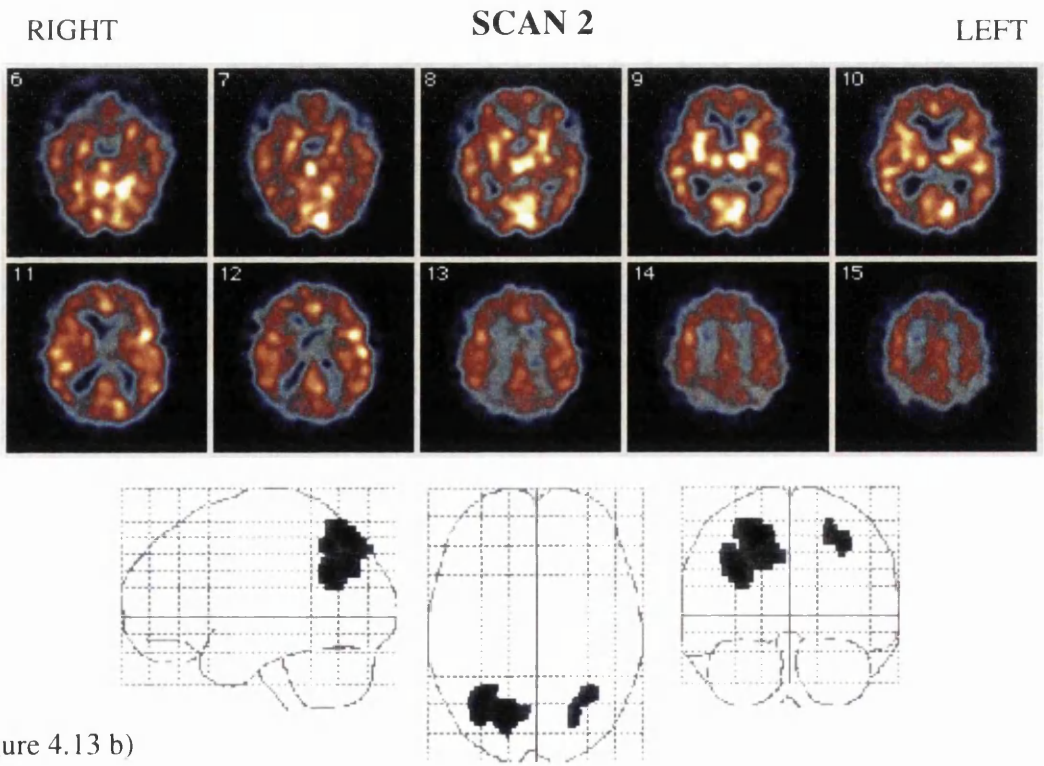

Figure 4.13 b)

Figure 4.13 a) and b) show 10 axial slices from above and below the ac-pc line of a ^{99m}Tc-HMPAO scan acquired from a patient whose clinical differential diagnosis included dementia taken 29 months apart. Below this is the glass brain display of the results (SPM(t)) calculated by the SPM96 analysis option "compare groups; 1 scan per subject". The results are thresholded at Pu<0.001 and Pk<0.5 (uncorrected).

However, the clinical symptoms became progressively worse and the patient was re-scanned at 29 months following. The visual reporting of both scans failed to confirm the presence of a progressive reduction in rCBF. On the basis of the results obtained using the SPM96 analysis on individual patients suffering from dementia it was reasoned that if an abnormality was present in either of the scans it would be detected and the number of significant voxels within the abnormality could be used to give an indication of the progression of the abnormality. Figure 4.13 shows two CBF SPECT scans of the same patient taken 29 months apart with their corresponding SPM(t) maps. The SPM analysis was able to detect an abnormality in the right parietal lobe (Zmax = 4.12 , no. of voxels = 421) in the original scan (figure 4.13a), an area associated with CBF patterns reported in patients with DAT clinical symptoms by other studies. Figure 4.13b shows that the SPM analysis confirmed the progression of the rCBF decrease located in the area of the right parietal lobe (Zmax = 4.61, no. of voxels = 788) and detected an additional abnormality in the left parietal lobe (Zmax = 3.65, no. of voxels = 110). The SPM(t) maps confirmed the progression of the rCBF decrease associated with progression of clinical symptoms of DAT. However, any changes observed between the two maps must be interpreted with caution as there is not yet sufficient data on the reproducibility of SPM(t) maps of ^{99m}Tc HMPAO scans of the same patient in the absence of physiological change. It is possible that a continuing clinical audit over many years, preferably involving histology, could be used to re-investigate the findings of this study to determine whether the additional SPM information shifted probabilities closer to the correct diagnosis.

4.5. Conclusions.

This investigation failed to show that there was any benefit to using an SPM96 analysis of individual patient data as an aid to the differential diagnosis of CBF SPECT scans. However, further use of this technique for the analysis of serial SPECT scans of a single patient provided evidence that the analysis may have potential for the objective monitoring of the progression of disease affecting blood flow in the cerebral cortex.

- There is no evidence to support the routine use of SPM96 at present in reporting CBF SPECT scans of dementia.

- SPM96 analysis of serial CBF SPECT scans of the same patient may provide an objective way of assessing for progression of disease when used in conjunction with both clinical and other imaging information.

CHAPTER 5

Modification of ^{99m}Tc HMPAO SPECT acquisition protocol for SPM type analysis of neuroactivation studies: Image quality versus statistical power.

This chapter describes the investigation to determine empirically whether an increase in statistical power, gained by using a scan replication paradigm, is significant enough to warrant the use of poorer image quality, due to decreased administered activity per scan, in neuroactivation studies. Section 5.1 describes the benefits of obtaining multiple images of a subject during one scanning session. Section 5.2 lists the materials and methods used for this investigation. Section 5.3 presents the results and section 5.4 and 5.5 discuss the implications and consequences of using a multiple scan paradigm with SPECT.

5.1 Introduction

These investigations focused on whether CBF SPECT studies of neuroactivation might benefit from an approach similar to that used in PET, i.e., increase the number of scans per task and accept poorer individual scan quality. When neuroactivation has been studied by emission tomography, PET (positron emission tomography) rather than SPECT (single photon emission computed tomography) has always been the modality of choice due to its higher sensitivity, better resolution and the shorter half life of [^{15}O] water which enables repeated measurements to be made. In practice up to 12 scans can

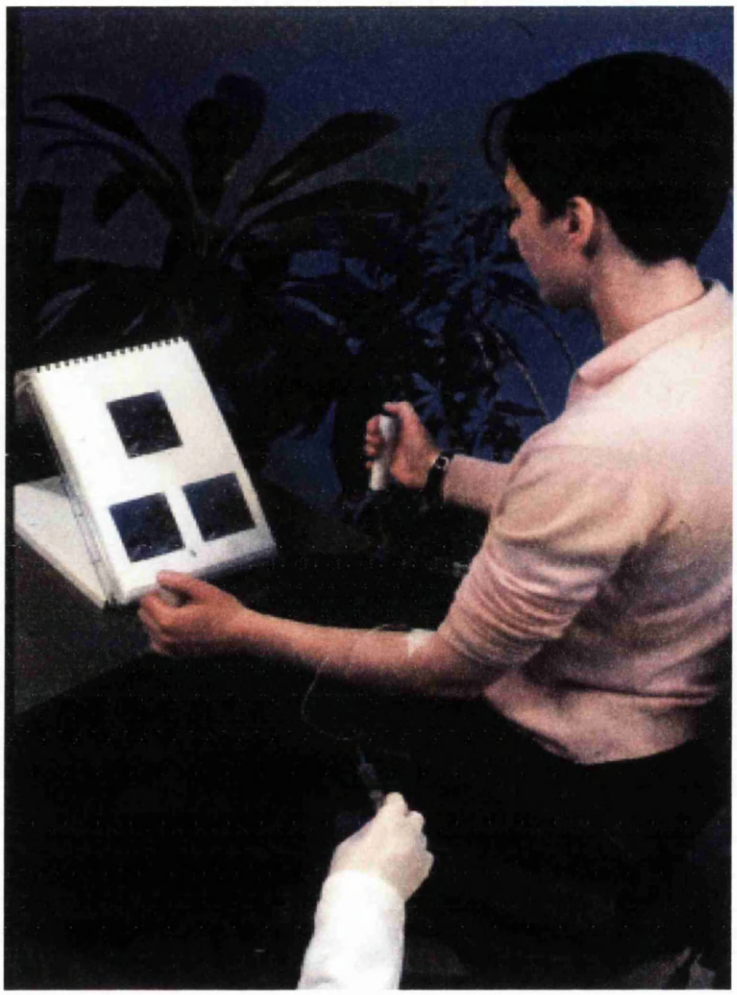

Figure 5.1 SPECT has its own unique features which make it attractive for neuroactivation work. In particular the trapping mechanism of the cerebral blood flow agents used in SPECT cerebral blood flow (CBF) studies provides the facility of performing tasks outwith the confines of the scanner in a more 'natural setting' as illustrated in the picture above.

be manipulated to obtain multiple data sets from one individual subject during one PET scanning session (101). SPECT, however, does have its own unique features which make it attractive for neuroactivation work. In particular the trapping mechanism of the cerebral blood flow agents used in SPECT studies provides the facility of performing tasks outwith the confines of the scanner in a more 'natural setting' (102) as illustrated in figure 5.1. The problems of setting up test equipment to provide tasks for the subjects to perform while lying in a scanner is not an insignificant problem faced by users of PET, and even more so for functional magnetic resonance imaging (fMRI) (103). The resolution of good neuroSPECT cameras is now approximately 7mm so inherently it should be possible to use SPECT for neuroactivation work and take advantage of the benefits which it offers at the task/scanning interface. The problem of obtaining multiple data sets and therefore the ability to assess within subject variance has not been tackled so far. To date a serious limitation of SPECT has been the poverty of information on within subject variation within the experimental paradigms which have been used. Most studies have only involved two measurements - baseline and activation.

The ability to detect change in regional CBF is dependent on (i) the noise in the imaging technique (statistical fluctuations, natural variation in CBF, variations in activation patterns), (ii) the signal i.e. the magnitude of the activation and the resulting change in CBF and, (iii) the measures taken to increase the signal/noise ratio (averaging between subjects). Parameter (ii) is unknown but is assumed to be directly related to the cognitive task being performed (73). For parameter (iii) the number of subjects can be estimated by using power analysis (104) if assumptions are made about the magnitude of activations that are expected. However, variations in the exact activation pattern between subjects are likely to make this an inexact science and the benefits of an increase in the number of subjects is not straightforward (105) since the differences in function and anatomy between subjects may start to impinge on the ability to detect change as described in parameter (i). These factors pertain to rCBF measurements whether PET or SPECT are used as the imaging modality. The main advantage of PET over SPECT has

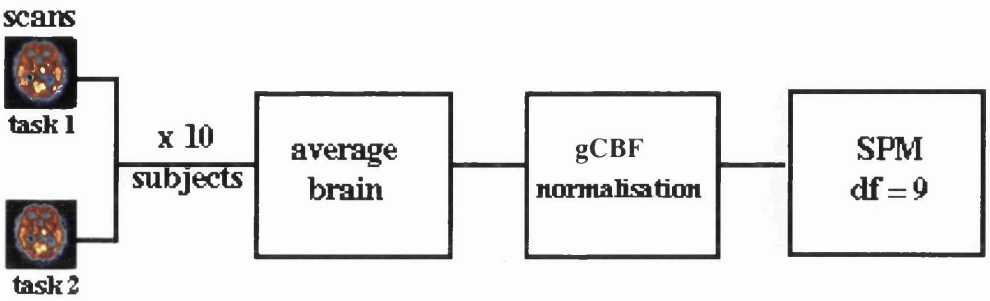

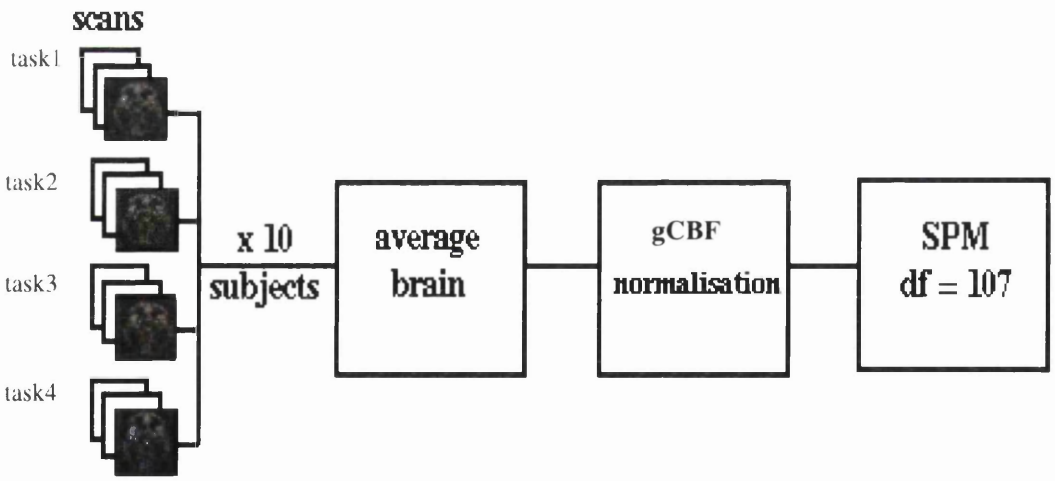

Figure 5.2a) (top of page) shows the degrees of freedom obtained with a typical SPECT paradigm. Fig 5.2b) (bottom of page) shows the vastly increased degrees of freedom obtained with typical PET paradigm.

been the ability to utilise multiple task within subject repetition paradigms which enable different aspects of a task to be studied and more importantly within subject variability of measurements to be estimated (104). Conventionally, SPECT studies use a non-replication paradigm i.e. one scan for each task (see fig5.2a). In PET studies of CBF it is common to obtain multiple data sets from each task, by including up to 12 scans in one scanning session (see fig5.2b). It is noticeable that the image quality of an individual neuroactivation PET CBF scan is not as good as that of many good quality SPECT scans obtained from trapped single photon emitters (IMP, HMPAO and ECD), mainly due to the longer data acquisition times which can be used with trapped compounds. Nevertheless, when these multiple task PET data sets are processed using a statistical parametric mapping (SPM) method, a high level of confidence can be achieved when measuring changes in regional functional activity (104).

Kapur et al 1995 (104) have shown using PET that to obtain reliable results for a single task design (non-replication paradigm) one should have a minimum of 15 subjects and for a repeat task design (replication paradigm) 9 subjects, based on a regional change in blood flow of 3% interpreted at a significance threshold of $p<0.01$. Most reported neuroactivation studies using SPECT currently involve 6 - 20 subjects performing two different cognitive tasks where one scan per task is produced. The total radiation dose received by a subject for research purposes is required to be as low as reasonably achievable. Most studies in the UK currently use 500MBq per scan although higher administered doses are common elsewhere. A few studies have used 250MBq of ^{99m}Tc HMPAO per scan for activation studies involving a non-replication paradigm. The lower count rate of using half the activity normally available for a single scan can be compensated for by using longer scanning times. Image quality is poorer using this dose protocol due to the increase in background noise as a consequence of prolonged acquisition times, nevertheless successful neuroactivation studies have been completed (13-15,106).

Radiation dose limits impose a ceiling on the amount of activity administered to each subject. Within that constraint the only factors available for manipulation are administered activity per scan and scanning time. This study investigates whether it is possible to manipulate these SPECT parameters in such away as to also obtain multiple data sets per cognitive task while achieving a significant return in statistical power when analysing data using a statistical parametric method.

5.2 Methods

In order to compare paradigms a controlled activation of known effect is required. A data simulation method was used to determine empirically whether an increase in statistical power, gained by using a replication paradigm, is significant enough to warrant the use of poorer image quality, due to decreased administered activity per scan.

As with chapter 3 the principle adopted in this study was to use 'real' clinical scans and superimpose a region of rCBF change on these data. Scans were chosen at random from those acquired in every day practice using ^{99m}Tc-HMPAO. The scans demonstrated no major abnormality. Duplicate copies of real scans were made for the purposes of this study, in order to have a paired data set that did not include noise due to natural variability of CBF or anatomy between subjects. This imposed condition of no anatomical variation makes the distinction between the paradigms clearer by removing noise due to inter and intra-subject variability without introducing bias in favour of any particular paradigm. To create the different experimental designs for testing the hypothesis the following method was used:-

- Create the acquisition parameters
- Create the image data sets
- Create the different paradigms

5.2.1 Creating the acquisition parameters.

The neuroactivation studies were simulated from past and current study protocols using the acquisition parameters

- unit dose per scan (500MBq) and unit scan time per slice (120 secs)
- half unit dose per scan (250MBq) and unit scan time per slice (120 secs)
- half unit dose per scan (250MBq) and double scan time per slice (240 secs)

For each of the three conditions a single SPECT scan was selected as representative of the conditions being tested. Scans were chosen at random from those acquired in every day practice using ^{99m}Tc-HMPAO. The scans used in the first study simulation (study 1) of 10 subjects imaged under two cognitive conditions were created from a previously used study protocol using an activity of 1 unit dose per scan and standard scanning time. A second study (study 2) was simulated as a 1/2 dose scan with standard acquisition time to investigate the benefits of a repeat task design in conjunction with the disadvantage of a drop of roughly half in the counting statistics. This was done in order that a replication paradigm might be offered that would keep the total acquisition time as standard thus minimising the discomfort to the volunteer. A further study (study 3) was simulated from another previous study protocol where the subjects had received 1/2 unit dose per scan with the scan acquisition time adjusted to obtain a similar number of total counts as a unit dose scan, however, the total scan time was chosen in light of experience to be the maximum acceptable duration of subject compliance. The procedure for study 2 and 3 simulated a replications paradigm of the activation tasks being investigated and so two scans for each condition were created. The maximum total radiation activity received by each simulated subject in all three groups was 2 unit doses, an effective dose of approximately 9.0 mSv (107). A summary of the study paradigms are given in table 5.1.

Study	*NO. OF SUBJECTS*	*DOSE UNITS PER SCAN*	*SCANS PER SUBJECT*	*UNITS OF SCAN TIME*
1	10	1	2 (A,B)	1
2	10	1/2	4 (A,B,A,B)	1
3	10	1/2	4 (A,B, A,B)	2

Table 5.1. Summary of scanning parameters used to simulate 3 different SPECT neuroactivation paradigms. All scan paradigms have been designed to deliver the same total radiation dose per subject.

5.2.2 Creating the image data sets.

The procedure for creating the image data sets is illustrated in figure 5.3. For each of these three paradigms simulating regional activations were introduced as follows. An exact copy of the original scan was made, in order to have a paired data set to represent two cognitive tasks, A and B, which did not include changes between the scans due to natural variability in CBF. The activation or difference between the two scans was achieved by using a customised graphics package, HIPS (108), to place a region of 'activation' in the duplicate scan. The image data was manipulated in HIPS format as a stack of images representing contiguous slices through the brain. An axial slice through the basal ganglia was chosen in which to place the region of activation. A rectangular region of interest was drawn in the left frontal lobe of size 9x11x1 voxels (1.56mm x1.56mm x6mm). The mean value of this slice was calculated and to each pixel in the designated region was added 3.0% of the slice mean. (The slice mean having been calculated as the number of counts in those pixels surviving an 80% threshold of the maximum number of counts in that slice divided by the area (mm^2) within the threshold boundary). Both scans, 'activation' and 'baseline', were then copied another 9 times in order to produce 10 SPECT scan pairs in total in order to exclude differences in anatomy between subjects. Gaussian noise was added to each of the 20 scans using a HIPS software facility, to emulate scanner noise across scans for each subject. The Gaussian noise generator function in HIPS adds pseudo-random, independent, identically distributed noise to an image. The noise values have zero-mean Gaussian distribution and the standard deviation of the noise must be specified. To provide a different Gaussian noise distribution for each stack of images a different seed for the pseudo-random number generators must be provided for each subject. For multiple frames, the normal operation of this function is to generate a noise frame for the first frame, and randomly permute its rows and columns for subsequent frames. Finally the images were re-formatted to ANALYZE™ compatibility for further analysis using SPM95.

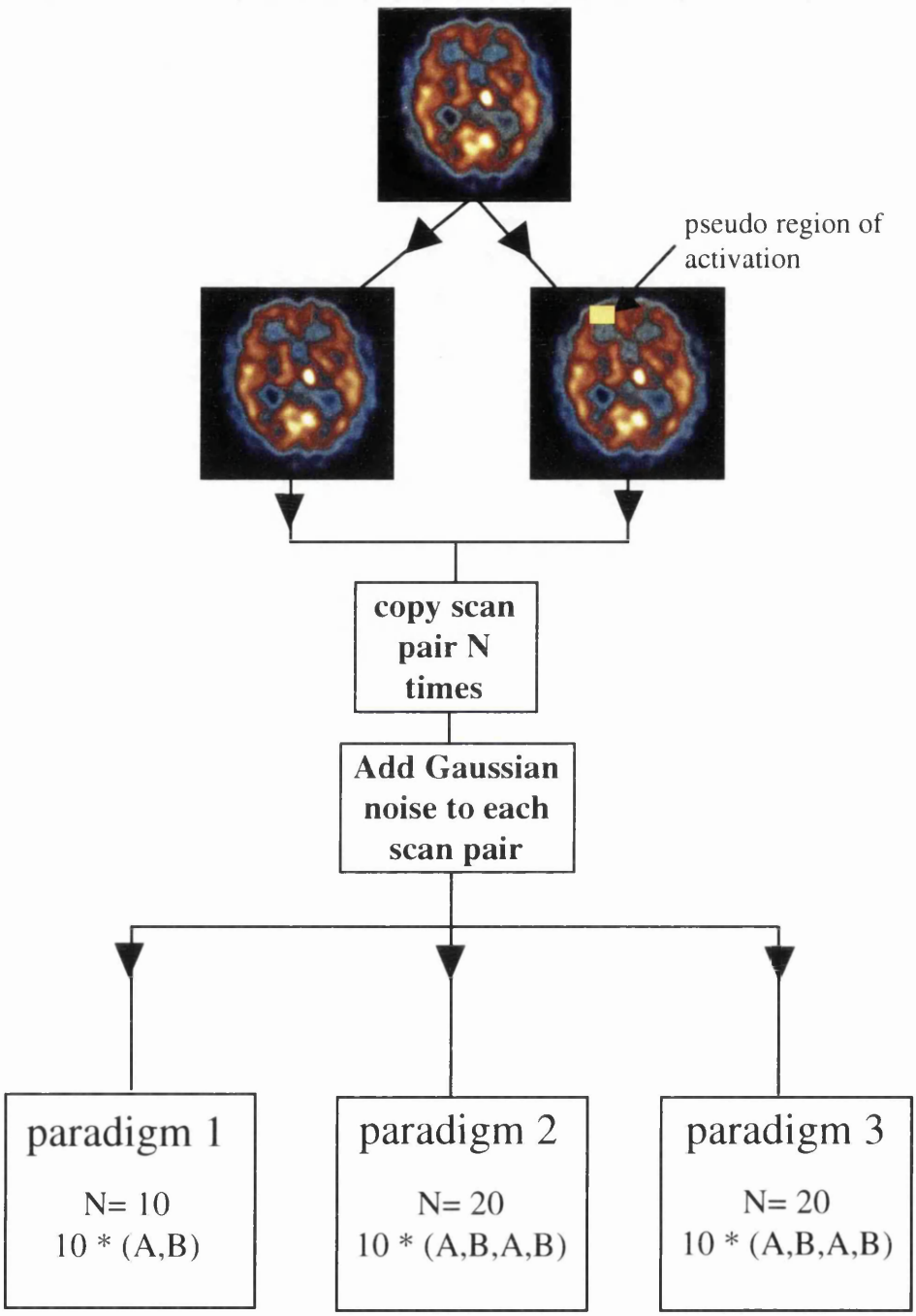

Figure 5.3 showing a schematic flow diagram of the procedure used to create the different study paradigms.

5.2.3 Creating the different paradigms.

The procedure described created a group of 10 subjects each with an activation scan (A) and a baseline scan (B) and is referred to as study 1. The same procedure was followed with the appropriate modifications; the original scan copied 4 times producing a total of 40 scans per study to which Gaussian noise was then added as before, to simulate the other paradigms involving a total of 4 scans per subject (ABAB). The simulated paradigms were then repeated using a 2.5%, 2.0%, 1.5% and 1.0% increased signal respectively, in the region of activation.

5.2.4 Reporting the different paradigm results.

In order to establish the statistical effects of the differences between the paradigms, the data sets were put through the SPM95 statistics package. Although all the scans were copies from an original single scan and therefore not anatomically different, before statistical analysis could be performed the scans had to be spatially standardised using the SPM95 linear spatial normalisation function and smoothed. Study 1 data was analysed using the software option 'multi-subject and different conditions' with global blood flow normalisation achieved using the proportional scaling option. Studies 2 and 3 were analysed using the option 'multi-subject with replications', global blood flow normalisation as before. The Z-score information was extracted from the SPMt.mat files produced by the SPM95 statistical analysis. The mean Z-score calculations were confined approximately to those voxels 'activated' in the original activation scans by using MATLAB.

5.3 Results

Results shown in Table 5.2 are the mean and standard deviation Z-scores for both the single task (study1) and repeat task designs (study 2 and 3). The mean Z-scores for study 1 and study 3 were significantly different at $p < 0.000001$ (independent t-test, one tailed) for changes in regional cerebral blood flow of 3.0%, 2.5% and 2.0% . No significant differences were found at changes in rCBF < 1.5%. Significant differences

were found between the mean Z-scores for study 1 and 2 at $p<0.003$ (independent t-test, one tailed) for changes in regional cerebral blood flow of 3% and 2.5 % only.

These results indicate that the best experimental design would be one that included replications of tasks. Within the limits set regarding the allowable total dose per subject the study design including replications combined with higher count rates associated with the increased scan time in study 3 gave the optimum Z-score results.

	study 1	***study 2***	***study 3***	***UNPAIRED ONE TAILED t-TEST***
% change in rCBF	*Z-score mean and std*	*Z-score mean and std*	*Z-score mean and std*	*significant differences*
3.00%	4.79 +/-0.84	5.83 +/-4.66	8.36 +/- 4.93	$p_{1,3} < 0.000001$ $p_{1,2} < 0.003$
2.50%	4.15 +/-0.6	5.83 +/-4.66	8.22 +/- 4.91	$p_{1,3} < 0.000001$ $p_{1,2} < 0.0001$
2.00%	3.34 +/-0.51	3.8 +/-1.06	5.46 +/- 0.84	$p_{1,3} < 0.000001$ $p_{1,2} <$ N.S.
1.50%	3.32 +/-0.51	2.4 +/-0.24	3.24 +/- 0.93	$p_{1,3} <$ N.S. $p_{1,2} <$ N.S.
1.00%	2.3 +/-0.27	2.4 +/-0.27	3.3 +/- 0.64	$p_{1,3} <$ N.S. $p_{1,2} <$ N.S.

Table 5.2. List of mean and standard deviation z-score for successive changes in rCBF in each paradigm listed in table 5.1.

5.4 Discussion.

This simulation was able to show that when an SPM investigation is used for data analysis, study replication is more important than the individual image quality typically available from a high performance SPECT system. Despite a reduction in administered activity per scan thus degrading the overall image quality, both studies 2 and 3 showed an improvement over study 1 ($p<0.003$ and $p<0.000001$ respectively). The reduction in administered activity per scan is partly compensated for in study 3 by increasing the scanning time. The image quality, however, is not fully restored since the increased scanning time also increases the fraction of background noise contained within the signal. Nevertheless this method used for study 3 obtains a gain in statistical power over studies

1 and 2 by using a replication paradigm that far outweighs the disadvantage of poorer image quality. This is not necessarily the case for low performance SPECT systems, where count rate is more of a limiting factor. However, the introduction of double and triple headed gamma cameras, coupled with the higher administered activity allowances in the rest of Europe and the US should make it possible for ^{99m}Tc-HMPAO SPECT to make valid contributions to the field of functional human brain mapping by following the methods presented here.

The experimental protocol selected for this study used a condition of no anatomical variation between scans. This should not affect the relative differences between the results of the different paradigms used. It should be noted, however, that the absolute significance values obtained are higher than one would expect for a neuroactivation study involving a similar number of different normal controls. Although the time taken to scan a single slice was defined as an independent acquisition parameter, it was actually defined by the total scan acquisition time of one hour which was chosen in the light of experience to be the maximum acceptable duration of subject compliance.

Adoption of a four study protocol does undoubtedly introduce logistical difficulties. It is important to consider the limiting factors in emission tomography studies of neuroactivation. The factors which must be considered are cost, number of volunteers who can be recruited, radiation dose, scanning time and consequently acceptable scan duration. Clearly a 4 scan paradigm is preferable but if it is not possible to arrange four independent scanning sessions then an alternative may be considered. One alternative would be to use two split dose studies, where up to one half of the dose is administered during one condition, obtaining the first scan, and then, on the same day administering the remainder of the dose during the second condition and obtaining the second scan (15). Another alternative would be to use two dual isotope acquisition studies. This would involve the administration of a half dose of one imaging agent (e.g. ^{123}I-IMP) during one condition and then another imaging agent (e.g. ^{99m}Tc HMPAO) is administered during another condition immediately following the first (109). A single scanning

session with two energy window settings would then be performed to obtain two images of the two different conditions. Fundamental to both these techniques, however, is the problem of noise from the initial scan/imaging agent interfering with the second scan/imaging agent.

A four scan design will be advantageous to SPECT studies of neuroactivation, which to date, have used two scan protocols (13,15,110). Within this context, the application of two additional scans could benefit neuroactivation studies of both patients and normal subjects. With respect to the former, one of the main limitations of the neuroactivation of for example, brain-injured patients, is the degree of neuroanatomical variability that is often present, even in patients displaying similar clinical or neuropsychological profiles. Therefore while grouping patients might be unwise in some circumstances, individual patients may present excellent opportunities to test specific neuropsychological hypotheses. However, in a two scan single case study, the reliability of the data may be limited, and in this case, the addition of two further scans, allowing for each condition to be replicated (i.e. ABAB), would greatly increase confidence in the results and their interpretation. With respect to the latter, the power of investigation of neuroactivation studies involving groups of normal healthy subjects, could be greatly enhanced by the addition of one, or perhaps two, additional cognitive conditions (i.e., ABAC or ABCD respectively). This would enable more subtle differences in cognitive processing to be investigated.

5.5 Conclusions.

This investigation was able to show that when using voxel-wise statistical data analysis, study replication is more important than the individual image quality typically available from a high performance SPECT system.

- When using CBF SPECT a 4 scan paradigm with the appropriate adjustment in scanning protocol should be used for neuroactivation studies.

CHAPTER 6

Applications of the 4 scan SPECT paradigm to neuroactivation studies: I. Investigation into the mechanisms of vagal nerve stimulation for the treatment of intractable epilepsy, using ^{99m}Tc HMPAO SPECT brain images.

This chapter describes the application of the multiple scan paradigm determined in chapter 5 for neuroactivation studies that use ^{99m}Tc HMPAO SPECT scans of cerebral blood flow. Section 5.1 provides a background to epilepsy and the newest form of treatment by stimulation of the vagal nerve (VNS). Sections 5.2 and 5.3 list the methods and the results of applying the 4 scan paradigm to the investigation of the affect of VNS on CBF using an SPM analysis. Section 5.4 discusses the benefits of using a repeat task design for this experiment and the implications that these results may have on explaining the action of VNS on rCBF.

6.1 Introduction

The previous chapter was able to show that SPECT studies of neuroactivation would benefit from a multi-task paradigm even though image quality would have to be compromised. This chapter describes the application of the 4 scan paradigm to investigate the stimulation of the vagus nerve for the treatment of epilepsy.

Epilepsy is a transitory disturbance of the function of the brain which develops suddenly, manifesting in uncontrolled movements or actions, ceases spontaneously and reoccurs at

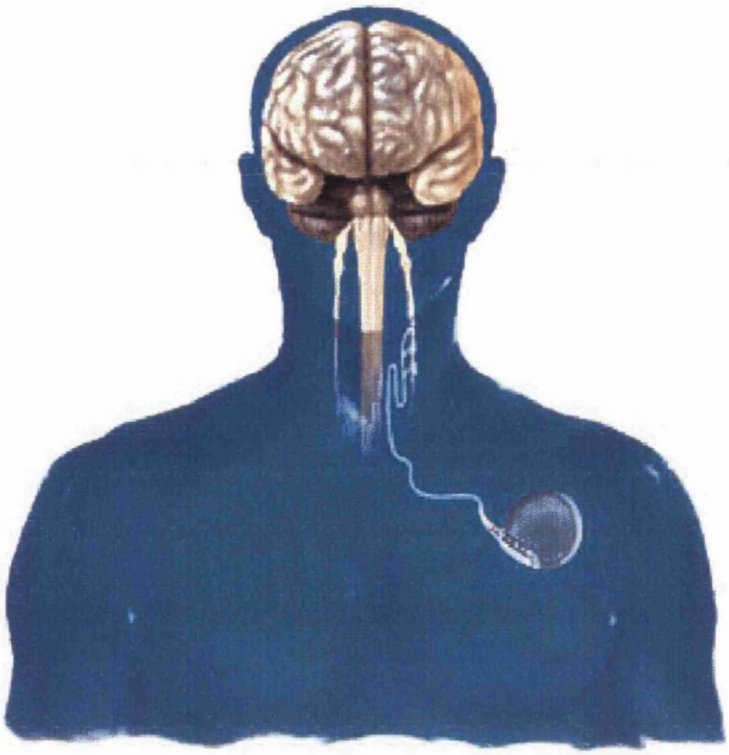

Figure 6.1. Schematic representation of the position of the implanted Cyberonics vagal nerve stimulator.

variable frequency in different patients. It is a common disorder affecting as many as 1 in 200 people in the USA and Europe. Epilepsies can be divided into two broad categories; those which are generalised, in which seizures appear to affect the whole brain and often have a genetic substrate, and those which are focal, in which seizures originate from a specific region (or regions) of the brain. The great majority of adult epilepsies are focal, most originating in the medial temporal lobe. About 20% of these are not brought under satisfactory control using drug treatment and surgical resection of the discrete region of the brain identified as the seizure focus is used in selected patients (111). Functional imaging has played a major part in improving the accuracy of localisation of such epilepsies, and in reducing the use of invasive (and hazardous) EEG techniques. In particular the SPECT CBF tracers (IMP, ECD and HMPAO), due to their unique trapping mechanism, provide the only means of imaging brain function during a seizure. However, surgery carries significant risks and for many patients is not suitable treatment (112) and alternative therapies are needed. One such treatment is the stimulation of the

vagus nerve using an implantable programmable device to decrease the frequency of seizures.

An implanted, programmable (Cyberonics Inc.)[16] electronic simulator is implanted in the left chest (infraclavicular subcutaneous pocket). The stimulating lead electrode contacts, embedded in silicone rubber, are wrapped around the left vagus nerve in the low cervical area. The vagus nerve is chosen for its absence of pain sensation. Once implanted, the stimulator can be programmed to deliver regular stimulation 24 hours a day regardless of seizure activity. Patients can also activate extra 'on demand' stimulation with a handheld magnet. Clinical studies have demonstrated VNS therapy to be a safe and effective mode of treatment when added to the existing treatment regimen for severe, refractory patients with epilepsy. Efficacy ranges from seizure free to no response with about half reporting a 50% reduction in seizure frequency (113,114). The side-effect profile includes stimulation-related sensations in the neck and throat (112,114).

The mechanism of action through which VNS modulates seizure activity is not clearly understood although two theories have emerged. First, the "direct connection" theory hypothesises that the anticonvulsant action of VNS is caused by a threshold raising effect within specific brain structures (114). The second is the concept that chronic stimulation of the vagus nerve increases the amount of inhibitory neurotransmitters and decreases the amount of excitatory neurotransmitters, basically calming down "hyperexcited" nerve cells and reverting the brain back to its normal patterns (115).

The vagus nerve is known to have connections through the nucleus of the solitary tract and so sites receiving projections from this area may also have changes in overall synaptic activity during VNS. Since the monitoring of cerebral blood flow using emission tomography has been shown to reflect changes in motor, sensory and cognitive processes, it should be possible to image the changes in blood flow induced during VNS

[16] Cyberonics Europe, S.A., Belgicastraat 2, 1930 Zaventem, Belgium.

and so use this information to provide clues as to the action of VNS on the central nervous system and its role in controlling or modifying epileptic seizures.

6.2 Methods

To confirm the hypothesis that the addition of two further scans, allowing for each condition to be replicated (i.e. ABAB), would greatly increase confidence in the results and their interpretation, the 4 scan paradigm was used to investigate the stimulation of the vagus nerve for the treatment of epilepsy. Ethics permission for the study was given by the Southern General Hospital-NHS Trust ethics committee and ARSAC (administration of radioactive substances advisory committee).

6.2.1 Subjects and VNS techniques.

Vagus nerve stimulation blood flow SPECT studies were performed in 6 subjects with intractable epilepsy. All patients had consented to participating in the protocol for Vagus Nerve Stimulation sponsored by Cyberonics. The group included 2 males and 4 females with a mean age of 29.5 range 21 - 39. Imaging was commenced 2 days after implantation. The protocol required that each patient had medically refractory epilepsy occurring 3 or more times monthly. 1 patient had primary generalised epilepsy causing generalised tonic clonic seizures, the remaining 5 patients had localisation related epilepsy, causing complex partial seizures. No patients had undergone cerebral resection. Each patient received 1 minute of VNS to establish the stimulator current level for each patient. The stimulation began at VNS current levels of 0.25mA and was increased to just enough to cause sensation in the throat to induce coughing. The shape of the stimulating waveform was square wave pulses of 500μsecs of duration at 30Hz.

6.2.2 Image acquisition.

Four CBF SPECT scans were acquired in four separate sessions for each subject, 2 scans when the stimulator was on and two when the stimulator was off. The time between consecutive scans was no less than 2 days and no more than 14 days No seizures occurred during injection of isotope but one subject had a seizure during an imaging

session. The scan was stopped and then repeated. CBF was imaged using 250 MBq of ^{99m}Tc HMPAO (1/2 unit dose) per scan. The images were acquired using the SME 810 scanner (described in chapter 2) with scanning parameters set at a slice acquisition time of 240 seconds (2 unit time) and a slice separation 8mm. Injection of ^{99m}Tc HMPAO was given at 2 mins of stimulation during which time the subject lay without speaking and eyes closed in a quiet environment. Patient movement during scanning was minimised as described in chapter 2.

6.2.3 Image analysis.

The reconstructed images were converted to ANALYZE^{TM} format, spatially standardised and smoothed as described in chapter 2. The statistical analysis was performed using the "multi subject: replication of conditions" option to check for the main effect of condition as well as the "multi subject: different conditions" to check the validity of a repeat task design. Proportional scaling to the global mean activity in each subject was used for global normalisation (see chapter 2). All results were displayed at a significance threshold of $P_u<0.001$ and $P_k<0.5$ (uncorrected).

6.3 Results

The contrasts used in this experiment were designed to look at:-

- the main effect of condition with repeat scans of tasks. (AA - BB)
- the main effect of condition with single scans of tasks. (A - B)
- the validity of repeated conditions. (A - A, B - B)

The first contrast investigated directly the effects (both increases and decreases) of VNS on CBF. The second contrast also showed the effect of VNS on CBF but this time with only a single scan per condition. This was used to look at the increase in statistical significance gained by an increase in the degrees of freedom of using a repeat scan design as opposed to a single scan design. The third contrast used a subtraction paradigm to check for the null hypothesis between two scans of the same task to confirm that the brain state had been replicated.

6.3.1 The main effect of condition with repeat scans of tasks.

Subtraction between activation states (A) and baseline states (B) with replications .

For the main effect of conditions the "multi subject: replication of conditions" option was used with the contrast (1 -1) to look for *increases* in blood flow in the stimulus condition with respect to the baseline condition and then (-1 1) to look for *decreases* in blood flow with respect to the baseline condition (figure 6.2).

The Z-score and location of the most significant voxel is listed below each SPM(t) map thresholded at $P_u<0.001$ and $P_k<0.5$ (uncorrected). For clarity, these maps are superimposed onto axial slices of the single MRI T1 template supplied with SPM96.

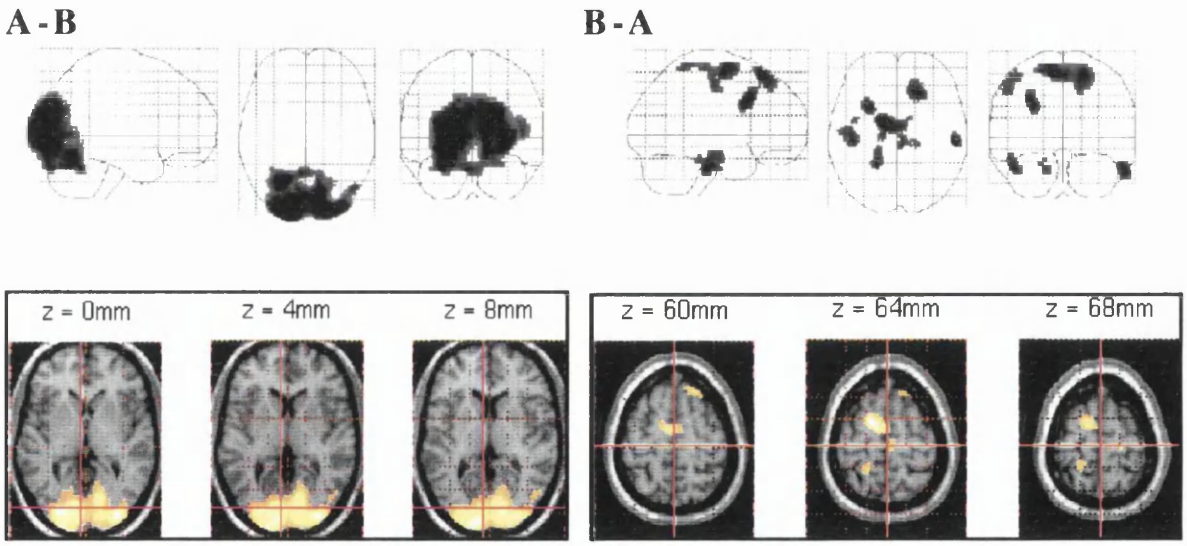

2*activation -2* baseline
Z= 5.45 K= 7144 voxels
(xyz) = -32 -90 0
increased BF in occipital cortex

2*baseline- 2*activation
Z= 5.07 K= 366 voxels
(xyz) = -14 -2 64
decreased BF in superior frontal gyrus (Brodmann 6)

Figure 6.2 The SPM(t) map of the subtraction of activation and baseline scans are displayed. The map on the left hand side shows the increases in rCBF in the activation condition (VNS) relative to the baseline condition (rest). The map on the right shows the decreases in rCBF in the activation condition relative to the baseline condition.

6.3.2 The main effect of condition with single scans of each task.

Subtraction between activation conditions (A1, A2) and baseline conditions (B1, B2) without replications

For the main effect of four conditions (A1, A2, B1, B2) the "multi subject: different conditions" option was used with the contrast of (1 0 -1 0) and (0 1 0 -1) to look for *increases* in blood flow in the stimulus condition with respect to the baseline condition and then (-1 0 1 0) and (0 -1 0 1) to look for *decreases* in blood flow with respect to the baseline condition (figure 6.3 a and b).

The Z-score and location of the most significant voxel is listed below each SPM(t) map thresholded at $P_u<0.001$ and $P_k<0.5$ (uncorrected).

A1-B1

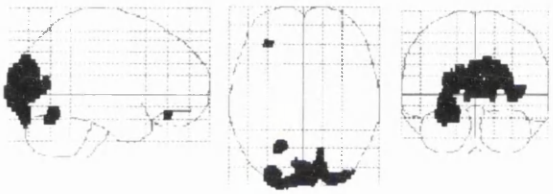

1*activation -1* baseline
Z= 4.17 K= 1417 (xyz) = -28 -94 -8
BF increases in occipital cortex

B1-A1

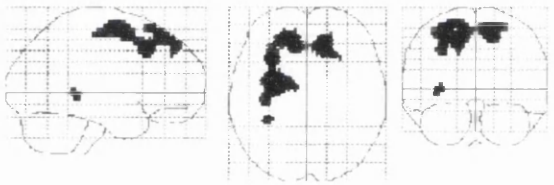

1* baseline - 1*activation
Z= 4.47 K= 796 (xyz) = -22 -2 64
BF decreases in L Superior Frontal Gyrus

A2-B2

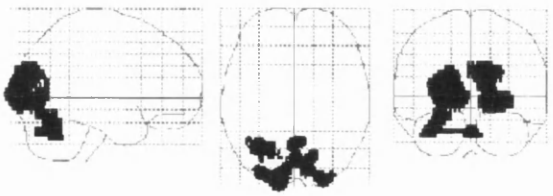

1*activation -1* baseline
Z= 4.18 K= 158 (xyz) = -30 -90 -4
BF increases in occipital cortex

B2-A2

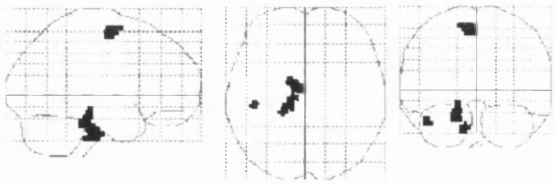

1* baseline - 1*activation
Z= 4.17 K= 59 (xyz) = -10 -4 64
BF decreases in L Superior Frontal Gyrus
Brodmann 6.

Figure 6.3a shows the SPM(t) maps of the subtraction of activation from baseline scans on the left and the subtraction baseline from activation scans on the right.

A1-B2

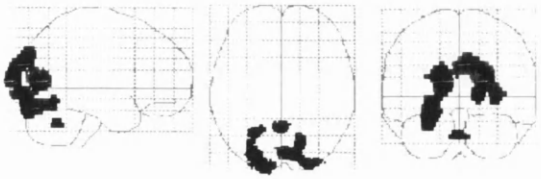

1*activation -1* baseline

Z= 4.08 K= 385 (xyz) = -28 -84 -20

BF increases in occipital cortex

B2-A1

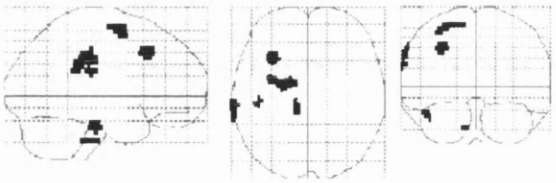

1* baseline - 1*activation

Z= 4.07 K= 57 (xyz) = -32 -20 40

BF decreases in L Frontal lobe, sub gyral

A2-B1

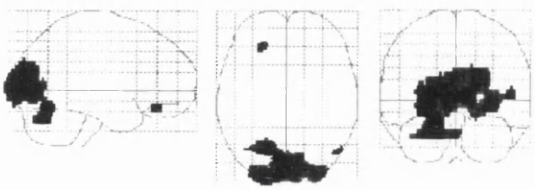

1*activation -1* baseline

Z= 4.08 K= 2315 (xyz) = -28 -84 -20

BF increases in occipital cortex

B1-A2

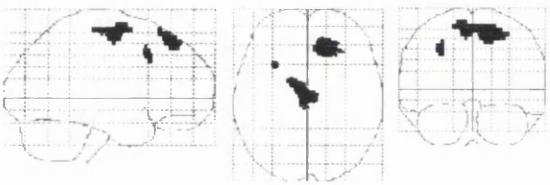

1* baseline - 1*activation

Z= 4.24 K =147 (xyz) = 16 38 56

BF decreases in R Frontal Lobe.

Figure 6.3b shows the SPM(t) maps of the subtraction of activation from baseline scans on the left and the subtraction baseline from activation scans on the right.

6.3.3 The validity of repeated conditions.

Subtraction within activation condition (A1, A2) and baseline condition (B1, B2).

To confirm the replication of conditions, the "multi subject: different conditions" option was used with contrasts designed to look at the subtractions between scans of the same condition. The SPM(t) maps (figure 6.4) confirm the null hypothesis that there are no differences in CBF between scans of the same condition.

A1-A2

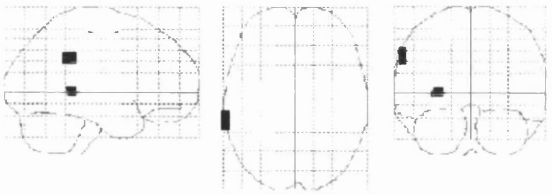

Z= 4.04 K= 21 (xyz) = -66 -26 32

Not significant

A2-A1

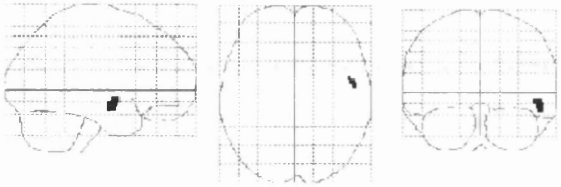

Z= 3.68 K= 16 (xyz) = 52 -4 -12

Not significant

B1-B2

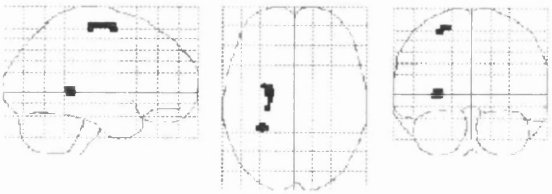

Z= 3.83 K= 34 (xyz) = -22 -6 64

Not significant

B2-B1

No significant voxels above this threshold K

Figure 6.4 Shows the SPM(t) maps produced by the contrast of the subtraction of within conditions (baseline - baseline) and (activation - activation).

6.4 Discussion.

The results of this investigation into the mechanisms involved in the anti-seizure effect of VNS confirm the hypothesis that more robust results can be found by sacrificing image quality for statistical power. The SPM(t) maps of the increases in CBF with respect to the baseline condition using only 2 scans show that the major activation region shows a corrected significance based on extent and height of $P_{u,k}<0.01$ thresholded at $P_u<0.001$ and $P_k<0.5$ (uncorrected). With 4 scans this corrected significance improves (to $P_{u,k}<0.0001$ at the same thresholds) by a factor of 100, strengthening the conviction that an activation has occurred. This becomes especially important when considering the omnibus nature of this test since there was no apriori definition of activation pattern requiring the application of a stringent thresholding to account for multiple statistical tests.

Neuronally active regions in the brain have been shown to be associated with increased levels of blood flow and so clues to the actions of VNS on the CNS may be made by

witnessing, in-vivo, the effect of VNS on blood flow to the brain. PET studies to date show inconsistent findings in response to VNS but this may be due to differences in study design, patient population, duration of VNS therapy and other factors confounding the measurement of rCBF. One study showed that changes occurred in the ipsilateral anterior thalamus and cingulate gyrus but two of the subjects out of five had seizures during scanning (116). Another study showed involvement of the ipsilateral cerebellum, contralateral thalamus and contralateral temporal lobe cortex but two of these subjects had already undergone cerebral resection (117). In a study that investigated patients immediately after insertion of the device changes in rCBF were evident bilaterally in the hypothalami, insular cortices, and inferior cerebellum as well as increased flow to the contralateral thalamus and post central gyrus (118). Furthermore PET studies on the sensation of pain in the throat, a side effect associated with the activation of the stimulator, have reported the following activation patterns, on the sensation of pain; increased blood flow in the central sulcus, bilateral insular cortices and frontal-parietal operculum and anterior cingulate gyrus (119). This pattern would seem to account for at least some of the activation seen in other studies investigating the VNS alone.

The results of this study into the effect of VNS on CBF does not confirm any of the CBF patterns described above. Differences in protocol with regard to the timing between imaging and the switching on of the stimulator as well as the randomisation of the baseline and activation conditions may well account for these differences. However, the location of the main activated region in the occipital cortex might simply be explained by the fact that the scanning protocol of eyes closed during the injection of ^{99m}Tc HMPAO was not adhered to for every subject. A study of the variability of activation results during cognitive processing by Crivello et al 1995 (120) point out that if an activation occurring in just one subject is very strong it will remain significant even when included in the group analysis. Studies of visual stimulation (109,110) have reported rCBF changes of between 15-20% in the occipital cortex during stimulation. Measurements in the occipital cortex of the 6 subjects (13.12%, 23.24%, 1.35%, 4.08%, 8.6%, 14.91%)

in this study show that at least 3 of the subjects had a significant increase in the occipital region between the two conditions indicating that the protocol had not been adhered to. In addition a further study to investigate specifically the differences in rCBF of having eyes open compared to eyes closed (appendix D) showed that there was significant change in the occipital cortex that did not require the application of intense visual stimulation in the eyes open condition. The percentage changes in rCBF associated with VNS have not been reported but are no doubt much less than those reported for the changes observed in the occipital cortex.

The SPM(t) maps of the decreases in CBF with respect to the baseline condition also show a similar increase in corrected significance but in this case the location of the most significant voxel in each of these separate contrasts using the single scan design is not stable. However, the most significant voxel for the original contrast of the main effect using the replication of conditions design is located in the superior frontal gyrus (Brodmann area 6) an area known to be affected by the stimulation of the sympathetic nervous system as shown by evoked potential experiments in animals (121). It has been suggested that these results could be proof that the stimulation of the parasympathetic nervous system by VNS causes inhibition in Brodmann area 6 an effect that has not been measured by evoked potential experiments (personal comm. from Dr Peter Julu)[17]. Clearly more subjects need to imaged with a tighter control on the visual stimulation status to confirm this result.

6.5 Conclusion.

This study was able to confirm that SPECT studies of neuroactivation would benefit from a multi-task paradigm even though image quality is compromised. This application of a 4 scan paradigm demonstrates that:-

- it can be used in practice
- the results are robust (as can be seen in the validity of repeated conditions contrast).

[17]Dr Peter O.O Julu, university lecturer, Department of Neurology, Central Middlesex Hospital, London, UK.

CHAPTER 7

Applications of the 4 scan SPECT paradigm to neuroactivation studies: II. Contrasting the role of the medial temporal lobes in novelty detection with their role in the encoding and/or consolidation into long-term memory of associative information.

This chapter describes the application of the multiple scan paradigm determined in chapter 5 to neuroactivation studies that use ^{99m}Tc HMPAO SPECT scans of cerebral blood flow. Section 7.1 provides a background to current opinion of the role of the medial temporal lobes in memory processing and an explanation of how a typical neuroactivation paradigm might be designed to investigate certain aspects of this role. Section 7.2 describes the design of the cognitive tasks and the image analysis used to isolate specific components of these tasks. Section 7.3 presents the results of applying the 4 scan paradigm and sections 7.4 and 7.5 discuss the findings and benefits of using a repeat task design.

7.1 Introduction

Chapter 5 hypothesised that a multi-task paradigm used with SPECT studies of neuroactivation could be greatly enhanced by the addition of one, or perhaps two, additional cognitive conditions and that this would enable more subtle differences in cognitive processing to be investigated. This chapter illustrates how the addition of two additional cognitive tasks to the conventional two-task SPECT paradigm enabled the role

of the medial temporal lobe in novelty detection to be contrasted with its role in the encoding of associative information into long term memory.

There exists good evidence, obtained from PET and fMRI studies, that the encoding of information from pictures or faces produces activations within the medial temporal lobes (MTL) (122-126). The reliability of this MTL finding is strengthened by the fact that the studies adopted a variety of different comparison baselines. However, it remains unclear exactly what processes are producing the MTL activations. They could be a result of novelty alone, the encoding and/or consolidation of associative information into long-term memory, or both of these. A recent study using verbal stimuli (127), has concluded that the left MTL is responsible for novelty detection and not directly for the processes involved in the formation of new associations. While the study used a task which manipulated novelty of associations it did not strictly match associative encoding across the conditions. The present study manipulated novelty while stringently matching levels of associative encoding across novel and familiar conditions, with two major aims:

- To test whether associative encoding and/or consolidation alone is responsible for the MTL activations or whether novelty alone can also produce such an activation.
- To investigate what activation pattern is produced in the frontal and parietal cortex when contrasting the processing of novel and familiar stimuli using different levels of encoding.

Memory refers to the brain processes of encoding, storage and retrieval of facts and events for later use. Traditionally psychologists were confined to cognitive investigations of memory (and other cognitive processes) whereby manipulations within memory tasks allowed the testing of cognitive hypotheses by observing resultant behaviour under different conditions. This type of investigation has been carried out both with normal healthy controls and with patients with organic amnesia. The comparison of normal subject and patient data in this way has allowed neuropsychologists to investigate the

neural basis of memory by relating cognitive deficits to underlying neuropathology (128). Over the years this type of investigation has been enhanced by developments in structural imaging, particularly that of MRI, since this has provided researchers with detailed confirmation of the location and extent of the brain lesion. However, lesion research is limited for two related reasons. First, human brain lesions are rarely selective to the extent that is required for testing specific functional hypotheses. Second, patients with selective brain lesions, when they do occur, occur in small numbers and therefore work on such patients is limited. The advent of functional neuroimaging and the development of techniques to study changes in CBF (SPECT) and corresponding changes in glucose metabolism and oxygen extraction (PET and fMRI) known to be associated with areas of neuronal activity, neuropsychologists have been provided with a "window to the brain" through which they can "observe" the neuronal activity associated with particular cognitive processes. In order to do this, however, studies require very careful cognitive design to ensure that the cognitive process of interest is indeed "isolated" by the experiment.

The first generation of neuroactivation experiments employed a simple subtraction paradigm, where the functional images acquired during one brain state were subtracted from the functional images in another brain state (45) in order to isolate the process of interest. But this model has it limitations. Although two tasks might be carefully designed to isolate a single cognitive process, the standard subtraction paradigm assumes that the interaction between this and the other components of the task is negligible, but this is probably not the case. Using newly developed voxel-wise statistical analysis techniques that are now available the subtraction paradigm can be extended further to investigate the interaction between different memory processes (129). By introducing more than two tasks into one experiment it is possible to use "cognitive conjunctions" to strengthen the power of the activations and "factorial designs" to investigate the interaction between processes. A conjunction analysis combines a series of subtractions that have a single cognitive process common to all task subtractions (130). A factorial design involves investigating two or more factors within a task. The interaction between

these factors identifies changes in rCBF brought about by another processing demand. For example if we consider the difference between naming familiar objects and categorising familiar objects compared to naming novel objects and categorising novel objects, the single subtractions will tell us about the differences between naming and categorising but will not be able to show the effect of the nature (familiar or novel) of the objects in the task. A conjunction analysis instead, will show us both the common difference between the two tasks i.e. naming vs. categorising, independent of the nature of the objects (novel or familiar) and the common difference attributable to the nature of the objects independent of the task . A factorial analysis will inform us of the interaction between the tasks and the nature of the objects.

7.2 Methods

7.2.1 Subjects

SPECT scans were performed on ten healthy right-handed subjects, 5 male and 5 female, age range 27-54. Normal memory performance was established using the Doors and People Test (131).

7.2.2 Cognitive Activation tasks

Four conditions were designed to manipulate both level of associative encoding and level of novelty. Two forced-choice matching-to-sample tasks were used, in which a sample complex scene and two choices were presented simultaneously. Each task was carried out under two different conditions of novelty (novel and familiar). The design was counterbalanced with respect to stimuli, task order and novelty condition.

Thematic Matching Task (TM). In this task, the three pictures were different perceptually, but similar in terms of meaningful content. However, one of the two choices shared a theme (e.g., family life, greeting, instruction) with the sample picture which the other picture did not portray. The subjects were required to identify this matching picture (left or right) by studying the pictures in a way that would identify

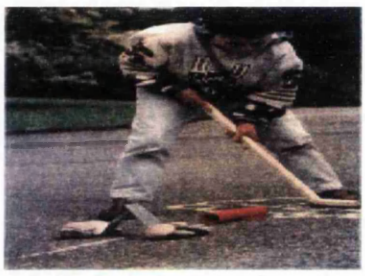

Figure 7.1 a. The material used in the thematic matching task. In this example the left hand image matches with the top image as they are both ice sports

Figure 7.1 b. The material used in the perceptual matching task. In this example the right hand image matches with the top image since the left hand image has been translated to the left slightly.

themes within the pictures, not focusing on individual items alone. The nature of this processing therefore involved high level semantic associative encoding.

Perceptual Matching Task (PM). In this task, all three pictures were extracted from a single original picture with the sample and one of the two choices being identical while the non-matched picture involved a slight shift (vertical or horizontal) from the other two. Subjects were required to decide which of the two choices (left or right) was identical to the sample picture. The three pictures were identical in teRMS of meaningful content so any attention paid to the theme of the pictures would not help discriminate between them and subjects were encouraged to use a low level superficial scanning strategy to compare the pictures.

Novelty conditions (familiar (F) and novel (N)) Each task was carried out twice (using different stimuli) once with familiar stimuli and once with novel stimuli. Familiarity was established by displaying the stimuli to the subjects 8 minutes prior to the activation task, subjects were instructed to point quickly and accurately to the centre of activity or interest, in each picture. Piloting of this familiarisation procedure ensured that exposure times produced equal and high familiarity levels (>90%) across the two matching tasks.

Behavioural data

Following each activation task, performance on an associative recognition test was measured to establish the extent of associative encoding that had taken place. The level of associative encoding was significantly greater during the Thematic Matching (TM) tasks than in the Perceptual Matching (PM) tasks ($p<0.0001$). Subjects were also debriefed regarding their awareness of the use of novel or familiar stimuli in each task. The results suggest that subjects were aware when novel stimuli were used. Moreover, subjects' thematic matching performance on the TE task was found to be significantly better in the familiar condition ($p<0.007$) compared to novel. This indirectly confirms that subjects accurately differentiated between novel and familiar stimuli.

7.2.3 Image acquisition

1 minute into each cognitive task, a maximum dose of 250 MBq ^{99m}TcHMPAO was injected intravenously through a forearm cannula while the subject performed the task. Each subject received 4 SPECT scans, one for each cognitive condition. Scanning was commenced 15 - 30 mins after the injection. The images were acquired using the SME 810 scanner (described in chapter 2) with scanning parameters set at a slice acquisition time of 240 seconds (2 unit time) and a slice separation 8mm. Patient movement during scanning was minimised as described in chapter 2.

7.2.4 Image analysis

The reconstructed images were converted to ANALYZE™ format, spatially standardised and smoothed as described in chapter 2. The statistical analysis was performed using the "multi subject: different conditions" option to check for the main effect of condition. Proportional scaling to the global mean activity in each subject was used for global normalisation (see chapter 2). Clusters of contiguous voxels greater than 40, activated at an overall threshold of $p<0.01$ (uncorrected), with peak z-scores > 3.0, were considered significant. All results were displayed at a significance threshold of $P_u<0.01$ and $P_k<1.0$ (uncorrected).

7.3 Results.

The contrasts used in this experiment were set up to look at:-

- the main effect of associative encoding
- the main effect of familiarity
- the main effect of novelty

In order to explore the independent effects of encoding and novelty, as well as the interaction between the two, the following subtraction and conjunction analyses were carried out.

7.3.1 The main effect of associative encoding.

TM familiar (TM_F), PM familiar (PM_F), TM novel (TM_N), PM novel (PM_N).

Conjunction

$(TM\text{-}PM)_F + (TM\text{-}PM)_N$

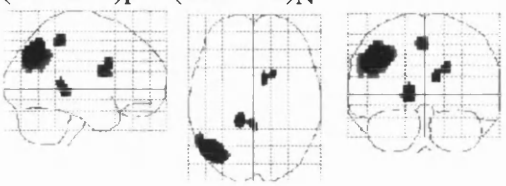

Figure 7.2a

left medial temporal lobe (parahippocampal gyrus)

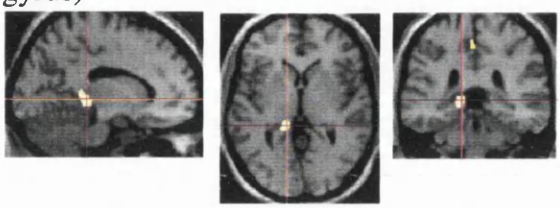

Z= 3.21 K= 77 (xyz) = -36 -68 40

Figure 7.2b

Left parietal cortex

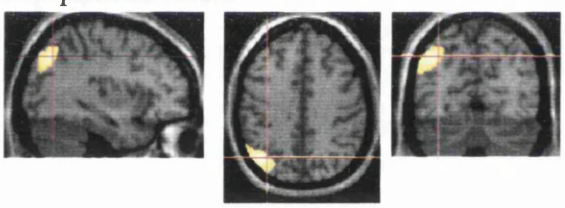

Z= 3.76 K= 568 (xyz) = -14 -36 0
Figure 7.2c

Subtraction

$(TM\text{-}PM)_F$

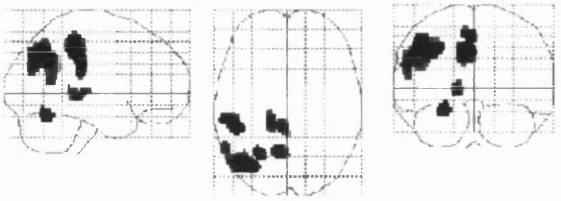

Figure 7.3a

left cerebellum

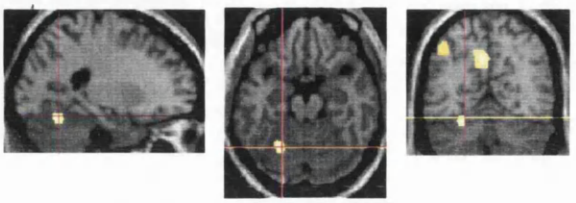

Z= 3.33 K= 66 (xyz) = -24 -62 -20

Figure 7.3b

Figure 7.2 and 7.3 show the contrasts of the main effect of associative encoding. Figure 7.2a shows the SPM(t) map produced by the conjunction analysis (combining TM familiar - PM familiar with TM novel - PM novel). Figure 7.2 b and c show the two major activations superimposed on the T1 MRI template. Figure 7.3a shows SPM(t) map produced by the single subtraction contrast (TM familiar - PM familiar). Figure 7.3 b shows the cerebellum activation superimposed on the T1 MRI template.

This conjunction of contrasts (figure 7.2 - $(TM\text{-}PM)_F + (TM\text{-}PM)_N$) produced activations in the left medial temporal lobe (parahippocampal gyrus) and left parietal cortex and are displayed above. A subtraction analysis of $(TM\text{-}PM)_F$ (figure 7.3) produced encoding-specific familiarity activations in the left cerebellum. This activation is also displayed superimposed on the corresponding axial slices of the T1 MRI template supplied with SPM96 (figure 7.2 a, b and figure 7.3 b).

7.3.2 The main effect of familiarity

TM familiar (TM_F), PM familiar (PM_F), TM novel (TM_N), PM novel (PM_N).

$(TM_F\text{-}TM_N) + (PM_F\text{-}PM_N)$

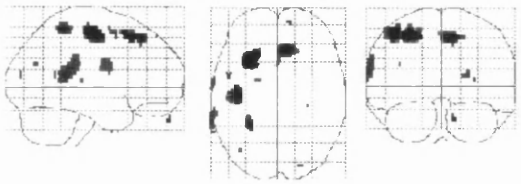

Figure 7.4 a

$TM_F\text{-}TM_N$

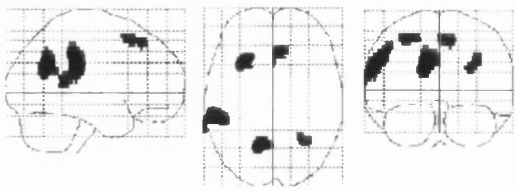

Figure 7.5 a

Right superior frontal lobe

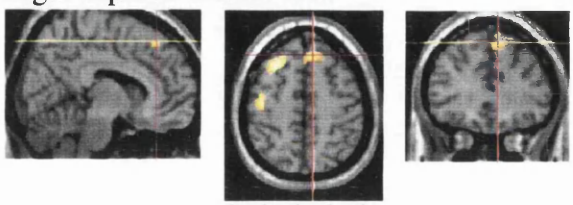

Z= 4.16 K= 97 (xyz) = -28 22 52

Figure 7.4 b

Left superior frontal lobe

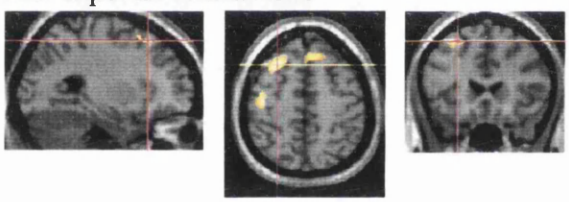

Z= 3.77 K= 149 (xyz) = -40 -18 56

Figure 7.4 c

Figure 7.4 (a,b,c) and 7.5 show the contrasts of the main effect of familiarity. Figure 7.4 a shows the SPM(t) map produced by the conjunction analysis (combining TM familiar - TM novel with PM familiar - PM novel). Figure 7.4 b and c show the two major activations superimposed on the T1 MRI template. Figure 7.5a shows SPM(t) map produced by the single subtraction contrast (TM familiar - TM novel).

This conjunction of contrasts (figure 7.4 - $(TM_F\text{-}TM_N) + (PM_F\text{-}PM_N)$) produced significant bilateral superior frontal activations activations. A subtraction analysis of $TM_F\text{-}TM_N$ revealed that these activations were a result of the encoding-specific familiarity condition. These activations are also displayed superimposed on the corresponding axial slices of the T1 MRI template supplied with SPM96 (figure 7.4 a, b).

7.3.3 The main effect of novelty detection

TM familiar (TM_F), PM familiar (PM_F), TM novel (TM_N), PM novel (PM_N).

Subtraction

PM_N-PM_F

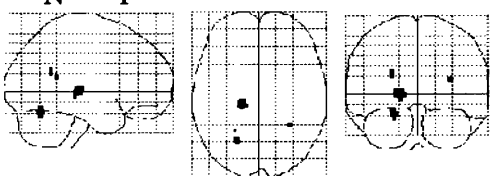

Z= N.S (xyz) = N.S

Figure 7.6 a

Subtraction

TM_N-TM_F

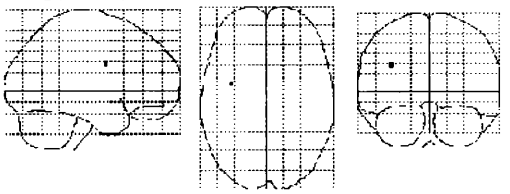

Z= N.S (xyz) = N.S

Figure 7.6b

Conjunction

(PM_N-PM_F) + (TM_N-TM_F)

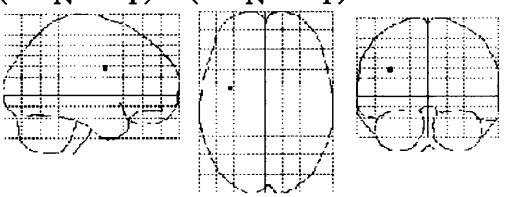

Z= N.S (xyz) = N.S

Figure 7.6c

Figure 7.6 a, b, c show the contrasts of the main effect of novelty detection. Figure 7.6a shows the subtraction (PM_N - PM_F) and Figure 7.6b shows the subtraction (TM_N - TM_F). Figure 7.6c shows the conjunction analysis (combining TM_N - TM_F with PM_N - PM_F)

This conjunction of contrasts produced no significant activations. Separate subtraction analyses also revealed no novelty activations for either task. This finding is clearly illustrated in the SPM(t) maps above.

7.4 Discussion.

The left MTL is involved in the associative encoding of both novel and familiar stimuli [see contrast "The main effect of associative encoding" - $(TM\text{-}PM)_F$ + $(TM\text{-}PM)_N$] as reported in the literature (121-126). Novelty alone (when encoding is stringently matched) does not produce MTL activations [see contrasts 'The main effect of novelty detection' - (PM_N-PM_F) + (TM_N-TM_F)], or any other neuroactivation. This suggests that novelty itself did not produce the activations seen previously (126,132), but rather

the processes generally driven by novelty (i.e. spontaneous encoding) did. The left parietal cortex is involved in the associative encoding of complex scenes irrespective of level of familiarity [contrast conjunction $(TM\text{-}PM)_F + (TM\text{-}PM)_N$]. While memory-related parietal activations have been reported before (124), the strength of this finding is remarkable and should encourage further investigation . The activations in the bilateral superior frontal regions are involved in the processing of familiar material only, irrespective of the level of associative encoding [see contrast "The main effect of familiarity conjunction" - $(TM_F\text{-}TM_N) + (PM_F\text{-}PM_N)$]. Again, these results are consistent with the literature (129, 133, 134, 135) and moreover, the involvement of bilateral frontal regions, rather than right-sided frontal regions alone, in processing familiar material, both in the encoding and matching tasks, will itself be, an important contribution to the literature.

These findings clearly illustrate that

- the MTL is involved in the associative encoding of pictures, whether novel or familiar. Moreover, the results also suggest that
- the MTL does not respond to the detection of novelty alone as might be suggested by the work of Knight 1996 (136).

The use of the 4 condition SPECT procedure allowed these two conclusions to be drawn from within one experiment. A 2 condition paradigm could only have addressed one question. , and two, two-condition experiments would have introduced unwanted inter-subject variability, and greatly reduced the impact of these important findings.

7.5 Conclusions.

This experiment was able to confirm that a multi-task paradigm greatly enhances the power of a SPECT CBF neuroactivation by the addition of two cognitive conditions enabling more subtle differences in cognitive processing to be investigated.

CHAPTER 8

Conclusions and future developments.

Aim: To investigate whether the functional brain mapping technique (SPM) can be extended to embrace the widely available imaging technique of SPECT and to determine whether the combination can contribute to routine diagnosis of abnormalities in brain function and to research investigations involving functional neuroactivation.

Objective 1: To assess the use of the SPM technique in analysing CBF SPECT images of individual subjects, and therefore whether it would be applicable to routine diagnosis.

Conclusion 1: Providing that the procedures described in chapter 3 are followed, i.e. rigid body transformation of non-optimal images to an ideal CBF SPECT image prior to image standardisation followed by manual editing of blurred edges, adequate results were obtained.

Objective 2: To investigate SPM96 as an aid in a specific diagnostic area i.e. the differential diagnosis of dementia using ^{99m}Tc HMPAO SPECT images of rCBF.

Conclusion 2: There is no evidence that the use of SPM96 improved inter-observer agreement in this study.

Objective 3: To investigate the potential benefits of using a 4 scan paradigm compared to a 2 scan paradigm in CBF SPECT neuroactivation

studies within the constraints of the total allowed radiation dose per subject.

Conclusion 3: The addition of a replication of condition allowed by the 4 scan paradigm significantly increased the statistical power of an SPM analysis.

Objective 4: To apply the 4 scan paradigm with a replication of conditions to an exploratory study of the affect of vagal nerve stimulation (as a treatment for intractable epilepsy) on rCBF and investigate

- the reliability of the rCBF pattern within the replication of conditions
- the localisation of rCBF increases and decreases produced by VNS

Conclusion 4: Application of the four scan paradigm to investigate the effect of VNS on rCBF was able to show that the stimulation of the parasympathetic nervous system by VNS causes inhibition in Brodmann area 6.

Objective 5: To apply the 4 scan paradigm with multiple conditions to contrast the role of the medial temporal lobes in novelty detection with their role in the encoding and/or consolidation into long-term memory of associative information.

Conclusion 5: Application of the multi scan paradigm was able to show that the medial temporal lobe is involved in the associative encoding of pictures, whether novel or familiar and that this activation is not due to the detection of novelty alone.

This thesis has shown that the SPM technique originally developed for use with positron emission tomography (PET) radiolabelled water studies of normal brain function during neuroactivation experiments can be used with ^{99m}Tc HMPAO SPECT images.

The use of SPM for the assessment of individual patient data while not of obvious benefit in reporting CBF SPECT scans of dementia, did focus attention on the involvement of the temporal lobes in frontal lobe dementia and therefore played a role in the continuing eductation of scan interpretation. SPM had no problems detecting the abnormal areas of cortical perfusion within the images. The limited benefit found in this study could be due in part to the fact that the observers were very familiar with the standard image display but had relatively little experience of SPM displays. It is possible that a study like this should be repeated in a few years time as familiarity with SPM image presentation grows. This could be accelerated by using SPM(t) maps produced from CBF images showing the classic patterns associated with a particular dementia type as part of an extended learning process of visual reporting for junior radiologists and/or physicists. Familiarity with the SPM results could lead to the robust information provided by the SPM(t) map being more easily incorporated into the existing knowledge base of disease (including post mortem data) and the associated CBF pattern.

The results from this thesis strongly recommend the adoption of a 4 scan paradigm for use with CBF SPECT scan studies of neuroactivation. Although adoption of this protocol will undoubtedly place an increased demand on the subjects, the ability to gain more information for the same effective radiation dose as a 2 scan protocol justifies this inconvenience.

When designing neuroimaging experiments consideration must always be made as to the most suitable technique available. With the growing availability of fMRI capabilities of most MR scanners the newest activation experiments are being designed for this environment. The most obvious advantage of this technique is that it involves no ionising radiation and potentially an unlimited number of acquisitions per subject. However, there are cases where the MR scanner environment is unsuitable. For example, the study described in chapter 6 of VNS stimulation as a treatment for epilepsy could not have been carried out in a MR scanner. Instead PET could have been the modality of choice but the limited clinical application of PET, because of its expense has limited its availability for

use by most groups and as a consequence those groups using PET find that their access to patients is limited. For the investigation of neuroactivation experiments in the clinical population SPECT is ideally placed and the trapping mechanism of SPECT blood flow tracers also means that neuroactivation experiments can be carried out in a more natural setting. The development of this 4 scan technique allows CBF SPECT images to be analysed using powerful voxel-wise techniques such as SPM.

This thesis has focused on cerebral blood flow images. The application of SPM methods to images of neuroreceptor function may be more important in the future and cannot be obtained with MR techniques. The images obtained using tracers such as ^{123}I QNB which map muscarinic receptors in the cerebral cortex could be analysed using the SPM method. Studies looking at the differences in muscarinic receptor distribution between patients suffering from dementia and a normal reference database could be used to monitor the progress of a particular treatment. For example, covariate analysis of voxel intensities could be used to study the relationship between cognitive response to an anti-dementia drug (e.g. Donepezil[18]. used in Alzheimer's disease) and receptor binding potential.

The results from these investigations, both the individual assessment of clinical images and the 4 scan neuroactivation paradigm, have shown that valid results can be obtained from ^{99m}Tc HMPAO SPECT images of the brain. Although PET has advantages as an imaging modality for this type of analysis because of the better resolution and the shorter half life of radiolabelled water (enabling repeated measurements to be made) use of SPM as developed here can help to make SPECT a viable option. This should not place SPECT in direct competition with PET, but it should bring the two modalities closer together, each contributing their specific advantages to the study of human brain function.

[18] donepezil ~Aricept^{TM} Pfizer Inc., New York, NY 10017, USA.

APPENDIX A

There are 3 options for the interpolation method used to reslice the images after spatial normalisation. a) nearest neighbour (Figure A.1) b) bilinear (Figure A.2) c) sinc interpolation (Figure A.3). Option b) is preferred for ^{99m}Tc HMPAO SPECT rCBF images based on empirical evidence. SPM results generated using option a) are noisier, i.e. there are more single voxels that are significant. Results generated using sinc interpolation seem to be no less noisy than using option b) but the registration algorithm takes much longer (approx. 30 mins per scan) to compute.

APPENDIX A

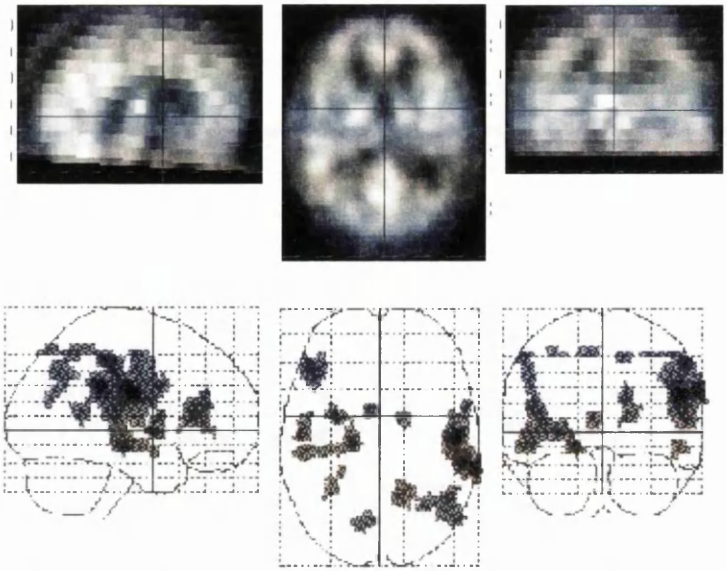

Figure A.1. 3D section display of CBF image after standardisation where the images have been resliced using the nearest neighbour interpolation with the corresponding SPM(t) map of results below.

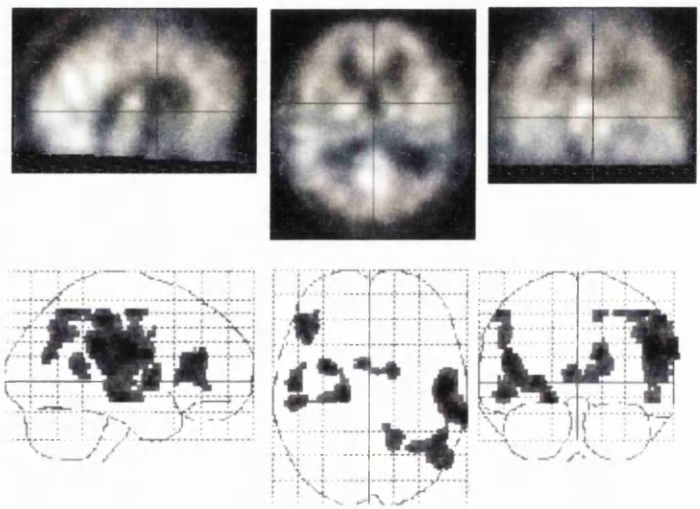

Figure A.2 3D section display of CBF image after standardisation where the images have been resliced using the bilinear interpolation with the corresponding SPM(t) map of results below.

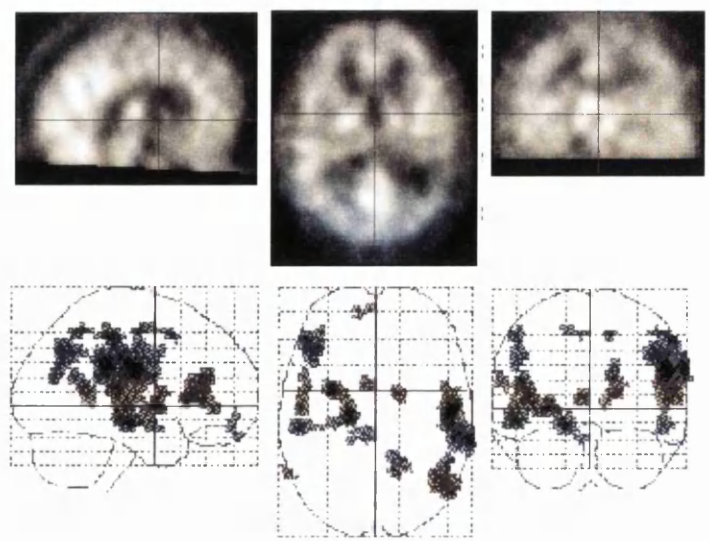

Figure A.3 3D section display of CBF image after standardisation where the images have been resliced using the sincinterpolation with the corresponding SPM(t) map of results below.

Empirical determination of the spatial smoothing filter

The method used to determine empirically which was the best smoothing filter to use with the CBF SPECT scans acquired from the SME810 scanner is described below. To do this a dataset of scans was simulated to represent a subtraction paradigm of activation minus baseline with 10 subjects with 2 scans each (1 scan per task). A pseudo lesion was introduced in order to follow the effects of the different spatial filters on the resulting SPM(t). Two different sized lesions were investigated (99 and 199 voxels respectively). In the first instance the effect of different smoothing filters was investigated in scans acquired using a standard 500MBq dose of Tc99m HMPAO and secondly using a half standard dose of Tc99m HMPAO. The results of those investigations are listed below in tables A1 and A2.

smoothing	LESION SIZE 99 VOXELS			LESION SIZE 199 VOXELS		
filter	region size	amplitude	Zmax * K	region size	amplitude	Zmax * K
xyz mm	(K)	(Zmax)		(K)	(Zmax)	
0	N/S			N/S		
8	129	4.77	615.33	222	6.95	1542.9
10	**152**	**7.67**	**1165.84**	**244**	**8.09**	**1973.96**
12	123	7.62	937.26	236	8.2	1935.2
14	104	7.9	821.6	203	8.9	1806.7
16	68	4.52	307.36	165	8.21	1354.65
18	55	4.55	250.25	121	7.94	960.74
20	36	3.74	134.64	88	7.95	699.6
22	N/S			11	4.41	48.51

Table A.1. Data showing effect of smoothing filters on region size and maximum z-score for a 500MBq dose scan original activation region size a) 99 voxels and b) 199 voxels (1 voxel = 1.57x1.57x6mm) Pu<0.001, Pc< 0.1

smoothing filter xyz mm	LESION SIZE 99 VOXELS region size (K)	amplitude (Zmax)	Zmax * K	LESION SIZE 199 VOXELS region size (K)	amplitude (Zmax)	Zmax * K
0	46	5.51	253.46	104	5.70	592.8
8	188	8.16	1534.08	352	9.95	3502.4
10	207	19.96	4131.72	395	19.57	7730.15
12	**208**	**22.52**	**4684.16**	429	28.45	12205.05
14	197	23.51	4631.47	436	26.76	11667.36
16	185	8.73	1615.05	**432**	**30.78**	**13296.96**
18	169	8.81	1488.89	399	33.3	13286.7
20	140	7.38	1033.2	355	31.37	11136.35
22	11	5.72	62.92	349	31.22	10895.78
	72	5.45	392.4	10	5.14	51.4

Table A.2. Data showing effect of smoothing filters on region size and maximum z-score for a 250MBq dose scan original activation region size a) 99 voxels and b) 199 voxels (1 voxel = 1.57x1.57x6mm) Pu<0.001, Pc< 0.1

The nature of the statistical analysis carried out in SPM95/96 means that the calculation of Z-scores is inherently dependent on the spatial filter used to reduce the variance in the data across each image and across all subjects. The empirical results showed that the optimum, filter based on maximum region size, is different from that with regard to optimum Zmax score. Instead a product of Zmax and region size (Zmax * K) gives an overall view of optimum filter size. The optimum filter size for a standard (500MBq) ^{99m}Tc HMPAO dose is determined as 10 FWHM for both sizes of activation. The optimum filter size for a half standard (250MBq) ^{99m}Tc HMPAO dose is determined as 12mm FWHM for an activation size of 99 voxels and 16 FWHM for an activation size of 199 voxels. If the 12mm FWHM spatial filter is used then the error in this choice in teRMS of Zmax * K for an estimated ROI of 99 voxels is zero and for 199 voxels is 1091 (Zmax * K_{16} - Zmax * K_{12} = 13296 - 12205 = 1091). If the 16mm FWHM spatial filter

is used then the error in this choice is zero for an estimated ROI size of 199 voxels and 3069 for 99 voxels (Zmax * K_{12} - Zmax * K_{16} = 4684-1615 = 3069). Due to the unknown size of the activation region in a "real" neuroactivation experiment a choice of 12mm FWHM filter size was chosen for the half dose scans as it gave the smaller error .

APPENDIX B

The results are listed below (Tables B1-3) for each of the challenge conditions analysed using the "compare groups: 1 scan per subject" option where group 1 was the 10 average scans in the reference data set and group 2 was a single challenge condition sample scan. Global blood flow normalisation was achieved using the proportional scaling option and SPM(t) maps were generated using the default thresholding of $P_u<0.001$, and $P_k<0.5$ (uncorrected).

METHOD 1

ΔZ

DIRN. OF ROTN. (degrees)		AXIAL TRUNCATION 0	18	30
SAG	0	0	0.33	0.89
	6	0.09	0.32	0.67
	9	0.07	0.3	0.54
	12	0.46	0.3	0.56
	15	0.33	0.46	0.59
COR	0	0	0.33	0.89
	6	0.09	0.28	0.09
	9	0.12	0.27	1.03
	12	0.17	0.21	1.03
	15	0.14	0.15	1.05
AX	0	0	0.33	0.89
	6	0.03	0.32	0.89
	9	0.01	0.33	0.89
	12	0.01	0.32	0.89
	15	0.01	0.32	0.89

RMS

DIRN. OF ROTN. (degrees)		AXIAL TRUNCATION 0	18	30
SAG	0	0.00	9.17	52.95
	6	0	5.66	52.95
	9	0	5.66	52.95
	12	9.17	52.95	52.95
	15	52.95	52.95	52.95
COR	0	0.00	9.17	52.95
	6	5.66	5.66	5.66
	9	5.66	5.66	52.95
	12	5.66	5.66	52.95
	15	5.66	5.66	52.95
AX	0	0.00	9.17	52.95
	6	0	9.17	43.86
	9	0	9.17	43.86
	12	0	9.17	43.86
	15	0	9.17	43.86

Table B1. List of all the error teRMS of the average in absolute change in Z score (ΔZ) and root mean squared (RMS) error in location (defined by Talairach co-ordinates) of the most significant voxel within the two pseudo lesions with respect to that reported in the reference scan for the first method of image standardisation. The **first method** involved image standardisation of each of the challenge condition sample images by direct matching to the standard PET template supplied with SPM96, linear spatial standardisation function.

METHOD 2

ΔZ

DIRN. OF ROTN. (degrees)		AXIAL TRUNCATION 0	18	30
SAG	0	0	0.33	0.89
	6	0.25	0.22	0.69
	9	0.23	0.26	0.74
	12	0.34	0.3	0.79
	15	0.09	0.34	0.82
COR	0	0	0.33	0.89
	6	0.11	0.29	0.09
	9	0.07	0.33	0.11
	12	0.08	0.4	0.82
	15	0.11	0.59	N/A
AX	0	0	0.33	0.89
	6	0.12	0.11	0.49
	9	0.12	0.1	0.48
	12	0.12	0.09	0.48
	15	0.12	0.09	0.48

RMS

DIRN. OF ROTN. (degrees)		AXIAL TRUNCATION 0	18	30
SAG	0	0.00	9.17	52.95
	6	0	7.48	5.66
	9	0	7.48	5.66
	12	7.48	7.48	9.80
	15	5.66	7.48	9.80
COR	0	0.00	9.17	52.95
	6	0	2	0
	9	0	2	2
	12	0	2	2
	15	0	2	N/A
AX	0	0.00	9.17	52.95
	6	0	4.47	4.47
	9	0	4.47	4.47
	12	0	4.47	4.47
	15	0	4.47	4.47

Table B2. List of all the error teRMS of the average in absolute change in Z score (ΔZ) and root mean squared (RMS) error in location (defined by Talairach co-ordinates) of the most significant voxel within the two pseudo lesions with respect to that reported in the reference scan for the second method of image standardisation. The **second method** used a rigid body registration step prior to standardisation. Each challenge condition sample image was co-registered to the reference image (the sample image no rotation, no truncation) using a 6 parameter rigid body transform before it was matched to the PET template.

METHOD 3

ΔZ

DIRN. OF ROTN. (degrees)		AXIAL TRUNCATION 0	18	30
SAG	0	0	0.33	0.89
	6	0	0.09	0.36
	9	0	0.09	0.21
	12	0.03	0.04	0.2
	15	0.03	0.04	0.12
COR	0	0	0.33	0.89
	6	0	0.02	0
	9	0	0.03	0.34
	12	0	0.1	0.35
	15	0	0.24	0.51
AX	0	0	0.33	0.89
	6	0	0	0.12
	9	0	0	0.09
	12	0	0	0.1
	15	0	0	0.09

RMS

DIRN. OF ROTN. (degrees)		AXIAL TRUNCATION 0	18	30
SAG	0	0.00	9.17	52.95
	6	0	9.80	5.66
	9	0	9.80	5.66
	12	0	9.80	5.66
	15	5.66	9.80	5.66
COR	0	0	9.17	52.95
	6	0	5.65	0
	9	0	0	2
	12	0	2	2
	15	0	2	2
AX	0	0	9.17	52.95
	6	0	0	4.47
	9	0	0	4.47
	12	0	0	4.47
	15	0	0	4.47

Table B3. List of all the error teRMS of the average in absolute change in Z score (ΔZ) and root mean squared (RMS) error in location (defined by Talairach co-ordinates) of the most significant voxel within the two pseudo lesions with respect to that reported in the reference scan for the third method of image standardisation. The **third method** includes editing of the final standardised sample image after co-registration, standardisation and smoothing to remove spurious data contained in the smoothed edges.

APPENDIX C

Percentage likelihood of diagnosis from CBF SPECT Scan information only.

Case no.	obs1 DAT	obs2 DAT	obs1 DFLT	obs2 DFLT	obs1 DVaT	obs2 DVaT	obs1 Othr	obs2 Othr	obs1 Norm	obs2 Norm
1	100	90	0	0	0	10	0	0	0	0
2	30	40	10	20	30	20	30	20	0	0
3	0	0	0	0	90	70	10	0	0	30
4	0	0	0	50	0	0	0	0	100	50
5	20	10	0	0	40	20	0	0	40	70
6	80	20	0	0	20	80	0	0	0	0
7	100	100	0	0	0	0	0	0	0	0
8	0	90	0	0	10	10	0	0	90	0
9	0	10	50	80	50	0	0	0	0	10
10	0	0	40	100	60	0	0	0	0	0
11	0	0	90	100	10	0	0	0	0	0
12	0	0	100	80	0	0	0	20	0	0
13	0	0	0	0	100	100	0	0	0	0
14	0	0	0	0	60	20	20	0	20	80
15	10	0	0	0	50	70	40	0	0	30
16	10	0	0	0	70	10	0	0	20	90
17	0	0	0	0	0	0	0	0	100	100
18	0	0	0	0	80	60	20	0	0	40
19	20	30	0	0	0	0	0	30	80	40
20	0	0	0	0	50	60	0	0	50	40
21	0	0	0	0	20	20	0	0	80	80
22	20	0	0	20	60	80	20	0	0	0
23	0	0	0	0	20	10	0	0	80	90
24	0	0	0	0	100	100	0	0	0	0
25	0	0	0	10	70	20	0	0	30	70
26	0	0	0	10	0	20	0	0	100	70
27	0	0	0	10	50	0	0	0	50	90
28	50	0	0	50	50	50	0	0	0	0
29	0	0	20	20	80	80	0	0	0	0
30	0	10	0	0	100	90	0	0	0	0
31	0	20	0	0	0	0	0	0	100	80
32	0	0	0	0	100	100	0	0	0	0
33	0	0	0	30	40	70	0	0	60	0
34	50	80	0	0	0	20	0	0	50	0
35	0	30	0	0	100	70	0	0	0	0
36	0	0	0	0	100	80	0	0	0	20
37	0	0	0	0	20	0	0	0	80	100
38	80	80	0	0	20	20	0	0	0	0
39	0	0	20	10	20	80	20	0	40	10

DAT - Dementia of the Alzheimer's type, DFLT - Dementia of the frontal lobe type, DVaT - Dementia of the Vascular type, othr - other dementia, norm -normal (no abnormalities)

Table C1. Percentage likelihood of diagnosis from CBF SPECT Scan information only for observer 1 and 2.

Percentage likelihood of diagnosis from CBF SPECT scan with additional information from SPM analysis

Code no.	obs1 *DAT*	obs2 *DAT*	obs1 *DFLT*	obs2 *DFLT*	obs1 *DVaT*	obs2 *DVaT*	obs1 *Othr*	obs2 *Othr*	obs1 *Norm*	obs2 *Norm*
1	90	95	10	0	0	0	0	0	0	5
2	90	90	0	0	10	10	0	0	0	0
3	0	0	0	0	100	80	0	0	0	20
4	0	0	0	70	0	0	0	0	100	30
5	40	0	0	0	60	20	0	0	0	80
6	80	0	0	0	20	80	0	0	0	20
7	100	100	0	0	0	0	0	0	0	0
8	10	100	0	0	10	0	0	0	80	0
9	0	10	50	10	50	80	0	0	0	0
10	0	0	50	60	50	0	0	0	0	40
11	0	0	90	30	10	70	0	0	0	0
12	0	0	100	60	0	20	0	20	0	0
13	0	0	0	0	100	100	0	0	0	0
14	0	0	20	0	60	40	20	0	0	60
15	20	0	0	0	70	90	10	0	0	10
16	30	20	0	0	60	20	0	0	10	60
17	0	0	0	0	0	10	0	0	100	90
18	0	0	0	0	70	70	30	0	0	30
19	10	0	0	0	0	0	0	0	90	100
20	50	0	0	0	40	40	0	0	60	60
21	20	0	0	0	20	70	0	0	60	30
22	10	0	0	0	70	80	20	20	0	0
23	0	0	0	0	0	0	0	0	100	100
24	0	0	0	0	100	100	0	0	0	0
25	30	70	0	0	70	20	0	0	0	10
26	0	0	0	0	20	30	0	0	80	70
27	0	0	20	0	30	10	0	0	50	90
28	50	0	0	0	50	70	0	0	0	30
29	0	0	20	0	50	60	30	40	0	0
30	0	10	0	0	100	90	0	0	0	0
31	0	0	0	0	0	30	0	0	100	70
32	0	0	0	0	100	100	0	0	0	0
33	0	0	0	0	60	100	0	0	40	0
34	40	0	0	0	40	100	20	0	0	0
35	0	60	20	0	80	40	0	0	0	
36	0	10	0	0	100	90	0	0	0	
37	0	0	0	0	20	10	0	0	80	90
38	80	20	0	0	0	80	20	0	0	
39	0	0	30	0	30	80	20	0	20	20

DAT - Dementia of the Alzheimer's type, DFLT - Dementia of the frontal lobe type, DVaT - Dementia of the Vascular type, othr - other dementia, norm -normal (no abnormalities)

Table C2. Percentage likelihood of diagnosis from CBF SPECT Scan and additional information from SPM(t) map for observer 1 and 2.

AGREEMENT OF RESULTS FROM CBF SPECT DATA ONLY.

KAPPA calculation for overall agreement (95).

		obs2 DAT	DFLT	DVaT	othr	norm	expected	
	DAT	3				1	4 (5x4)/39	0.513
obs1	DFLT		3	1			4 (3x4)/39	0.308
	DVaT	2		13	1	2	18(18x18)/39	8.308
	othr				1		1 (1x2)/39	0.051
	Norm			4		8	12(12x16)/39	3.385
		5	3	18	2	11	39	12.56

Table C3a. Frequency table for a kappa calculation of agreement between 2 observers of diagnosis from CBF SPECT data only.

K = (sum obs-sum exp)/(N-sum exp)

$$= \frac{(3+3+13+1+8) - (0.51+0.3+8.3+0+3.39)}{39 - (0.51+0.3+8.3+0+3.39)}$$

K = (28 - 12.56)/(39 - 12.56) = **0.584** moderate agreement

AGREEMENT OF RESULTS FROM CBF SPECT AND SPM(t) DATA .

KAPPA calculation for overall agreement

		obs2* DAT	DFLT	DVaT	othr	NORM	expected	
	DAT	3		2			5 (5x7)/39	0.897
obs1*	DFLT		2	2			4 (4x3)/39	0.308
	DVaT	2		13		3	18(18x18)/39	8.308
	othr			1			1 (1x0)/39	0
	NORM	2	1			8	11(11x11)/39	3.103
		7	3	18	0	11	39	12.62

Table C3b. Frequency table for a kappa calculation of agreement between 2 observers of diagnosis from CBF SPECT data and additional information from SPM(t) map.

K = (sum obs-sum exp)/(N-sum exp)

$$= \frac{(3+2+13+0+8) - (0.9+0.3+8.3+0+3.1)}{39 - (0.9+0.3+8.3+0+3.1)}$$

K = (26 - 12.62)/(39 - 12.62) = **0.507** moderate agreement

Weighted KAPPA (K_w) calculations for agreement between observers of diagnosis.

$$K_{(w)} = (Po_{(w)} - Pe_{(w)})/(1 - Pe_{(w)})$$

and

$$W_{ij} = 1 - (|i - j| / g - 1)$$

where i is the row number and j the column number and g the number of categories or rating levels .

$$P_{o(w)} = (1/n)(\Sigma \Sigma w_{ij} * f_{ij})$$

$$P_{e(w)} = (1/n^2)(\Sigma \Sigma w_{ij} * F_i * F_j)$$

where f_{ij} is the entry in the frequency table for row i and column j.

where F_i is the total number of observations entered in the frequency table for row i.

where F_j is the total number of observations entered in the frequency table for column j.

Weighted
Kappa

	0	1	2	3	4	5	6	7	8	9	10
0	1	0.9	0.8	0.7	0.6	0.5	0.4	0.3	0.2	0.1	0
1	0.9	1	0.9	0.8	0.7	0.6	0.5	0.4	0.3	0.2	0.1
2	0.8	0.9	1	0.9	0.8	0.7	0.6	0.5	0.4	0.3	0.2
3	0.7	0.8	0.9	1	0.9	0.8	0.7	0.6	0.5	0.4	0.3
4	0.6	0.7	0.8	0.9	1	0.9	0.8	0.7	0.6	0.5	0.4
5	0.5	0.6	0.7	0.8	0.9	1	0.9	0.8	0.7	0.6	0.5
6	0.4	0.5	0.6	0.7	0.8	0.9	1	0.9	0.8	0.7	0.6
7	0.3	0.4	0.5	0.6	0.7	0.8	0.9	1	0.9	0.8	0.7
8	0.2	0.3	0.4	0.5	0.6	0.7	0.8	0.9	1	0.9	0.8
9	0.1	0.2	0.3	0.4	0.5	0.6	0.7	0.8	0.9	1	0.9
10	0	0.1	0.2	0.3	0.4	0.5	0.6	0.7	0.8	0.9	1

Table C4. Weighting values used to calculate a weighted kappa measure of agreement.

Weighted KAPPA (K_W) calculations for agreement between observers of diagnosis.

$$K_{(w)} = (Po_{(w)} - Pe_{(w)})/(1 - Pe_{(w)})$$

and

$$W_{ij} = 1 - (|i - j| / g - 1)$$

where i is the row number and j the column number and g the number of categories or rating levels .

$$P_{o(w)} = (1/n)(\Sigma \Sigma w_{ij} * f_{ij})$$

$$P_{e(w)} = (1/n^2)(\Sigma \Sigma w_{ij} * f_{ij})$$ $F_i * F_j$

where f is the entry in the frequency table for row i and column j.

F_i is the total n° of observations in row i

F_j is the total n° of observations in column j.

Weighted Kappa

	0	1	2	3	4	5	6	7	8	9	10
0	1	0.9	0.8	0.7	0.6	0.5	0.4	0.3	0.2	0.1	0
1	0.9	1	0.9	0.8	0.7	0.6	0.5	0.4	0.3	0.2	0.1
2	0.8	0.9	1	0.9	0.8	0.7	0.6	0.5	0.4	0.3	0.2
3	0.7	0.8	0.9	1	0.9	0.8	0.7	0.6	0.5	0.4	0.3
4	0.6	0.7	0.8	0.9	1	0.9	0.8	0.7	0.6	0.5	0.4
5	0.5	0.6	0.7	0.8	0.9	1	0.9	0.8	0.7	0.6	0.5
6	0.4	0.5	0.6	0.7	0.8	0.9	1	0.9	0.8	0.7	0.6
7	0.3	0.4	0.5	0.6	0.7	0.8	0.9	1	0.9	0.8	0.7
8	0.2	0.3	0.4	0.5	0.6	0.7	0.8	0.9	1	0.9	0.8
9	0.1	0.2	0.3	0.4	0.5	0.6	0.7	0.8	0.9	1	0.9
10	0	0.1	0.2	0.3	0.4	0.5	0.6	0.7	0.8	0.9	1

Table C4. Weighting values used to calculate a weighted kappa measure of agreement.

Agreement for the dementia of the Alzheimers type category from CBF SPECT Scan information only

DAT

obs1 \ obs2	0	1	2	3	4	5	6	7	8	9	10	
0	22	3	1	0	0	1	0	0	0	0	0	27
1	2	0	1	0	0	0	0	0	0	0	0	3
2	1	0	0	0	0	0	0	0	1	0	0	2
3	1	0	1	1	0	0	0	0	0	0	0	3
4	0	0	0	0	0	0	0	0	0	0	0	0
5	0	0	0	0	0	0	0	0	0	0	0	0
6	0	0	0	0	0	0	0	0	0	0	0	0
7	0	0	0	0	0	0	0	0	0	0	0	0
8	0	0	0	0	0	0	0	0	1	0	0	1
9	1	0	0	0	0	0	0	0	0	0	1	2
10	0	0	0	0	0	0	0	0	0	0	1	1
	27	3	3	1	0	1	0	0	2	0	2	39

Table C5. Frequency table of agreement for the disease category DAT.

obs1 \ obs2	0	1	2	3	4	5	6	7	8	9	10	
0	22	2.7	0.8	0	0	0.5	0	0	0	0	0	
1	1.8	0	0.9	0	0	0	0	0	0	0	0	
2	0.8	0	0	0	0	0	0	0	0.4	0	0	
3	0.7	0	0.9	1	0	0	0	0	0	0	0	
4	0	0	0	0	0	0	0	0	0	0	0	
5	0	0	0	0	0	0	0	0	0	0	0	
6	0	0	0	0	0	0	0	0	0	0	0	
7	0	0	0	0	0	0	0	0	0	0	0	
8	0	0	0	0	0	0	0	0	1	0	0	
9	0.1	0	0	0	0	0	0	0	0	0	0.9	
10	0	0	0	0	0	0	0	0	0	0	1	
												0.91

Table C6. Frequency table of weighted agreement

obs1 \ obs2	0	1	2	3	4	5	6	7	8	9	10	
0	676	70.2	62.4	18.2	0	13	0	0	10.4	0	0	
1	70.2	9	8.1	2.4	0	1.8	0	0	1.8	0	0.6	
2	41.6	5.4	6	1.8	0	1.4	0	0	1.6	0	0.8	
3	54.6	7.2	8.1	3	0	2.4	0	0	3	0	1.8	
4	0	0	0	0	0	0	0	0	0	0	0	
5	0	0	0	0	0	0	0	0	0	0	0	
6	0	0	0	0	0	0	0	0	0	0	0	
7	0	0	0	0	0	0	0	0	0	0	0	
8	5.2	0.9	1.2	0.5	0	0.7	0	0	2	0	1.6	
9	5.2	1.2	1.8	0.8	0	1.2	0	0	3.6	0	3.6	
10	0	0.3	0.6	0.3	0	0.5	0	0	1.6	0	2	
												0.78

Table C7. Frequency table of the weighted agreement expected by chance.

$$K_w = (0.91 - 0.78)/(1-0.78) = 0.59$$

Agreement for the dementia of the frontal lobe type category from CBF SPECT Scan information only.

DFLT

obs1 \ obs2	0	1	2	3	4	5	6	7	8	9	10	
0	30	0	1	0	0	0	0	0	0	0	0	31
1	0	1	1	0	0	0	0	0	0	0	0	2
2	2	0	0	0	0	1	0	0	0	0	0	3
3	0	0	0	0	0	0	0	0	0	0	0	0
4	0	0	0	0	0	0	0	0	0	0	0	0
5	0	0	0	0	0	0	0	0	0	0	0	0
6	0	0	0	0	0	0	0	0	0	0	1	1
7	0	0	0	0	0	0	0	0	0	0	0	0
8	0	0	0	0	1	0	0	0	0	0	0	1
9	0	0	0	0	0	0	0	0	0	1	0	1
10	0	0	0	0	0	0	0	0	0	0	0	0
	32	1	2	0	1	1	0	0	0	1	1	39

Table C8. Frequency table of agreement for the disease category DFLT.

obs1 \ obs2	0	1	2	3	4	5	6	7	8	9	10
0	29	0	0.8	0	0	0	0	0	0	0	0
1	0	1	0.9	0	0	0	0	0	0	0	0
2	1.6	0	0	0	0	0.7	0	0	0	0	0
3	0	0	0	0	0	0	0	0	0	0	0
4	0	0	0	0	0	0	0	0	0	0	0
5	0	0	0	0	0	0	0	0	0	0	0
6	0	0	0	0	0	0	0	0	0	0	0.6
7	0	0	0	0	0	0	0	0	0	0	0
8	0	0	0	0	0.6	0	0	0	0	0	0
9	0	0	0	0	0	0	0	0	0	1	0
10	0	0	0	0	0	0	0	0	0	0	0

0.953

Table C9. Frequency table of weighted agreement

obs1 \ obs2	0	1	2	3	4	5	6	7	8	9	10
0	930	27	48	0	18	15	0	0	0	3	0
1	55.8	2	3.6	0	1.4	1.2	0	0	0	0.4	0.2
2	74.4	2.7	6	0	2.4	2.1	0	0	0	0.9	0.6
3	0	0	0	0	0	0	0	0	0	0	0
4	0	0	0	0	0	0	0	0	0	0	0
5	0	0	0	0	0	0	0	0	0	0	0
6	12.4	0.5	1.2	0	0.8	0.9	0	0	0	0.7	0.6
7	0	0	0	0	0	0	0	0	0	0	0
8	6.2	0.3	0.8	0	0.6	0.7	0	0	0	0.9	0.8
9	3.1	0.2	0.6	0	0.5	0.6	0	0	0	1	0.9
10	0	0	0	0	0	0	0	0	0	0	0

0.851

Table C10. Frequency table of the weighted agreement expected by chance.

$$K_w = (0.953 - 0.851)/(1-0.851) = 0.685$$

Agreement for the dementia of the vascular type category from CBF SPECT Scan information only.

DVaT

obs1 \ obs2	0	1	2	3	4	5	6	7	8	9	10	
0	6	1	1	2	1	0	0		0	0	0	11
1	1	1	1	0	0	0	0	1	0	0	0	4
2	1	0	2	0	1	0	1	1	0	0	0	6
3	0	0	0	1	0	0	0	0	0	0	0	1
4	0	0	0	0	0	0	0	0	0	0	0	0
5	0	0	0	0	0	1	0	0	0	0	0	1
6	0	0	1	0	0	0	0	0	1	0	0	2
7	0	0	0	0	1	1	0	0	0	1	1	4
8	0	0	2	0	0	0	1	0	1	0	1	5
9	0	0	0	0	0	0	0	0	1	0	1	2
10	0	0	0	0	0	0	0	0	0	0	3	3
	8	2	7	3	3	2	2	2	3	1	6	39

Table C11. Frequency table of agreement for the disease category DVaT.

obs 1 \ obs 2	0	1	2	3	4	5	6	7	8	9	10
0	6	0.9	0.8	1.4	0.6	0	0	0	0	0	0
1	0.9	1	0.9	0	0	0	0	0.4	0	0	0
2	0.8	0	2	0	0.8	0	0.6	0.5	0	0	0
3	0	0	0	1	0	0	0	0	0	0	0
4	0	0	0	0	0	0	0	0	0	0	0
5	0	0	0	0	0	1	0	0	0	0	0
6	0	0	0	0	0	0	0	0	0.8	0	0
7	0	0	0	0	0.7	0.8	0	0	0	0.8	0.7
8	0	0	0.8	0	0	0	0.8	0	1	0	0.8
9	0	0	0	0	0	0	0	0	0.9	0	0.9
10	0	0	0	0	0	0	0	0	0	0	3

0.832

Table C12. Frequency table of weighted agreement

obs 1 \ obs 2	0	1	2	3	4	5	6	7	8	9	10
0	88	19.8	52.8	23.1	19.8	11	8.8	6.6	6.6	1.1	0
1	28.8	8	21.6	9.6	8.4	4.8	4	3.2	3.6	0.8	2.4
2	38.4	10.8	36	16.2	14.4	8.4	7.2	6	7.2	1.8	7.2
3	5.6	1.6	5.4	3	2.7	1.6	1.4	1.2	1.5	0.4	1.8
4	0	0	0	0	0	0	0	0	0	0	0
5	4	1.2	4.2	2.4	2.7	2	1.8	1.6	2.1	0.6	3
6	3.2	1	3.6	2.1	2.4	1.8	2	1.8	2.4	0.7	3.6
7	9.6	3.2	12	7.2	8.4	6.4	7.2	8	10.8	3.2	16.8
8	8	3	12	7.5	9	7	8	9	15	4.5	24
9	1.6	0.8	3.6	2.4	3	2.4	2.8	3.2	5.4	2	10.8
10	0	0.6	3.6	2.7	3.6	3	3.6	4.2	7.2	2.7	18

0.589

Table C13. Frequency table of the weighted agreement expected by chance.

$$K_w = (0.832 - 0.589)/(1-0.589) = 0.591$$

Agreement for the normal category from CBF SPECT Scan information only.

norm

obs 1 \ obs 2	0	1	2	3	4	5	6	7	8	9	10	
0	18	0	0	0		0	1	0	0	0	0	19
1	1	0	0	0	1	0	0	0	0	0	0	2
2	1	0	0	0	0	0	0	0	0	0	0	1
3	2	0	0	0	0	0	0	0	0	0	0	2
4	1	0	0	0	0	0	0	0	1	0	0	2
5	0	0	0	0	0	0	0	0	0	0	1	1
6	0	0	0	0	0	0	0	0	0	0	0	0
7	0	0	0	1	1	0	0	0	0	0	1	3
8	0	0	1	0	0	0	0	0	1	0	1	3
9	0	0	1	0	0	1	0	0	1	0	0	3
10	0	0	0	0	0	0	0	0	1	1	1	3
	23	0	2	1	2	1	1	0	4	1	4	39

Table C14. Frequency table of agreement for the normal category.

obs 1 \ obs 2	0	1	2	3	4	5	6	7	8	9	10
0	18	0	0	0	0	0	0.4	0	0	0	0
1	0.9	0	0	0	0.7	0	0	0	0	0	0
2	0.8	0	0	0	0	0	0	0	0	0	0
3	1.4	0	0	0	0	0	0	0	0	0	0
4	0.6	0	0	0	0	0	0	0	0.6	0	0
5	0	0	0	0	0	0	0	0	0	0	0.5
6	0	0	0	0	0	0	0	0	0	0	0
7	0	0	0	0.6	0.7	0	0	0	0	0	0.7
8	0	0	0.4	0	0	0	0	0	1	0	0.8
9	0	0	0.3	0	0	0.6	0	0	0.9	0	0
10	0	0	0	0	0	0	0	0	0.8	0.9	1

0.836

Table C15. Frequency table of weighted agreement

obs 1 \ obs 2	0	1	2	3	4	5	6	7	8	9	10
0	437	0	30	13.3	22.8	9.5	7.6	0	15	1.9	0
1	41.4	0	3.6	1.6	2.8	1.2	1	0	2.4	0.4	0.8
2	18.4	0	2	0.9	1.6	0.7	0.6	0	1.6	0.3	0.8
3	32.2	0	3.6	2	3.6	1.6	1.4	0	4	0.8	2.4
4	27.6	0	3.2	1.8	4	1.8	1.6	0	4.8	1	3.2
5	11.5	0	1.4	0.8	1.8	1	0.9	0	2.8	0.6	2
6	0	0	0	0	0	0	0	0	0	0	0
7	20.7	0	3	1.8	4.2	2.4	2.7	0	11	2.4	8.4
8	13.8	0	2.4	1.5	3.6	2.1	2.4	0	12	2.7	9.6
9	6.9	0	1.8	1.2	3	1.8	2.1	0	11	3	10.8
10	0	0	1.2	0.9	2.4	1.5	1.8	0	9.6	2.7	12

0.639

Table C16. Frequency table of the weighted agreement expected by chance.

$$K_w = (0.836 - 0.639)/(1-0.639) = 0.546$$

Agreement for the dementia of the Alzheimers type category from CBF SPECT Scan and SPM(t) data.

DAT

obs 1 \ obs 2	0	1	2	3	4	5	6	7	8	9	10	
0	22	2	2	0	1	1	0	0	1	0	0	29
1	3	0	0	0	0	0	0	0	0	0	0	3
2	0	0	0	1	0	0	0	0	1	0	0	2
3	0	0	0	0	0	0	0	0	0	0	0	0
4	0	0	0	0	0	0	0	0	0	0	0	0
5	0	0	0	0	0	0	0	0	0	0	0	0
6	0	0	0	0	0	0	0	0	0	0	0	0
7	0	0	0	1	0	0	0	0	0	0	0	1
8	0	0	0	0	0	0	0	0	0	0	0	0
9	0	0	0	0	0	0	0	0	0	2	0	2
10	0	1	0	0	0	0	0	0	0	0	1	2
	25	3	2	2	1	1	0	0	2	2	1	39

Table C17. Frequency table of agreement for the disease category DAT.

obs 1 \ obs2	0	1	2	3	4	5	6	7	8	9	10
0	21	1.8	1.6	0	0.6	0.5	0	0	0.2	0	0
1	2.7	0	0	0	0	0	0	0	0	0	0
2	0	0	0	0.9	0	0	0	0	0.4	0	0
3	0	0	0	0	0	0	0	0	0	0	0
4	0	0	0	0	0	0	0	0	0	0	0
5	0	0	0	0	0	0	0	0	0	0	0
6	0	0	0	0	0	0	0	0	0	0	0
7	0	0	0	0.6	0	0	0	0	0	0	0
8	0	0	0	0	0	0	0	0	0	0	0
9	0	0	0	0	0	0	0	0	0	2	0
10	0	0.1	0	0	0	0	0	0	0	0	1

0.856

Table C18. Frequency table of weighted agreement

obs 1 \ obs 2	0	1	2	3	4	5	6	7	8	9	10
0	672	75.6	44.8	39.2	16.8	14	0	0	11.2	5.6	0
1	64.8	0	0	0	0	0	0	0	0	0	0
2	38.4	0	4	3.6	1.6	1.4	0	0	1.6	1.2	0.4
3	0	0	0	0	0	0	0	0	0	0	0
4	0	0	0	0	0	0	0	0	0	0	0
5	0	0	0	0	0	0	0	0	0	0	0
6	0	0	0	0	0	0	0	0	0	0	0
7	7.2	0	1	1.2	0.7	0.8	0	0	1.8	1.6	0.7
8	0	0	0	0	0	0	0	0	0	0	0
9	4.8	0	1.2	1.6	1	1.2	0	0	3.6	4	1.8
10	0	0	0.8	1.2	0.8	1	0	0	3.2	3.6	2

0.686

Table C19. Frequency table of the weighted agreement expected by chance.

$$K_w = (0.856 - 0.686)/(1-0.686) = 0.541$$

Agreement for the dementia of the frontal lobe type category from CBF SPECT Scan and SPM(t) data.

DFLT

	obs 2											
obs 1	0	1	2	3	4	5	6	7	8	9	10	
0	28	1	4	1	0	0	0	0	0	0	0	34
1	0	0	0	0	0	1	0	0	0	0	0	1
2	0	0	0	0	0	0	0	0	0	0	0	0
3	0	0	0	0	0	0	0	0	0	1	0	1
4	0	0	0	0	0	0	0	0	0	0	0	0
5	0	0	0	0	0	0	0	0	0	0	0	0
6	0	0	0	0	0	1	0	0	0	0	1	2
7	1	0	0	0	0	0	0	0	0	0	0	1
8	0	0	0	0	0	0	0	0	0	0	0	0
9	0	0	0	0	0	0	0	0	0	0	0	0
10	0	0	0	0	0	0	0	0	0	0	0	0
	29	1	4	1	0	2	0	0	0	1	1	39

Table C20. Frequency table of agreement for the disease category DFLT.

	obs 1											
obs 1	0	1	2	3	4	5	6	7	8	9	10	
0	28	0.9	3.2	0.7	0	0	0	0	0	0	0	
1	0	0	0	0	0	0.6	0	0	0	0	0	
2	0	0	0	0	0	0	0	0	0	0	0	
3	0	0	0	0	0	0	0	0	0	0.4	0	
4	0	0	0	0	0	0	0	0	0	0	0	
5	0	0	0	0	0	0	0	0	0	0	0	
6	0	0	0	0	0	0.9	0	0	0	0	0.6	
7	0.3	0	0	0	0	0	0	0	0	0	0	
8	0	0	0	0	0	0	0	0	0	0	0	
9	0	0	0	0	0	0	0	0	0	0	0	
10	0	0	0	0	0	0	0	0	0	0	0	
												0.913

Table C21. Frequency table of weighted agreement

	obs 2											
obs 1	0	1	2	3	4	5	6	7	8	9	10	
0	986	30.6	108.8	23.8	0	34	0	0	0	3.4	0	
1	26.1	1	3.6	0.8	0	1.2	0	0	0	0.2	0.1	
2	0	0	0	0	0	0	0	0	0	0	0	
3	20.3	0.8	3.6	1	0	1.6	0	0	0	0.4	0.3	
4	0	0	0	0	0	0	0	0	0	0	0	
5	0	0	0	0	0	0	0	0	0	0	0	
6	23.2	1	4.8	1.4	0	3.6	0	0	0	1.4	1.2	
7	8.7	0.4	2	0.6	0	1.6	0	0	0	0.8	0.7	
8	0	0	0	0	0	0	0	0	0	0	0	
9	0	0	0	0	0	0	0	0	0	0	0	
10	0	0	0	0	0	0	0	0	0	0	0	
												0.854

Table C22. Frequency table of the weighted agreement expected by chance.

$$K_w = (0.913 - 0.854)/(1-0.854) = 0.4$$

Agreement for the dementia of the vascular type category from CBF SPECT Scan and SPM(t) data.

DVaT

obs 1 \ obs 2	0	1	2	3	4	5	6	7	8	9	10	
0	5	1	0	0	0	1	0	0	0	0	0	7
1	1	1	1	1	0	0	0	0	0	0	0	4
2	1	0	0	0	0	0	2	1	0	0	0	4
3	1	0	1	0	0	0	0	0	0	0	0	2
4	0	0	0	0	1	0	1	0	1	0	0	3
5	0	0	0	0	0	0	0	0	0	0	0	0
6	0	0	0	0	0	1	0	0	0	0	0	1
7	0	1	1	0	0	1	0	1	0	0	0	4
8	1	0	1	1	0	1	0	1	0	0	1	6
9	0	0	0	0	0	0	0	1	0	0	2	3
10	0	0	0	0	0	0	1	0	0	0	4	5
	9	3	4	2	1	4	4	4	1	0	7	39

Table C23. Frequency table of agreement for the disease category DVaT.

obs 1 \ obs 2	0	1	2	3	4	5	6	7	8	9	10	
0	5	0.9	0	0	0	0.5	0	0	0	0	0	
1	0.9	1	0.9	0.8	0	0	0	0	0	0	0	
2	0.8	0	0	0	0	0	1.2	0.5	0	0	0	
3	0.7	0	0.9	0	0	0	0	0	0	0	0	
4	0	0	0	0	1	0	0.8	0	0.6	0	0	
5	0	0	0	0	0	0	0	0	0	0	0	
6	0	0	0	0	0	0.9	0	0	0	0	0	
7	0	0.4	0.5	0	0	0.8	0	1	0	0	0	
8	0.2	0	0.4	0.5	0	0.7	0	0.9	0	0	0.8	
9	0	0	0	0	0	0	0	0.8	0	0	1.8	
10	0	0	0	0	0	0	0.6	0	0	0	4	
												0.79

Table C24. Frequency table of weighted agreement

obs 1 \ obs 2	0	1	2	3	4	5	6	7	8	9	10	
0	63	18.9	22.4	9.8	4.2	14	11.2	8.4	1.4	0	0	
1	32.4	12	14.4	6.4	2.8	9.6	8	6.4	1.2	0	2.8	
2	28.8	10.8	16	7.2	3.2	11.2	9.6	8	1.6	0	5.6	
3	12.6	4.8	7.2	4	1.8	6.4	5.6	4.8	1	0	4.2	
4	16.2	6.3	9.6	5.4	3	10.8	9.6	8.4	1.8	0	8.4	
5	0	0	0	0	0	0	0	0	0	0	0	
6	3.6	1.5	2.4	1.4	0.8	3.6	4	3.6	0.8	0	4.2	
7	10.8	4.8	8	4.8	2.8	12.8	14.4	16	3.6	0	19.6	
8	10.8	5.4	9.6	6	3.6	16.8	19.2	21.6	6	0	33.6	
9	2.7	1.8	3.6	2.4	1.5	7.2	8.4	9.6	2.7	0	18.9	
10	0	1.5	4	3	2	10	12	14	4	0	35	
												0.581

Table C25. Frequency table of the weighted agreement expected by chance.

$$K_W = (0.79 - 0.581)/(1-0.581) = 0.498$$

Agreement for the normal category from CBF SPECT Scan and SPM(t) data.

norm

obs 1 \ obs 2	0	1	2	3	4	5	6	7	8	9	10	
0	16	0	0	0	1	0	0	0	1	0	0	18
1	2	0	0	0	0	0	0	0	0	0	0	2
2	2	0	1	0	0	0	0	0	0	0	0	3
3	2	0	0	0	0	0	1	0	0	0	1	4
4	1	0	0	0	0	0	0	0	0	0	0	1
5	0	0	0	0	0	0	0	0	0	0	0	0
6	1	1	0	0	0	0	1	0	0	0	0	3
7	0	0	0	0	0	0	0	0	1	0	1	2
8	1	0	0	0	0	0	0	0	0	0	0	1
9	0	0	0	0	0	1	0	0	1	0	1	3
10	0	0	0	0	0	0	0	0	0	1	1	2
	25	1	1	0	1	1	2	0	3	1	4	39

Table C26. Frequency table of agreement for the normal category.

obs 1 \ obs 2	0	1	2	3	4	5	6	7	8	9	10
0	16	0	0	0	0.6	0	0	0	0.2	0	0
1	1.8	0	0	0	0	0	0	0	0	0	0
2	1.6	0	1	0	0	0	0	0	0	0	0
3	1.4	0	0	0	0	0	0.7	0	0	0	0.3
4	0.6	0	0	0	0	0	0	0	0	0	0
5	0	0	0	0	0	0	0	0	0	0	0
6	0.4	0.5	0	0	0	0	1	0	0	0	0
7	0	0	0	0	0	0	0	0	0.9	0	0.7
8	0.2	0	0	0	0	0	0	0	0	0	0
9	0	0	0	0	0	0.6	0	0	0.9	0	0.9
10	0	0	0	0	0	0	0	0	0	0.9	1

0.826

Table C27. Frequency table of weighted agreement

obs 1 \ obs 2	0	1	2	3	4	5	6	7	8	9	10
0	450	16.2	14	0	10.8	9	14.4	0	11	1.8	0
1	45	1.8	2	0	1.6	1.4	2.4	0	2.4	0.6	0
2	60	2.4	2.7	0	2.7	2.4	4.2	0	4.5	1.2	0
3	70	2.8	3.2	0	4	3.6	6.4	0	7.2	2	6.4
4	15	0.6	0.7	0	0.9	1	1.8	0	2.1	0.6	2
5	0	0	0	0	0	0	0	0	0	0	0
6	30	1.2	1.5	0	2.1	2.4	5.4	0	8.1	2.4	8.4
7	15	0.6	0.8	0	1.2	1.4	3.2	0	6	1.8	6.4
8	5	0.2	0.3	0	0.5	0.6	1.4	0	2.7	1	3.6
9	7.5	0.3	0.6	0	1.2	1.5	3.6	0	7.2	2.7	12
10	0	0	0.2	0	0.6	0.8	2	0	4.2	1.6	7.2

0.632

Table C28. Frequency table of the weighted agreement expected by chance.

$$K_w = (0.826 - 0.632)/(1-0.632) = 0.53$$

Appendix D

The following pages list the the results from an SPM analysis to investigate the impact of visual stimulus on CBF, using two groups of subjects. The first group contains five patients who were injected with ^{99m}Tc HMPAO with their eyes shut, the second group were injected with their eyes open. The statistical option chosen was 'compare groups; 1 scan per subject'. The contrast design was (1, -1) and (-1, 1). Global normalisation was acheived using proportional scaling.

Figure D1. A list of the scan numbers, group number, subject number and the global mean voxel intensity scaled to 50 ml/min/100g

Figure D2. Design matrix of the SPM analysis described above.

Figure D3. SPM(F) map of the results of an F test on every voxel in the analysis and represents any unexplained variance in the data. The contrasts are listed below.

Figure D4. SPM(t) contrast 1 (1 -1) represents the increases in the eyes closed condition with respect to the eyes open condition.

pg 5 SPM(t) contrast 2 (-1 1) represents the increases in the eyes open condition with respect to the eyes closed condition.

Statistical analysis

Base directory:
/homes/abarnes/work_in_progress/VNS/occ_act/nformat

Scan Index	Group	Subject	Global	Filename Tails
01 :	1	1	52.5178	/snA509B.img
02 :	1	2	46.3219	/snD615B.img
03 :	1	3	46.8641	/snD705B.img
04 :	1	4	50.2058	/snD707B.img
05 :	1	5	51.634	/snD709B.img
06 :	2	1	49.1376	/snD699S.img
07 :	2	2	51.7105	/snP157S.img
08 :	2	3	52.3154	/snD701S.img
09 :	2	4	47.0633	/snP253S.img
10 :	2	5	52.2296	/snD719S.img

Images scaled to an overall grand mean of 50
Gray matter threshold is 80% of the whole brain mean
Covariates are centered before inclusion in design matrix

Design Matrix

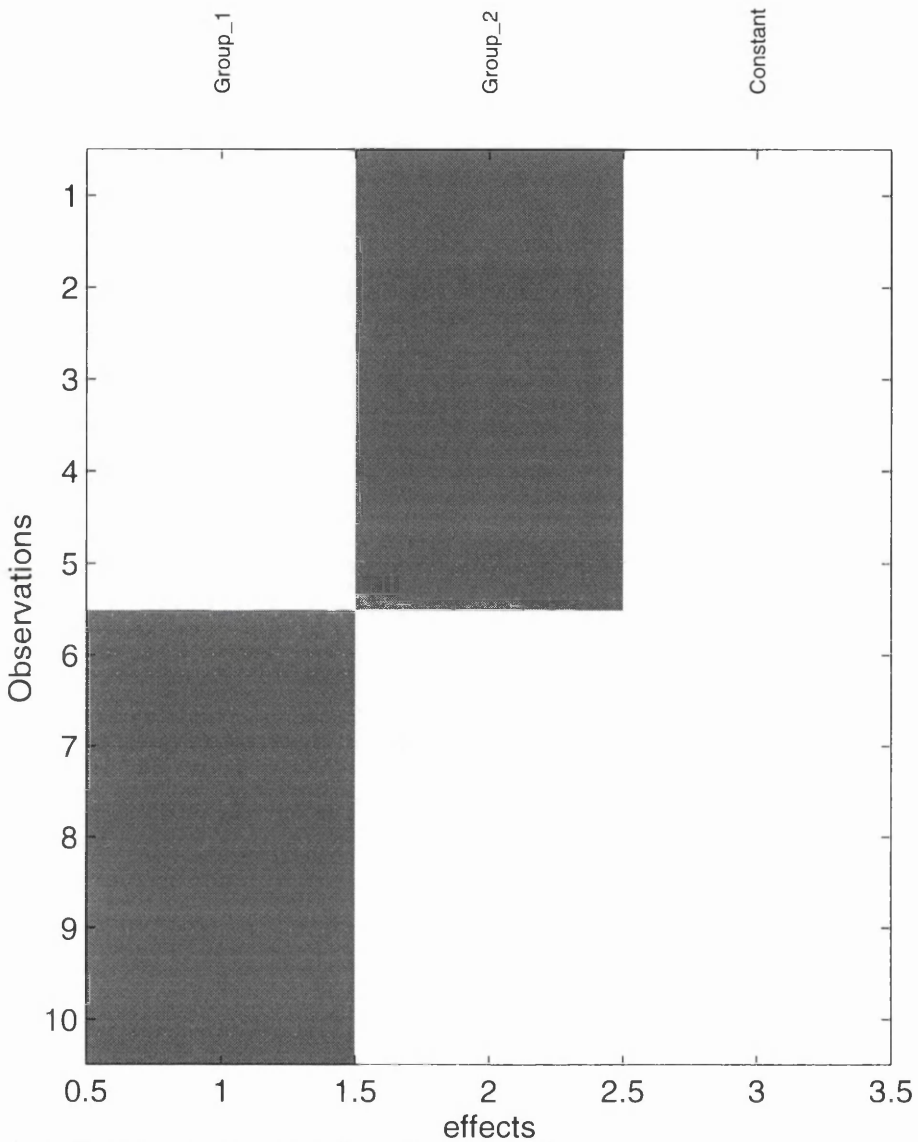

Design: Compare–groups: 1 scan per subject

Global normalisation: Proportional scaling

Parameters:

2 Condition + 0 Covariate + 1 Block + 0 Confound

= 3 parameters, having 2 degrees of freedom, giving 8 residual df (10 scans).

SPM{F} p < 0.05, df: 1.0,8.0

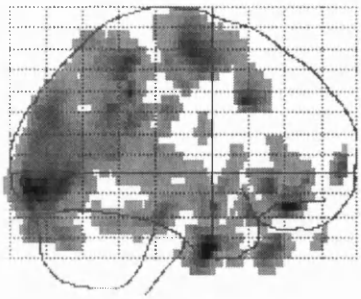

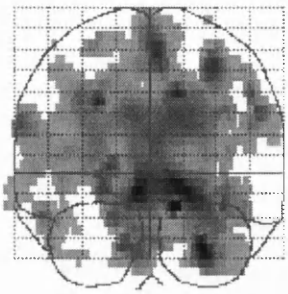

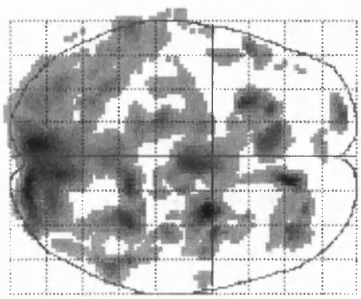

Search volume: 110114 voxels
Image size: 79 95 34 voxels
Voxel size 2.0 2.0 4.0 mm
Resolution {FWHM} 17.2 18.8 19.8 mm

Results directory:**/homes/abarnes/work_in_progress/VNS/occ_act/selected_scans**

Contrasts	1	2
Group_1	1	–1
Group_2	–1	1

SPM{Z}

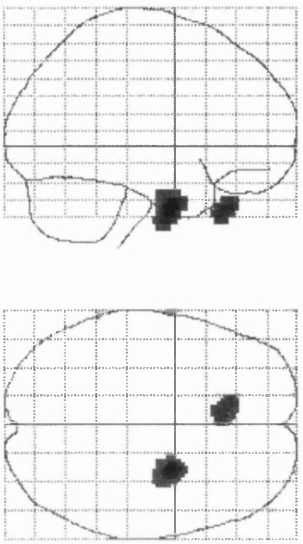

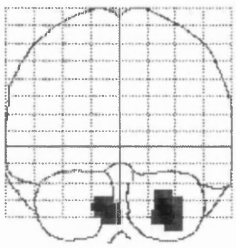

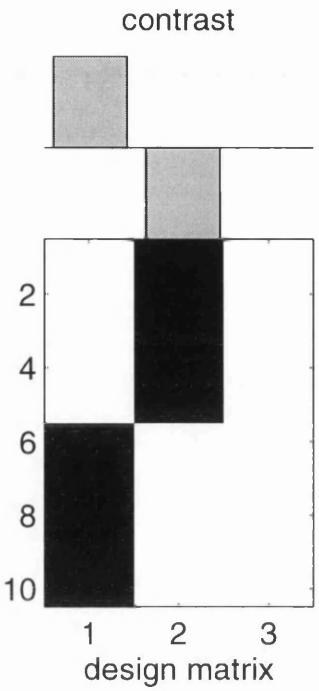

P values & statistics: ../VNS/occ_act/all_scans

set–level {c}	cluster–level {k,Z}	voxel–level {Z}	uncorrected k & Z		x,y,z {mm}
0.863 (2)	0.247 (224, 3.95)	0.187 (3.95)	0.116	0.000	26 −2 −36
	0.908 (125, 3.14)	0.897 (3.14)	0.233	0.001	−14 34 −36

Height threshold {u} = 2.33, p = 0.010
Extent threshold {k} = 94 voxels, p = 0.299
Expected voxels per cluster, E{n} = 94.3
Expected number of clusters, E{m} = 3.5

Volume {S} = 110114 voxels or 276.1 Resels
Degrees of freedom due to error = 8.0
Smoothness FWHM {mm} = 17.2 18.8 19.8
{voxels} = 8.6 9.4 4.9

SPM{Z}

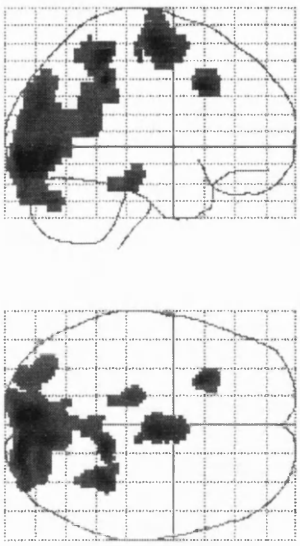

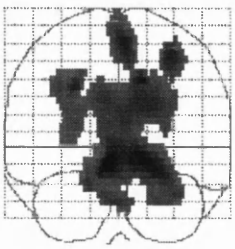

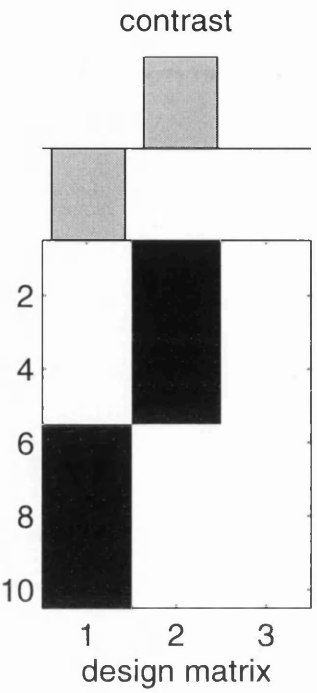

P values & statistics: ../VNS/occ_act/all_scans

set–level {c}	cluster–level {k,Z}	voxel–level {Z}	uncorrected k & Z		x,y,z {mm}
0.273 (5)	**0.002 (3555, 3.83)**	**0.264 (3.83)**	**0.000**	**0.000**	**−6 −88 −8**
		0.349 (3.73)		0.000	14 −92 −4
		0.619 (3.46)		0.000	10 −76 −8
	0.646 (103, 3.48)	**0.602 (3.48)**	**0.278**	**0.000**	**−26 16 36**
	0.424 (416, 3.39)	**0.698 (3.39)**	**0.039**	**0.000**	**4 −8 60**
		1.000 (2.46)		0.007	10 −20 56
	0.749 (198, 3.37)	**0.716 (3.37)**	**0.138**	**0.000**	**32 −40 56**
	0.972 (94, 2.97)	**0.969 (2.97)**	**0.299**	**0.002**	**−18 −24 −20**
		1.000 (2.46)		0.007	−14 −36 −24

Height threshold {u} = 2.33, p = 0.010
Extent threshold {k} = 94 voxels, p = 0.299
Expected voxels per cluster, E{n} = 94.3
Expected number of clusters, E{m} = 3.5

Volume {S} = 110114 voxels or 276.1 Resels
Degrees of freedom due to error = 8.0
Smoothness FWHM {mm} = 17.2 18.8 19.8
{voxels} = 8.6 9.4 4.9

Appendix E

The following pages contain copies of the personal communications referred to in the text and footnotes, available from the spm mailbase facility for a limited time.

SPM-mailbase letter dated Jan/98 at http://www.mailbase.ac.uk/lists/spm/1998-01/0078.html
SPM-mailbase letter dated feb/98 at http://www.mailbase.ac.uk/lists/spm/1998-02/0001.html
SPM help line letter dated - http://www.mailbase.ac.uk/lists/spm/1998-04/0014.html
SPM help line letter dated - http://www.mailbase.ac.uk/lists/spm/1998-06/0076
SPM help-line http://www.mailbase.ac.uk/lists/spm/1997-12/0009.html

Re: normalization

John Ashburner (*john@fil.ion.ucl.ac.uk*)
Mon, 26 Jan 1998 12:25:43 GMT

- **Messages sorted by:** [date][thread][subject][author]
- **Next message:** John Ashburner: "Bounding Box"
- **Previous message:** Andrew Holmes: "Re: Stats"

> *#1) With regards to the basis functions options in SPM, I had reviewed*
> *your correspondence with Matthew Brett and S. Kapur... but I would*
> *appreciate some clarification.*
>
> *I thought increasing the number of basis functions in x, y, or z*
> *would usually improve the solution in each respective axis i.e.*
> *4 4 4 will not give as close a mathematical solution as 8 8 8.*
> *However, sometimes the mathematical solution with more parameters*
> *is vulnerable to local minima and may not result in the best solution.*
> *So I thought the best empirical use would be to choose the lowest*
> *number of basis functions needed for each axis. I would increase*
> *basis functions from the default until the normalized image no longer*
> *improved. Improvement could be assessed visually and by choosing*
> *coordinate points.*
>
>
> *With this in mind I normalized full head MRIs that had been coregistered*
> *to the SPM96 T1 MRI template (the MRIs are degraded to PET voxel size*
> *of about 2X2X3).*

You don't need to work on the degraded resliced MRI. The associated '.mat' file contains the information required to map the original MRI to the PET images. This information is used by the spatial normalization, enabling you to work from the full sized MRI. In fact, one main danger of estimating parameters from the resliced MRI is that there may be artificial edges in the resliced image (from where you may have data in the PET images, but none in the original MRI). Similarly, it is better to estimate spatial normalization parameters from the mean of the PET images that can be generated by the realignment routine. This image does not have artificial edges that are generated by the 'masking'.
Another similar issue is what to do with the edge of the FOV. The images are smoothed before estimating the registration parameters. Because the values outside the FOV are unknown, there are inevitably edge artifacts in the smoothed images. In SPM96, the whole of the image is used - including the bits near the edge - and this occasionally causes problems. However, in the next release, the bits at the edges will be ignored by the parameter estimation part. This should improve the results.

> *I initially used the default 4 5 4 and noticed that*
> *the cerebellum seemed stretched in the z axis grossly. Thinking that*
> *an MRI should have more information than a PET image, I would expect*
> *better normalization. Thus I thought increasing the basis functions*

> *in the z axis would inprove the situation because a better mathematical*
> *solution from more basis functions would result in a better template*
> *solution. Empirically 4 6 9 seemed better but there was still downward*
> *displacement in the z axis of about 4mm in the inferior frontal and*
> *occipital cortex as compared to template. In general, coordinates*
> *located seemed no more than 8mm apart.*
> *I found that 4 6 11 made unpleasant (some z axis distortions?) in the*
> *temporal cortex giving a wide appearance in the transverse view.*
>
>
> *Does this seem general approach seem rational to you? Would you approach*
> *this any differently?*

This approach is rational for the spatial normalization of SPM96. Fit as many parameters as possible until the registration becomes unstable. See the answer to Q (#4).

> *#2) My other question is what set of basis functions do you find provides*
> *the best normalization for a coregistered quality MRI? (Consider the*
> *MRI coregistered by the SPM96 program - which probably gives similar*
> *quality images to our coregistration)*

I don't know for SPM96. There are so many parameters to think of.

> *#3) T1 MRI template with 12 subjects - Would you concur that this seems*
> *to be the best template? Why do you think so?*
>
> *12 MRIs have more entropy than 305 averaged MRIs which may provide better*
> *coregistration. (The 305 have a homogenous cortex with limited information)*
>
> *Why 12 is better than 1? : Maybe 12 provide a spatial distribution that*
> *will be more likely to have more mutual information with an average subject*
> *than a single MRI. Based on this, I would anticipate that a greater*
> *proportion of subjects would normalize well to the 12 averaged. I would*
> *also anticipate that the single MRI template would be better for spatial*
> *normalization for some but worse for others (a wider variance of quality*
> *of normalization in the single template normalized images). Could you*
> *clarify whether you agree with these thoughts and perhaps suggest some*
> *other reasons?*

I agree with you.

I think that the voxel values in the template should be unbiased estimates of what the voxel values in spatially normalized images should be. The best unbiased estimate I could think of would be the mean of a number of spatially normalized images. The images should be normalized as well as possible to within the limits of the spatial normalization routine that is to be used. The more images the better, but I expect that adding much more than about 12 images to the template would not improve it greatly.
Possibly a slightly better approach would be to model the intensity distribution of the normalized images. Rather than just the mean of the images, the mean and covariance of the normalized images could be modelled (possibly by fitting to a

inear combination of 'eigenimages' and their associated variances).

Another issue relates to the choice of what is matched. With T1 MRI, much of the matching information is around the ventricles, brain and scalp. Because the deformations are only defined by a few hundred parameters, the overall shape of the head (rather than just the brain) tends to be matched. This leads to inaccuracies in brain matching that result from variability outside the brain. This is particularly evident for T1 MRI, but less so for PET blood flow images where there is less signal in the scalp.
The next SPM release will give you an option for weighting the registration so that the parameters are just based on the shape of the brain.

> *#4) What is a good normalization?*

This is a good question for which different people are likely to give different answers. I guess for SPM, it is the spatial normalization that gives you the best Z-scores for multi-subject experiments.

I believe that Bayesian statistics need to be applied in order to obtain a maximum a posteriori (MAP) estimate (the single most probable solution), minimum variance estimate (MVE - a weighted average of all possible solutions, where the weights are the probabilities that the solutions are correct), or something in between. With little or no smoothing before doing the stats, then a MAP estimate may be preferable, but with more smoothing then I think a solution closer to the MVE would be better. Unfortunately, MVE solutions require a lot of computation.

In order to adopt Bayesian statistics, it is necessary to have a good model describing the a priori probability distribution of the parameters. This means that by plugging in some data that represents the true variability of brain shape, then a better estimate of the spatial normalization parameters can be made. This is comparable to a statistics test that was sent around our unit a few months ago:

o----------o
| *You feel perfectly healthy. However, one in a thousand persons of your age group,* |
| *gender and life style suffer from a specific cancer without showing any clinical* |
| *symptoms. Therefore you decide to participate in a screening test.* |
| *The screening test is very reliable. The probability that the test is positive* |
| *given that the person has the disease is 99%, i.e. only 1% of false negative* |
| *results. The probability that the test is negative given that the person does not* |
| *have the disease is 98%, i.e. only 2% of false positive results.* |
| *You are informed that in your case the result of the test is positive.* |
| *What is the probability that you actually suffer from the disease?* |
o----------o

By knowing the a priori distribution of the disease (1 in 1000 sufferers), it is possible to obtain a much more accurate estimate of the answer (0.047 if you are interested).

A Bayesian solution also requires an estimate of the error that would be made by using only a maximum likelihood solution (ML). This is comparable to knowing the false positive and false negative error rate in the above example. A bit more work has been done on this for the next SPM release (see NeuroImage 6:344-352 (1997)).

The spatial normalization of SPM96 slightly overestimates the a priori variability

of the parameters, and the errors on the fits are slightly underestimated, so the fitting may be a little bit under-regularized (although it seemed to work OK at the time with our images). This means that the algorithm can have problems when it attempts to fit too many parameters. Any modeller will tell you that you can only fit so many parameters to any data, and that occasionally any nonlinear optimization algorithm will mess up - especially when it tries to converge too rapidly. Only when you start using constraints and priors can you begin to attempt to fit lots of parameters.

Another issue is what to do with voxels that shrink and grow dramatically. This is easier to conceptialize with PET, where the simple question would be:
"Should concentration, or absolute amount of tracer be preserved in the spatially normalized images?"
With lots of warping, the relative volumes of the voxels will be more variable. The way it is done now results in concentration being preserved. So, if any particular region shrinks after spatial normalization, this results in the absolute amount of tracer in this region also shrinking. This may or may not be a good thing.

> *I have been assessing our application of your normalization process upon*
> *summed WAY ligand images over time.*
>
> *I have been sampling the location of points on normalized images (finding*
> *their mean coordinate for each image) In general, the average distance*
> *between subjects ranges from 2mm (anterior insula) to 6mm (midline posterior*
> *occipital cortex). The greatest distance between a pair of subjects for a*
> *given point is 10mm.*
>
> *How does this compare to water images and MRI images?*

I don't honestly know. I haven't evaluated the registration this way. Most of the evaluations have involved looking at the decrease in the residual squared differences between the templates and images, as well as a few purely qualitative evaluations.

> *I am not aware of a paper that states mean distances between normalized*
> *images -could you refer me to one? I am aware of 1991 JCBF by Friston*
> *et al. which states mean template and image coordinates for points (but*
> *not standard deviation or greatest distance).*

There isn't one for the current nonlinear spatial normalization of SPM.

> *#5) Will SPM actually change the values within voxels?*

It will try not to, but when it has to interpolate between 8 neighbouring voxels, changes in voxel values are inevitable.

> *#6) With regards to interpolation, I am aware that sinc interpolation has*
> *been demonstrated to be the best for MR images. What evidence (if any)*
> *supports the use of sinc interpolation for PET images?*

I think sinc interpolation should be better for all images. However, there is so much noise in PET images, they are relatively smooth, PET signals are usually much higher than fMRI signals, and the degrees of freedom are so much

ower in PET experiments that sinc and bilinear interpolation should not make oo much difference. However, it is worth noting that when you use sinc nterpolation with PET, you will find that the estimates of smoothness have ower FWHMs. This is because bilinear interpolation takes a weighted average of the 8 nearest neighbours - which is essentially a smoothing step.

> *Is there any way to choose one kind of interpolation for choosing the*
> *location of resliced data and a different interpolation i.e. nearest*
> *neighbour or bilinear to the actual values?*

The estimation of spatial normalization parameters always uses bilinear interpolation, whereas you get a choice about how you resample the data.

Regards,
-John

%%%

- **Next message:** John Ashburner: "Bounding Box"
- **Previous message:** Andrew Holmes: "Re: Stats"

AnCova & proportional scaling [Was: Basic fMRI covariates...]

Andrew Holmes (*andrew@fil.ion.ucl.ac.uk*)
Mon, 2 Feb 1998 10:56:21 GMT

- **Messages sorted by:** [date][thread][subject][author]
- **Next message:** Daniel Welti: "Realign - matlab problems"
- **Previous message:** John Ashburner: "Re: coregister, normalize"

Dear Dr Allison,

You suggested that Dr. Makuuchi employ Global Normalization using "Scaling". Please comment on the use of "Scaling" versus "ANCOVA" for Global Normalization. When is each appropriate in the realm of fMRI studies? Why did you suggest "Scaling"?

AnCova and proportional scaling imply very different models for the effect of changes in global measurement. There has been much disagreement and much written about the pro's and con's of the two approaches, but to my mind there's no general answer as to which is best: It's a simple case of using the model most appropriate for the data at hand. Here are my general thoughts...

AnCova uses a local linear model for a small range of global values, with constant variance, and assummes activations are additive. Proportional scaling (followed by Anova) implies a proportional model the effect of global changes on regional values, assummes activations are proportional to the underlying global, and (crucially) also that variance increases with global. This last attribute is oft overlooked, makes a formal comparison of AnCova and Prop.Scale/Anova models on a data set non-trivial, but is really what differentiates the two models.

In short: If global measurements vary as a result of a gain effect, such as scanner sensitivity (fMRI) or introduced activity (PET), then the noise should increase with the signal and a proportional model would be appropriate. If global measurements truly reflect a normal range of an underlying physiological process (i.e.CBF), then there is little evidence for globally dependent variance, and the non-linear relationship global and regional values is best modelled with a local linear model - AnCova.

(Note that global normalisation implies assessing other changes)
(relative to the global, via the chosen model. In general then,)
(you're in trouble if the global measurement and effects of interest)
(are correlated. See the Ch3 of the SPMcourse notes for further)
(discussion.)

So, for quantified PET with true rCBF measurements, I'd use AnCova

within subjects, with a different parameter for each subject (subject specific AnCova in SPMspeak). With relative "counts" data obtained from a tightly controlled input dose, I'd again use subject specific AnCova, but would consider scaling across subjects (prior to AnCova) if there are obvious subject differences. Such a scaling would involve scaling all a subjects images by the *same* factor, such that the Grand mean (mean of the global means) for each subject was the same. For PET with a very variable input dose, the Poisson nature of radioactive decay immediately suggests variance increasing with intensity, and hence proportional scaling.

With fMRI it's a bit trickier, mainly because we're not sure what BOLD is actually measuring. However, we've found that many (older) scanners recalibrate prior to acquiring every image volume. This is clearly a gain effect. Empirically, for a tight range of global values, there appears to be little difference in the results from a proportional scaling and a subject-specific AnCova. I therefore suggested "Scaling" to Dr. Makuuchi on the grounds that it's safest for fMRI in the absence of additional knowledge.

For further comments I suggest the SPM course notes (Ch3), and a review of the literature. There's a plethora of assessments for various data published, and I look forward to reading of other groups thoughts and experience.

Hope this helps,

-andrew

+- Dr Andrew Holmes -----------------------a.holmes@fil.ion.ucl.ac.uk-+
| -___ __ __ *Wellcome Department of Cognitive Neurology* - |
| *(_)( )( ) Functional Imaging Laboratory, Stats &* |
| *) _))( )(__ 12 Queen Square, Systems* |
| *(_) (__)(____) London. WC1N 3BG. England, UK* |
+---------------------------------------http://www.fil.ion.ucl.ac.uk/-+

%%

- **Next message:** Daniel Welti: "Realign - matlab problems"
- **Previous message:** John Ashburner: "Re: coregister, normalize"

single subject analyses

BSwartz (*BSWARTZ@ucla.edu*)
Thu, 02 Apr 1998 14:10:06 -0800

- **Messages sorted by:** [date][thread][subject][author]
- **Next message:** Andrew Holmes: "Re: the filters again"
- **Previous message:** Andrew Martin: "Re: Statistics crashes"

I have been using spm to do single subject analyses and have encountered some interesting if vexing problems.
1. A single subject who has hydrocephalus compared to a normal data base shows less activity in the temporal horns of the lateral ventricle areas (interpreted as grey matter, but easily understood). Curiously he shows greater activity on the SPM in the atria of the lateral ventricles. How can this be?
2. A subject with a large R frontal lobe lesion simply wouldn't run. We tried no affine, our own iterations, etc. The normalization chops off the right frontal lobe in a clean line. Our hypothesis is that if a lesion exceeds the voxel size after smoothing the normalization transformation is "funky" but what exactly happens - just curious?
3. Similar to number one. One subject was tested who has a normal brain on MR. Unfortunately he was badly positioned during the scan and lost large parts of both the basal temporal lobes and the superior frontal parietal cortex instead of small parts of both. Tested against the normal group spm says the normals have greater activity than all of the brain that was included in the scan. It says he has greater activity at the lower edge of the scan, where it was cut off. Again I would like to know how an edge effect can look like too much activity in an area that doesn't really exist and how relatively normal brain can be judged as all significantly depressed "between the edges"?

In case it isn't obvious, we are using a single subjects, 2-conditions, 1 with replications to run the tests, which has worked well in other subjects.

Why bother with bad or distorted scans in the first place you ask? Good question! Hopefully it will be a learning experience?

%%

- **Next message:** Andrew Holmes: "Re: the filters again"
- **Previous message:** Andrew Martin: "Re: Statistics crashes"

(no subject)

Karl Friston (*karl@fil.ion.ucl.ac.uk*)
Tue, 23 Jun 1998 15:08:30 +0100

- **Messages sorted by:** [date][thread][subject][author]
- **Next message:** Debbie Hall: "PhD research studentship"
- **Previous message:** Debbie Hall: "Re: Talairach vs. MNI space"
- **Maybe in reply to:** Lesley Peters: "(no subject)"
- **Next in thread:** nancy c. andreasen: "(no subject)"

Dear Darren,

This is a recurrent issue. The following was posted some time ago but remains, I think, a reasonable answer to your question:

I think it is appropriate to re-iterate a few points about standard anatomical spaces.

(i) The 'standard' space into which data are normalized is defined operationally by the template employed (not by any atlas or system)

(ii) The Talairach 'system' is used by most people in the imaging neuroscience community. This system is a coordinate referencing system and can be used with any template.

(iii) Any template that is used to implement the Talairach system can be said to effect a normalization into 'a' Talairach space.

(iv) The relationship between the template used and the Talairach atlas drawings may, or may not, be a tight one. The closer this relationship, the better the atlas will serve as a guide for labelling the Talairach x,y,z designation.

Clearly to maximize the face (and construct) validity of anatomical labels it would best if we all used the same template (and this template was as canonical as possible). To this end SPM has adopted templates that conform to those used by the ICBM project (USA) that will create a probabilistic atlas and that will, possibly, supervene over the Talairach atlas in the years to come. This template is based on a single subject that has been matched to the MNI 305 average.

In short all the templates available with SPM conform to the Talairach system with varying degrees of 'closeness' to the atlas drawings. They are all variants of 'a' Talairach space. The most recent templates have been designed to make them compatible with the MNI 305 average and implicitly the ICBM atlases that will ensue in the future.

This is a difficult issue and other comments would be valued.

I hope this helps - Karl

Specifically:-

> *Dear SPM-folks*
>
> *A series of questions have come up regarding the relationship between the*
> *MNI brain (as provided in SPM96) which defines one version of "Talairach"*
> *space and the brain space identified in the 1988 Talairach atlas itself. It*
> *appears these are not the same (the 1988 brain is smaller) and comments to*
> *that effect were made at HBM98 by Dr. Passingham.*
>
> *Is there any way to map between MNI space (SPM96) and Talairach-88' space?*
> *Are there any algorithms for that mapping? How can one compare coordinates*
> *obtained by matching the MNI template (ala SPM96) with coordinates*
> *published in the literature supposedly in Talairach space.*

There is no unique 'Talairach space' (see above). Clearly the mappings from one 'Talairach space' to another are easily obtained by normalizing the underlying template of one to that of the other. Given that the drawings in the T&T atlas do not conform to a 'template' the T&T space is operationally less useful than any other (because its relationship to other spaces is less easy to define).

> *Many functional imaging studies published today compare results by listing*
> *"Talairach" coordinates for various studies. The possibility exists that*
> *one can't compare results in this way at all if the brain spaces are*
> *different. Is there a crisis in normalization?*

No. There will be a variance component in the stereotactic metrics due to different normalization procedures and the use of different templates. The exitance of this component is important but does not engender a 'crisis'. This component will be minimized with a convergence of nonlinear techniques and when we all adopt the same template. This is why we switched to a template that conforms to the MNI space and implcitly the ICBM space. The priority for us was to promote convergence within the community (not to ensure any backward compatibility or contruct validity in relation to a particular set of atlas drawings).

With best wishes - Karl

%%

- **Next message:** Debbie Hall: "PhD research studentship"
- **Previous message:** Debbie Hall: "Re: Talairach vs. MNI space"
- **Maybe in reply to:** Lesley Peters: "(no subject)"
- **Next in thread:** nancy c. andreasen: "(no subject)"

Re: n=? normal database

karl@fil.ion.ucl.ac.uk
Tue, 2 Dec 1997 18:52:22 GMT

- **Messages sorted by:** [date][thread][subject][author]
- **Next message:** hgupta@grip.cis.upenn.edu: "Resplicing necessary?"
- **Previous message:** 896371ba@udcf.gla.ac.uk: "n=? normal database"
- **Maybe in reply to:** 896371ba@udcf.gla.ac.uk: "n=? normal database"
- **Next in thread:** jra@plato.neurology.bgsm.edu: "Re: n=? normal database"

Dear Anna,

> *We are about to embark on a study involving the comparison of*
> *individual patients to a 'normal' database using SPM96. Does anybody*
> *have any feeling for the number of scans needed in the normal*
> *database? I have seen quoted in abstracts from the FIL n but I have*
> *also seen users on the mailing list quoting numbers of n0. I have*
> *tried searching the mailing list archives for more info but had no*
> *luck. If anybody could point me in the right direction I would be*
> *grateful.*

I don't think there is any absolute answer. The more normals you include then the more powerful (increased probablity of detecting an effect, if it is there, for a given false positive rate) it will be.

There is the ancillary issue of the approximation implicit in Gaussianization of the SPM{t} that is special to SPM. This means that a SPM analysis is more conservative than the normal t test for very low degrees of freedom (e.g. < 16). I like the number n2 but n would be acceptable in terms of power. Of course if you detect an effect with n=8 then it is perfectly justifiable to report it (as long as you don't try to interpret negative findings and say that the analysis is not powerful).

I hope this helps - Karl

%%

- **Next message:** hgupta@grip.cis.upenn.edu: "Resplicing necessary?"
- **Previous message:** 896371ba@udcf.gla.ac.uk: "n=? normal database"
- **Maybe in reply to:** 896371ba@udcf.gla.ac.uk: "n=? normal database"
- **Next in thread:** jra@plato.neurology.bgsm.edu: "Re: n=? normal database"

References

1. Functional neuroimaging: Technical foundations. 1994. San Diego: Academic Press.

2. Penfield W , Rasmussen AT . The cerebral cortex of man. A clinical study of localisation of function. 1950. New York: Macmillan.

3. Collins R C. Basic aSPECTs of functional brain metabolism. In Exploring Brain Functional Anatomy with Positron Tomography Chadwick D J, Whelan J L editors. 1991. Chichester, UK.. John Wiley & Sons Ltd.. 6-22.

4. Jueptner M, Weiller C . Review: does measurement of regional cerebral blood flow reflect synaptic activity? Implications for PET and fMRI. Neuroimage, 1995; 2: 148-156.

5. Ogawa S, Lee T M, Kay A R, Tank D W . Brain magnetic resonance imaging with contrast dependent on blood. Proc Natl Acad Sci U S A, 1990; 87: 9868-9872.

6. Ackerman R H, Subramanyam R, Correia J A, Alpert N M, Taveras J M . Positron imaging of cerebral blood flow during continuous inhalation of carbon dioxide. Stroke, 1980; 11: 45-9.

7. Fox P T, Mintun M A, Raichle M E, Herscovitch P . A noninvasive approach to quantitative functional brain mapping with $H_2{}^{15}O$ and positron emission tomography. J Cereb Blood Flow Metab, 1984; 4: 329-333.

8. Mazziotta J C , Phelps M E , Plummer D , Kuhl D E . Quantitation in positron emission computed tomography: 5. Physical-anatomical effects. Journal of Computer Assisted Tomography, 1981; 5: 734-743.

9. Lassen N A, Andersen A, Vorstrup S . Cerebral blood flow by SPECT using diffusible tracers as xenon -133 or technetium -99m-HM-PAO. Italian Current Radiology, 1986; 5: 21-24.

10. Sharp P F, Smith F W, Gemmell H G, et . Technetium-99m HM-PAO stereoisomers as potential agents for imaging regional cerebral blood flow: human volunteer studies. Journal of Nuclear Medicine, 1986; 27: 171-177.

11. Costa D C, Ell P J, Nowotnik D P . HM-PAO: a new technetium-99m labelled agent for brain SPECT. J Nucl Med Allied Sci, 1985; 29: 337-338.

12. Devous M, Duara R, Jagust W, Oconnell R A, Markand O, Tikofsky R, Van Heertum R, Mazziota J, Masdeu J C, Brass L C, Holman B L, Kushner M J, Altrocchi P H, Brin M, Ferguson J H, Goldstein M L, Gorelick P B, Hanley D F, Lange D J, et al. Assessment of brain SPECT: report of the therapeutics and technology assessment subcommittee of the american academy of neurology. Neurology, 1996; 46: 278-285.

13. Montaldi D, Mayes A R, Barnes A, Pirie H, Hadley D M, Patterson J, Wyper D J . Associative encoding of pictures activates the medial temporal lobes. Hum Brain Mapp, 1998; 6: 85-104.

14. Riddle W, Ocarroll R E, Dougall N, Van Beck M, Murray C, Curran S M, Ebmeier K P, Goodwin G M . A single photon emission computerised tomography study of regional brain fuction underlying verbal memory in patients with alzheimer- type dementia. British Journal of Psychiatry, 1993; 163: 166-172.

15. Ebmeier K P, Murray C L, Dougall N J, Ocarroll R E, Goodwin G M . Unilateral voluntary hand movement and regional cerebral uptake of technetium-99m-exametazime in human control subjects. Journal of Nuclear Medicine, 1992; 33: 1623-1627.

16. Thornton A F Jr, Ten Haken R K, Gerhardsson A, Correll M . Three-dimensional motion analysis of an improved head immobilization system for simulation, CT, MRI, and PET imaging. Radiother Oncol, 1991; 20: 224-228.

17. Bettinardi V, Scardoni R, Gilardi M C, Rizzo G, Perani D, Paulesu E, Striano G, Triulzi F, Fazio F . Head holder for PET, CT and MR studies. Journal of Computer Assisted Tomography, 1991; 15: 886-892.

18. Graham J D, Warrington A P, Gill S S, Brada M . A non-invasive, relocatable stereotactic frame for fractionated radiotherapy and multiple imaging. Radiother Oncol, 1991; 21: 60-62.

19. Thornton A F Jr, Ten Haken R K, Weeks K J, Gerhardsson A, Correll M, Lash K A . A head immobilization system for radiation simulation, CT, MRI, and PET imaging. Med Dosim, 1991; 16: 51-56.

20. Evans A C, Beil C, Marrett S, Thompson C J, Hakim A . Anatomical-functional correlation using an adjustable MRI-based region of interest atlas with positron emission tomography. Journal of Cerebral Blood Flow and Metabolism, 1988; 8: 513-530.

21. Van den Elsen P A, Viergever M A . Marker-guided multimodality matching of the brain. Neuroradiology, 1994; 4: 45-51.

22. Pohjonen H, Nikkinen P, Sipila E, Launes J, Salli E, Salonen O, Karp P, Yla-Jaaski J, Katila T, Liewendahl K . Registration and display of brain SPECT and MRI using external markers. Neuroradiology, 1996; 38: 108-114.

23. Strother S C, Anderson J R, Xu X L, Liow J S, Bonar D C, Rottenberg D A . Quantitative comparisons of image registration techniques based on high- resolution MRI of the brain. J Comput Assist Tomogr, 1994; 18: 954-962.

24. Evans A C, Marrett S, Torrescorzo J, Ku S, Collins L . Mri-PET correlation in three dimensions using a volume-of-interest (voi) atlas. Journal of Cerebral Blood Flow and Metabolism, 1991; 11: A69-A78.

25. Collins D L, Neelin P, Peters T M, Evans A C . Automatic 3D intersubject registration of mr volumetric data in standardized talairach space. Journal of Computer Assisted Tomography, 1994; 18: 192-205.

26. Hill D L G, Hawkes D J, Crossman J E, Gleeson M J, Cox T C S, Bracey E E C M L, Strong A J, Graves P . Registration of MR and CT images for skull base surgery using point- like anatomical features. British Journal of Radiology, 1991; 64: 1030-1035.

27. Ge Y, Fitzpatrick J M, Votaw J R, Gadamsetty S, Maciunas R J, Kessler R M, Margolin R A . RetroSPECTive registration of PET and MR brain images: an algorithm and its stereotactic validation. Journal of Computer Assisted Tomography, 1994; 18: 800-810.

28. Levin D N, Pelizzari C A, Chen G T Y, Chen C T, Cooper M D . RetroSPECTive geometric correlation of MR, CT, and PET images. Radiology, 1988; 169: 817-823.

29. Andersson J L R. A rapid and accurate method to realign PET scans utilizing image edge information. Journal of Nuclear Medicine, 1995; 36: 657-669.

30. Pallotta S, Gilardi M C, Bettinardi V, Rizzo G, Landoni C, Striano G, Masi R, Fazio F . Application of a surface matching image registration technique to the correlation of cardiac studies in positron emission tomography (PET) by transmission images. Physics in Medicine and Biology, 1995; 40: 1695-1708.

31. Venot A, Lebruchec J F, Golmard J L, Roucayrol J C . An automated method for the normalization of scintigraphic images. J Nucl Med, 1983; 24: 529-531.

32. Mintun M A, Fox P T, Raichle M E . A highly accurate method of localizing regions of neuronal activation in the human brain with positron emission tomography. J Cereb Blood Flow Metab, 1989; 9: 96-103.

33. Junck L, Moen JG, Hutchins GD, Brown MB, Kuhl DE . Correlation methods for the centring, rotation and alignment of functional brain images. Journal of Nuclear Medicine, 1990; 31: 1220-1276.

34. Venot A, Liehn J C, Lebruchec J F, Roucayrol J C . Automated comparison of scintigraphic images. J Nucl Med, 1986; 27: 1337-1342.

35. Minoshima S, Berger K L, Lee K S, Mintun M A . An automated method for rotational correction and centering of three- dimensional functional brain images. J Nucl Med, 1992; 33: 1579-1585.

36. Stoddart H A, Stoddart H F . New multi-dimensional reconstructions for the 12-detector, scanned focal point, single-photon tomograph. Physics in Medicine and Biology, 1992; 37: 579-586.

37. Eberl S, Kanno I, Fulton R R, Ryan A, Hutton B F, Fulham M J . Automated interstudy image registration technique for SPECT and PET. J Nucl Med, 1996; 37: 137-145.

38. Barber D C, Tindale W B, Hunt E, Mayes A, Sagar H J . Automatic registration of SPECT images as an alternative to immobilization in neuroactivation studies. Physics in Medicine and Biology, 1995; 40: 449-463.

39. Studholme C, Hill D L G, Hawkes D J . Automated three-dimensional registration of magnetic resonance and positron emission tomography brain images by multiresolution optimization of voxel similarity measures. Medical Physics, 1997; 24: 25-35.

40. Woods R P, Cherry S R, Mazziotta J C . Rapid automated algorithm for aligning and reslicing PET images. Journal of Computer Assisted Tomography, 1992; 16: 620-633.

41. Ashburner J, Friston K . Multimodal image coregistration and partitioning - a unified framework. Neuroimage, 1997; 6: 209-217.

42. Bartenstein P, Minoshima S, Hirsch C, Buch K, Willoch F, Mosch D, Schad D, Schwaiger M, Kurz A . Quantitative assessment of cerebral blood flow in patients with Alzheimer's disease by SPECT. J Nucl Med, 1997; 38: 1095-1101.

43. West J, Fitzpatrick M, Wang M Y, Dawant BM, Maurer C R, Kessler R M, Maciunas R J, Barillot C, Lemoine D, Collignon A, Maes F, Suetens P, Vandermeulen D, van den Elsen P A, Napel S, Sumanaweera T S, Harkness B, Hemler P F, Hill D L G, Hawkes D J, Studholme C, Maintz J B A, Viergever M A, Malandain G, Pennec X, Noz M E, Maguire Jr G Q, Pollack M, Pelizzari C A, Robb R A, Hanson D, Woods R P. Comparison and evaluation of retrospective intermodality brain image registration techniques. Journal of Computer Assisted Tomography, 1997; 21: 554-566

44. Woods R P, Mazziotta J C, Cherry S R . MRI-PET registration with automated algorithm. Journal of Computer Assisted Tomography, 1993; 17: 536-546.

45. Fox P T, Perlmutter J S, Raichle M E . Stereotactic method for determining anatomical localization in physiological brain images [letter]. J Cereb Blood Flow Metab, 1984; 4: 634.

46. Talairach J. , Tournoux P. Co-Planar stereotaxic atlas of the human brain. 1988. New York: Thieme Medical Publishers, Inc.

47. Friston K J, Passingham R E, Nutt J G, Heather J D, Sawle G V, Frackowiak R S J . Localisation in PET images: direct fitting of the intercommissural (AC-PC) line. Journal of Cerebral Blood Flow and Metabolism, 1989; 9: 690-695.

48. Friston K J, Frith C D, Liddle P F, Frackowiak R S J . Plastic transformation of PET images. Journal of Computer Assisted Tomography, 1991; 15: 634-639.

49. Ashburner J, Neelin P, Collins D L, Evans A, Friston K . Incorporating prior knowledge into image registration. Neuroimage, 1997; 6: 344-352.

50. Bookstein F L. Landmarks, edges, morphometrics, and the brain atlas problem. In Functional Neuroimaging: Technical foundations Thatcher R W, Hallet M, Zeffiro T, Roy John E, Huerta M editors. 1994. London. Academic Press. 107-119.

51. Bajcsy R, Lieberson R, Reivich M . A computerized system for the elastic matching of deformed radiographic images to idealized atlas images. J Comput Assist Tomogr, 1983; 7: 618-625.

52. Toga A W, Ambach K, Quinn B, Hutchin M, Burton J S . Postmortem anatomy from cryosectioned whole human brain. Journal of Neuroscience Methods, 1994; 54: 239-252.

53. Minoshima S, Koeppe R A, Frey K A, Kuhl D E . Anatomic standardization: linear scaling and nonlinear warping of functional brain images. J Nucl Med, 1994; 35: 1528-1537.

54. Rizzo G, Gilardi M C, Prinster A, Grassi F, Scotti G, Cerutti S, Fazio F . An elastic computerized brain atlas for the analysis of clinical PET/SPET data. Eur J Nucl Med, 1995; 22: 1313-1318.

55. Bohm C, Greitz T, Eriksson L . A computerized adjustable brain atlas. Eur J Nucl Med, 1989; 15: 687-689.

56. Seitz R J, Bohm C, Greitz T, Roland P E, Eriksson L, Blomqvist G, Rosenqvist G, Nordell B . Accuracy and precision of the computerized brain atlas programme for localization and quantification in positron emission tomography. J Cereb Blood Flow Metab, 1990; 10: 443-457.

57. Fox P T, Mintun M A, Reiman E M, Raichle M E . Enhanced detection of focal brain responses using intersubject averaging and change-distribution analysis of subtracted PET images. J Cereb Blood Flow Metab, 1988; 8: 642-653.

58. Grabowski T J, Frank R J, Brown C K, Damasio H, Ponto L L B, Watkins G L, Hichwa R D . Reliability of PET activation across statistical methods, subject groups, and sample sizes. Human Brain Mapping, 1996; 4: 23-46.

59. Friston K J, Holmes A P, Worsley KJ, Poline J B, Frith C D, Frackowiak R S J. Statistical Parametric Maps in Functional Imaging: A general linear approach. Human Brain Mapping, 1995; 12: 189-210.

60. Worsley K J, Evans A C, Marrett S, Neelin P . Detecting and estimating the regions of activation in CBF activation studies in human brain. Annals of Nuclear Medicine, 1993; 7: S108-S109.

61. Worsley K J, Evans A C, Marrett S, Neelin P . A three-dimensional statistical analysis for CBF activation studies in human brain. Journal of Cerebral Blood Flow and Metabolism, 1992; 12: 900-918.

62. McIntosh A R, Bookstein F L, Haxby J V, Grady C L . Spatial pattern analysis of functional brain images using partial least squares. Neuroimage, 1996; 3: 143-157.

63. Minoshima S, Frey K A, Koeppe R A, Foster N L, Kuhl D E . A diagnostic approach in Alzheimer's disease using three-dimensional stereotactic surface projections of fluorine-18-FDG PET. J Nucl Med, 1995; 36: 1238-1248.

64. Julin P, Lindqvist J, Svensson L, Slomka P, Wahlund L O . MRI-guided SPECT measurements of medial temporal lobe blood flow in Alzheimer's disease. J Nucl Med, 1997; 38: 914-919.

65. Strother S C, Anderson J R, Schaper K A, Sidtis J J, Liow J S, Woods R P, Rottenberg D A . Principal component analysis and the scaled subprofile model compared to intersubject averaging and statistical parametric mapping: I. "Functional connectivity" of the human motor system studied with [15O]water PET. J Cereb Blood Flow Metab, 1995; 15: 738-753.

66. Houston A S, Kemp P M, MacLeod M A . A method for assessing the significance of abnormalities in HMPAO brain SPECT images. Journal of Nuclear Medicine, 1994; 35: 239-244.

67. Holmes A P, Blair R C, Watson J D G, Ford I . Nonparametric analysis of statistic images from functional mapping experiments. Journal of Cerebral Blood Flow and Metabolism, 1996; 16: 7-22.

68. Poline J B, Mazoyer B M . Analysis of individual positron emission tomography activation maps by detection of high signal-to-noise-ratio pixel clusters. J Cereb Blood Flow Metab, 1993; 13: 425-437.

69. Poline J B, Worsley K J, Evans A C, Friston K J . Combining spatial extent and peak intensity to test for activations in functional imaging. Neuroimage, 1997; 5: 83-96.

70. Friston K J, Holmes A, Poline J B, Price C J, Frith C D . Detecting Activations in PET and fMRI: Levels of Inference and Power. 1996 Dec;4(3):223-35.

71. Mazziotta J C. Physiologic neuroanatomy: new brain imaging methods present a challenge to an old discipline. J Cereb Blood Flow Metab, 1984; 4: 481-483.

72. Chang W, Henkin R E, Buddemeyer E . The sources of overestimation in the quantification by SPECT of uptakes in a myocardial phantom: concise communication. J Nucl Med, 1984; 25: 788-791.

73. Friston KJ. Statistical Parametric Mapping. In Functional neuroimaging, technical foundations Thatcher R, Hallet M, Zeffiro T, RoyJohn E, Heurta M editors. 1994. San Diego. Academic Press. 49-55.

74. Friston K J. Imaging cognitive anatomy. Trends in Cognitive Sciences, 1997; 1: 21-27.

75. Pelizzari CA, Levin DN, Chen C, Chen GTY . Registration of PET and SPECT with MRI by anatomical surface matching. In Functional neuroimaging, technical

foundations Thatcher R, Hallet M, Zeffiro T, RoyJohn E, Heurta M editors. 1994. San Diego. Academic Press. 233-241.

76. Piez Cw J, Holman B L . Single photon emission computed tomography. Computerized Radiology, 1985; 9: 201-211.

77. Holman B L, Johnson K A, Gerada B, Carvalho P A, Satlin A . The scintigraphic appearance of Alzheimer's disease: a proSPECTive study using technetium-99m-HMPAO SPECT [published erratum appears in J Nucl Med 1992 Apr;33(4):484]. J Nucl Med, 1992; 33: 181-185.

78. Talbot P R, Lloyd J J, Snowden J S, Neary D, Testa H J . A clinical role for 99mTc-HMPAO SPECT in the investigation of dementia? J Neurol Neurosurg Psychiatry, 1998; 64: 306-313.

79. Jagust W J, Johnson K A, Holman B L . SPECT perfusion imaging in the diagnosis of dementia. Journal of Neuroimaging, 1995; 5: S45-S52.

80. Gemmell H G, Sharp P F, Smith F W, Besson J A O, Ebmeier K P, Davidson J, Evans N T S, Roeda D, Newton R, Mallard J R . Cerebral blood flow measured by SPECT as a diagnostic tool in the study of dementia. Psychiatry Research, 1989; 29: 327-329.

81. Smith F W, Besson J A, Gemmell H G, Sharp P F . The use of technetium-99m-HM-PAO in the assessment of patients with dementia and other neuropsychiatric conditions. J Cereb Blood Flow Metab, 1988; 8: S116-S122.

82. Smith F W, Gemmell H G, Sharp P F . The use of Tc99m-HM-PAO for the diagnosis of dementia. Nucl Med Commun, 1987; 8: 525-533.

83. Gemmell H G, Sharp P F, Besson J A, Crawford J R, Ebmeier K P, Davidson J, Smith F W . Differential diagnosis in dementia using the cerebral blood flow agent 99mTc HM-PAO: a SPECT study. J Comput Assist Tomogr, 1987; 11: 398-402.

84. American Psychiatric Association. Diagnostic and statistical manual of mental disorders. 1987. Washington, DC: American Psychiatric Association.

85. Jobst K A, Barnetson L P, Shepstone B J . Accurate prediction of histologically confirmed Alzheimer's disease and the differential diagnosis of dementia: the use of NINCDS-ADRDA and DSM- III-R criteria, SPECT, X-ray CT, and APO E4 medial temporal lobe dementias. The Oxford Project to Investigate Memory and Aging. Int Psychogeriatr, 1997; 9 Suppl 1: 191-222; discus.

86. Miller B L, Ikonte C, Ponton M, Levy M, Boone K, Darby A, Berman N, Mena I, Cummings J L . A study of the Lund-Manchester research criteria for frontotemporal dementia: clinical and single-photon emission CT correlations. Neurology, 1997; 48: 937-942.

87. Butler R E, Costa D C, Greco A, Ell P J, Katona C L E . Differentiation between alzheimer's disease and multi-infarct dementia: SPECT vs MR imaging. International Journal of Geriatric Psychiatry, 1995; 10: 121-128.

88. Gemmell H G, Evans N T S, Besson J A O, Roeda D, Davidson J, Dodd M G, Sharp P F, Smith F W, Crawford J R, Newton R H, Kulkarni V, Mallard J R . Regional cerebral blood flow imaging: a quantitative comparison of technetium-99m-HMPAO SPECT with $C^{15}O_2$ PET. Journal of Nuclear Medicine, 1990; 31: 1595-1600.

89. Powers W J, Perlmutter J S, Videen T O, Herscovitch P, Griffeth L K, Royal H D, Siegel B A, Morris J C, Berg L . Blinded clinical evaluation of positron emission

tomography for diagnosis of probable Alzheimer's disease. Neurology, 1992; 42: 765-770.

90. Bonte F J, Weiner M F, Bigio E H, White C L . Brain blood flow in the dementias: SPECT with histopathologic correlation in 54 patients. Radiology, 1997; 202: 793-797.

91. Burdette J H, Minoshima S, Vander Borght T, Tran D D, Kuhl D E . Alzheimer disease: improved visual interpretation of PET images by using three-dimensional stereotaxic surface projections. Radiology, 1996; 198: 837-843.

92. Masterman D L, Mendez M F, Fairbanks L A, Cummings J L . Sensitivity, specificity, and positive predictive value of technetium 99-HMPAO SPECT in discriminating Alzheimer's disease from other dementias. J Geriatr Psychiatry Neurol, 1997; 10: 15-21.

93. Pasquier F, Lavenu I, Lebert F, Jacob B, Steinling M, Petit H . The use of SPECT in a multidisciplinary memory clinic. Dement Geriatr Cogn Disord, 1997; 8: 85-91.

94. McMurdo M E T, Grant D J, Kennedy N S J, Gilchrist J, Findlay D, McLennan J M . The value of HMPAO SPECT scanning in the diagnosis of early Alzheimer's disease in patient's attending a memory clinic. Nuclear Medicine Communications, 1994; 15: 405-409.

95. Altman Douglas G . Practical Statistics for Medical Research. 1991. London: Chapman and Hall.

96. Ebmeier K P, Glabus M F, Prentice N, Ryman A, Goodwin G M . A voxel-based analysis of cerebral perfusion in dementia and depression. Neuroimage, 1998; 7: 199-208.

97. Imran M B, Kawashima R, Awata S, Kazunori S, Kinomura S, Ono S, Yoshioka S, Sato M, Fukuda H . Parametric mapping of cerebral blood flow defecits in Alzheimer's disease: A SPECT study using HMPAO and image standardization technique. Journal of Nuclear Medicine, 1999; 40: 244-249.

98. Ishii K, Sasaki M, Yamaji S, Sakamoto S, Kitagaki H, Mori E . Relatively preserved hippocampal glucose metabolism in mild Alzheimer's disease. Dement Geriatr Cogn Disord, 1998; 9: 317-322.

99. Ishii K, Sasaki M, Yamaji S, Sakamoto S, Kitagaki H, Mori E . Paradoxical hippocampus perfusion in mild-to-moderate Alzheimer's Disease. Journal of Nuclear Medicine, 1998; 39: 293-8.

100. Ishii K, Sakamoto S, Sasaki M, Kitagaki H, Yamaji S, Hashimoto M, Imamura T, Shimomura T, Hirono N, Mori E . Cerebral glucose metabolism in patients with frontotemporal dementia. Journal of Nuclear Medicine, 1998; 39: 1875-1878.

101. Frackowiak R S J, Friston K J . Functional neuroanatomy of the human brain: positron emission tomography - a new neuroanatomical technique. Journal of Anatomy, 1994; 184: 211-225.

102. Fukuyama H, Ouchi Y, Matsuzaki S, Nagahama Y, Yamauchi H, Ogawa M, Kimura J, Shibasaki H . Brain functional activity during gait in normal subjects: a SPECT study. Neuroscience Letters, 1997; 228: 183-186.

103. Nadeau S E, Crosson B . A guide to the functional imaging of cognitive processes. Neuropsychiatry,Neuropsychology and Behavioral Neurology, 1995; 8: 143-162.

104. Kapur S, Hussey D, Wilson D, Houle S . The statistical power of [^{15}O]-water PET activation studies of cognitive processes. Nuclear Medicine Communications, 1995; 16: 779-784.

105. Woods R P, Mazziotta J C, Cherry S R . Optimizing activation methods: Tomographic mapping of functional cerebral activity. In Functional neuroimaging: Technical foundations Thatcher R W, Hallet M, Zeffiro T, Roy John E, Heurta M editors. 1994. San Diego. Academic press. 47-57.

106. Shedlack KJ, Hunter R, Wyper D, McLuskie R, Fink G, Goodwin GM . The pattern of cerebral activity underlying verbal fluency shown by split-dose single photon emission tomography (SPECT or SPECT) in normal volunteers. Psychological Medicine, 1991; 21: 687-696.

107. International commission on radiological protection, addendum 1 to publication 53. 1993. Oxford. ICRP Publication 62 Pergamon Press.

108. Cohen Y, Landy M S . The HIPS image processing software V2.0. Turing Institute, Dumbarton Rd, Glasgow G11, 1991.

109. O'Leary D.S. , Madsen M.T. , Hurtig R. , Kirchner P.T. , Rezai K. , Rogers M. , Andreasen N.C. . Dual isotope brain SPECT imaging for monitoring cognitive activation: initial studies in humans. Nuclear Medicine Communications, 1993; 14: 397-404.

110. Woods S W, Hegeman I M, Zubal I G, Krystal J H, Koster K, Smith E O, Heninger G R, Hoffer P B . Visual stimulation increases technetium-99m-HMPAO distribution in human visual cortex. Journal of Nuclear Medicine, 1991; 32: 210-215.

111. Butler R E, Costa D C, Ell P J, Katona C L, Creco A . Diagnosing Alzheimer's disease [letter]. BMJ, 1992; 304: 574-575.

112. Amar AP, Heck CN, Levy ML, Smith T, DeGiorgio CM, Oviedo S, Apuzzo ML . An institutional experience with cervical vagus trunk stimulation for medically refractory epilepsy: rationale, technique, and outcome. Neurosurgery, 1998; 43: 1265-1276.

113. McLachlan R S. Vagus nerve stimulation for intractable epilepsy: a review. J Clin Neurophysiol, 1997; 14: 358-368.

114. Ben-Menachem E. Modern management of epilepsy: Vagus nerve stimulation. Baillieres Clinical Neurology, 1996; 5: 841-848.

115. Snively C, Counsell C, Lilly D . Vagus nerve stimulator as a treatment for intractable epilepsy. J Neurosci Nurs, 1998; 5: 286-289.

116. Garnett E S, Nahmias C, Scheffel A, Firnau G, Upton A R . Regional cerebral blood flow in man manipulated by direct vagal stimulation. Pacing Clin Electrophysiol, 1992; 15: 1579-1580.

117. Schachter S C, Saper C B . Vagus nerve stimulation. Epilepsia, 1998; 39: 677-686.

118. Henry T R, Bakay R A, Votaw J R, Pennell P B, Epstein C M, Faber T L, Grafton S T, Hoffman J M . Brain blood flow alterations induced by therapeutic vagus nerve stimulation in partial epilepsy: I. Acute effects at high and low levels of stimulation. Epilepsia, 1998; 39: 983-990.

119. Aziz Q, Andersson JL, Valind S, Sundin A, Hamdy S, Jones AK, Foster ER, Langstrom B, Thompson DG . Identification of human brain loci processing esophageal sensation using positron emission tomography. Gastroenterology, 1997; 113: 50-59.

120. Crivello F, Tzourio N, Poline J B, Woods R P, Mazziotta J C, Mazoyer B . Intersubject variability in functional neuroanatomy of silent verb generation: assessment by a new activation detection algorithm based on amplitude and size information. Neuroimage, 1995; 2: 253-263.

121. Cechetto D F, Saper C B . Role of the Cerebral Cortex in Autonomic Function. In Central Regulation of Autonomic Functions Loewy A D, Spyer M K editors. 1990. Oxford. Oxford University Press. 208-223.

122. Gabrieli J D E, Brewer J B, Desmond J E, Glover G H . Separate neural bases of two fundamental memory processes in the human medial temporal lobe. Science, 1997; 276: 264-266.

123. Grady C L, McIntosh A R, Horwitz B, Maisog J M, Ungerleider L G, Mentis M J, Pietrini P, Schapiro M B, Haxby J V . Age-related reductions in human recognition memory due to impaired encoding. Science, 1995; 269: 218-221.

124. Roland P E, Gulyas B . Visual memory, visual imagery and visual recognition of large field patterns by the human brain: Functional anatomy by positron emission tomography. Cerebral Cortex, 1995; 1: 79-93.

125. Stern C E, Corkin S, Gonzalez R G, Guimaraes A R, Baker J R, Jennings P J, Carr C A, Sugiura R M, Vedantham V, Rosen B R . The hippocampal formation participates in novel picture encoding: Evidence from functional magnetic resonance imaging. Proceedings of the National Academy of Sciences of USA, 1996; 93: 8660-8665.

126. Tulving E, Markowitsch H J, Kapur S, Habib R, Houle S . Novelty encoding networks in the human brain: positron emission tomography data. Neuroreport, 1994; 5: 2525-2528.

127. Dolan, R.J., & Fletcher, P.C. Dissociating prefrontal and hippocampal function in episodic memory. Nature, 1997; 388, 582-585.

128. Mayes A R. Human Organic Memory Disorders: Problems in the Behavioural Sciences. 1988. Cambridge: Cambridge University Press.

129. Friston K J, Price C J, Fletcher P, Moore C, Frackowiak R S, Dolan R J . The trouble with cognitive subtraction. Neuroimage, 1996; 4: 97-104.

130. Price CJ, Friston KJ. Cognitive conjunction: A new approach to brain activation experiments. Neuroimage, 1997; 5: 261-270.

131. Baddeley A, Emslie H, Nimmo-Smith I . Doors and People. 1994. Flempton: Thames Valley Test Company.

132. Tulving, E., Markowitsch, H.J., Craik, F.I.M., Habib, R. & Houle, S. (1996) Novelty and familiarity activations in PET studies of encoding and retrieval. Cerebral Cortex, 6, 71-79.

133. Kelley, W.M., Miezin, F.M., McDermott, K.B., Buckner, R.L., Raichle, M.E., Cohen, N.J., Ollinger, J.M., Akbudak, E., Conturo, T.E., Snyder, A.Z. & Petersen, S.E. (1998) Hemispheric specialization in human dorsal frontal cortex and medial temporal lobe for verbal and nonverbal memory encoding. Neuron, 20, 927-936.

134. Wagner, A.D., Poldrack, R.A., Eldridge, L.L., Desmond, J.E., Glover, G.H. & Gabrieli, J.D.E. (1998) Material-specific lateralization of prefrontal activation during episodic encoding and retrieval. Neuroreport, 19, 3911-3717.

135. Wiggs, C.L., Weisberg, J. & Martin, A. (1996) Neural correlates of semantic and episodic retrieval. Neuropsychologia, 37, 103-118.

136. Knight R T. Contribution of human hippocampal region to novelty detection. Nature, 1996; 383: 256-259.

Published abstracts and papers

Montaldi, D, Mayes, AR, Barnes, A, et al. Use of HMPAO to investigate memory function in patients with amnesia. Acta Neurologica Belgica , 1995, Supp.95: 19.

Montaldi, D, Mayes, AR, Barnes, A, et al. Activations produced by memory encoding and retrieval using a SPECT-MRI co-registration technique: Comparison with SPM results. Neuroimage, 3, S551, 1996.

Barnes, A, Wyper, D, Montaldi, D, Patterson, J. Effect of restricted image data on automated co-registration algorithms: A method of investigation. Neuroimage S48,1996.

Montaldi, D., Mayes, A.R., Barnes, A., Pirie, H., Patterson, J., Hadley, D. and Wyper, D. Medial Temporal Lobe activations are produced by visual associative encoding and auditory verbal retrieval. Neuroimage, 5: 4, S614, 1997.

Barnes, A., Dai, D., Montaldi, D., Patterson, J. and Wyper, D. Image quality versus statistical power in neuroactivation. Neuroimage, 5:4 S447, 1997.

Barnes A, D Dai, D Montaldi, J Patterson and D Wyper. Image Quality vs. Statistical Power. Nuclear Medicine Communications December 1997 18: 1155-1160

Montaldi D, Mayes A, Barnes A, Pirie H, Hadley D, Patterson J, Wyper D. Associative Encoding of Pictures Activates the MedialTemporal lobes. Human Brain Mapping 6:85-104 (1998)

Montaldi D., Mayes A.R., Pirie H., Barnes A., Patterson J., Hadley D., Wyper D. Dissociating novelty detection and associative encoding in the processing of complex scenes. Neuroimage 7:4 S816, 1998

Montaldi D., Mayes A.R., Pirie H., Barnes A., Patterson J., Hadley D., Wyper D., Jauhar P. Alcoholic Korsakoff syndrome: One disorder or two? Evidence from structural and functional imaging. Neuroimage 7:4 S214, 1998